Development and characterization of solid lipid nanoparticles (SLN) as a vehicle of biomolecules

Marta Eduviges Bustos Araya

UNIVERSITAT DE BARCELONA

FACULTAT DE FARMÀCIA I CIÈNCIES DE L'ALIMENTACIÓ

DEVELOPMENT AND CHARACTERIZATION OF SOLID LIPID NANOPARTICLES (SLN) AS A VEHICLE OF BIOMOLECULES

MARTA E. BUSTOS ARAYA, 2022

UNIVERSITAT DE BARCELONA

FACULTAT DE FARMÀCIA I CIÈNCIES DE L'ALIMENTACIÓ

Ph.D. PROGRAM IN BIOTECHNOLOGY

DEVELOPMENT AND CHARACTERIZATION OF SOLID LIPID NANOPARTICLES (SLN) AS A VEHICLE OF BIOMOLECULES

Report submitted by Marta Eduviges Bustos Araya for the achievement of the Doctor degree in Biotechnology for the Universitat de Barcelona:

Dr. Montserrat Miñarro Carmona
Director and Tutor

Dr. Josep Ramon Ticó Grau
Director

Marta E. Bustos Araya
Ph.D. Student

MARTA E. BUSTOS ARAYA, 2022

ACKNOWLEDGEMENTS

These have been wonderful years of study and research, in which I have learned a lot and have received the support and help of many people. First, I thank God for the strength and guidance, my husband and son for being my driving force and strength. To my family and close friends, your words of support and encouragement also count in achieving my goals.

Thanks to my academic tutors Dr. Montserrat Miñarro Carmona who has been a fundamental column to guide me and to solve even the smallest detail in this training process, always with the precise and timely guidance, and to Dr. Josep Ramon Ticó Grau for guidance in the formulation of the research design and in the logistical support for the execution of the proposed methodology. Thank you for accepting me as your PhD student. In my future professional development, I will always keep in mind the patience, guidance, advice, and professional contributions that you gave me during my formative years.

In general, to the staff of the Department of Pharmacy and Pharmaceutical Technology, and Physiochemistry, who support us as doctoral students, always willing to provide us with equipment, teach us analytical techniques and help us solve problems, thank you again.

Special thanks to the government institutions Ministry of Science, Innovation, Technology and Telecommunications of Costa Rica and the University of Costa Rica, for their support and sponsorship of this academic project.

I am grateful to Dr. Tang Bin, from the Department of Biomedical Engineering, Southern University of Science and Technology, Shenzhen, Guangdong, Republic of China, and to Dr. Peter Smooker of the School of Science, RMIT University, Bundoora, Australia, for receiving me at their laboratories and allowing me to obtain greater expertise and knowledge in Molecular Biology techniques, to Jasmine, Ivana and Debolina, wonderful people, and friends. Thanks to all the work team of both laboratories, more than colleagues, they were friends and selflessly

shared their knowledge and made it a true experience of integral growth and learning.

1.

ABSTRACT

The interest of this work was to manufacture solid lipid nanoparticles that serve as a vehicle for biomolecules, specifically Chondroitin sulfate and pEGFP plasmid DNA. In the experimental part, the reagents and equipment used, and the methodology applied for the production and characterization of the nanoparticles are exposed, in accordance with the latest scientific trends contrasted bibliographically.

The nanoparticles were manufactured by the hot Microemulsion method, and the final formula was optimized by means of a 3x3x2 Experimental Factorial Design, where the critical operating parameters Concentration (mg/ml), Agitation Speed (rpm) and Reaction Time were evaluated. (min).

Five valid formulas to encapsulate CHON demonstrated stability both nanoparticles in aqueous media and lyophilized nanoparticles. The physicochemical characterization of the formulations as CHON vehicle presented sizes smaller than 200nm, negative zeta potential and mainly circular morphology. At the level of biomolecular studies, the nanoparticles did not show cellular toxicity, they demonstrated the ability to internalize different cell lines and the ability to modify the inflammatory activity in inflamed cells. The ex vivo studies support the possibility of applying the nanoparticles as a CHON vehicle to be administered in a living being.

On the other hand, two nanoparticle formulations also proved to be useful as pDNA vehicles, presenting sizes smaller than 170 nm, positive zeta potential, and protecting DNA against enzymes that degrade this nucleic acid. The lipoplexes, formed between the nanoparticles and the DNA, did not show cytotoxicity and were able to transfect cells through the expression of the green fluorescent protein (EGFP).

With the study carried out, it will be possible in the future to propose said nanoparticles to treat certain diseases or that are useful in other applications in the pharmaceutical field.

RESUMEN

El interés de este trabajo fue fabricar nanopartículas lipídicas sólidas que sirvieran como vehículo para biomoléculas, específicamente Condroitín sulfato y ADN plásmido pEGFP. En la parte experimental se exponen los reactivos y equipos utilizados y la metodología aplicada para la producción y caracterización de las nanopartículas, de acuerdo con las últimas tendencias científicas contrastadas bibliográficamente.

Las nanopartículas fueron fabricadas por el método de Microemulsión en caliente, y la fórmula final fue optimizada mediante un Diseño Factorial Experimental 3x3x2, donde se evaluaron los parámetros críticos de operación Concentración (mg/ml), Velocidad de Agitación (rpm) y Tiempo de Reacción (min).

Cinco fórmulas válidas para encapsular CHON demostraron estabilidad tanto en medio acuoso como liofilizadas. La caracterización fisicoquímica de las formulaciones como vehículo CHON, presentó tamaños menores a 200nm, potencial zeta negativo y morfología principalmente circular. A nivel de estudios biomoleculares las nanopartículas no mostraron toxicidad celular, demostraron capacidad de internalizar de diferentes líneas celulares y capacidad de modificar la actividad inflamatoria en células inflamadas. Los estudios ex vivo avalan la posibilidad de aplicar las nanopartículas como vehículo de CHON para ser administrado en un ser vivo.

Por otro lado, dos formulaciones de nanopartículas también demostraron ser útiles como vehículo de pDNA, presentando tamaños menores a 170 nm, potencial zeta positivo y protegiendo al ADN contra enzimas que degradan este ácido nucleico. Los lipoplexos, formados entre las nanopartículas y el ADN, no presentaron citotoxicidad y fueron capaces de transfectar células mediante la expresión de la proteína verde fluorescente (EGFP).

Con el estudio realizado, será posible en un futuro proponer dichas nanopartículas para tratar determinadas enfermedades o que sean útiles en otras aplicaciones en el campo farmacéutico.

ABBREVIATIONS

ACN	Acetonitrile
<	Less than
>	Greater than or equal to
±	Plus or minus
± SEM	± Standard error of the mean
≤	Less than or equal to
≥	Greater than
°C	Degrees Celsius
µg	microgram
µL	Microlitre
µm	Micrometre
2D	2 Dimensions
3D	3 Dimensions
Abs	Absorbance
ACAN	Aggrecan
AFM	Atomic Force Microscopy
AMP	Ampicillin
ANOVA	Analysis of variance
API	Active pharmaceutical ingredients
BJ	Human skin fibroblast cell line
BMP2	Bone morphogenetic protein-2
bp	Base pairs
CHON	Chondroitin sulfate
cm^2	Square centimeter
CO_2	Carbon dioxide
Col10	Collagen 10

COL10	Collagen type 10
Col2	Collagen 2
COLII	Collagen type II
D[3,2]	Average surface diameter
D50	The point in the size distribution, up to and including which, 50% of the total volume of material in the sample is contained.
D90	The point in the size distribution, up to and including which, 90% of the total volume of material in the sample is contained.
DAPI	4,6-diamidino-2-phenylindole
DC	Dendritic cell
DC2.4	Immature murine dendritic cell line
dH2O	Distilled water
DLS	Dynamic light scattering
DMEM	Dulbecco's modified eagle medium
DMSO	Dimethyl sulfoxide
DNA	Deoxyribonucleic acid
DNase I	DNA-specific endonuclease
DOE	Experimental Factorial Design
DSC	Differential Scanning Calorimetry
EDTA	Ethylenediamine tetra acetate
EE	Entrapment efficiency of CHON
EGFP	Enhance Green fluorescent protein
ELISA	Enzyme-linked immunosorbent assay
EtOH	Ethanol
FBS	Fetal bovine serum
g	Gram
GAPDH	Glyceraldehyde-3-phosphate dehydrogenase
h	Hour

H2O	Water
HACAT	Human keratinocyte cells
HCL	Hydrochloric acid
HEPES	4-(2-hydroxyethyl)-1-piperazineethanesulfonic acid
HPLC	High performance liquid chromatography
HT 29	Human colon adenocarcinoma cell line
ICH	International Council for Harmonisation of Technical Requirements
ICH	International Council for Harmonisation of Technical Requirements for Pharmaceuticals for Human Use
IL	Interleukin
IL-18:	Interleukin-18
IL-1β	Interleukin-1β
IL-1β:	Interleukin-1 beta
IL-6	Interleukin-6
iNOS	NO sintasa
J/g	Joule/gram
kDa	Thousand daltons
kg	Kilogram
LB brother	Luria-Bertani (LB) brother
Matrix	SLN prepared without CHON
MeOH	Methanol
mg	Milligram
MGH2O	Molecular grade water
Min	Minute
ml	Mililitre
mm	Millimeter
MMP-13	Matrix metalloproteinase 13
MMP-13	Matrix metallopeptidase 13

MMP-9	Matrix metallopeptidase 9
mPa·s	millipascal per second
MQH2O	Milli Q water
MTT	3-(4,5-dimethylthiazol-2-yl)-2,5-diphenyltetrazolium bromide
mV	Millivolts
NaOH	Sodium hydroxide
ng	Nanogram
nm	Nanometre
nm	Nanometre
NTA	Nanoparticle Tracking Analysis
OA	Osteoarthritis
p	Probability value
Pa	Pascal
PBS	Phosphate buffered saline
PCR	Polymerase chain reaction
PDI	Polydispersity index
pDNA	DNA plasmid
pg	Picogram
pH	Negative algorithm of hydrogen ion concentration
Ph. Eur.	European pharmacopoeia
Pot Z	Zeta Potential
R	Correlation coefficient
R^2	Coefficient of determination
RMIT	Universidad Real Instituto de Tecnología de Melbourne
RNA	Revolution per minute
RP-HPLC	Reverse phase high performance liquid chromatography
RP-HPLC	Reverse-phase chromatography
RSD	Relative standard deviation

RT-qPCR	Reverse transcription and quantitative polymerase chain reaction
SD	Standard deviation
SDS	Sodium dodecyl sulphate
SEM	Scanning electron microscopy
SLN	Solid lipid nanoparticles
SUSTech	Southern University of Science and Technology
TAE	Tris-Acetate-EDTA
TEM	Transmission Electron Microscopy
TNF-α	Tumour necrosis factor-α
USP	United states pharmacopeia
UV	Ultraviolet
UV-Vis	Ultraviolet Visible
v/v	Volume per volume
w/v	Weight by Volume
WGA	Wheat Germ Agglutinin
XRD	X-Ray Diffraction
Δ	Delta

INDEX

LIST OF FIGURES

LIST OF TABLES

INTRODUCTION

In the pharmaceutical industry there is a great variety of pharmaceutical forms according to the drug used and its pharmaceutical application. At present, nanotechnology has taken a great growth in many areas of knowledge (1,2). The use of nanoparticles as a vehicle for the transport of active substances can result in the modification of the contact surface, an increase in the permeability of biological barriers, resistance to chemical degradation, the administration of several substances together or stimulate the biological response(1). In the pharmaceutical sector at the nanotechnological level, methods and techniques are proposed to improve the bioavailability and/or access of active ingredients, whether of synthetic, natural, or biotechnological origin, among others (3).

There are many efforts to apply nanotechnology to cancer therapies, gene therapy, skin applications and many other areas of knowledge (1,4–12). Due to their composition and characteristics, nanoparticles can be lipid, cationic, anionic, neutral, biodegradable, metallic, among others, depending on the existing needs and possibilities (4,9,10,13–19). Solid lipid nanoparticles (SLN) have been highly relevant in the field of scientific research (8–10,14–17,19–26). The average diameter of SLN is from 50 nm to 1000 nm and they are composed of physiologically tolerable lipids, dispersed in water using surfactants (1). Some general methods for manufacturing are divided into high pressure homogenization, microemulsion, emulsification and solvent evaporation and double emulsion or a combination of them (1,27).

At the Faculty of Pharmacy and Food Sciences of the University of Barcelona, efforts have been made to obtain cationic solid lipid nanoparticles with an average size of less than 200 nm, by means of the hot microemulsion method, which have been tested as a vehicle for pDNA and siRNA, in the transfection of cell lines (28,29). This type of formulation becomes a basis of scientific interest to evaluate the possibility of transporting different types of biomolecules with pharmacological potential, whether they are not being administered by any pharmacological route or require an improvement in their bioavailability.

OBJECTIVES

The main objective of this study is to develop and characterize a formulation of solid lipid nanoparticles (SLN) that work as a vehicle of biomolecules.

The research work is based on the following goals:

Objective 1: Definition and study of critical operating parameters in obtaining SLN for biomolecules.

- Selection of the SLN manufacturing technique, preformulation, components to be used and physicochemical characteristics, as well as parameters that can influence the formulation.

- Evaluation of the critical operational physical parameters regarding particle size and surface electric potential, to obtain SLN as carriers of biomolecules, through a multifactorial design of the experimental study.

- Optimization and standardization of the conditions of the SLN obtaining method. Manufacture of different formulations with changes in some of the ingredients to evaluate the consistency of the results.

- Structural and thermal characterization of the components and the SLN obtained. Study the morphology and size of the nanoparticles through analytical techniques such as SEM, TEM, AFM, as well as the main interactions between the components of the formulation through XRD and DSC.

- Study of the binding capacity or efficiency of encapsulation of biomolecules to SLN, using the validated analytical methods Volumetric

titration and Uv-Vis Spectroscopy to determine the amount of CHON bound to the nanoparticles..

Objective 2: Stability study of SLN for the delivery of biomolecules.

- Evaluation of the stability of SLN under different temperature conditions (4 °C, room temperature and 37 °C) for fresh SLN samples in aqueous medium and at room temperature for lyophilized SLN samples.

- Measurement of critical physical parameters such as particle size and surface electric potential of the nanoparticles at different times and storage conditions.

Objective 3: Study of the applicability of SLN in ex-vivo models and cell models

- Study of transfection and cytotoxicity of SLN in cell models. Culture and maintenance of BJ, HaCaT, HT-29, DC and OA chondrocyte cell lines, used in the MTT cell cytotoxicity assay, internalization of labeled SLN and EGFP plasmid transfection.

- Study of inflammation markers in cell models. To characterize the potential of SLN as a vehicle for CHON, in the inflammatory response of OAchondrocytes and HaCaT cells previously induced to inflammation.

- Biopharmaceutical study of the ex-vivo permeation of SLN through the skin. To assess the ability of SLN to act as a vehicle for CHON to pass through the skin of pig ears, using the Franz Diffusion Cell.

BIBLIOGRAPHIC PART

1 The role of nano-biotechnology in the pharmaceutical field

1.1 Definition of Nano-biotechnology

The word nano-biotechnology refers to the set of two areas of knowledge: nanotechnology and biotechnology.

Nanotechnology is a study that synthesizes, through the characterization, production and application at the anatomical and molecular level, structures, devices, and systems at the nanometric scale (30). Nanotechnology-guided drug delivery improves permeability through cell membranes, which is the fundamental basis for promoting genetic-based drug development. In the same way, it is considered that nanotechnology seeks to understand the creation, manipulation, and use of different materials of nanometric order and its application in the chemical, biological, physical, and engineering fields, but essentially in medicine, allowing significant advances. scientists that achieve significant improvements in people's health (30,31).

Biotechnology is considered the use of living organisms, or products extracted from them for the benefit of beings (or the benefit of their environment) to develop a product or achieve the solution of a problem (32). Biotechnology through technological developments emphasizes the search for medical treatments whose contributions to medicine allow the advancement of science, this has the need to solve the problems of men from a scientific and technical perspective at the same time, which will be proportional individuals and their need to achieve changes in their health and constitute medical fields that can work together with technological supports (33).

Those types of science allow the improvement of human environments, emphasizing the need to innovate and improve people's health with updated and certified techniques and

procedures, which promise to improve people's health.

Nano-biotechnology is a combination of nanotechnology that involves the development and application of nanomaterials and devices on a nanometric scale, on the other hand, biotechnology that includes a diversity of functions that correspond to the biological aspect, such as microorganisms (34). This technology has the promise of creating access in the research field that allows the diagnosis and treatment of many pathologies in the future, using nano-materials, that can interact with complex biological organ and consumption low level of biomolecules. (35).

It is considered a strategy that allows the interaction of nanotechnology and biotechnology, to achieve the design and improvement of the properties of different therapeutic agents, in the treatment of many acute, chronic, or terminal diseases, nanotechnology focuses to improve diagnose methods, improved drug loaded delivery system for the effective and enhanced therapy (35). As shown in Figure 1, nanobiotechnology seeks, among other objectives in the pharmaceutical field, the redirection of the drug under study towards a specific therapeutic target, achieving a more personalized therapy with fewer adverse effects.

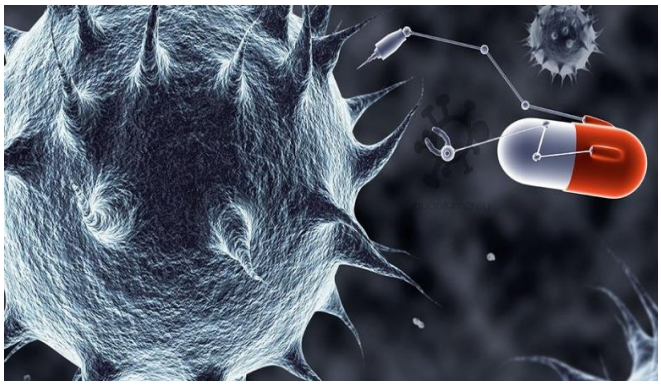

Figure 1. Nanobiotechnology in the improvement of pharmaceutical forms reproduced from Olvera Carranza, 2017 (36). Illustration of the potential use of nanobiotechnology in the redirection and improvement of therapeutic agents for the specific treatment of diseases.

1.2 Advantages of nanobiotechnology

There are many expectations for the future regarding the medical applications and the improvement of people's quality of life that nanobiotechnology may have. Many advantages are attributed to this area of knowledge, which causes more and more research groups to emerge (37,38).

Among the advantages obtained from the application of nanotechnology in the therapeutic field, we can name (35,37):

1. Obtaining molecular images for brain tissue engineering
2. Drug delivery across the blood-brain barrier
3. An improvement in the neuroprotection or regeneration of the CNS is achieved
4. Improvements in drug absorption, achieving fewer side effects compared to conventional molecules
5. Improved biodistribution and high bioavailability of biomolecules such as DNA and RNA providing high affinity and binding at a specific target site, without enzymatic degradation
6. Availability of non-toxic and biodegradable nanomaterials that improve the effectiveness of drugs against cancer and other pathologies.
7. In the field of biomedical research, it allows the realization of simple methods of drug selection in vivo and in vitro.

Given the variety of benefits and applications of nanobiotechnology, this es having a wide impact on the fields of science and technology and presenting some unique possibilities in medicine, diagnosis, and biomedical sciences, with a diversity of nanosystem proposals for the development and discovery of new therapeutic alternatives (35).

2 Nanosystems in drug discovery and development

Currently, in the field of drug discovery and development of strategies diagnostics, researchers are starting to use nanotechnology, creating different nanosystems functional with different applications (35,39).

A well-structured nanosystem has defined dimensions and properties that are manageable and capable of achieving the transport of functional biomolecules, such as small molecules, proteins, genes, among others. This type of systems allows effective interaction to generate diagnoses or treatments of various diseases that affect man (40).

Nanotechnology from the pharmaceutical approach seeks to develop components that fulfill individualized functions and at the same time achieve integration in a multifunctional architecture, together with biomolecular machines that have managed to revolutionize over time and allow the assembly of nanodevices with multiple degrees of freedom (41). This science, to achieve a better purpose in therapy, is based on the response of nanomaterials that release active substances under external stimuli that consider the unique physicochemical characteristics and properties (40).

Among the nanosystems studied are: Nanocrystals (QDs) and nanoparticles (solid lipid nanoparticles, gold colloids, magnetic nanoparticles, nanobarcodes, nanobodies, dendrimers, fullerenes, and nanoshells) (35,39). The nanosystems become nanocarriers, which provide protection against the biodegradation of the different therapeutic agents, which means that the release of the active principles occurs in a sustained manner and with prolonged circulation kinetics. Given this, nanocarriers increase the solubility and bioavailability of pharmacological drugs, reducing the use of large doses and the administration of injectables. (42).

3 Nanoparticles and their importance in the biomedical field

The nanoparticles have made significant contributions to drug discovery and development of devices for biomedical purposes, and given their versatility, they become strategies that promise to improve and optimize the treatment of diseases (43).

These nanostructures may be able to avoid the immune system, and thus cross some barriers that the body uses to reduce the risk of penetration of substances that are not part

of it and therefore are not wanted by the body (44). Therefore, it is considered that pharmaceutical compounds that have been reformulated as nanoparticles may be more biologically active, coupled with the broad surface area that increases their bioavailability (41).

4 Types of Nanoparticles

There is a great diversity of nanoparticles in terms of composition, functionality, and characteristics. Among which the following nanoparticles with application in the biomedical field can be mentioned, they are shown in Figure 2.

The use and application of each type of nanoparticles will depend both on the physicochemical properties of the drugs, namely, aqueous solubility, oil/water partition coefficient, ionization constant, stability at various pH prevalent in the gastrointestinal tract, as well as on the characteristics biopharmaceutical properties along with permeability across cell barriers, tissue distribution, cellular uptake, metabolic and excretion pattern, route of drug administration, general pharmacodynamics, and adverse effects (45).

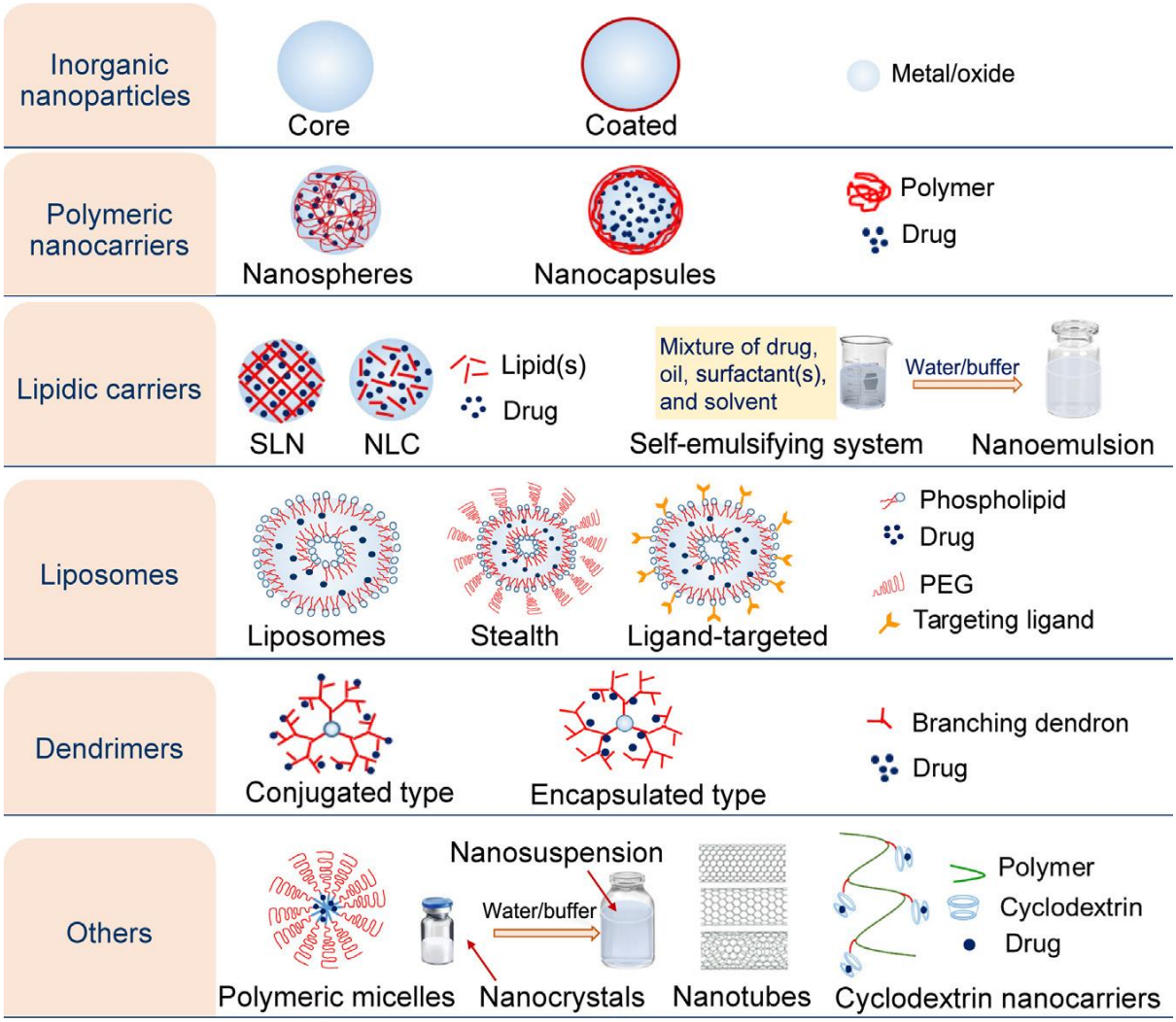

Figure 2. Some types of nanoparticles with application in the biomedical field. Reproduced from Pund &Joshi 2017 (45)**.** There are different forms of nanoparticles such as inorganic, polymeric, lipidic, liposomes, dendrimers, and others, presenting paricular structural arrangements and variation in the ingredients according to each formulation.

Some relevant aspects of the types of nanoparticles will be briefly described in table 1, finally focusing in detail on the Solid Lipid Nanoparticles, which are the object of the present investigation.

Table 1. Brief description of some types of nanoparticles with application in the biomedical field.

Nanoparticle	Description
Inorganic Nanoparticles	Among the components you can use: Metals, such as gold, copper, and silver, and inorganic carriers, such as silica or alumina, and/or their oxides/ sulfides. Inert, nontoxic, highly stable nature. Gold nanoparticles are one of the most studied in cancer therapy (45,46).
Polymeric Nanoparticles	Matrix composed of biodegradable and biocompatible polymers of synthetic or natural origin. Natural polymers like alginate, albumin, or chitosan have been widely explored. can be get for different methods of preparation: solvent evaporation, spontaneous emulsification, solvent diffusion, or polymerization (44,45,47).
Lipid-Based Carriers	Solid lipid nanoparticles (SLN) and nanostructured lipid carriers (NLC) were initially developed as a pharmaceutical alternative to liposomes and emulsions (45).
Liposomes	Liposomes are concentric, microscopic, bilayered, spherical vesicles with central aqueous compartment enclosed by phospholipids. Their suffer from a major drawback of rapid elimination from blood by reticuloendothelial system. Various novel liposomes have been developed to help improve the targeting ability of liposomes, like virosomes, archaeosomes, pH sensitive, magnetic liposomes, and photodynamic liposomes (45).
Dendrimers	Dendrimers are polymer-based biocompatible core–shell nanostructures constructed from monomeric or oligomeric units, with precise architecture and low polydispersity. Dendrimers may be hydrophobic or hydrophilic and accordingly affect the degree of encapsulation of drug (45,47).

4.1 Lipid-Based Carriers

The development of nanostructured lipid carriers and solid lipid nanoparticles dates to the early 1990s (48). These types of nanoparticles are described as colloidal solid particles that range in size from 1 nm to 1000 nm, they are made up of lipids which have the ability to disperse in solutions such as water and, act as dosing agents in drug delivery (41,49). Therefore, the significant reduction of drug particles at a nanoscale level increases the speed at which dissolution occurs and the saturation limit of solubility, which allows a better pharmacological action (41).

Lipid nanoparticles include:

- Solid lipid nanoparticles (SLN)
- Nanostructured lipid carriers (NLC)
- Lipid drug conjugate (LDC)
- Polymer-lipid hybrid nanoparticle (PLN).

These entities emerged as a pharmaceutical alternative to liposomes and emulsions. The main difference between SLN and NLC is the liquid or solid state of the lipids that make it up. SLN are composed of rigid cores of biodegradable hydrophobic solid lipids with high levels of surfactants, while, NLC have a mixture of liquid and solid lipids (Figure 2) (45).

4.1.1 Nanostructured lipid carriers (NLC)

Nanostructured lipid transporters (NLC) are among effective drug delivery systems, they have aroused increasing interest as a potential drug vehicle due to their high drug loading capacity, physical stability, easy preparation, and protection of the bioactive compound. encapsulated against degradation, and low toxicity (50,51).

NLCs are lipid-based colloidal systems characterized by a solid lipid core containing a mixture of solid and liquid lipids, and with an average particle size in the nanometer range (50,52).

NLC have appeared as novel systems composed of physiological lipid materials appropriate for topical, dermal, and transdermal administration (52). The main components of NLC are lipid, surface active agent and water (51).

4.1.2 Solid lipid nanoparticles (SLN)

SLN have certain characteristics that make them an alternative of pharmaceutical interest for the entry of biomolecules into the cell interior, being considered as a valuable therapeutic tool, among which are (49):

a. The ability to convert lipophilic drugs into solubles.
b. Allow stabilization with emulsifiers or surfactants.
c. Have the ability to be incorporated with the drug creating a lipid-drug matrix.
d. Confer high loads to the drug, allow drug release in a controlled manner.
e. Increase the degree of absorption of various drugs and do not generate toxicity due to its nature.

The speed at which the SLN-Drug complexes degrade is dependent on the size of the SLN particle, according to Villafuerte (2008), SLN with sizes between 180-300nm have a higher degradation speed compared to 800nm SLN (53).

SLN are heterogeneous systems with a solid at room and body temperature lipid inner phase and an external aqueous phase stabilized by surfactants; they are composed by three main components: lipids, surfactants, and the active ingredient (drug) loaded (Figure 3).

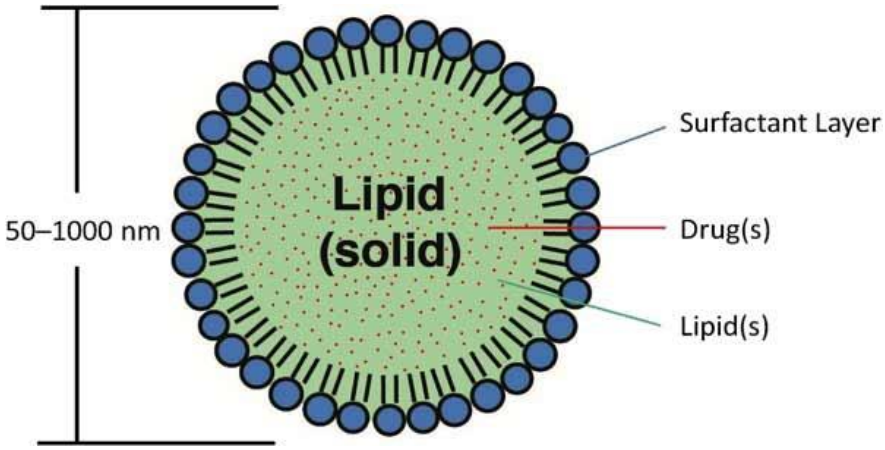

Figure 3. Structure of solid lipid nanoparticle, reproduced (54)**.**

SLN have a solid core that contains the drug and a surfactant substance in its outer layer. The size of SLNs is large and can range from 50 to 1000 nm.

The solid inner matrix allows the controlled release of encapsulated molecules and protects them from degradation, increasing the long-term stability whereas the external phase produces interactions with the skin and help to dissolve the nanoparticles. These characteristics present several advantages for cutaneous use, such as protection from degradation of the encapsulated molecules due to the solid matrix, which leads to the possibility of modulating molecules release and ease to adhere to the horny layer and penetrate deeper layers because of the hydrophilic interactions between the surfactant of the external layer and lipids present in the stratum corneum (55,56).

In general, there are potential advantages of solid lipid nanoparticles (57)

- Longer shelf life
- Biocompatible and biodegradable colloidal carrier
- Prevention of degradation of drug in body fluids due to encapsulation
- Longer half-life of drug
- Increased drug payload
- Possibility of sustained-release and controlled-release of drugs
- Increased drug dissolution and absorption, improved bioavailability

- Drug targeting
- Feasibility of sterilization
- Large scale manufacturing

4.1.3 Solid lipid nanoparticles applications

In the scientific field, SLN have many areas of application and study. Within the applications of SLN in biomedicine, one can find the delivery of nucleic acids as well as other biomolecules of pharmaceutical interest.

4.1.3.1 SLN as a vehicle for nucleic acids

Nucleic acids contain the genetic information of living beings, they are made up of fundamental units called nucleotides.

Nucleotides are organic-type molecules involved in reactions related to cell reproduction and maintenance, as well as the storage of genetic code information. The decoding of the genetic code contained in a nucleotide sequence transcribes all types of essential proteins for cell development, among which are: structural, catalytic, functional proteins, factors involved in the transcription process, among others (58).

This type of molecules is made up of a sugar (ribose or deoxyribose) and a nitrogenous base. Table 2 shows the nucleotides present in nucleic acids, which in solutions have a negative charge due to the phosphate group present, giving it the ability to easily bind to positively charged molecules through electrostatic interactions, as evidenced by the formation of complexes with cationic nanoparticles used to transport nucleic acids (59).

Table 2. Nucleotides that make up nucleic acids (59).

Base	Nucleoside	Nucleotide
Adenine	• Adenosine • Deoxyadenosine	• Adenosine monophosphate • Deoxyadenosine monophosphate
Guanine	• Guanosine • Deoxyguanosine	• Guanosine monophosphate • Deoxyaguanosine monophosphate
Thymine	• Thymidine	• Thymidine monophosphate
Cytosine	• Cytidine • Deoxycytidine	• Cytidine monophosphate • Deoxycytidine monophosphate
Uracil	• Uridine	• Uridine monophosphate

Both DNA and RNA have become therapeutic targets for the treatment of various diseases. These molecules are defined as:

DNA

Deoxyribonucleic acid is made up of nucleotides such as: Adenine, Thymine, Cytocine and Guanine, linked by a phosphodiester bond with a 5' to 3' direction, which form chemically complementary chains by means of hydrogen bonds, thus creating it forms a double helix structure. From a thermodynamic perspective, the nucleotides that follow one another are found forming interactions with the pi orbitals present in the aromatic rings of the bases, called π stacking, being the characteristic that allows the structure to double at low energy levels, thus creating a stable molecule (60).

DNA (Deoxyribonucleic Acid) is known as the molecule which gives the instructions that are given from adult organisms to their offspring in the process of reproduction (61).

RNA

Ribonucleic acid (RNA) is created from the polymerization of ribonucleotide complexes, linked by phosphodiester bonds in the 5' to 3' direction, formed by union with a phosphate group, a nitrogenous base (guanine, cytosine, uracil, and adenine) and a ribose.

Combination of ribonucleotide complexes forms single-stranded RNA (58).

It is present in all those living cells and has some structural similarities with DNA. However, compared to DNA, RNA is made up of a single strand. This is how there are also several types of RNA in cells, such as: ribosomal RNA (rRNA), messenger RNA (mRNA) and transfer RNA (tRNA); even participating, some RNA in the regulation of gene expression (62).

Previous studies show great potential for the use of SLN in the delivery of nucleic acids, such as the cases presented by:

- SLN are systems that promise a lot in terms of the administration of lipophilic and hydrophilic drugs, basically consisting of a solid lipid core that is stable thanks to a layer of surfactants. By incorporating cationic lipids in the formulation, positively charged SLN can be generated, taking charge of properly transporting nucleic acids (DNA, siRNA). Taking into account this beneficial effect that auxiliary lipids have on the efficiency of transfection with cationic liposomes of nucleic acids that allow controlling the expression of certain proteins and thus reversing the development of any disease, Rodríguez et al, 2016 (63) indicates that lipid vectors are considered safe, but have low efficiency in the transfection process, the compiled scientific evidence shows that an effective formulation is related to the improvement of parameters such as the disposition at the intracellular level and the internalization of nucleic acids. The authors affirm that the SLN, according to the present scientific evidence, can induce the production of proteins after the complex has been administered intravenously, which would indicate that the route of administration would also be conditioning the efficiency parameter of the process. The information collected shows that SLN have been used in the treatment of certain hereditary and acquired diseases such as: X-linked juvenile retinoschisis.

- This type of degenerative disease that affects the retina is due to a mutation in the RS1 gene, which viral and non-viral vectors have been evaluated for treatment by

gene therapy, as demonstrated by Gallegos, 2015, through the design and evaluation of a non-viral vector based on SLN and addition of dextran and protamine, which managed to transfect the retina after its delivery via the eye in HEK-293 and ARPE-19 cells, indicating that gene therapy presents a high efficiency in the process of transfection with this type of vector (64).

- Previous applications demonstrate the potential of SLN, as indicated by Torrecilla, 2016 in their research, which demonstrated the capacity of non-viral vectors based on SLN, in the administration of the shRNA74 plasmid, this in order to inhibit "in vitro" the replication of the hepatitis C virus (HCV, English hepatitis C virus). The vectors were characterized by: size, surface charge, as well as binding capacity, release and inhibition of plasmid degradation against DNases. Wherein the size of all the complexes was less than 240 nm in diameter together with a surface charge around +35 mV. Likewise, all the vectors showed a good binding capacity to genetic material, with the ability to protect it against DNases and to release it (65).

- Fàbregas et al., 2017 in their research used a selected and optimized formulation of SLN to carry out an effective transfection of circular DNA molecules together with linear RNA in eukaryotic cells. The authors were in charge of carrying out a physicochemical characterization of SLN together with its binding capacity, evidencing that they deliver DNA and RNA molecules in those target cells where there is complete bioactivity (the ability of cells to interact with molecules from the external environment). in concentrations that are not toxic, using techniques based on fluorescence and luminescence. Therefore, the authors were able to establish a novel and simple SLN formula for future therapeutic use (26).

- Suñé-Pou et al., 2019, present in their study the use of cholesteryl oleate, which is a new excipient for SLN in terms of the development of vehicles to administer highly efficient and non-toxic nucleic acids. The authors fully described the

physicochemical and biological characterization of the cholesteryl oleate-loaded SLN, ensuring the reproducibility of this formula along with the preservation of their characteristics before and after lyophilization. The results indicated that this improved formulation is appropriate for gene therapy and has the potential to scale up nanoparticle manufacturing under Good Manufacturing Practice conditions (66).

- Parashar, 2020, indicates that for the transfection of interfering RNA (siRNA) useful in the genetic silencing of diseases, it is necessary to have efficient vehicles that are alternatives for the instability presented by the use of immunogenicity and serum, for which he affirms that The lines of research have focused on the creation of SLN for the administration of siRNA towards the exact symptomatic points, with lipid nanoparticle formulations being the most suitable alternative for transfection and important for the efficient development of gene therapy (67).

- Limeres et al., 2019 characterized and formulated cholesteryl oleate (coSLN) SLN into DNA:Protamine:coSLN complexes for gene transfer with high uptake efficiency and low cell toxicity. The results presented an efficiency of 100% with respect to the load and likewise a positive analysis regarding the protection of DNase I in relation to the protective action of DNA. Another important contribution made by the authors is regarding the use of protamine, which induced an increase in the capacity of the transfection process without toxic effects (68).

Other DNA delivery systems have been studied, presenting disadvantages in their application:

***Viral transfection*:** it is a delivery system which uses a virus as an auxiliary vector for the transfection process. Among the viruses used we find retroviruses made up of RNA, which can be able to couple to the host genome, allowing a constant expression process with respect to the transgene, an important characteristic for the care of chronic or hereditary diseases. One of the disadvantages of the use of this type of transfection is that the integration of the viral RNA is random in the host genome, being a risk for the

development of insertional mutagenesis, which can cause an alteration of a suppressor. of a tumor by inhibiting gene expression or causing the expression of an oncogene. Another disadvantage of using these systems is due to the inability to enter cells that are dividing. Table 3 shows the advantages and disadvantages of the use of viral transfection systems used in gene therapy (69).

Table 3. Advantages and disadvantages of viral vectors (69)

Vector	Advantages	Disadvantages
AAV (45-60 nm)	• Avoids the immune response • Translates into the great diversity of cells • Constant expression	• Generation of low titles • Limited in size of the transgene.
Ad (90-110 nm)	• Does not have the ability to integrate • Transduces only those cells that are in the replication or resting phase • Ability to integrate with large genes.	• High immune response • It is only expressed temporarily • Single dose
Retrovirus (123-145 nm)	• Stability in gene expression • Ability to integrate with large genes	• Their integration occurs randomly • Translates only when cells are dividing.

***Transfection with cationic liposomes*:** refers to the use of cationic lipids forming complexes with genetic material which will be transferred from the cell membrane or outside to the intracellular medium, to deposit the gene load of interest. The advantage of using lipids as vectors for transfection is based on the ability to selectively transport genetic material to any region of the body, as well as its entry into the intracellular medium and its deposit at the correct destination. These types of vectors act as mechanical protectors of the genetic material, avoiding degradation by means of DNAses, achieving controlled distribution that does not depend on the size of the genetic material to be expressed. Due to their nature, this type of biomolecules is not immunogenic or carcinogenic; however, they have problems in the efficiency of the transfection process,

as well as temporary expression, which only allows them to be used in the treatment of chronic or acute diseases that do not require replace a faulty gene (70).

4.1.3.2 SLN as a vehicle of other Biomolecules -CHON

Since living beings are made up of a series of substances classically known as "immediate principles", biomolecules are currently known as those molecular organizations that are part of or integrate living matter (71).

They are chemical compounds that make up the living matter of all beings that inhabit the Earth. These result from the link of bioelements through chemical bonds, highlighting those of the covalent type. Within the universal biomolecules are amino acids, carbohydrates, lipids, proteins, vitamins, and nucleic acids. Similarly, some of the characteristics that these biomolecules present are:

- They allow the formation of covalent bonds between them, sharing electrons; these links being very stable.
- Carbon atoms can form a kind of three-dimensional skeletons, allowing living beings to present different compounds compared to their carbon skeleton.
- Bioelements allow the formation of double and triple bonds between them, and likewise allow the synthesis of various structures such as branched, cyclic, etc.
- With smaller amounts of bound bioelements, it is possible to synthesize a considerable amount of functional groups, with different chemical and physical properties (72).

An important biomolecule is chondroitin sulfate (CHON), which is known as a chemical, which is present in human and animal cartilage. It is commonly used orally with glucosamine or other ingredients to treat osteoarthritis. In this disease, the cartilage in the joints breaks down, so the consumption of chondroitin sulfate could delay this. Usually made from animal sources, such as cow and shark cartilage, it can also be made in a laboratory. Chondroitin sulfate may also be used to treat many other conditions, however there is little scientific evidence to support these uses (73).

CHON presents characteristics such as a size between 5-50kDa, it is the most abundant glycosaminoglycan in the human body, it is found in cartilage, tendon, ligaments and the aorta. CHON binds to proteins (like collagen) to form proteoglycan aggregates (74).

CHON, in addition to being part of the group of glycosaminoglycans, is one of the main elements that make up cartilage, which binds to a central protein, thus constituting the so-called "proteoglycan"; who gives cartilage elastic and mechanical properties. Due to its nature and properties, CHON is considered a drug with an effect similar to those reported by non-steroidal anti-inflammatory drugs, which is why clinical studies have reported that the supply of CHON presents an effective action in the control group compared to placebos related to reducing the level of pain, increasing the functional capacity of patients with osteoarthritis in fingers and knees, and reducing the use of other types of medications such as gastroprotectors. Therefore, the authors indicate that the use of CHON is an effective tool to prevent progression in diseases such as joint injury (74,75)

The main use of CHON is in the treatment of osteoarthritis. It is part of the so-called SYSADOA, which stands for *symptomatic slow acting drugs for osteoarthritis*, which refers to a group of slow-acting drugs for the symptomatic treatment of osteoarthritis (OA). However, there is also a body of evidence that is growing, demonstrating its DMOAD effect (disease modifying osteoarthritis drugs), which means slow-acting drugs for OA, with the ability to modify the structure. There are also other uses or applications of chondroitin sulfate, as evidenced by Cañas, 2008 in their study evidencing the neuroprotective properties in in vitro models linked to the pathophysiology of cerebral ischemia, where it had previously shown antioxidant and anti-inflammatory properties (76).

Another very interesting use reported by the literature is in the treatment with sodium chondroitin sulfate in intravescial instillation in painful bladder syndrome. Where it has been shown that it improves aspects related to pain, micturition frequency and in general the quality of life in the long term (77).

4.1.3.2.1 CHON and his relationship with Arthritis

Arthritis is defined as an inflammatory process of the articular synovium. The synovium is the tissue that, like a membrane, covers the bone and cartilage surfaces that come into contact in a joint. Arthritis appears when cartilage and synovium suffer destruction due to various causes, such as trauma, infectious agents such as bacteria, viruses, fungi and parasites, and immunological factors (78).

The signs and symptoms of arthritis are in one or several joints, being typical of an inflammatory response (78):

- Joint pain
- Swelling, or increased joint size.
- Redness of the skin of the joint.
- Heat or increased temperature in the affected area.
- Limitation of joint mobility.

From 2013 to 2015, an estimation of 54.4 million adults in the United States reported doctor-diagnosed arthritis (osteoarthritis, rheumatoid arthritis, gout, lupus, or fibromyalgia), with 23.7 million describing arthritis-attributable activity limitation (79).

The progressivity of this type of pathology leads to joint destruction with consequences that become disabling for patients, progressively decreasing not only its mobility, but also influencing extra-articular manifestations such as development and affection of other internal organs (80).

Arthritis can be caused by various diseases such as rheumatoid arthritis (RA) and osteoarthritis (OA) (Langford & Mandell, 2022).

4.1.3.2.2 ***Rheumatoid Arthritis (RA)***

Rheumatoid Arthritis is considered one of the main types of arthritis, this being a chronic pathology and aggressive etiology in the patient, since it generates irreversible damage to the joints and cartilage, in addition to inducing the patient in severe pain and disability. Medically, it is considered that this pathology has no cure, however it is worth considering that there are a variety of treatments that are aimed at treating the symptoms, reducing severe pain, and preventing both the damage that occurs in the joints and the disability that the disease generates in the patient (82).

Rheumatoid Arthritis presents a chronic inflammatory etiology of systemic origin, where its most relevant clinical expression is erosive polyarthritis coupled with serological tests of autoreactivity. This type of pathology is more frequent in the female population than in the male population, its main characterization consists of chronic pain and joint destruction, which leads to the patient presenting a high risk of disability, which means an increase in medical costs and treatment coupled with the progressivity of the disease (83).

In terms of disability, the World Health Organization considers that Arthritis is one of the main degenerative diseases that present and generate disability in people, with high percentages of absenteeism and premature retirement from work due to disability (82)]. According to estimates made, the World Health Organization estimates that between 1 and 1.5% of the population worldwide suffers from this type of pathology and currently there are around 34 million people with permanent disabilities associated with the disease, and 140 million with temporary disability related to diseases of rheumatic origin (82). The diagnosis of this pathology depends to a large extent on the compilation of the information that is collected, the patient's medical history, the medical-physical diagnosis, and the support that one has from laboratory tests and imaging. (84).

This, like other pathologies that generate immobility in patients, inhibits the individual's ability to function in an environment that facilitates daily activities, considering that the disease degenerates and limits the patient. This pathology affects the lining of synovial

joints, which is the cause of progressive disability, premature death, as well as socioeconomic burdens on patients (84).

Radu & Bigau, 2021 describe RA as a multifactorial autoimmune disease with unknown etiology, which usually mainly affects the joints, while some extra-articular manifestations may appear later. Given its complexity, based on an incompletely elucidated pathophysiological mechanism, assertively managing RA requires a multidisciplinary approach. Thanks to medical advances in terms of diagnosis and treatment, thus allowing the activity of the disease to decrease, as well as preventing systemic complications from occurring (85).

Rheumatoid Arthritis are classified according to the presence or absence of anti-citrullinated protein antibodies (ACPAs). This citrullinated protein is catalyzed by a calcium-dependent enzyme called peptidylarginine deaminase (PAD), which modifies a positively charged arginine to a polar but neutral origin citrulline, as the product of a modified post-translational process. These antibodies can manage to detect rheumatoid arthritis in 67% of cases, and at the same time can be considered a reference to achieve diagnosis in patients with early undifferentiated arthritis and thus have a dimension of the progression of the pathology (84,86).

It is reported that the most relevant or promising results were obtained through the development of disease-modifying antirheumatic drugs (DMARDs), belonging to the class of biologic, conventional synthetic, and targeted synthetic drugs. The continuous development of drugs has also managed to obtain molecules with better profiles in terms of efficacy and safety (85). Methotrexate is usually an agent in the first-line treatment of rheumatoid arthritis; however, nonsteroidal anti-inflammatory drugs and simple analgesia are also important in controlling symptoms (78,87). In the case of rheumatoid arthritis, both glucosamine and chondroitin sulfate are not described as disease-modifying agents for use (88).

4.1.3.2.3 Osteoarthritis (OA)

Osteoarthritis (OA) is a joint and bone disease with pathological characteristics such as synovial and subchondral bone reactive hyperplasia and articular cartilage degeneration damage (Figure 4). Osteoarthritis is a common feature, most often affecting the shoulders, knees, hips, and hands (Figure 5) (89,90). OA is a disease of the cartilage that presents a failure in the functioning of the chondrocytes to maintain the proper balance between the formation and destruction of cartilage (79).

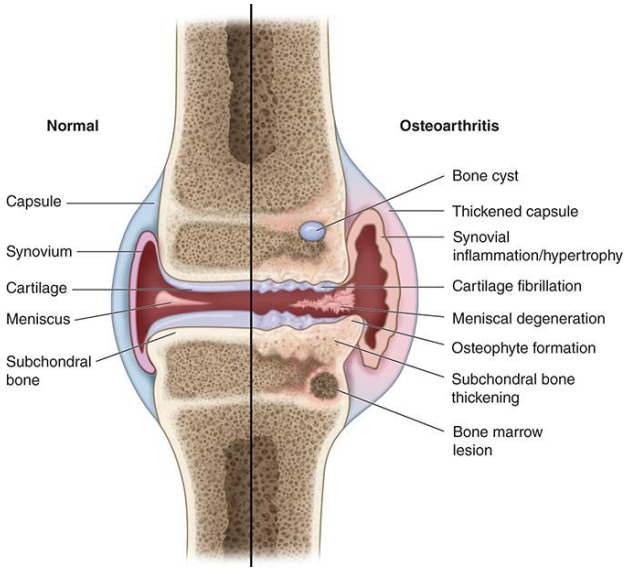

Figure 4. Characteristics of osteoarthritis in the diarthrodial joint. Reproduced from Buys et al 2019 (79)**.** The cartilage joint is shown in normal condition on the left and the cartilage alterations in OA, on the right side of the image.

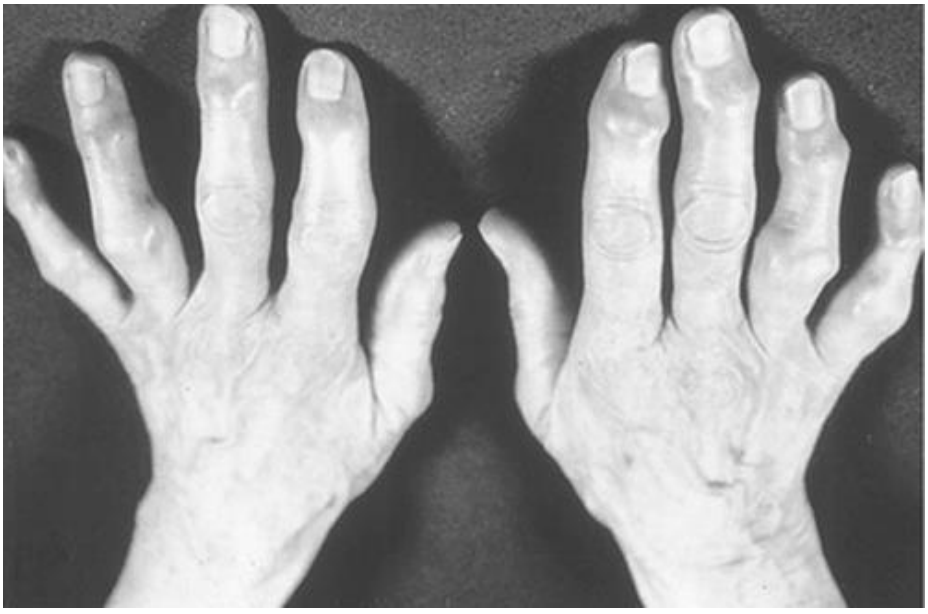

Figure 5. Representation of the hands of a patient affected by OA. Reproduced from Johnson 2015 (91). Heberden nodes (distal interphalangeal joint) noted on all fingers and Bouchard nodes (proximal interphalangeal joint) noted on most fingers.

Prevalence by Age, Sex, and Race (79,92)

- OA is more prevalent with increasing age: affecting 1.6% of those between ages 30 and 39, up to a prevalence of 14% in those over 85 years of age.
- Physician-diagnosed arthritis has a prevalence of 26.3% in White populations, 11.1% in Asian populations and 21.8 % for Black populations.
- Women are more commonly affected than men. Women are also more likely to have inflammatory OA of the proximal and distal interphalangeal joints of the hands.

4.1.3.2.4 Etiology of OA

The etiology of OA is multifactorial and complex. The risk factors most common are age, obesity, occupation, sex, the practice of certain sports, history of joint injury or surgery, and genetic predisposition (79).

4.1.3.2.5 Treatment of OA

The treatment of OA includes measures such as (78)

- Rest, exercise such as swimming, walking, having a healthy and well-balanced diet.
- Learn to use joints correctly and avoid being overweight.
- Pharmacological treatment with selective inhibitors of cyclooxygenase 2 (Coxibs or COX-2), non-steroidal anti-inflammatory drugs (NSAIDs). In the most serious cases, steroid anti-inflammatory drugs, corticosteroids and their derivatives, and opiate analgesics such as tramadol or codeine are usually prescribed.
- Glucosamine sulfate, chondroitin sulfate, and diacerein, with different mechanisms of action, have been successfully associated with the treatment of OA.

It has been established for CHON as its main use the treatment of Osteoarthritis (OA) and generally is well tolerated. As CHON is a glycosaminoglycan that has a slight anti-inflammatory action, it stimulates chondrocytes to produce cartilage, thus serving as a source of sulfur for the generation of molecular bonds within cartilage and inhibits leukocyte elastase, an enzyme responsible for cartilage degradation (93).
In animal models, CHON has been shown to influence chondrocyte metabolism, favorably influencing cartilage restoration or preventing further degradation of the matrix during the course of the disease. It is proposed that the therapeutic action of CHON is due, at least, to the following mechanisms of action: it has anti-inflammatory activity with respect to the cellular components of inflammation (tumor necrosis factor alpha (TNF-α),

IL-1β, cyclooxygenase 2 (COX-2), prostaglandin E2 (PGE2), nuclear factor kappa B (NFκB)), stimulates the synthesis of endogenous proteoglycans and hyaluronic acid, reduces catabolic activity of chondrocytes (by inhibiting proteolytic enzymes such as collagenase, elastase , proteoglycanase, phospholipase A2, NAG, MMP-3, MMP-9, MMP-13, MMP-14, cathepsin B, and aggrecanase 1 and 2), reduces apoptosis, nitric oxide, and free radicals, and protects cellular components from cartilage. At the subchondral bone level, CHON exerts a positive effect on the bone imbalance produced in arthritic subchondral bone, by regulating the expression and production of OPG (factor involved in subchondral bone remodeling) (94).

4.1.3.2.6 Inflammation in Osteoarthritis

Osteoarthritis presents inflammation markers that have been studied in recent years, since previously it was not considered an inflammatory arthropathy (95). Biological mediators involved in the pathological processes of OA include cytokines, chemokines, GFs, adipokines, lipid mediators such as prostaglandins and leukotrienes, nitric oxide (NO) and proteinases (Figure 6) (96).

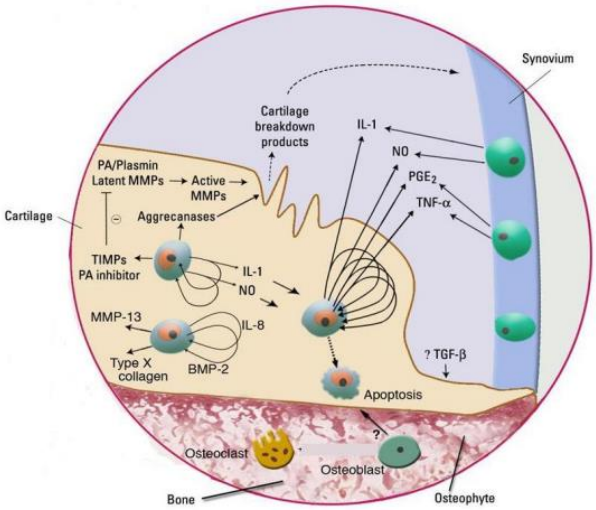

Figure 6. Biological mediators involved in OA. Reproduced from Gato 2019 (96). Many biological mediators are activated in the OA condition like cytokines, chemokines, GFs, adipokines, lipid mediators such as prostaglandins and leukotrienes, nitric oxide

(NO) and proteinases.

Different researches show that different proinflammatory mediators, such as the cytokines interleukin 1β (IL-1β) and tumor necrosis factor alpha (TNF-α), may be important in the development of this pathological condition. Chondrocytes from OA-affected patients and activated macrophages have been found to release similar inflammatory mediators. Stimulation of chondrocytes with proinflammatory cytokines increases the production of enzymes responsible for degrading cartilage, known as metalloproteinases (MMPs) (95,97).

Among the cytokines with proinflammatory activity in OA, there are IL-1β / IL-8 / MMP-13 / MMP-9 / IL-6 / iNOS / BMP-2 / COL-X or COL-10 and with regenerative activity of chondrocyte action are ACAN /COLII (97–99)

Among the inflammation markers that mediate osteoarthritis, such as IL-6, studies reveal that endogenous IL-6 exerts a crucial anti-inflammatory role in acute inflammatory responses, both local and systemic, by managing or controlling the level of pro-inflammatory, but not anti-inflammatory cytokines. In addition, said anti-inflammatory activities of IL-6 do not they can be carried out by IL-10 or other members of the IL-6 family (100).

IL-6 is considered to have a dual role, one of which is related to increasing the expression of IL-1Ra, the soluble tumor necrosis factor (TNF) receptor together with tissue inhibitors of metalloproteinases (TIMPs); while boosting immune cell function along with inflammation. It is necessary for the IL-6 receptor to be soluble in its activity to create synergy with IL-1, thus stimulating gene expression of the Matrix Metalloproteinases (MMPs) and family of proteases enzymes (ADAMTS), as well as downregulating the COL2A1 and ACAN genes in cultured chondrocytes. Chondrocytes also produce a macrophage migration inhibitory factor or MIF, which increases in osteoarthritic patients, with a gene inactivation of this MIF, which is linked to the development of osteoarthritis and aging. In the same way, IL-11 shares several activities with IL-6, such as stimulation by producing TIMP, without affecting the production of MMP by chondrocytes, thus

achieving inhibition of cartilage destruction. In the case of the Cytokine of the interleukin 6 (LIF) family, it participates in a positive feedback loop, increasing the production of IL-6 by chondrocytes, processes linked to the development of osteoarthritis (98).

In OA, high levels of **IL-1β** (inflammation marker) cause damage, as well as joint inflammation by regulating the synthesis of OA-inducing factors, such as cyclooxygenase-2 (Cox-2) and matrix metalloproteinase (MMP). These being inflammatory mediators that suppress collagen synthesis in chondrocytes after stimulating with prostaglandin E2 and effecting collagenase secretion. Recent investigations have revealed that nuclear factor-κB (NF-κB) promotes the expression of COX-2, MMP-3, and MMP-13, while decreasing cartilage extracellular matrix (ECM) proteins, also including collagen type II alpha 1 (Col2a1) synthesis (101).

Another of the markers is matrix metallopeptidase 13 (MMP-13), which is regulated by the development of human osteoarthritis (OA), correlating with its progression (Zhong et al., 2016). For Ma et al., 2017, MMP-13 expression is linked to the deformation of cartilage (decreasing of COLII, ACAN) together with the inflammation (IL-1 and IL-6) in OA cell line (96,103).

For López et al., 2007, the stimulation of chondrocytes with proinflammatory cytokines increases the synthesis of enzymes responsible for degrading cartilage. These are called metalloproteinases (MMPs), which inhibit the production of proteoglycans and/or type II collagen, thus stimulating the generation of reactive oxygen species (Nitric Oxide) and increasing the synthesis of prostaglandin E2 (PGE2). Likewise, they are classified into 5 subgroups:

1. Collagenases that separate the triple helix of collagen fibers into MMP-1, MMP-8 and MMP-13.
2. Gelatinases, responsible for degrading gelatin and type IV collagen, MMP-2 and MMP-9.
3. Stromelysins, whose function is to degrade lamin, proteoglycans and fibronectin, among other proteins, MMP-3 and MMP-10.
4. Membrane stromelysins that includes MMP-14 and MMP-15.

5. Includes others such as MMP-7 and MMP-12 (97).

IL-17 and IL-18 are another type of cytokines with important catabolic effects in the chondrocyte, since both increase the expression of IL-1 in human chondrocytes as well as stimulate the synthesis of NO synthase or iNOS (marker inflammation) (104).

On the other hand, proinflammatory cytokines such as IL-1 and TNFα produce Nitrogen Monoxide (NO) by increasing the inducible form of NO synthase. And as mentioned in the literature, mechanical stress causes an increase in inflammatory mediators in cartilage (105).

Bone morphogenetic protein-2 (BMP-2) has been studied as a potent osteoinductive cytokine of the transforming growth factor beta (TGF-β) family and is currently used as a protein-based bone graft substitute. Although its clinical use has increased significantly in recent years, BMP-2 has also exhibited various adverse effects, including induction of inflammation. As evidenced, an increase in the levels of the inflammatory cytokines interleukin (IL)-1b, IL-6, IL-10, IL-17, IL-18 and tumor necrosis factor (TNF-α) has been found (106–109).

4.1.3.2.7 Controversy CHON effectiveness

There are several controversies regarding the forms of treatment used in arthritis, whether it's osteoarthritis (OA) or Rheumatoid arthritis, including the treatment with chondroitin sulfate (CHON).

CHON has low oral availability, the bioavailability of CHON administered orally reaches about 20%, the problem associated with absorption may be due to the saturation of the receptors present in the cell membrane, likewise the present parameters are dependent on characteristics and structures that presents the CHON molecule such as charge density, disulphated disaccharides and molecular mass (110).

The controversy in the results evidenced in clinical trials carried out regarding the

therapeutic efficiency of CHON for patients with OA, due to its reduced oral bioavailability and its action as an active ingredient, have led to the recommendation of the use of effective topical systems through nanotechnology, such as an alternative that allows the therapeutic action of CHON to be efficient (111,112)

Likewise, in a recent study, the purpose was to critically elucidate the efficacy of this type of therapy in delaying the progression of osteoarthritis, this by evaluating the impact on the tissues of the synovial joint of the knee and biochemical markers in preclinical studies through a systematic review of the last two decades of peer-reviewed publications on experimental osteoarthritis. Showing in these preclinical studies a great heterogeneity between the experimental designs and the results themselves. The products evaluated, either alone or in combination, did not show the ability to prevent changes in the subchondral bone, the formation of osteophytes, or synovial inflammation. Furthermore, it is mentioned that the beneficial effects were related to preventive administrations, as well as higher doses together with multimodal approaches with some combination therapies. Thus, affirming that more long-term studies are needed, with good quality and a systematic design. (113).

Chondroitin sulfate together with glucosamine sulfate are two drugs that have the approval of the Spanish Agency for Medicines and Health Products, as symptomatic treatment of osteoarthritis. However, their efficiency and safety, which has already been demonstrated through meta-analysis and clinical trials, were questioned in another meta-analysis published by the British Medical Journal (2010) in addition to pointing out that they do not provide or imply an advantage at the therapeutic level compared to other older drugs (114).

4.1.3.3 Solid lipid nanoparticles composition

The diversity of Lipids that can be used in the formulation of nanoparticles is high, they include highly purified triglycerides, monoglycerides, hard fats, complex glyceride mixtures, or even waxes (115).

Lipids are the main ingredient of lipid nanoparticles that influence their drug loading capacity, stability, and release of the formulations. Because of that it's essential to choose appropriate lipids. The most important factors to consider are adequate solubility of the drug in the lipid, which influences the drug encapsulation efficiency and loading capacities, and lipid polymorphism, which defines crystalline forms in solid lipids and provide structural defects for the drug molecules to fit in (57). Based on their structural diversity, lipids used in the production are broadly categorized into fatty acids, fatty esters, fatty alcohols, triglycerides, or partial glycerides (116).

Given the diversity of options in the composition of the SLN, the components of the formulations that are the object of this investigation are briefly described, whose molecular structure is shown in Figure 7.

1. Among the lipids used to prepare the nanoparticles there is **stearic acid**, a saturated solid fatty acid with an 18- carbon chain and melting point way above human temperature, neutral charge and similar to skin lipids, which facilitates penetration, being a good choice for lipid matrix (116).

2. Another one is **cholesterol oleate**, an esterified form of cholesterol, also solid at human temperature, which has proven to be also a good choice for assembling lipid matrix (117).

3. **Octadecylamine,** a saturated cationic 18-carbon chain lipid solid at human temperature, is used to induce cationic charge in the nanoparticle when the molecule loaded has anionic charge, such as nucleic acids, and cause condensation of nucleic acid by electrostatic interactions with the phosphate groups (118).

4. **Oleylamine** it's also a cationic 18-carbon chain lipid, but in this case, unsaturated and liquid at human body temperature, so can also be used to induce cationic charge but giving liquid nature to the SLN matrix (119).

5. Surfactants are amphipathic molecules half hydrophilic, half lipophilic. As said before, they form the external layer of the nanoparticle and its importance lies in their role of dispersing the lipid melt in the aqueous phase during the production phase and stabilizing the nanoparticles in dispersions (57). One of the most used surfactants is **poloxamer 188**, a poloxamine non-ionic tryblock synthetic copolymer is a very common choice to achieve good emulsifier properties in the external layer (120,121).

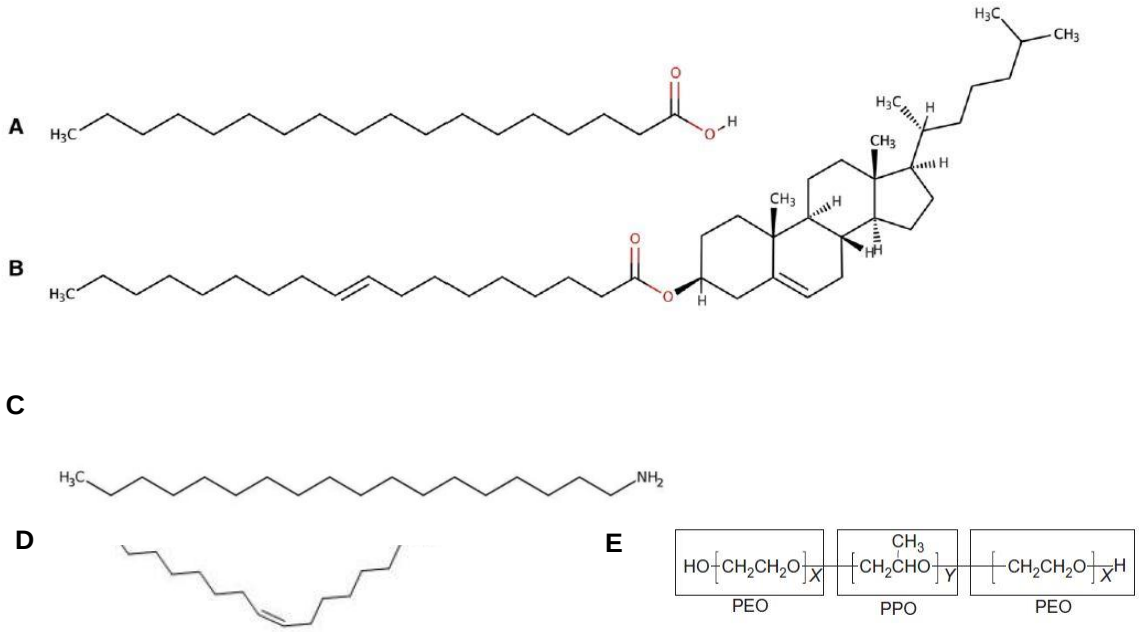

Figure 7. Chemical structure of components used in SLN of this research. Reproduced from (122–124)**.** Stearic acid (A), cholesteryl oleate (B), octadecylamine (C), oleylamine (D) and poloxamer 188.

4.2 Nanoparticle Manufacturing Methods

Since research began on lipid nanoparticles, a multitude approaches for the preparation and manufacturing methods have been developed. There are a few general aspects to consider first. The main characteristics of the SLN, such as particle size, degree of size dispersion, zeta potential, loading efficiency and release kinetics, are determined by the nature of the lipid matrix, by the mixture of surfactants, the viscosity of the lipid phase,

the aqueous phase at the time of emulsification, and production parameters, mainly by the homogenization conditions and the temperature (125).

As for choosing an appropriate preparation technique for lipids preparations, the most important factors to consider are physicochemical properties of the drug to be incorporated, stability of the drug, desired particle characteristics of the lipid nanoparticle dispersion, stability of the lipid nanoparticle dispersion and availability of the production equipment (57).

4.2.1 Stages in nanoparticles elaboration

In general terms, there are four stages in nanoparticles elaboration:

1. First one, oily phase preparation by melting or dissolving fats, choosing the proper lipids by their ability to dissolve the drug and form a crystalline matrix with imperfections where the drug is loaded.

2. Second stage is the preparation of the aqueous phase, that is, the surfactant layer. Two useful considerations are the use of surfactant mixtures, which generally have a synergistic effect, producing an interface film with high coating capacity and sufficient viscosity to reduce particle aggregation during production and storage, and addition of co-emulsifiers, which improves physical stability of the particles by increasing the steric effects and the rigidity of the external film, and by modifying the surface charge of the particles.
3. Third stage is the mixture of solid and aqueous phases to form a pre-emulsion.
4. Last stage is the concentration of the aqueous dispersion of nanoparticles through processes of evaporation, centrifugation, ultrafiltration, drying or lyophilization, to make its handling and administration easier (126).

4.2.2 Production techniques of SLN

Regarding production techniques, the main varieties are discussed below.

a. ***High pressure homogenization***

Consists of the application of strong amounts of energy that generate high shear force, turbulence, and cavitation in the oily material, being able to process dispersions of up to 40 % lipids, giving rise to nanoparticles with a low polydispersity index. In general, the formation of fine particles is favored by increasing the temperature, the pressure, and/or the number of homogenization cycles.(R. Müller & Stefan Lucks, 1996; Jenning et al., 2000)

There are two variants, hot and cold homogenization.

a.1. Hot homogenization

Hot homogenization is an emulsification that consists of heating the mixture of lipid and drug to 5ºC-10ºC above the melting point of the lipid and adding it, by means of high-speed mechanical agitation or ultrasound, to an aqueous solution of surfactant maintained at the same temperature (Figure 8). It's recommended to destroy any crystalline nuclei of the oily starting material by prolonged heating before the addition of the drug, to form entirely different solid during cooling (125).

The pre-emulsion obtained in this way is processed in a high-pressure homogenizer for 3 to 5 cycles, at a controlled temperature. When the nanoemulsion is cooled to room temperature, it crystallizes in the form of SLN. The pressure and the number of cycles used in the homogenization process determine the particle size (129). The main disadvantage of the hot method is that it can increase the rate of degradation of active ingredients and/or carrier lipids and cause conformational changes in proteins (130).

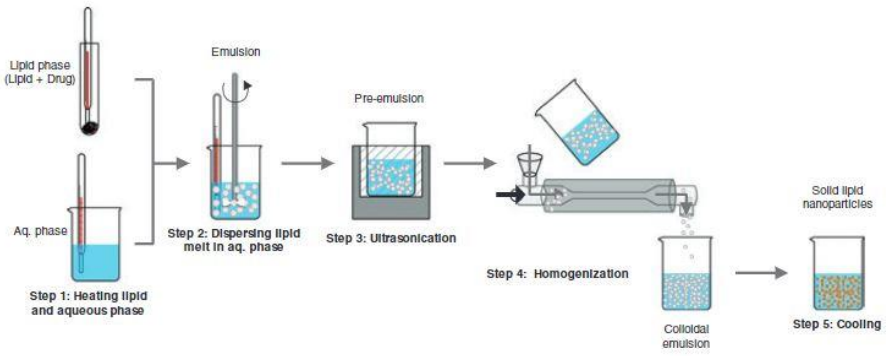

Figure 8. Schematic depiction of steps involved in the hot homogenization technique, reproduced from Shah et al, 2015 (57)**.**

a.2. Cold homogenization

Cold homogenization consists of grinding a suspension of solid particles, by applying high pressure (Figure 9). This process minimizes temperature exposure, so it is suitable for encapsulating thermolabile or hydrophilic drugs. Dispersions obtained in this way generally produce particles of larger size and distribution than those obtained by hot homogenization, which is less trouble for drug encapsulation and during crystallization (131).

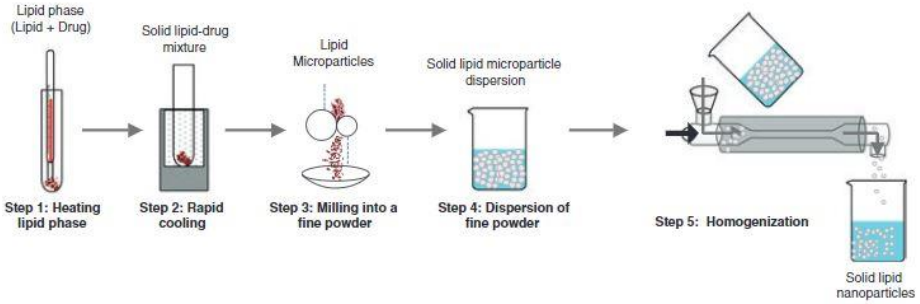

Figure 9. Schematic depiction of steps involved in the cold homogenization technique, reproduced from Shah et al., 2015 (57)**.**

b. Microemulsion Technique

This technique consists in the preparation of a microemulsion, a thermodynamically

stable system comprising of water and oil, stabilized by surfactant and is optically isotropic (Figure 10).

The lipid phase and aqueous surfactant system are separately heated to a temperature above the melting point of the solid lipid. The drug and the lipid are heated together to solubilize the drug in the molten lipid. The lipid melt is later emulsified in the hot surfactant/co-surfactant system under continuous stirring to yield a hot microemulsion, which is then dispersed in cold water (typically 2–4 °C), under mechanical stirring, to yield SLN (48).

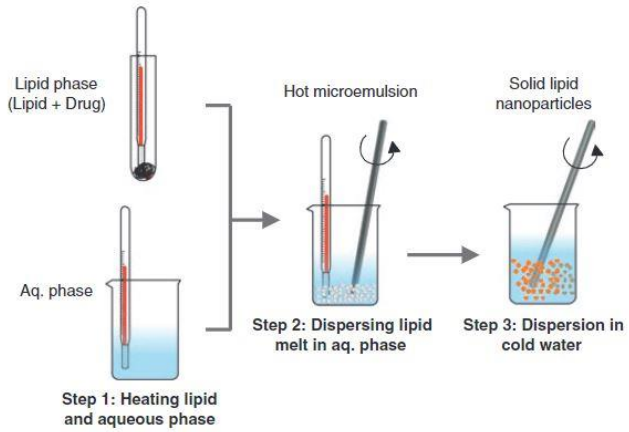

Figure 10. Schematic steps involved in the microemulsion technique, reproduced from Shah et al., 2015 (57)**.**

c. Microwave-Assisted Microemulsion Technique

In this technique, the drug, lipid and aqueous surfactant/co-surfactant system are subjected to controlled microwave heating at a temperature above the melting point of the solid lipid (Figure 11). Constant stirring while heating the formulation components in a controlled microwave environment yields a hot micro-emulsion. One important difference with conventional microemulsion technique is that all ingredients are heated in a single synthesis vessel. The hot microemulsion obtained from the micro-wave is again then dispersed in cold water (at 2–4 °C) to generate SLN (132).

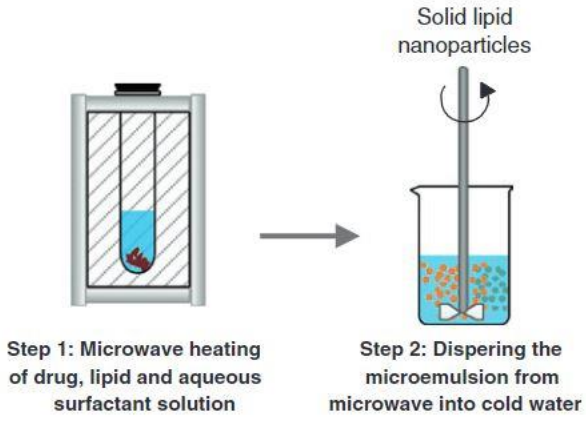

Figure 11.. Schematic steps involved in the microwave-assisted microemulsion technique, reproduced from Shah, et al., 2015 (57)**.**

d. ***Other techniques***

The previously mentioned techniques are considered the main ones, but there are some additional techniques that are mentioned below (133).

- Solvent emulsification/evaporation Technique.
- Ultrasonic solvent emulsification Technique.

5 Topical Route of Administration for Nanoparticles

The topical application of medications, especially for skin diseases, is a very useful route for treatments. Among the advantages are a reduced load of active pharmaceutical ingredients (API) and therefore, systemic side effects are reduced compared to parenteral or oral drug administration, avoidance of major fluctuations of plasma levels and bypass the first passage of API trough liver (134).

On the other hand, there are a few handicaps that are linked to this method of drug application. The efficient barrier function of the horny layers impairs absorption of toxic agents, but also of API, especially for hydrophilic compounds. Thus, drug vehicles facilitating it to overcome the barrier formed by the stratum corneum (or horny layer) are currently researched (135).

The horny layer of skin is the main penetration barrier for humans to protect them from excessive water loss and harm due to toxic agents and microorganisms from the environment (134). Its structure is formed by corneocytes, which are the product of keratinocytes apoptosis during their passage from the basal layer of the epidermis to the surface, and extracellular matrix composed of lipids (ceramides, cholesterol, long chain free fatty acids and cholesteryl sulphate), which are secreted by these cells to the intercellular space during the surface migration (136).

These two elements form a structure with 15 layers of corneocytes and lipids with a 5-8 μm thickness. Thus, corneocytes are embedded in hydrophobic lipids grouping together by dozens, forming clusters which represent the basic permeation unit. Junctions between the clusters protrude into underlying skin as small furrows of up to some micrometres (Figure 12). Hydrophilic nanopores of up to 20 nm in average, however, are reported to create conduits in the inter-corneocyte spaces (137).

Another important structure are the micrometer wide hair follicles reaching from the dermis (1-2 mm) or the subcutis to the skin surface and passing through the epidermis

(50–100μm). These hair follicles allow direct access of compounds applied to the outer skin layers to the blood vessels, but they penetrate and permeate the skin by passing the horny layer, using the intercellular pathway between the corneocytes. Therefore, skin absorption varies with the physicochemical nature of the compound and the anatomical region of application (138).

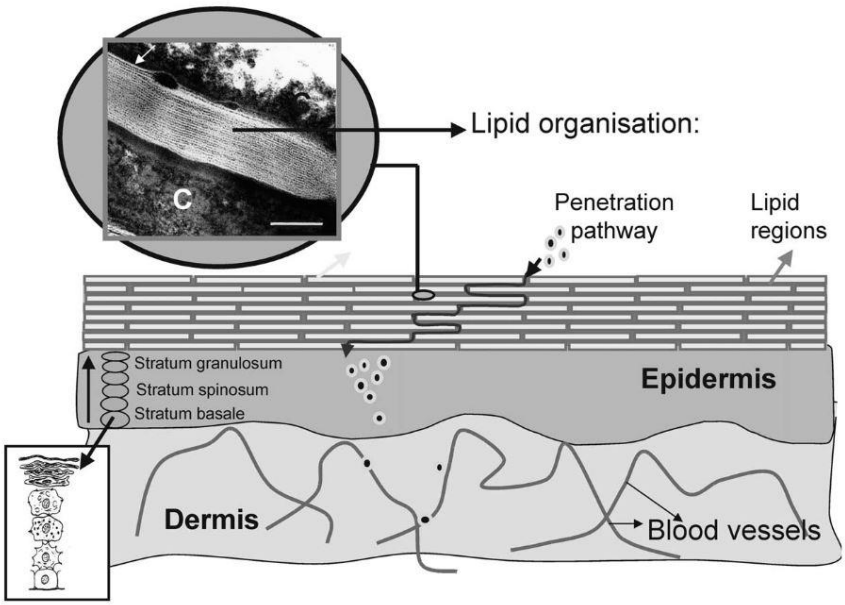

Figure 12. A schematic drawing of skin cross-section, reproduced from Bouwstra et al., 2003 (136)**.**

Some of the characteristics of a substance to present good absorption are an under 0.6 kDa molecular mass, adequate solubility in oil and water, and a high partition coefficient, and should be applied saturated or supersaturated (139,140).

Because of the attributes mentioned to the horny layer and the disadvantages of hair follicles absorption, adequate skin penetration for topical treatments is a difficult task to overcome, since conventional drug carriers such as creams and ointments result in low drug uptake, with leads to high interindividual variation of uptake rates (141).

To overcome this challenge, a promising strategy to improve molecular penetration

throughout the horny layer is the use of lipid nanoparticles, since their lipophilicity ease the intact lipid layer crossing. These nanoparticles have been showing promising results to enhance molecular penetration up to epidermis, reducing systemic absorption, and provide chemical stability of compounds sensitive to light oxidation and hydrolysis (142).

6 Characterization of nanoparticles

There are a variety of methods to characterize SLN, to know their structure, application and effectiveness. According to Villafuerte(53), the main methods used to characterize these nanoparticles include: differential scanning calorimetry, X-rays, nuclear magnetic resonance, determination of zeta potential and determination of particle size and its distribution. Showing each of these techniques particular features that can be considered largely complementary to each other.

Below are details of the characterization techniques used in the development and characterization of SLN as a vehicle for the CHON and pEGFP biomolecules.

6.1 Factorial experimental design

Factorial design is an experiment strategy whose design consists of two or more factors, each with discrete possible values or levels, and whose experimental units take on all possible combinations of these levels across all such factors. Although there are many specific implementations of factorial design, all such implementations involve the simultaneous variation of multiple components within the input vector. These designs differ from classical strategies based on changes in only one input variable at a time. If we consider an input–output process relating the input vector x to the scalar output *z*, we can say that *x* is composed of factors, quantitative or qualitative, that represent the inputs that can be adjusted in the experiment, we can assume that there is full control over levels of the factors. The factorial design formula then is $n^{m,}$ where *n* is the levels and *m* the factors of the experimental design (143,144).

As for factorial design for SLN analysis, this statistical technique, which allows to extract the maximum amount of information data, has proven to be very useful to analyze the multiple factors that need to be considered when doing experiments with SLN variables, such as type of emulsifiers, composition of oil phase, effect of emulsifiers, etc.(145)

6.2 Determination of Encapsulation Efficiency

The study of the encapsulation efficiency of the nanoparticles will depend mainly on the encapsulated analyte and the characteristics of the SLN. To determine the percentage of CHON bound to the SLN, the Hight Performance Liquid Chromatography, Volumetric titration and Ultraviolet -visible spectroscopy methods were tested.

Finally, two validated methods were used: Volumetric titration and aviolet-visible spectroscopy.

6.3 High performance liquid chromatography

High performance liquid chromatography (HPLC) is a column chromatography analytical technique used to separate, identify, and quantify each component in a mixture. In liquid chromatography, the mobile phase is a liquid that flows through a column containing the fixed phase. Chromatographic separation in HPLC is the result of specific interactions between sample molecules in both the mobile and stationary phases. HPLC is capable of separating macromolecules and ionic species, labile natural products, polymeric materials, and a wide variety of other high molecular weight polyfunctional groups. With an interactive liquid mobile phase, another parameter is available for selectivity, in addition to an active stationary phase. HPLC offers a greater variety of stationary phases, allowing for a greater range of these selective interactions and more possibilities for separation. The most common variation used is reverse phase, where is used a non-polar stationary phase with a polar mobile phase, which allows to separate hydrophobic analytes (146).

Its basic components (Figure 13) are the infusion pump that propels the mobile phase through the chromatograph at a specific flow rate, the injector, which introduces the liquid sample into the flow stream pf the mobile phase, the column, which contains the stationary phase where the analytes are separated, the detector, a device that monitors the composition changes of the effluent separated in the column and the data processing system (147).

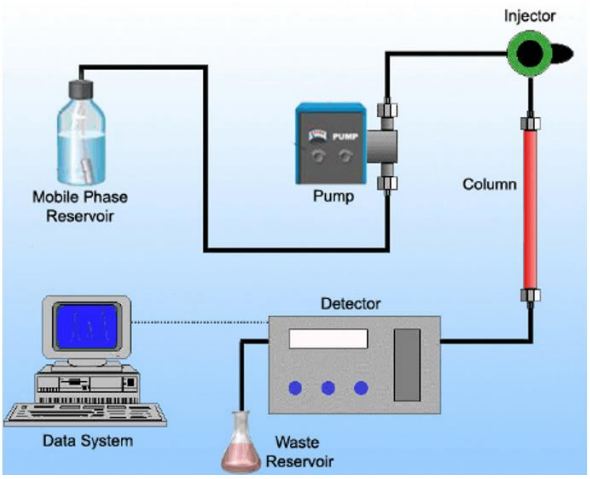

Figure 13. Main High-Performance Liquid Chromatography (HPLC) Components. Reproduced from Creative Proteomics, 2022 (148)**.**

6.4 **Volumetric analysis**

The titration is defined as that process in charge of determining the amount of a substance A by means of the addition of measured increments of a substance B, the titrator, with whom it reacts until the exact chemical equivalence is reached or also known as the point of equivalence. Most of the titrations or assessments are carried out in an aqueous solution, however, although different solvents can also be used, especially organic solvents (149).

In general, conventional volumetric analysis requires the basic components shown in figure 14, a buret containing the titrant, a buret holder, a flask for the analyte studied, and

a color indicator can be used to see the end point. A stirring tablet and a magnetic stirring base. There are various types of titrations depending on the chemical reaction that is carried out, such as: acid-base titration, redox titration, and precipitation titration (150).

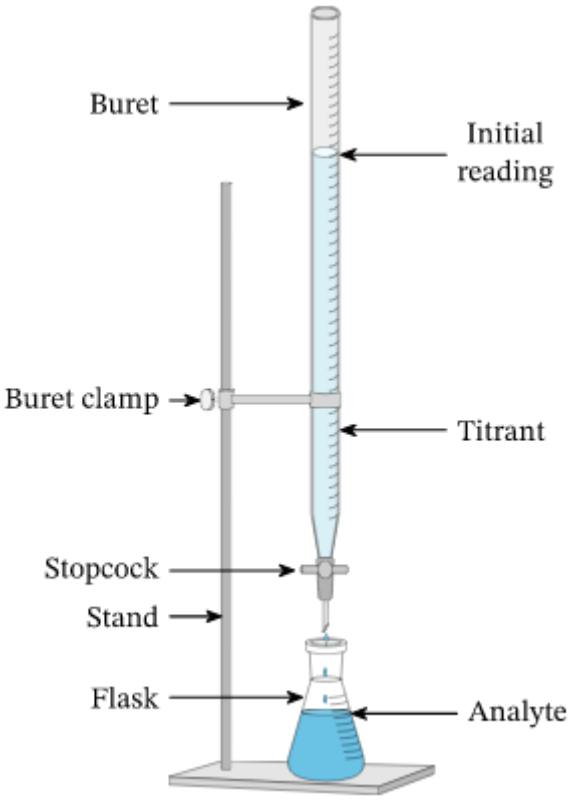

Figure 14. Components used for the volumetric titration method. Adapted from Nagwa, 2022 (151)**.**

The precipitation titration is based on reactions that are accompanied by the formation of a slightly soluble product according to the general reaction (150):

$A^+ + B^- \longrightarrow AB_{(S)}$

Even though many reactions are known that culminate in the formation of a precipitate, only very few of them can be used in volumetric analysis. This is due to a set of requirements that a chemical reaction must meet to be used in precipitation titration, for example.

1. The precipitate formed must be practically insoluble.

2. The precipitation should be fast, that is, the phenomenon of formation of supersaturated solutions should not take place.

3. The results of the titration must not be affected by adsorption or coprecipitation phenomena. 4. There must be the possibility of establishing the equivalence point of the titration (150).

6.4.1 **Advantages and disadvantages of volumetric titration** (152)**.**

Advantages

1. The main advantage of volumetric titration is that it is a simple and cost-effective method.
2. Volumetric titration is not sophisticated, so no skill is required to handle it
3. Volumetric titration is fast and gives accurate results.
4. It is a simple method compared to other types of evaluation.
5. The reaction can be identified visually at the equilibrium or at the endpoint.

Disadvantages

1. The titration results can be affected by factors such as pH, temperature, and humidity, because it is an open system.
2. Human error may occur during processing and may affect accuracy.
3. Requires an indicator for reactions to occur.
4. The biggest disadvantage of this technique is that it can produce large volumes of chemical residues that need to be removed.
5. It requires reactions to occur in the liquid phase.

6.5 **Ultraviolet-visible spectroscopy**

Ultraviolet-visible spectroscopy (UV-VIS) is an analytical quantitative technique based on the interaction of electromagnetic radiation in the ultraviolet-visible region (10-800 nm) with matter (Figure 15). It is a very useful technique to quantify compounds (from ions to organic macromolecules), due to its speed and robustness. Its functioning is based on the Beer–Lambert law , which states that the absorbance of a solution is directly proportional to the concentration of the absorbing species in the solution and the path length, and the main parameters measured are transmittance and absorbance (153).

Ultraviolet-visible spectroscopy or UV-VIS is known as a powerful technique, used in various applications in different industries and market segments. In the moment that a substance absorbs the maximum of light at a certain wavelength, a unique relationship is obtained between the substance and its UV-VIS spectrum, this relationship being useful in qualitative analysis, which means, to determine the presence of certain substances (154)

The technique is based on the measurement of the interaction that occurs between molecules or atoms present in a chemical solution and electromagnetic radiation, which is used for pharmaceutical evaluation through the UV spectrum, with the use of a spectrophotometer through the selection of the wavelength of light which passes through the solution and measures the absorbance or amount of light that is absorbed (155).

The components of a UV-VIS spectrophotometer are a radiation source, usually a deuterium of xenon lamp that provides the correct wavelength radiation, a wavelength selector, monochromator or polychromator, a cuvette that loads the sample and allow the radiation to pass through and detector, which consists of phototubes or photomultipliers (156).

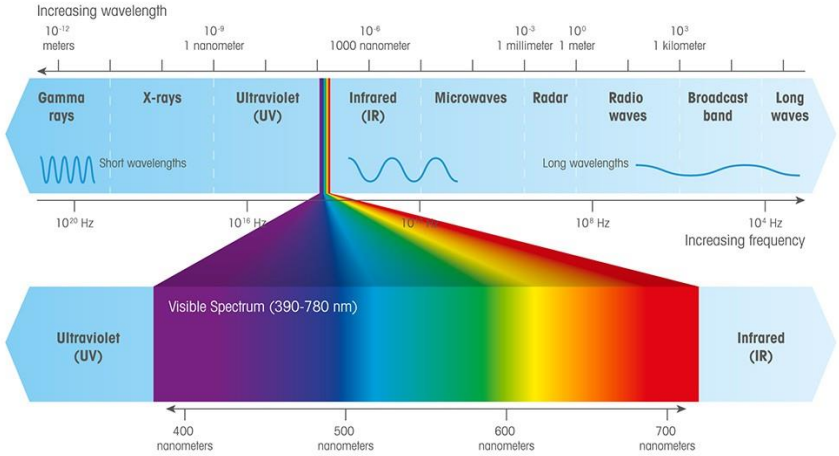

Figure 15. Electromagnetic spectrum. Reproduced from Mettler Toledo, n.d. (154)

6.6 Validation of Analytical Procedures

Validation of an analytical method is the process by which it is established, through laboratory studies, that the performance characteristics of the method meet the requirements for its intended analytical applications (157).

Among the parameters that are validated for an analytical methodology, such as UV/VIS spectroscopy and volumetric titration, are: specificity, linearity, accuracy, precision, intermediate precision and robustness (157–160).

2. **Specificity or selectivity:** refers to the unequivocal evaluation of the analyte when it is part of a solution where the results of the degradation components and the matrix, as well as impurities, are evident. When a method is not specific, it uses the support of other procedures.

3. **Linearity:** this is the ability to achieve directly proportional analysis results, using a mathematical model that makes it possible to predict the concentration of the studied molecule with respect to an established interval.

4. **Accuracy:** it is defined as the value calculated by the difference between the value obtained and the real value or percentage of analyte recovered.

5. **Precision:** refers to the level of similarity with respect to the results of the data obtained from all the samples of a homogeneous sample.

6. **Intermediate precision**: refers to the similarity between the data obtained in a laboratory, by different analysts or teams and on different days.

7. **Robustness:** refers to a measure of the capacity of analytical methods, as well as the ability to not vary the study parameters and provides reliable results during normal use.

6.7 Transmission electron microscopy (TEM)

TEM is known as a method used in microscopy based on the passage of a beam of electron light through an ultra-thin sample, with which it establishes an interaction through its passage (161). Following this by means of an imaging device, an amplified and focused image of the interaction of electrons with the sample is obtained, that is, the formation of an image is observed by means of a fluorescent screen, a layer of photographic film, or it can be detected by a sensor such as a CCD camera (162).

With the TEM technique, images are obtained to study the morphology, size, shape, arrangement of particles on scale of atomic diameters (163).

In a TEM, the monochromatic beam of electrons is increased by a potential of 40 to 100 kilovolts (kV), which passes through the electromagnetic field that fulfills the function similar to a lens. Currently, a TEM has a resolution of approximately 0.1 nm (164),

referring to the distance between two atoms in a solid. This resolution is 500,000 times better compared to the human eye and 1000 times better compared to a light microscope (LM). The main difference between an LM and a TEM is that the LM allows direct observation through light transmittance for image formation, unlike TEM, which the image is observed through a CRT or video. Cathode ray tube, while this image is formed by the transmitted electrons that impinge on the phosphor-coated screen (162).

6.8 **Scanning Electron Microscopy (SEM)**

SEM uses equipment for the visualization of samples on the surface, allowing the projection of the sample or object in detailed and enlarged images at a high resolution (165).

Scanning Electron Microscope has many components (Figure 16), the main ones used in SEM are an electron column, a scanning system, detectors, display, vacuum system, and electronic controls. The column of electrons, it is made up of an electron gun together with two or more electromagnetic lenses operated in a vacuum, generating free electrons while accelerating them to energies in the range of 1-40 KeV, it is responsible for creation and alignment of the electron beam (165,166).

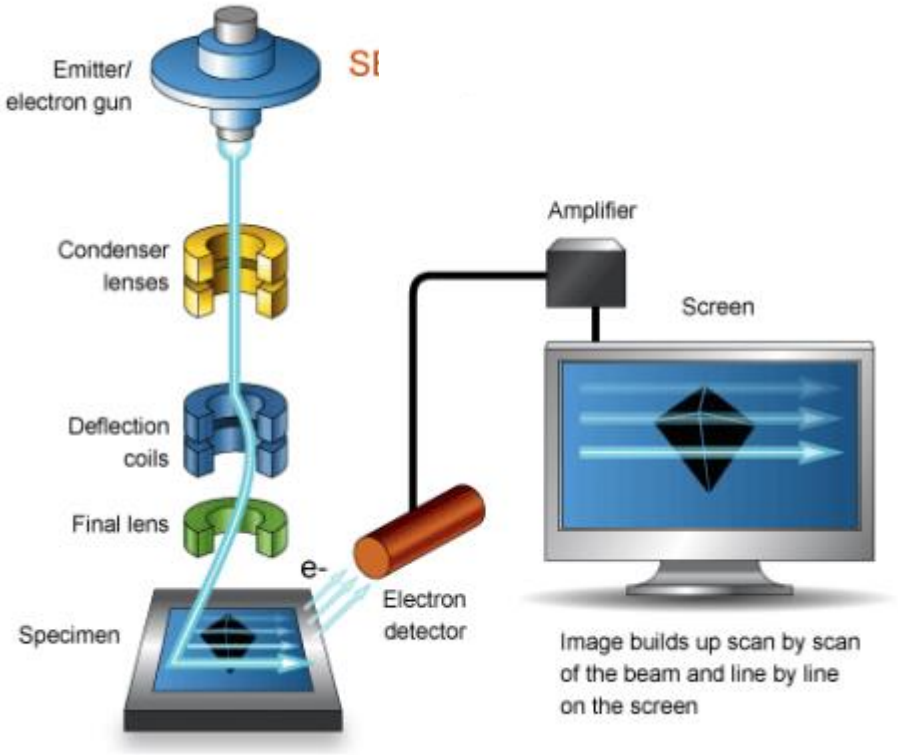

Figure 16. Components of Scanning Electron Microscopy (SEM). Modify from Azad & Avin, 2018 (165).

Electron lenses fulfill the function of generating a small electron probe that is focused on the sample, because SEM allow the production of an electron beam in the surface region of the sample, over a diameter of less than 10 nm, Likewise, current transport causes the formation of an acceptable image. For imaging, "the electron beam is focused onto a fine probe, which is scanned along the surface of the sample with the help of scanning coils. Each point of the sample that is hit by the accelerated electrons gives off a signal in the form of electromagnetic radiation"(166).

6.9 **Atomic Force Microscopy (AFM)**

Atomic force microscopy, or AFM, is known as a surface measurement technique based on the interaction of a tip with the sample surface. This technique makes it possible to perform surface analysis of samples with nanometer or even atomic resolution. As one of its advantages, the main one refers to the possibility of making measurements without any prior treatment of the sample to be measured, and without the need to use a vacuum (167).

Fundamentally, AFM consists of capturing topographic images of a sample, controlling the distance between the surface and the probe, while scanning the probe over a surface, in a surface plane, xy (168).

The acquired topographic image is that of the measured height values, z (x,y), for a given area, A, defined by a window scan size L. Individually, each height value is related to a pair of surface coordinates, (x,y) , and the image can be described by a matrix with N lines and M columns that refer to the points of the surface (x,y) where the elements of the matrix are the height z (x,y) (169).
The basic components of an Atomic Force Microscope are Electronics, detector, laser spring cantilever and tip (Figure 17).

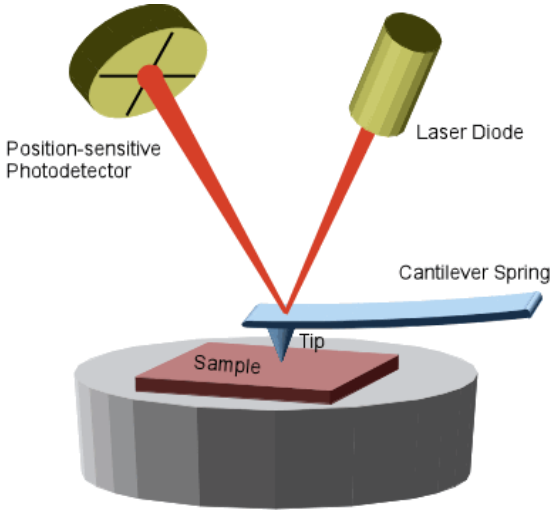

Figure 17. Basic parts of an Atomic Force Microscope. Reproduced from University of Greifswald, 2022 (170)**.**

The atomic force microscope consists basically of an extremely small and sharp probe attached to a spring-loaded cantilever that moves over the surface of a sample. A photodiode captures light from a laser shining on the cantilever and the signal is interpreted by analysts in electronic devices. The tip can typically be made of a ceramic or semiconductor material, or currently carbon nanotubes (171).

6.10 X-ray diffraction (XRD)

X-ray diffraction is a technique that allows differentiating crystalline and amorphous compounds. Therefore, it is valid to affirm that this technique provides relevant information, in relation to the particles produced and the raw materials used utilizadas (Bunjes & Unruh, 2007). Both nanometer-sized and larger diameter particles can be analyzed by X-ray diffraction (173).

Through XRD it is feasible to study the structure corresponding to the short lattice distances that are between the hydrocarbon chains of the solid lipid (lateral packing in wide-angle X-ray diffraction), as well as in the spaced lengths (interplanar distances with nanometric dimensions in short-angle X-ray diffraction). Thus, X-ray diffraction makes it possible to determine the different polymorphic forms of a substance and, therefore, can offer information about its crystalline state (174).

6.11 Differential Scanning Calorimetry or DSC

Differential scanning calorimetry or DSC is known as a technique used to characterize the stability of a protein or other biomolecule directly in its native form. The analysis measures the heat change associated with the thermal denaturation of the molecule when it is heated at a constant rate (175).

DSC consists of measuring the temperature difference between a reference material and

the sample under study, when both systems are subjected to controlled heating. The applied temperature has to increase linearly with the temperatures. This procedure causes the sample to present a temperature difference with respect to the reference material. Graphically, the temperature applied to the sample is reported with the temperature difference between that of the sample and that of the reference material, obtaining a characteristic differential thermogram of each sample. The thermogram reflects the changes induced in the sample as a consequence of the application of the controlled temperature, these changes can be changes of state, oxidation, decomposition, among others, which will occur depending on the structure of the sample and the eventual interaction between its components (29,176).

6.12 Determination of Surface Charge (Zeta-Potential)

Zeta potential is usually denoted by the Greek letter zeta and is a property of materials that measure the electrokinetic potential in colloidal systems in colloidal chemistry. From a physical point of view, the zeta potential is the electrical potential in the interfacial double layer (Figure 18) (177).

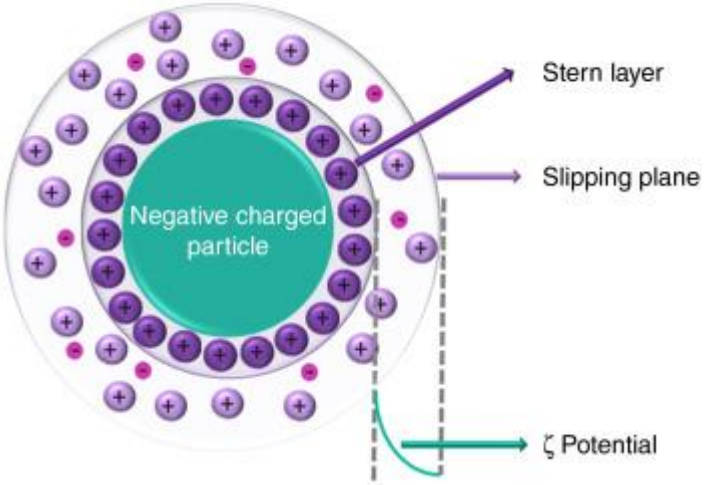

Figure 18. Illustration of zeta potential, as the electrical potential in the interfacial double layer. Reproduced from Gumustas et al., 2017 (178)**.**

It can be said that the zeta potential is the potential difference between the dispersion medium and the stationary layer attached to the dispersed particle (179,180).
The zeta potential indicates the degree of repulsion between adjacent charged particles in a dispersion, hence its importance since its value may be related to the stability of colloidal dispersions (177).

For very small molecules and particles, a high zeta potential value confers stability, that is, the solution or dispersion will resist aggregation. When the value of the zeta potential is low, there is attraction between the particles, the repulsion is overcome and the formation of flocs occurs, instead of carrying out the dispersion of the particles. Hence, samples with high zeta potentials are electrically stabilized, while samples with low zeta potentials tend to coagulate or flocculate (177,181). Also, the stability of the dispersions depends on the balance between the attractive van der Waals forces and the repulsive electrostatic charges on the colloidal particle (182).

The Z potential is considered a primary indicator of the stability of the dispersion of nanomaterials and by convention a value below -25 mV and above 25 mV is considered stable. Among the factors that affect the obtained value of potential Z, the concentration and type of ions, as well as the pH of the solution, strongly affect the zeta potential (183).

Cationic, positively charged nanoparticles can present high cellular cytotoxicity since they have greater interaction with the lipid bilayer of the cell surface (184–186). However, several investigations have reported that the positive charges on the particles favored their action as vehicles for the delivery of antigens and nucleic acids, being effective and biocompatible (186–188).

6.13 Determination of Particle Size

Particle size in SLN characterization aims to quantitatively define the size of particles as a function of diameter, area, or volume.
The particle sizing kit provides results from a distribution of three-dimensional particles that may not be perfectly spherical. Therefore, it is necessary to proceed as if they were spherical fossils or adapt the final amount measured to that of an equivalent sphere (176).

Particle size is often used to characterize lipid nanoparticles and several factors have an impact on the mean diameter of lipid nanoparticles, for example the excipient composition, drug, production procedure, process variables, sterilization, dispersion medium, storage conditions and others (57).

Particle size, therefore, is an important indicator of physical stability. In a formulation, this characteristic will generally increase if some destabilizing mechanism is present. An increase in particle size is usually observed before the appearance of macroscopic changes. Previous research has used increased particle size to predict poor SLN stability (57,189,190)

To determine particle size of lipid nanoparticles is regularly performed by light scattering methods such as photon correlation spectroscopy and/or laser diffraction (57).

6.14 Viscosity Measurement

"*Viscosity is a measure of resistance to flow or thickness, and elasticity refers to stickiness or structure. The higher the magnitude of viscosity, the more resistant the material will be to flow*" (191).

In general, the viscosity in a property of liquid materials, each liquid has a certain viscosity; however, "viscous" is commonly used to describe materials that are highly

resistant to flow. Viscosity is framed in the science of rheology, and the flow of a substance is normally described by the relationship between viscosity and applied force (191).

In Figure 19 is shown, the *shear stress* with consist in the application of horizontal force (*F*) over a unit area (*A*). Newton proposed that the applied shear stress is directly proportional to the velocity (δ*v*) of the material over the small distance (δ*x*) that it travels (191).

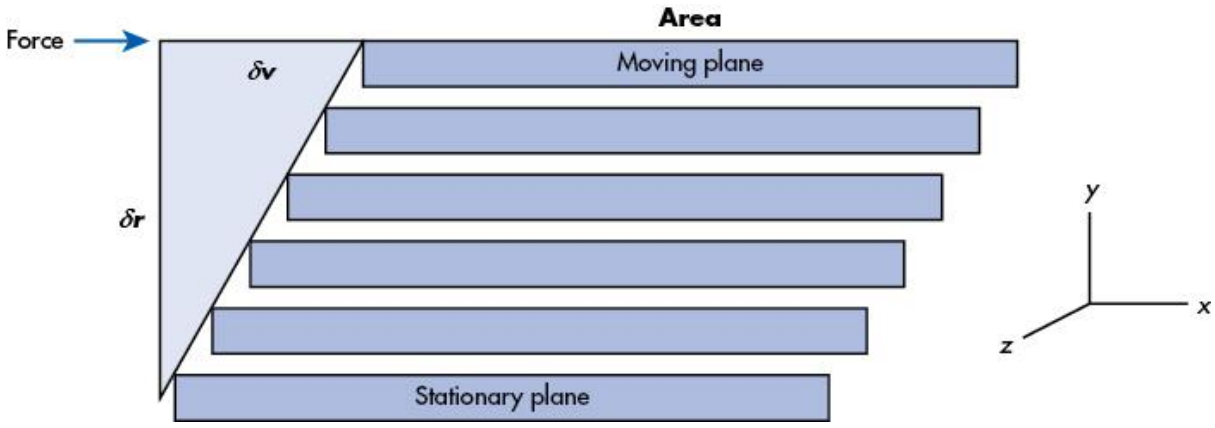

Figure 19. Dynamic viscosity (η). Reproduced from Lambros, 2013 (191)**.** Diagrammatic representation of the relationship between shear stress and the rate of shear in a Newtonian system.

"*The coefficient of proportionality between the shear stress and the shear rate is defined as the shear viscosity or dynamic viscosity (η), which is a quantitative measure of the internal friction of the fluid and is associated with damping or loss of kinetic energy in the system.*"(192).

If the viscosity in the system remains constant as the applied force changes, they are called Newtonian fluids, where the shear stress is linearly related to the shear rate. Newtonian flow is one of the simplest types of flow, such as the flow of water and low molecular weight oils. If the viscosity changes according to the applied force, it is a non-Newtonian fluid, the viscosity varies depending on the applied shear speed or the shear stress. The most common type of fluids with non-Newtonian behaviour is shear thinning or

pseudoplastic flow, in which the viscosity of the fluid decreases with increasing shear (191,192).

6.15 Techniques in Molecular and Cellular Biology

There are a large number of techniques, molecules and assays at the molecular and cellular biology level, which can be used to characterize the plication and functionality of SLN.

6.15.1 Cell lines

The study in cell lines allows obtaining *in vitro* results that will provide guidance for studies at the level of animal experimentation or other tests with more complex living beings. Stable cell lines are cell populations established from a single clone, which has previously been modified by genetic engineering so that it expresses the desired phenotype. These types of cell lines are used in many important applications, including: the production of biological drugs, such as recombinant proteins and monoclonal antibodies; drug screening is also included along with gene functional studies (193).

6.15.2 Plasmids

A plasmid is a small molecule that is made up of circular DNA which is present in bacteria, among other microorganisms. These molecules are separate from chromosomal DNA and have the ability to replicate independently. Plasmids present a limited number of genes, which can be transmitted cell to cell. For this reason, they are preferred transfer vectors for various areas of scientific research, where rDNA or recombinant DNA methods are used for the insertion of the genes to be evaluated into the plasmid (194).
Usually, the purification of plasmids is used for processes such as: molecular cloning, transformation, and expression of recombinant proteins. Therefore, it is necessary to have plasmid purification kits considering the size of the bacterial culture and the

corresponding plasmid yield. These plasmid kits provide reliable isolation of high-quality plasmid DNA. In general, these products allow researchers to maximize workflow reproducibility and minimize the time spent obtaining plasmid DNA for transfection, sequencing, PCR, and other downstream applications (195).

6.15.3 Real-Time Quantitative Polymerase Chain Reaction (RT qPCR)

The RT qPCR is a useful method for quantifying the expression level of genes, which is performed by relative and absolute quantitative analysis (196).

These are the most used to analyze data from quantitative experiments carried out by PCR in real time: absolute and relative quantification. In absolute quantification, the amount or copy number of input genes is determined, usually by relating the PCR signal to a standard curve. On the other hand, relative quantification relates the PCR signal of the transcribed target, in a treatment-only group, to the other sample; as if it were an untreated control. Being then, the method $2^{-\Delta\Delta C_T}$ is used to analyze the relative changes in gene expression, from quantitative PCR experiments in real time. (197).

The absolute quantitative analysis is based on the identification of the total input genes with respect to a standard curve and the relative quantitative analysis is based on the determination of the gene expression variants with respect to the sample proposed as reference, this requires Less reagent usage compared to absolute quantitation, since creation of a standard curve is not required, as well as less hassle in curve calibration (196).

The $2^{-\Delta\Delta C_T}$ method used for relative quantitative analysis is present in most of the software programs currently used for the development of QR-PCR research, where gene expression is compared and measured with respect to a gene used as a reference, to which takes into account the threshold cycle, defined as the cycle in which the degree of fluorescence reaches a certain amount (196).

For Rao et al., 2013 The $2^{-\Delta\Delta C_T}$ method has been widely used as a relative quantification strategy to analyze quantitative data pertaining to real-time polymerase chain reaction

(qPCR). Likewise, this method is conveniently a way to calculate the relative levels of gene expression between different samples, since the threshold cycles (TC) that are generated by the qPCR system are used directly for the calculation (196).

6.15.4 Enzyme-linked immunosorbent assay (ELISA)

ELISA is known as a technique for detecting the presence of antigens in biological samples. Similar to other types of immunoassays, the ELISA test relies on antibodies to identify a target antigen, through highly specific antigen-antibody interactions. Part of the basic principles of this test is that the antigen is immobilized on a solid surface; this being done directly or using a capture antibody immobilized on the surface. The antigen is then complexed with a detection antibody conjugated to a susceptible detection molecule (eg an enzyme or a fluorophore). Typically, this assay is performed in a multiwell plate between 96 or 384 wells, providing the solid surface that immobilizes the antigen (198,199)

Indirect ELISA The steps of this are identical to the direct ELISA, with the only difference being an additional washing step together with the types of antibodies that are added after removing the buffer. This indirect ELISA requires 2 antibodies: a primary detection antibody that binds to the protein of interest, and the other is an enzyme-related secondary antibody complementary to the parent antibody. The first thing to do is add the primary antibody, then wash and then add and incubate the secondary antibody already conjugated with the enzyme. After this, it is when the steps remain the same as those of the direct ELISA (washing, addition of substrate and detection of color change). It should be noted that the indirect ELISA has much higher sensitivity compared to the indirect ELISA, it is also less expensive and more flexible because of the large number of possible primary antibodies that can be used. However, its only major disadvantage is the risk of cross-reactivity between the secondary detection antibodies (198,200).

6.15.5 Gel Retardation Assay

The electrophoretic mobility shift or gel delay assay (EMSA) is a sensitive technique for studying protein-DNA interactions and can be used to assess the interaction of DNA with SLN. The EMSA technique is based on the observation that complexes migrate more slowly than free linear DNA fragments when subjected to non-denaturing agarose or polyacrylamide gel electrophoresis. Because the migration rate of DNA changes or is delayed when it binds to protein, the assay is also called a gel shift or gel retardation assay (201,202). Many researchers have applied Gel retardation assay to determine complex formation between SLN:pDNA (68,186,203).

6.15.6 DNase protection study and SDS-induced release assay

The DNA Protection Assay is used in in vitro assays to assess the protective properties of proteins or chemicals against bound DNA; it has become a simple, fast and robust tool for the characterization of protective complexes. It involves exposing DNA to a damaging oxidative reaction, such as exposing DNA to DNases and adding varying concentrations of the compound of interest to see if it has the ability to protect DNA from the damaging agent. The reduction or increase in DNA damage as a function of compound concentration is then visualized by gel electrophoresis (204).

6.15.7 Cell transfection

Transfection is a technique that allows foreign nucleic acids to be introduced into cells to generate genetically modified cells. Transfection is a useful analytical tool for the study of gene function and regulation and protein function. Advances in molecular biology make it possible for cell transfection to achieve the delivery of nucleic acids to specific subcellular regions of cells and to be visualized with instruments such as precisely controlled laser microscope systems (205).

There are different systems used for cell transfection, including solid lipid nanoparticles (SLN) introduced as non-viral transfection systems (206).

6.16 Biopharmaceutical Studies

6.16.1 Ex vivo permeation studies by Franz Diffusion Cell

Franz cells are an analytical method developed in 1975, which allows the evaluation of transepithelial penetration and drug release (207). It is a system composed of two chambers, one donor and one acceptor, separated by a membrane of animal, human or synthetic origin that allows the study of the diffusion of biologically active molecules from one chamber to another (208).

Franz cells make it possible to evaluate the release kinetics from different pharmaceutical systems, especially those with controlled release of biologically active molecules, such as nanoparticles as a vehicle for biomolecules (209).

The figure 20 shows a typical Franz Diffusion Cell representation, in the upper compartment (Donor compound) the solution or dispersion containing the active compound is added and in the lower one (Receptor chamber) the study samples are taken, which are later quantified by analytical techniques such as HPLC, UV-Vis spectroscopy. During the analysis, influential parameters in the diffusion process of the evaluated substance must be controlled, such as temperature, agitation speed, the type and nature of the membrane and the medium of the receptor compartment (208).

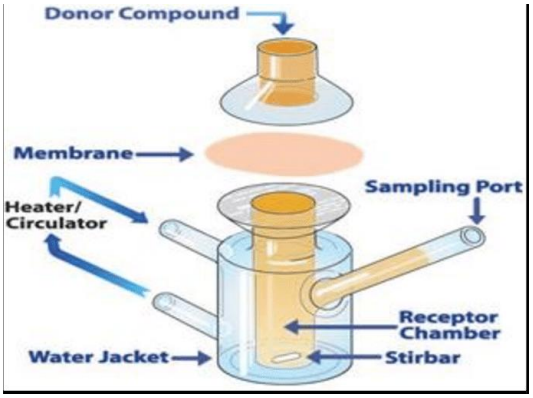

Figure 20. Franz Diffusion Cell. Reproduced from Vats et al., 2014 (210)**.** The Franz diffusion cell has a donor chamber, where the analyte under study is placed, a membrane that can be manufactured commercially or directly from human or animal skin, and a receptor chamber, which contains the receptor liquid with the analyte that has passed through the membrane during analysis.

EXPERIMENTAL PART

MATERIALS AND REAGENTS

FORMULATION OF NANOPARTICLES

- Hot Microemulsion Method
- Experimental Factorial Design
- Stability Study - Lyophilization

PHYSICOCHEMICAL TECHNIQUES

Morphological Analysis by Transmission Electron Microscopy (TEM)

1. Differential Scanning Calorimetry (DSC)
2. Determination Of Surface Charge (Zeta-Potential) And Particle Size
3. Viscosity Measurement
4. Scanning Electron Microscopy (SEM)
5. Atomic Force Microscopy (AFM)
6. X-Ray Diffraction (XRD)
7. High-Performance Liquid Chromatography (HPLC)
8. Titration Method
9. UV-Vis Spectroscopy Method

VALIDATION OF ANALYTICAL METHODS

1. Specificity
2. linearity
3. Accuracy
4. Precision
5. Intermediate precision
6. Robustness

TECHNIQUES IN MOLECULAR AND CELLULAR BIOLOGY

1. Cell lines (culture conditions)
2. Plasmid preparation
3. Gel retardation assays
4. Cytotoxicity (MTT)
5. RT-qPCR
6. Enzyme-linked immunosorbent assay (ELISA)
7. Characterisation of SLN uptake by **Confocal Microscopy**
8. Confirmation of lipoplexes transfection by **Fluorescence Microscopy**

BIOPHARMACEUTICAL STUDIES

1. Permeation test
2. Drug retention inside the skin

7 MATERIALS AND REAGENTS

7.1 MATERIALS

7.1.1 OBTAINING NANOPARTICLES

- CHON from Bioiberica (Industrial Estate, Barcelona, Spain), batch F-042903.
- Stearic acid 50 vegetable grade, from Merk, Germany, batch K46563361.
- Myristic acid batch 61200918, Palmitic acid batch 10191598, Stearic acid > 98 %, batch 10201250 and Oleic acid batch 10204629, from Alfa Aesar by Thermo Fisher Scientific, Germany.
- Octadecylamine from Acros Organics, Geel, Belgium, batch A0307242.
- Poloxamer 188 from Sigma-Aldrich by Merck, United States, batch SLBF9298V.
- Cholesteryl oleate from Tokyo Chemical Industry Co., Tokyo, Japan. CAS RN: 303-43-5.
- Oleylamine (purity ≥ 70%), from Sigma-Aldrich by Merck, Madrid, Spain, CAS Number 112-90-3.
- Qualitative paper filters of 43-48 μm and 7–9 μm pore size from FILTER-LAB®, Filtros ANOIA, SA Barcelona.
- The water used was obtained using a Milli-Q A10 module (Millipore, France).

7.1.2 STABILITY STUDY - LYOPHILIZATION

- Trehalose (Cargill- Cerestar, State Units. Lot 120608).

7.1.3 SLN CHARACTERIZATION

7.1.3.1 PHYSICOCHEMICAL TECHNIQUES

MORPHOLOGICAL ANALYSIS BY TRANSMISSION ELECTRON MICROSCOPY (TEM)

- Uranyl acetate: (Sigma Aldrich, Germany) 1 % prepared in dH2O, filtered through 0.45 µm filter and aliquots stored at 4°C.

TITRATION METHOD

- 1-Cetylpyridinium chloride Monohydrate, from Merck, India, batch S5765108648.
- Cetylpyridinium chloride, from Alfa Aesar by Thermo Fisher Scientific, Germany, batch 10207196.
- Sodium hydroxide was purchased from Panreac Quimica (Barcelona, Spain), batch 0001030347.
- Methylene blue 1%v/v.

HIGH-PERFORMANCE LIQUID CHROMATOGRAPHY (HPLC)

- Acetonitrile (ACN) HPLC grade, acetic acid glacial Ph.Eur. grade and sodium hydroxide were purchased from Panreac Chemistry (Barcelona, Spain).
- Octanesulphonic acid from Romil Chemicals, Cambridge, UK.
- Ortho-Phosphoric acid 85% was purchased from Merck, and triethylamine, from Sigma-Aldrich by Merck, Germany.

UV-Vis SPECTROSCOPY METHOD

- Sodium tetraborate decahydrate, B3545, from Sigma-Aldrich by Merck, Saint Louis, USA.
- Sulfuric acid, from Sigma-Aldrich by Merck, Saint Louis, USA
- Carbazole C5132, from Sigma-Aldrich by Merck, Saint Louis, USA
- Ethanol absolute 1.07017, from Sigma-Aldrich by Merck, Germany. D-Glucuronic acid 98+%, L14350, from Alfa Aesar by Thermo Fisher Scientific, Germany.

7.1.3.2 TECHNIQUES IN MOLECULAR AND CELLULAR BIOLOGY

If not otherwise indicated, all solutions were prepared with reverse osmosis double distilled water (MQH2O) from the Millipore Milli-Q® water system (Millipore, USA). All media was prepared with distilled water (dH2O).

If not otherwise indicated, all chemicals used were analytical grade and stored at ambient temperature. Sterilisation of all media and glassware by autoclaving was undertaken at 121ºC for 20 min. Samples were filter sterilised using the Acrodisc® 0.22 μm filters (Pall, USA).

All media were prepared following standard recipes at room temperature using MQH2O. The media was autoclaved at standard conditions (121 °C, 20 min) and stored at 4 °C until use.

7.1.3.2.1 CELL LINES

- DC2.4 cells-Murine dendritic cell line was provided by Dr. Dodie Pouiniotis, Royal Melbourne Institute of Technology (RMIT) University.
- HT-29 and BJ cell lines were purchased from LGC Standards (Barcelona, Spain).
- HaCaT cell line was purchased from Cell Line Services (Eppelheim, Germany) and the reagents used for this cell cultures were obtained from Gibco (Cacavelos, Portugal).
- Primary chondrocytes were extracted from the articular cartilage disposal of an OA patient after total joint arthroplasty.

7.1.3.2.2 REAGENTS AND SUPPLIERS FOR CELL BIOLOGY TESTS

- Molecular grade Milli-Q water (MQH2O): DNAse and RNase free from Millipore, USA.
- Culture plates and lenses (Nalge Nunc International, United States),
- Lipofectamine® 2000 Transfection Reagent: (Invitrogen, USA).
- DMEM culture media of different compositions (Dulbecco's Modified Eagle Medium, Gibco, United States)
- Molecular grade water (MGH2O): Double distilled, RNase and DNAse free (Gibco, USA).
- Opti-MEM® I (Reduced Serum Medium): stored at 4 ºC (Gibco, USA) stored at 4ºC.
- PBS/Tween: PBS (Oxoid, England) with 0.05% (v/v) Tween 20® (Sigma-Aldrich, Germany).
- Phosphate buffered saline (PBS) tablets: (Invitrogen, Australia), prepared 1x buffer by

  dissolving 1 tablet per 100 ml and stored at 4 ºC. (sodium chloride 0.8 %, potassium chloride 0.02 %, disodium hydrogen phosphate 0.115 %, potassium dihydrogen phosphate 0.02 %). pH 7.4.

- SDS running buffer (10x): Tris-HCl-3 % (w/v) (Merck, Germany), glycine-14.2 % (w/v). (Amresco, USA), SDS-1% (w/v) (Merck, Germany).
- SDS loading buffer: (5x): 60 mM Tris-HCl (Merck, Germany), 25% (v/v) glycerol (BDH, USA), 2% (w/v) SDS (Merck, Germany), 1.4 mM β-mercaptoethanol (Bio-Rad, USA), 0.1% (w/v) bromophenol blue (Sigma-Aldrich, Australia), stored at −20°C.
- Tris-Acetate-EDTA (TAE) electrophoresis buffer (1x): Tris-HCl-40 mM (pH 8.0) (Merck, Germany), acetic acid-20 mM (Merck, Germany), EDTA 2 mM (Merck, Germany).
- Sodium Chloride (NaCl): 0.15 M-0.5 M NaCl from BDH, USA.
- Sodium dodecyl sulphate (SDS): 10% (w/v) from Merck, Germany.
- Sodium Hydroxide (NaOH): 0.1-3 M NaOH from Merck, Germany.
- Triton X-100**:** 0.1% (v/v) from Sigma-Aldrich, Australia, in MQH2O
- ELISA coating buffer: 4% of 84 g/L NaHCO3 (BDH, Germany) and 8% of 106 g/L Na2CO3 (BDH, Germany) were mixed immediately before use. Stored at 4°C.
- Trypan blue stain: 0.4 % (Life Technologies, USA).
- Cell internalization: Nile Red (EMD Millipore).
- Alexa Fluor-488 (Molecular Probes) from Thermo Fisher Scientific (Life Technologies, USA).
- Roswell Park Memorial Institute (RPMI) 1640 GlutaMAX ™: (Gibco, USA), stored at 4°C.
- Dimethyl Sulfoxide (DMSO) from Merck, Germany.
- DAPI (4',6-diamino-2-phenylindole) from Invitrogen, USA and Sigma Aldrich St. Louis, USA). Stored at −20°C
- Tetrazolium bromide (MTT) were purchased from Sigma Aldrich (St. Louis, USA).
- Fetal bovine serum (FBS), IL-6, IL-8 and TNFα Human ELISA Kit were purchased from Thermo Fisher Scientific (Life Technologies, USA).
- Fetal bovine serum (FBS): heat-inactiated, Australian-certified (Gibco, USA), stored at −20°C.

- ProLong. Gold Antifade Mountant (Invitrogen, Thermo Fisher Scientific, Scoresby, VIC, Australia).
- Ethanol: 96% (v/v) from Merck, Germany.
- Tween 20: polyoxyethylene sorbitan monolaurate from Sigma-Aldrich, Australia.
- Ethylenediamine tetra acetate (EDTA): 0.5 M EDTA from Merck, Germany.

7.1.3.2.3 PLASMID PREPARATION

- Plasmid pEGFP from Addgene. Bacterial Resistance to Ampicillin.
- Plasmid Pred Mini Spin kit (GE Healthcare).
- HindIII, ApaI and EcoRI digestion enzymes from New England Biolabs, USA. All enzymes were used in the supplied buffer according to the manufacturer's instructions and stored at −20°C.
- Escherichia coli DH5alpha, strain was obtained from Smooker lab, RMIT University, Australia.
- Luria-Bertani (LB) broth: 1% (w/v) tryptone (Oxoid, England), 0.5% (w/v) yeast extract from Oxoid, England, 1% (w/v) NaCl from BDH, USA. Prepared in MQH2O.
- Luria-Bertani (LB) agar: 1% (w/v) tryptone (Oxoid, England), 0.5% (w/v) yeast extract from Oxoid, England, 1% (w/v) NaCl from BDH, USA, 1% (w/v) bacteriological agar from Oxoid, England. Prepared in MQH2O.
- Ampicillin: (CSL, Australia) 100 mg/ml stock prepared in MQH2O, filtered through a 0.22 µ m filter and the aliquots stored were at -20 ° C. Final working concentration of 100 µg /ml was used in the media.

7.1.3.2.4 GEL RETARDATION ASSAYS

- Agarose gel: (1% w/v) agarose, molecular grade (Bio-Rad-Laboratories, USA) prepared in 1 x.
- TAE buffer by heating using a microwave and stained with SYBR Safe DNA gel stain.

- Bio-Rad GelDoc imaging system from Bio-Rad, USA.
- HyperLadder™ 1kb DNA ladder from Bioline, USA.
- Bacteriological agar from Oxoid, England.
- DNA loading buffer (5x): 10% (w/v) ficoll®-400 (BDH, USA), 50% (v/v) glycerol (BDH, USA), 0.5% (w/v) Orange G (Sigma-Aldrich, Australia), 1% (w/v) SDS (Merck, Germany), 10 mM EDTA (BDH, USA), 50 mM Tris-HCl (pH 8.0) (Merck, Germany).

7.1.3.2.5 RT-qPCR

- BeyoFast™ SYBR Green qPCR Mix (2×, High ROX) (Beyotime).
- PrimeScript 1st Strand cDNA Synthesis Kit (Takara, Dalian, China).
- qPCR Master Mix (Promega, Madison, WI, United States).
- Primers from Sangon Biotech (Shanghai) Co., Ltd.

7.1.3.2.6 BIOPHARMACEUTICAL STUDIES

- 0.05% solution of Sodium lauryl sulphate from Sigma-Aldrich by Merck, Madrid, Spain.

7.2 EQUIPMENT

7.2.1 OBTAINING NANOPARTICLES

The following equipment was used for the synthesis and characterization of the components and of the solid lipid nanoparticles themselves:

- Dual Range XS105 analytical balance (Mettler-Toledo, Switzerland)
- Mastersizer 2000 laser diffractor coupled to Hydro 2000SM module (Malvern Instruments, United Kingdom).
- Measurement of the Z potential in Zetasizer Nano-Z equipment (Malvern Instruments, United Kingdom).
- Centrifuge Digicen 20-R (OrtoAlresa, Spain)
- Agimatic heating plate (P Selecta, Spain)
- Polystat K6 thermostatic bath with Polystat cc3 thermostat (Huber, Germany)
- Mechanical shaker Ultraturrax T25 Digital (Ika, Germany).
- Ultrasonic processors, Vibra-Cell™ VCX 130

7.2.2 STABILITY STUDY - LYOPHILIZATION

For the short-term stability studies of SLN, the following equipment has been used:

- Refrigerator (LG, South Korea)
- Stoves (Heraeus, Germany)
- Lyobeta 20 pilot freeze-drying system (Telstar, Terrassa, Spain).

7.2.3 SLN CHARACTERIZATION

7.2.3.1 PHYSICOCHEMICAL TECHNIQUES

- Burette SB Straight s/cock from VWR, tolerance of ±0.030 ml.
- Thermo Scientific Helyos B Uv-Vis Dual Beam Spectrophotometer, used with 1 cm matched quartz cells.
- Dionex UltiMate 3000, equipped with pump (LPG-3400 M), autosampler (WPS3000), thermostated column compartment (TCC-3100, 6P), DAD (PDA-3000) and Chromeleon datasystem software (version 6.80 SR15, Dionex).
- Extended-C18 (YMC pack ODS-250 x 4.6 mm, packed with 5 micron) column.
- 1010 microscope at an accelerating voltage of 80 kV from JOEL, Japan.
- Tecnai Spirit microscope equipped with a LaB6 cathode (FEI Company, Hillsboro, OR, USA), from the Centers Cientifics i Tècnològics de la Universitat de Barcelona (CCiTUB).
- Tecnai SPIRIT (FEI Co.) electronic microscope at 120 kV.
- Emitech 950 X Vacuum Carbon Evaporator (Quorum Technologies, UK).
- Zetasizer Nano ZS (Malvern, UK).
- Mastersizer 2000 (Malvern Instruments, UK), coupled to a Hydro 2000SM module.
- Zetasizer Nano ZS90 and Zetasizer Nano-Z (Malvern Instruments, UK).
- Malvern Panalytical NanoSight NS300 Instrument from Malvern Panalytical.
- Calorimeter DSC30 (Mettler-Toledo, Switzerland).
- Multimode 8 AFM atomic force microscope coupled to a Nanoscope V Electronics (Bruker, Germany) electronic module.
- Bruker's Sharp Nitride Lever (SNL) probes and analysis software Nanoscope Analysis (Bruker).
- X-ray diffractor PANalyticalX'Pert PRO MPD Θ/Θ.

7.2.3.2 TECHNIQUES IN MOLECULAR AND CELLULAR BIOLOGY

- DNA was quantified using NanoDrop Lite Spectrophotometer.
- Bio-Rad Gene Pulser™ apparatus. UV gel doc imaging system from Bio-Rad, USA.
- Step one Plus real-time PCR System (Applied Biosystems).
- Nanodrop 1000 (GE Healthcare Bio-sciences, Uppsala, Sweden).
- Eppendorf microcentrifuge MiniSpin® Plus.
- Beckman Allegra 21R centrifuge or the Heraeus Multifuge 1S-R centrifuge.
- EPS 3000xi power pack Bio-Rad, USA
- Milli-Q® water filtration system from Millipore, USA
- Mini-PROTEAN® tetra system PAGE unit from Bio-Rad, USA
- MiniSpin® Plus microcentrifuge from Eppendorf, Germany
- NanoDrop™ One from ThermoFisher, Australia
- pH meter Metrohm from AG, Switzerland
- NanoDrop Lite Spectrophotometer, Invitrogen, USA
- Automatic Modulus™ Microplate Photometer (Turner BioSystems).
- Leica TCS SP5 confocal laser scanning microscope (Leica Microsystems, Germany)
- Leica Epifluorescence microscope (Wetzlar, Hesse, Germany)
- The Finnpipette® digital pipette range (Thermo Fisher Scientific, USA) was used to dispense solutions. The range included 0.5-10 μL, 5-50 μL, 20-200 μL, 100-1000 μL, 1-5 ml, 2-10 ml pipettes and 20-200 μL or 50-300 μL multi-channel pipettes. Volumes above 10 ml were measured with a measuring cylinder.
- Mettler Toledo XS105 Dual Range top loading analytical balance.
- ISSCO model 300 top loading balance.
- Biological safety cabinet class II, BH2000 series from Clyde-Apac, Australia
- CO2 incubator fom Sanyo, Japan
- Countess® automated cell counter from Thermo Fisher, USA
- Dry heating block from Ratek, Australia

- IX51 inverted phase contrast microscope from Olympus, Japan
- POLARSTAR Omega microplate reader from BMG Labtech, Germany
- Sonicator wash from Soniclean, Australia
- Suspension mixer from Ratek, Australia
- Water bath from Ratek, Australia

7.2.3.3 BIOPHARMACEUTICAL STUDIES

- Vertical Franz-type cells of diffusion (Vidra Foc, Barcelona, Spain).
- Dermatome, Aesculap® Acculan 3Ti, Germany.
- DermaLab® module, Cortex Technology, Hansund, Denmark for trans epidermal water loss (TEWL).

8 METHODOLOGY

8.1 OBTAINING SOLID LIPID NANOPARTICLES

8.1.1 HOT MICROEMULSION METHOD

The SLN with CHON were produced by hot microemulsion technique described previously (211), including improvements to the method, by reducing manufacturing times and improving the filtration technique. The centrifugation parameters were set to 19,000 rpm instead of 15,000 and 15 minutes instead of 30 minutes. To obtain a more homogeneous suspension it was used two filters (43–48 μm and 7–9 μm) instead of only one (7–9 μm).

For the optimization of the production of solid lipid nanoparticles, the experimental factorial design was performed with the formulation SLN-1. Lipid matrix was composed by stearic acid 50 vegetable grade, corresponding to a range from (35-40) % of the formulation, and octadecylamine was the cationic lipid used as charged carrier, representing to (42-48) % of the formulation (26) The aqueous matrix contained the Chondroitin Sulphate sodium WS (CHON) representing (5-11) % of the mix, and Poloxamer 188 from EMD Millipore corresponding to (7-8) % of the formulation.

Briefly, the aqueous solution of CHON in ultrapure water (EMD Millipore) was prepared. Subsequently, both the lipids of the lipid matrix and the components of the aqueous matrix were separately heated to a temperature above their melting point. Next, they were mixed and stirred at 80 °C to obtain a hot emulsion. According to the proposed experimental factorial design, several reaction times, stirring rates and CHON concentrations were assessed. Each tested formulation was stirred at different timeframes, then the microemulsion was dispersed into refrigerated ultrapure water at 4 °C in continuous agitation and containing different concentrations of CHON, to produce the core

solidification of the CHON-SLN. Later, the emulsion was centrifuged at defined stirring rates (19 000 rpm) and reaction times (15 minutes). Then, the emultion was filtered with two qualitative filter papers of 43–48 μm and 7–9 μm from FILTER-LAB®, Filtros ANOIA, SA Barcelona and storage. Plain SLN was formulated without CHON in the aqueous matrix.

For the NLC-3 formulation, a change in the manufacturing process was introduced in order to evaluate the option of using ultrasound for the manufacturing of nanoparticles. The results are presented in the table 18, of the section *9.4 Stability Study - Lyophilization*, of the stability study. Briefly, all the components were weighed in a test tube, together with the hot water. It was sonicated in hot water, at 80 °C to obtain a hot emulsion, for 5 minutes at 40 % amplitude. Then the emulsion was transferred to a container with ultrapure water at 4 °C and sonicated for 5 minutes with an amplitude of 40 %. Subsequently, centrifugation and filtration followed the steps of the procedure set forth above.

Starting from the best-defined formulation conditions, other nanoparticles were manufactured, introducing changes in the amount or composition of the ingredients, as shown in Tables 4 and 5.

Different nanoparticles were formulated, to be evaluated in different tests during the investigation, according to the test carried out and the reagents and equipment available at each stage.

Table 4. Composition of the solid lipid nanoparticles studied.

Composition (%)	Formulation							
	SLN-1	**SLN-2**	**NLC-3**	**SLN-4**	**NLC-5**	**40/60**	**70/30**	**95/5**
CHON	5	5	5	-	-	5	5	5
Stearic acid*	40	16	16	17	17	40	40	40
Cholesteryl oleate	-	24	24	25	25	-	-	-
Octadecylamine	48	48	-	50	-	48	48	48
Oleylamine	-	-	48	-	50	-	-	-
Poloxamer 188	8	8	8	8	8	8	8	8
Total (%)	**100**	**100**	**100**	**100**	**100**	**100**	**100**	**100**

* the composition of stearic acid was different in some formulations, see table 5.

In general, to synthesize the SLN (SLN-1, SLN-2, NLC-3, SLN-4, SLN 5) stearic acid 50 vegetable grade was used, however, the impact of varying the composition of stearic acid in the formulation of some nanoparticles was evaluated (40/60, 70/30 and 95/5), the following proportions were used.

Table 5. Composition of stearic acid used in different SLN formulations.

Composition (%)	Stearic acid ratio		
	40/60	**70/30**	**95/5**
Myristic acid	<2	<4	-
Palmitic acid	52-65	25-34	<5
Stearic acid (purity > 98 %)	33-46	60-69	>95
Oleic acid	<1	-	<1

8.1.2 EXPERIMENTAL FACTORIAL DESIGN

An experimental factorial design was employed to optimize the production of SLN as vehicle of CHON. A 3x3x2 full-factorial experimental design was used for the optimization of CHON- SLN formulations. The factors tested at various levels (table 6), were CHON final concentration (mg/ml) in the formulation, Stirring rate during the synthesis reaction, and Reaction time which means the time during which the synthesis reaction occurs, in which it is stirred with the ultraturrax both hot and at 4 °C.

Table 6. Factors and levels used in the experimental factorial design to optimize the production of SLN as vehicle of CHON.

Factors	Levels
Concentration (mg/ml)	0.4 - 0.7 - 1.0
Stirring rate (rpm)	16,000 - 20,000 - 24,000
Reaction time (min)	10 - 15

In total, the DOE proposed 18 different combinations (table 7), for each experiment two different formulations were analyzed in triplicate, the average of the measurements for each sample is reported. Based on the results, the most optimal formulation of SLN was chosen.

Table 7. Design of experiments to optimize the production of SLN as vehicle of CHON.

Experiment	Concentration (mg/ml)	Stirring speed (rpm)	Reaction time (min)
1	0.4	16000	10
2	0.4	16000	15
3	0.4	20000	10
4	0.4	20000	15
5	0.4	24000	10
6	0.4	24000	15
7	0.7	16000	10
8	0.7	16000	15
9	0.7	20000	10
10	0.7	20000	15
11	0.7	24000	10
12	0.7	24000	15
13	1.0	16000	10
14	1.0	16000	15
15	1.0	20000	10
16	1.0	20000	15
17	1.0	24000	10
18	1.0	24000	15

For the selection of the best formulation, different properties were tested, including entrapment efficiency of CHON (EE%), zeta potential and particle size (table 8). TEM technique was used to characterize the morphology and confirm the size of the nanoparticles.

Table 8. Properties evaluated to optimize the production of SLN as vehicle of CHON.

Property	**Criterio**
Entrapment efficiency of CHON (EE%)	Highest % EE possible
Zeta potential (mV)	< -25 and > 25
Particle size (nm)	Minor size possible
Morphology	TEM technique to characterize SLN

The optimal factors were attained by Minitab® 18.1.0.0 program, using design of experiment (DOE), and pareto chart was used in the screening step to find the significant variables.

8.1.3 STABILITY STUDY - LYOPHILIZATION

To improve the feasibility and stability of the nanoparticle suspension, it was lyophilized by mixing it with a solution of the cryoprotectant trehalose (5%, w/v) and freeze-dried using a Lyobeta 20 pilot freeze-drying system (Telstar, Terrassa, Spain). For all assays performed using freeze-dried SLN, the vial of SLN used was re-dispersed in ultrapure water (3.0 ml).

The stability of the SLN was evaluated by measuring the Z potential and the size of fresh and stored samples at 4 °C, room temperature and 37 °C. For their part, these parameters were evaluated in lyophilized samples stored at room temperature, up to a maximum of 1 year from their manufacture and lyophilization.

8.2 SLN CHARACTERIZATION - PHYSICOCHEMICAL TECHNIQUES

8.2.1 MORPHOLOGICAL ANALYSIS BY TRANSMISSION ELECTRON MICROSCOPY (TEM)

TEM was used to analyze the content homogeneity and surface of reconstituted SLN. The SLN morphology was studied with different equipment and at different times since their manufacture.

For newly manufactured samples, morphology was evaluated using a Tecnai Spirit microscope equipped with a LaB6 cathode (FEI Company, Hillsboro, OR, USA). Images were recorded at 120 kV using a 1376 × 1024 pixel CCD Megaview camera. The samples were negatively stained with a 2.0 % uranyl acetate solution and adsorbed onto carbon-coated copper grids CF200-Cu.

After 12 months of lyophilized samples of SLN-4 and NLC-5 and lipoplexes (SLN:pDNA) were also analyzed. The lipoplexes were obtained by mixing an aqueous solution of 1µl of the EGFP plasmid (1 mg/ml) together with 20 µl of each SLN suspension (36 µg/µl), as described in section 8.10.4 Preparation of DNA-SLN Complexes.

The samples were applied to the TEM grids, 200 mesh formvar-carbon copper grids, by direct floating the grids on 40 µl drops of the sample, without any poststaining. The grids were washed twice with freshly filtered MQH2O to remove any excess sample. The stained grids were allowed to dry overnight before imaging by JEOL1010 TEM at an accelerating voltage of 80 kV.

8.3 DIFFERENTIAL SCANNING CALORIMETRY (DSC)

The objective was to study of possible CHON:Excipient interactions by Differential Scanning Calorimetry (DSC).

For SLN-1 differential scanning calorimetry was used for the evaluation of possible interactions between formulation components, as previously described (211), on a DSC-822e (Mettler-Toledo) equipment with a temperature program consisting of a heating rate of 10 ºC in the range of 30 ºC to 200 ºC, using the heat flow method. The ingredients were were weighed into a 40 µl aluminum pan, and an empty pan was used as a reference. Dry nitrogen (50 ml/min) was used to perform the assay in a nonoxidative atmosphere.

The study was proposed to obtain, by differential scanning calorimetry (DSC), useful information to anticipate possible interactions between CHON and the materials that are intended to be used as excipients in its formulation. The comparative analysis of the DSC thermograms of the primary active ingredient:excipient mixtures, in relation to the records of each component separately, is commonly used to quickly reveal chemical and physical interactions from the modifications produced in thermal events (Balasubramaniam & Panpalia, 2001; Ford & Timmins, 1989; Kerč et al., 2011; Malan et al., 1997; Wissing et al., 2000).

8.4 DETERMINATION OF SURFACE CHARGE (ZETA-POTENTIAL) AND PARTICLE SIZE

In the process of SLN formula optimization, analyzes of SLN sizes were determined by laser diffraction on a Mastersizer 2000 (Malvern Instruments, UK) equipped with a 4 mW He–Ne laser (633 nm). For the treatment of samples in solution, it was fixed at a stirring speed of 800 rpm. The results are expressed as average surface diameter (D [3,2]), in nanometers (nm), unless otherwise indicated. The zeta potential of some formulations was also measured by laser Doppler microelectrophoresis in a Zetasizer Nano-Z (Malvern Instruments, UK). The zeta-potential values were obtained from the electrophoretic mobility of the nanoparticles and lipoplexes under an electric field. All samples were analyzed in triplicate and results are expressed as mean voltage, in millivolts (mV) or nanometers (nm), depending on the measurement.

In the study of stability of SLN over time, the size, the polydispersity index (PDI) and loading of some samples were measured by dynamic light scattering on a Zetasizer Nano ZS90 (Malvern Instruments). These teams work on the principle of dynamic light scattering in which the light beam hits the particles moving in Brownian motion and measures their hydrodynamic diameter.

The size and charge of some SLN and the complexes formed (study of lipoplexes (SLN and pGFP), were determined by laser diffraction and light dispersion techniques using a Zetasizer Nano ZS (Malvern, UK), by dispersing the sample with distilled water.
A 100 µL aliquot of the sample diluted in 1 ml distilled water was used for measurement. All the measurements were done at room temperature using a disposable clear zeta-cell.

The size of the nanoparticles and the concentration of particles per milliliter were also studied using Nanoparticle Tracking Analysis (NTA). NTA utilizes the properties of both light scattering and Brownian motion to obtain the nanoparticle size distribution of samples in liquid suspension. In general, with this analytical technique, nanoparticles in

liquid suspension are loaded into a sample chamber, which is illuminated by a dedicated laser beam. Particles in the beam path scatter the laser light, and it is captured by the 20x microscope objective and viewed with a digital camera. The camera captures a video of the particles moving under Brownian motion. Nanoparticle Tracking Analysis (NTA) software analyzes many particles individually and simultaneously (particle by particle) and, using the Stokes Einstein equation, calculates their hydrodynamic diameters (212). For the analysis of the nanoparticles with NTA, the suspension was diluted 1:1000 in ultrapure water, before reading it in the equipment.

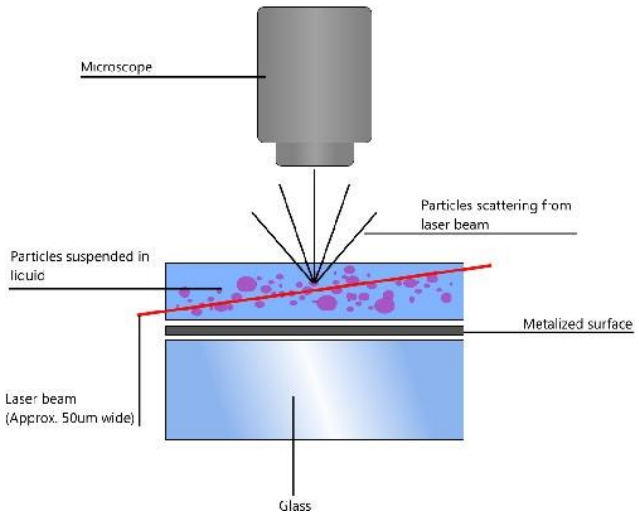

Figure 21. Nanoparticle Tracking Analysis (NTA) system to determine size of nanoparticles. Reproduced from Malvern Panalytical, n.d. (212)**.**

8.5 SCANNING ELECTRON MICROSCOPY (SEM)

Sample preparation of solid lipid nanoparticles (SLN) for scanning electron microscopy visualization was performed as follows: a thin layer of the fresh or lyophilized sample was placed on a circular double-sided carbon tape, which is deposited attached to a sample holder (stub). Excess sample was removed using a compressed air gun. Afterwards, it was coated with a conductive material in an Equip equipment Polaron ES100 (Polaron Instruments). The coating was carried out with carbon (C), in an inert atmosphere of argon (Ar). Images were acquired using a Hitachi S4300 field emission scanning electron

microscope (Hitachi High-Technologies), applying an electron flux corresponding to an energy of 10 keV (29).

8.6 VISCOSITY MEASUREMENT

The evaluation of the rheological characteristics was carried out in duplicate at 25 ℃, using a rotational rheometer Thermo Scientific Haake Rheostress 1 (Thermo Fischer Scientific, Kalsruhe, Germany), equipped with a cone plate set-up (0.105 mm gap between con and plate) with a fixed lower plate and a mobile upper cone Haake C60/2° Ti (60 mm diameter, 2nd angle). The apparatus was connected to a temperature control Thermo Haake Phoenix II + Haake C25P. The Rheometer was connected to a computer PC provided with the Haake Rheowin ® Job Manager software to perform the tests and Haake Rheowin ® Data Manager software to analyze the obtained data, respectively.

The rheological properties were observed from recently prepared samples. Viscosity curves $(\eta = f(\dot{\gamma}))$and flow curves $(\tau = f(\dot{\gamma}))$were recorded at 25℃, in two replicates. The shear rate ramp program included: Constant shear rate period: 100 s^{-1} during 1 min; Ramp-up period from 0 to 100 s^{-1} in 3 min; Ramp-down period: from 100 to 0 s^{-1} in 3 min. Data from the flow curves were fitted to different mathematical models: Newton, Bingham, Ostwald-De- Waele, Cross, Casson and Herschel - Bulkley (213). Viscosity mean value (Pa.s) were calculated from the constant share section at 100 s^{-1} for the samples kipped at 25 ℃ ±2 ℃.

Statistical analysis was compared by two-way analysis of variance (ANOVA), with Bonferroni's multiple Comparison Test, using Graphpad Prism (Graphpad Software Inc., San Diego, CA, USA).

8.7 ATOMIC FORCE MI CROSCOPY (AFM)

The atomic force microscopy technique is a tool that allows us to obtain surface images of samples with nanometric resolution and, by extension, the surface of any solid. The analyzed sample does not need to be electrically conductive and is not altered by the measurement, which gives it a great advantage over other microscopic techniques. For its part, it is not necessary to carry out any previous preparation of the sample, its microscope does not work with light or with an electron beam, but by palpating the sample and the visualization is carried out in ambient conditions (29).

Technically, the images are the result of measuring the force received by a very fine probe and transmitted in the form of deflection of a laser beam that hits a lever (acting, therefore, as a force sensor) that supports this probe. This force, of low intensity and which remains constant, is a consequence of its proximity to the surface of the sample. To determine the surface characteristics, the lever probe is moved following the contours of the sample. The AFM technique can operate in different modes, depending on whether the tip comes into contact with the sample surface, and how that contact occurs (continuous or discontinuous) (214).

Multimode 8 AFM atomic force microscope coupled with a Nanoscope V Electronics (Bruker) electronic module, using the peak mode. force tapping for surface analysis. SNL probes (Bruker) were used for analysis. Images made at 1Hz speed and 512 x 512 pixels. In this imaging mode, individual nanoindentations (one per pixel) are made in order to detect the presence of the surface by deflection of the probe lever. This deflection, which can be calculated as the applied vertical force, is held constant and is used as a feedback signal to track the sample surface.

The speed analysis is performed at a frequency of 1 kHz and vertical forces of the order of pN or approximately 1nN are applied. By using low forces, both the integrity of the sample and the probe apex are preserved. AFM probes consist of triangular silicon levers and a silicon oxide pyramid, with a nominal spring constant of 0.35 nN /nm (SNL-10 probes, Bruker).

The preparation of the sample for the morphological analysis of the different isolated SLN formulations was carried out as follows: 20 µl of the diluted SLN sample (100 uL of the nanoparticles in 1 ml of MQH2O) were deposited in a flat glass slide, previously glued on a teflon disc with two-component epoxy. It was left to rest for 2 minutes, and the sample was gently rinsed with MQH2O to later take the photographs in liquid. Before starting the imaging process, the samples were allowed to stabilize for 2 min to thermally equilibrate the sample and AFM probe with the environment, to prevent drift of the piezoscanner. Images were taken at 1 Hz and 512x512 pixels. Particle detection and analysis was performed using the analysis software Nanoscope Analysis (Bruker).

8.8 X-RAY DIFFRACTION (XRD)

A PANalyticalX'Pert PRO MPD Θ/Θ solid sample diffractometer was used to obtain an X-ray diffraction pattern of the bulk components and a molten mixture of CHON and octadecylamine, with a radius of 240 mm in a configuration with converging beams that give rise to monochromatic X-rays, which impinges on a focusing mirror, and a transmission geometry with the planar samples sandwiched between films of low absorption. The studied pulverized samples were sandwiched between 3.6-micron thick polyester films. Experimental conditions were set as follows: Cu K α radiation (λ = 1.5418 Å) and working power of 45 kV - 40 mA. The active length (aperture) of the PIXcel detector was 3.347º. 2Θ/Θ sweeps from 2 to 60° were performed with a step size of 0.026º and a measurement time of 200 seconds per step. The incident beam slits define a beam height of 0.4 mm, with 0.04 Söller radians, in both the incident and diffracted beams (211).

8.9 ENTRAPMENT EFFICIENCY OF CHON (EE%)

8.9.1 HIGH-PERFORMANCE LIQUID CHROMATOGRAPHY (HPLC)

Initially, preliminary studies were performed to determine the amount of CHON bound to the nanoparticles using High-performance liquid. chromatography (HPLC) technique, as described above (215). Briefly, prepare a solution of Chondroitin sulphate 0.8 mg/ml into a 50 ml volumetric flask and dissolved with 25ml of diluent and sonicated for 5 min and made up to volume with diluent. Obtained solution was mixed well, filtered through 0.45 µm PVDF filters and a road for HPLC was prepared.

All determinations were carried out in six injections. The contents of the mobile phase were filtered before use through 0.45 µm filter paper and pumped from the respective solvent reservoirs to the column at a specified flow rate of 1.0 ml/min. Prior to injection of the CHON solutions, the column was equilibrated for at least 30 min with the mobile phase flowing through the systems. Then, 20 µl of each of standard and sample solutions were injected into the HPLC system for six times to get the chromatograms. The retention time and average peak areas were recorded.

The mobile phase was compounded by Octane sulphonic acid in water: Acetonitrile: triethylamine at the ratio of 90.65:8.96:0.381 (adjusted the pH 4.0 with orthophosphoric acid). Diluent was made by addition of 0.3 ml of Acetic acid with 5.0 ml of Acetonitrile then it was made up to 100 ml with water. System suitability was evaluated with six consecutive injections of system suitabilitysolution under chromatography conditions described in analytical method. Software chromeleon was used to define capacity factor (k'), tailing factor (Tf), number of theoretical plates (N) and resolution between peaks (R_s).

Finally, for the determination of the % EE, we worked with two different methods, previously validated: the volumetric titration of CHON and the determination by UV-Vis spectrophotometry.

8.9.2 TITRATION METHOD

Based on the CHON determination assay described in the European Pharmacopeia and the American Pharmacopeia (216,217), the methodology was proposed to carry out a visual titration of CHON by means of a precipitation reaction.

A linear regression curve was prepared, with different concentrations of CHON reference solution in MQH2O. (from 0.10 mg/ml to 1.20 mg/ml). 15.0 ml of each: reference solution, samples of SLN containing CHON or plain SLN, were titrated. 1-Cetylpyridinium chloride Monohydrate 1.0 mg/ ml was used as titrant. The solution becomes turbid. At the end point, the liquid appears clear, with an almost-white precipitate in suspension. 0.1 ml of a 1 percent solution of methylene blue R was added before starting the titration.

From the regression equation, using the volumes of the titrant consumed as a function of the concentrations of the CHON standard solutions, the concentration of free CHON in the sample was determined and calculated with the value of r^2.

Where: **y = m*x + b**; **y**: ml titrant; **x**: mg/ml free CHON.

Knowing the initial concentration of CHON used per sample, the CHON difference that constituted the CHON bound to the nanoparticles was calculated. Entrapment was calculated efficiency of CHON (EE%) as well

$$EE\% = (Cx)/C \times 100$$

Where C= mg/ml initial CHON and x: mg/ml free CHON in the analyzed sample.

Matrix was titrated for each formulation of Item corresponding plain SLN.

8.9.2.1 CONFIRMATION OF CHON ENCAPSULATION

To determine the amount of total CHON in the formulation and free in the water after manufacturing, different procedures were proposed:

1. Acid treatment: concentrated HCL (37%) was added to the SLN formulation in a 50:50 ratio, gently stirred, allowed to react for 5 minutes at room temperature and by volumetric titration method, the amount of CHON was calculated. free of the formulation after heat treatment, compared to the same original untreated formulation. The study was analyzed in triplicate.

2. Heat break. 50 ml of the SLN sample were taken and heated to 15 °C above the highest melting point of the formulation components for 5 minutes, avoiding boiling and loss of the sample. It was allowed to cool to room temperature and by means of the volumetric titration method, the amount of free CHON in the formulation after heat treatment was calculated, with respect to the same untreated original formulation. Each sample was analyzed in triplicate.

3. Alkali treatment. 10 ml of 0.7% w/v NaOH was added according to the stoichiometric relationship with the stearic acid present in the formulation, it was stirred gently, it was left to react for 5 minutes at room temperature and by means of the volumetric titration method, the amount of free CHON of the formulation after heat treatment, compared to the same original untreated formulation. Each sample was analyzed in triplicate.

8.9.3 UV-Vis SPECTROSCOPY METHOD

The CHON concentration in the nanoparticle samples was determined, using a modified method (218,219), which consisted of the acid hydrolysis of glycosaminoglycans (CHON hydrolysis in monosaccharides) (220) and the reaction of hexuronic acid with carbazole, obtaining a red solution, colorimetrically quantifiable.

1 ml of the sample to be analyzed was added, either as a standard solution of glucuronic acid (100, 50, 25, and 10) mg/L, to a previously prepared solution of sodium tetraborate decahydrate or in sulfuric acid (0.08 mg/ml)., in an ice-cold stoppered test tube. It was stirred and heated at 95-100°C for 30 min. Then it was cooled in an ice bath and 0.20 ml of carbazol solution, prepared at a concentration of 1.25 mg/ml of absolute methanol, was added. Subsequently, it was shaken vigorously and heated again for 30 min.

Then it was cooled to room temperature and the final absorbance (A) of the standard solution or of the samples under study was measured at 520 nm against a blank prepared in the same way. The value of the corresponding bank was subtracted from each absorbance value. MQH2O was used for standard solutions and their respective plain SLN formulation was used for SLN. The analysis of each sample was carried out in triplicate. The linear regression equation of the absorbance of the standard solutions (A_{st}) against their concentration (C_{st} mg/L) was calculated. It was calculated with the value of r^2 and from the calibrator function, the hexuronic acid content was calculated, expressed as glucuronic acid in each sample. A conversion factor of 0.343 was used to pass the mg of glucuronic acid found to mg CHON of bovine origin.

% CHON = ($C_{mg/ml}$) / (initial $CHON_{mg/ml}$ x 0.343) *100

8.10 SLN CHARACTERIZATION - TECHNIQUES IN MOLECULAR AND CELLULAR BIOLOGY

8.10.1 CELL LINES (CULTURE CONDITIONS)

In the study in cell models, the cell lines described below were used:

Table 9. Cell lines used for molecular and biological studies of SLN.

Cell	Description	Cell Culture Medium
DC2.4	Dendritic cells (murine DC2.4 cells)	RPMI
HT-29	Human colon adenocarcinoma cell line (HT-29)	DMEM
HACAT	Human keratinocyte cells (HaCat)	DMEM
B.J.	Human skin fibroblast cell line (BJ)	DMEM
Chondrocytes	Extracted from articular cartilage disposal of OA patient	DMEM

8.10.1.1 Growth and maintenance of HaCaT, HT-29 and BJ cell lines

The human keratinocyte (HaCaT) cell line, the human colon adenocarcinoma (HT-29) cell line and Human skin fibroblast cell line (BJ), were maintained in high-glucose Dubelcco's Modified Eagle's medium (DMEM) supplemented with 25 mM hepes, 1 % non-essential amino acids, 100 μg /ml streptomycin, 100 U/ml penicillin, and 10 % heat inactivated fetal calf serum (FCS). Cells were cultured in a humidified incubator at 37 ºC in a 5% CO2 atmosphere and received fresh medium every 3 days. Experiments were performed at 80-90 % of confluence (passes between n=85-95).

8.10.1.2 Growth and maintenance of DC2.4 cell line

DC2.4 cells were routinely grown in RPMI 1640 media with 1 mM HEPES and 2 mM L-glutamine supplemented with 10% heat inactivated fetal bovine serum (FBS). Cells were incubated at 37 ºC with a 5% CO_2 humidified atmosphere and subcultured every 2-3 days. For detaching cells from flasks, cell scrapers were used.

8.10.1.3 Growth and maintenance of chondrocyte cells

The primary chondrocytes were extracted from the articular cartilage disposal of an OA patient after total joint arthroplasty. All experimental procedures were approved by the Research Ethics Review Committee of SUSTech, number 02557. The culture medium used for chondrocytes was HyClone medium containing DMEM (Dulbecco's Modified Eagle Medium) supplemented with 10% FBS (fetal bovine serum, Gemini). Cells were incubated at 37 ºC with a 5% CO_2 humidified atmosphere and subcultured every 2-3 days. For detaching cells from flasks, cell scrapers were used.

The proliferation tests of OA chondrocytes treated with SLN were performed with the Cell Counting kit-8 (DOJINDO) following the manufacturer's instruction. First, cells were seeded onto the 96well plate with identical density 4×10^4 cells/ml and incubated for 24 h before SLN treatment. After that, cells were treated with different concentrations of SLN-1, SLN-2 and NLC-3. Cytotoxicity assay (MTT assay) and determination of proinflammatory cytokines (was performed.

8.10.2 PLASMID PREPARATION

In the study of transfection capacity of the SLN-4 and NLC-5, a mammalian expression plasmid, pEGFP from Addgene was used as a reporter plasmid which contains a CMV promoter and ampicillin resistant genes (table 10).

Table 10. General description of the plasmid used in cell transfection studies of SLN.

Plasmid name	Description	Size of the plasmid	Source
pcDNA5/frt/EGFPN1 (CAT)	Plasmid DNA expression vector with EGFP reporter gene, Ampicillin Resistance	5.8kb	Health Innovations Research Institute, RMIT University

.

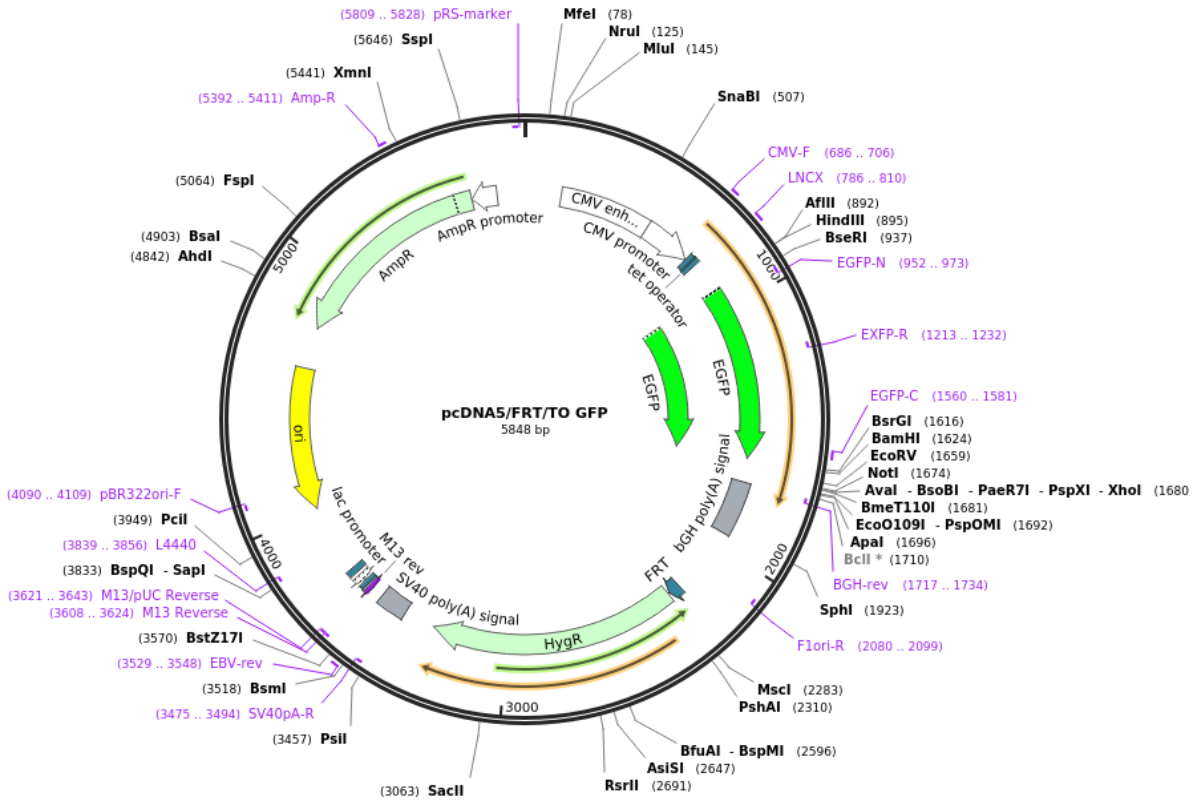

Figure 22. EGFP Plasmid map. Reproduced from Addgene, n.d. (221)

This plasmid was propagated in E. coli by a standard protocol and purified using a Plasmid Pred Mini Spin kit (GE Healthcare), following the manufacturer's instructions.

8.10.2.1 Bacterial growth conditions

E. coli DH5alpha was grown at 37 °C in an incubator overnight for plasmid isolation. The plates with transformed DH5alpha were grown at 37 °C overnight to observe colonies. This bacterium presents the following genotype:

F– Φ 80laczΔ M15 Δ (lacZYAargF) U169 recA1 endA1 hsdR17 (rK–, mK+) phoA supE44 λ – thi1 gyrA96 relA1

The media was autoclaved at standard conditions (121°C, 20 min) and stored at 40°C until use. Bacterial cultures were aseptically inoculated using a Bunsen burner flame and transformed colonies were selected by adding 100 ug/ml ampicillin. Bacterial cultures were maintained at 37°C at 220 rpm in a shaking incubator overnight unless otherwise specified. Bacteriological agar plates were used for the selective growth of transformant colonies. Plates were stored at 37°C for 16-18 h for selection and subculture of transformant colonies.

8.10.2.2 Plasmid Amplification

The plasmid was amplified in E. coli DH5alpha strain. A 50 ng of pEGFP was transformed to a 50 µL aliquot of competent E. coli DH5alpha cells at 2 V electric pulse using Bio-Rad gene pulser or chemical transformation. Next 1 ml of LB broth was added immediately to the transformed cells and incubated at 37°C for an hour, to get outgrowth of cells. Once the outgrowth was confirmed, 100 µL of mixture was added on to LB agar plates with antibiotics ampicilim. The plates were incubated at 37°C, overnight to observe transformants. A single isolated colony was inoculated in 10 ml LB broth and grown overnight at 37°C, 200 rpm in incubator cum shaker. Then the overnight culture was used to extract the pEGFP purified using a Plasmid Pred Mini Spin kit (GE Healthcare). The plasmid was eluted in a 50 µL of Elution buffer type 4 and the concentration was

measured using a NanoDrop Lite Spectrophotometer. Plasmid samples were stored at -20 °C in TE buffer.

8.10.2.3 Quantification of DNA by Nanodrop

pEGFP was quantified using NanoDrop Lite Spectrophotometer, by following the manufacturer's instructions. Briefly, 1.5 µL of elution buffer type 4 was used as a blank followed by 1.5 µL of sample. The purity of plasmid DNA was estimated based on the 260/280 ratio.

8.10.2.4 Restriction digestion of pEGFP

Restriction digestion was performed by following the manufacturer's instructions. To defined the suitable conditions for the set of enzymes 'Double digest finder' online tool from NEB labs was used. Briefly, 5 µL of plasmid was used in 20 µL reaction supplemented with 1x Cut Smart buffer solution containing 1 µL of each restriction enzyme. The following restriction digestion reaction was used to digest EGFP plasmid throughout the cloning process (table 11).

Table 11. Restriction digestion conditions of pEGFP for HindIII and EcoRI.

Double digestion	**Reaction set up**		**Incubation conditions**
HindIII and *EcoRI*	*HindIII*	1µL	
	EcoRI	1µL	
	CutSmart buffer	5µL	Incubated at 37°C for 30
	plasma	5µL	min
	Mol grade water	8µL	
Single digestion	**Reaction set up**		**Incubation conditions**
ApaI or EcoRI	*Restriction enzyme*	1µL	
	CutSmart buffer	5µL	Incubated at 37°C for 30
	plasma	5µL	min
	Mol grade water	9µL	

The DNA samples (plasmid double digests or plasmid single digest) were loaded onto 1% agarose gel stained with SYBR Safe DNA gel stain. The electrophoresis was carried out at 80 V for 60 min. The marker used was Hyperladder 1kb and the Restriction Enzymes used were HindIII, EcoRI and ApaI. The agarose gels were observed under Bio-Rad GelDoc imaging system and photographs were captured.

8.10.3 GEL RETARDATION ASSAYS

Various ratios of DNA-SLN complex formulations were analyzed on 1% agarose gels gel stained with SYBR Safe DNA gel stain. A 20 µl of sample along with 5 µL loading dye was loaded on the gel and run for 1 h at 100 V and visualised alongside HyperLadder™ 1kb DNA ladder. The gel image was taking using the Bio-Rad GelDoc imaging system from Bio-Rad, USA.

8.10.4 PREPARATION OF DNA-SLN COMPLEXES

The DNA-SLN complexes were prepared by a co-incubation method. Calculated amounts of plasmid DNA and SLN suspension were briefly vortexed and incubated at room temperature for 45 min to obtain lipoplexes. Different ratios of DNA-SLN complexes: 1:1, 1:2, 1:5, 1:10 and 1:20 (w/w), were obtained by mixing an aqueous solution of 1 µl of the EGFP plasmid (1 mg/ml) together with different amount of SLN suspension (36 µg/µl). These ratios (DNA:SLN) were selected to study the effect of various concentrations of SLN and DNA on transfection efficiency. These ratios were chosen to have an increasing amount of SLN with a constant DNA amount to determine the DNA holding capacity of SLN. The integrity of these complexes was analyzed by TEM and gel retardation assays.

8.10.5 DNASE PROTECTION STUDY AND SDS-INDUCED RELEASE ASSAY

For the DNase I protection assay, deoxyribonuclease I (Thermo-Fisher) was added to DNA-SLN complexes to a final concentration of 1 U DNase I/2.5 µg DNA, and the mixtures were incubated at 37 ºC for 30 min. Then, a sodium dodecyl sulphate (SDS) solution was added to a final concentration of 1% to liberate bound DNA from the complexes. All samples were then analyzed by agarose gel electrophoresis and the release pattern was compared to the controls.

8.10.6 CYTOTOXICITY (MTT)

8.10.6.1 SLN with CHON studies.

The effect on cell viability of SLN containing CHON, was evaluated *in vitro* using the MTT assay. For this, 100 µl of solution containing $1x10^5$ cells/ml were seeded in 96-well plates and incubated for 24 h at 37 ºC in 5% CO_2 humidified atmosphere overnight. Then, media were replaced by 90 ml fresh media plus 10 ml of media containing the formulation of nanoparticle diluted 1, 5, 10, 25, 50, 100 times, depending on the case studied. The initial concentration of the SLN formulations was 36 µg/µl. After a period of incubation (24, 48, 72 h or 1, 3 and 5 days), cells were washed with PBS and incubated with 0.25 % MTT in fresh medium for 2 h at 37 ºC in the dark. Subsequently, medium was removed, and cells were lysed by the addition of 99 % DMSO. Finally, the absorbance was measured at λ = 560 nm using an automatic Modulus™ Microplate Photometer (Turner BioSystems). The data were analyzed by calculating the percentage of MTT reduction compared to the control (untreated cells, 100 % viability).

8.10.6.2 Lipoplexes studies.

The effect on cell viability of lipoplexes, was evaluated *in vitro* using the MTT assay. For this, $1x10^4$ cells in 0.1 ml were seeded in 96-well plates and incubated for 24 h at 37 ºC in 5% CO_2 humidified atmosphere overnight. Then, media were replaced by 100 ml fresh media containing the final concentration of the nanoparticle or lipoplex formulations, according to the different dilutions evaluated (100, 250 and 500).

The initial concentration of the SLN formulations was 36 µg/µl and pDNA 1.0 µg/µl. After a period of incubation (24, 48, 72 h or 1, 3 and 5 days), cells were washed with PBS and incubated with 0.25 % MTT in fresh medium for 2 h at 37 ºC in the dark. Subsequently, medium was removed, and cells were lysed by the addition of 99 % DMSO. Finally, the absorbance was measured at λ = 560 nm using an automatic Modulus™ Microplate Photometer (Turner BioSystems). The data were analyzed by calculating the percentage of MTT reduction compared to the control (untreated cells, 100 % viability).

8.10.7 REAL TIME – qPCR

Total RNA was extracted from Chondrocytes cells with RNAiso plus (TAKARA) following the instructions provided by the supplier, after 5 days culture with 10 µl of different concentrations of nanoparticles (36 µg/µl). The dilutions applied according to the evaluated treatments are shown below, IIn the table 12

Table 12. Working dilution, according to the treatment evaluated in the study of proinflammatory cytokines.

Treatment	Dilution
SLN-1	5
SLN-2	25
NLC-3	25
Plain SLN	25
CHON (4.0 mg/ml)	25

The extracted RNA was purified using the phenol/chloroform method and dissolved in the RNase-free water. The concentration and the purity were assessed by Nanodrop 1000 (GE Healthcare Biosciences, Uppsala, Sweden). The cDNA synthesis was conducted by the PrimeScript 1st Strand cDNA Synthesis Kit (Takara, Dalian, China) according to the manufacturers' instructions.

Briefly, quantitative Reverse Transcript PCR (RT-qPCR) was performed in 10 μL reaction volumes consisting of 5 μL qPCR Master Mix (Promega, Madison, WI, United States), 0.5 μL each of cDNA and reverse primers (5 μM), and 3.5 μL nuclease-free water. The synthetic cDNA was analyzed by a Step one Plus real-time PCR System (Applied Biosystems) with BeyoFast™ SYBR Green qPCR Mix (2×, High ROX) (Beyotime) following the instructions. The PCR was processed at 95 ºC for 2 min, followed by 40 cycles of 95 ºC for 10 s and 60 ºC for 30 s. In addition, relative quantities (RQs) were measured with the comparative $2^{-\Delta\Delta C_T}$ Method. Data are present as mean ± SEM for at least three biological replicates. One-way ANOVA test was conducted. In those cases, p-values were < 0.05, a Bonferroni post-hoc test was conducted. The relative expression level of the target gene was normalized against the housekeeping gene GAPDH. The primers used for gene detection were as follows (Table 13):

Table 13. Primers used in the study of proinflammatory cytokines by the Real-time qPCR technique.

GENE	FORWARD	REVERSE
IL-1β	5- AGCTTCAAATCTCGCAGCAG-3	5-TCTCCACAGCCACAATGAGT-3
IL-6	5-CTCAGCCCTGAGAAAGGAGA-3	5-TGATTTTCACCAGGCAAGTCT-3
ACAN	5-TAGAGGATGTGAGTGGTCTT-3	5-TCCACTAAGGTACTGTCCAC-3
COLII	5-CCTCTGCGACGACATAATCT-3	5-CTCCTTTCTGTCCCTTTGGT-3
GAPDH	5-GTATGACTC TACCCACGGCAAGT-3	5-TTCCCGTTGATGACCAGCTT-3
MMP-9	5-GATCCCCAGAGCGTTACTCG-3	5-GTTGTGGAAACTCACACGCC-3
MMP-13	5-TGCTGCATACGAGCATCCAT	5-TGTCCTCAAAGTGAACCGCA-3
IL-8	5-TGGCCGACTTCACTGTACAAC-3	5-TGGGGTTCACTGGCACTTTG-3
iNOS	5-CCCTTCCGAAGTTTCTGGCAGCAGC-3	5- GGCTGTCAGAGCCTCGTGGCTTTGG -3
BMP2	5-TGTATCGCAGGCACTCAGGTCA-3	5-CCACTCGTTTCTGGTAGTTCTTC-3
COL 10	5- CGCTGAACGATACCAAATGCCC-3	5- TGGACCAGGAGTACCTTGCTCT-3

8.10.8 ENZYME-LINKED IMMUNOSORBENT ASSAY (ELISA)

To evaluate the anti-inflammatory activity of SLN-1, where $1x10^5$ HaCaT cells were seeded in 12-well plates and grown until 90 % confluency. Cells were induced to inflammation with TNFα 20 ng/ml for 6 h. Then SLN-1 were added to the culture medium at 10 µl of SLN-1 or SLN-2 (36 µg/µl). Cells stimulated only with TNFα were considered the positive control and untreated cells as the negative control. After 24 h incubation, the supernatants were collected and centrifuged (10,000 rpm for 5 min) at 4 ºC and stored at 80 ºC until use. Secreted levels of the pro-inflammatory cytokines IL-6 and IL-8 were quantified by enzyme-linked immunosorbent assay (ELISA) sets (BD Biosciences) according to manufacturer's instructions. The results were expressed as $pg \cdot ml^{-1}$.

8.10.9 CELLULAR UPTAKE STUDY

8.10.9.1 CHARACTERISATION OF SLN UPTAKE BY CONFOCAL MICROSCOPY

To assess the cellular internalization of the CHON-containing nanoparticles, dye-labeled SLN-1 and SLN-2 were prepared. SLN were prepared by adding 200 µl of 2 mg/ml Nile Red (EMD Millipore) in methanol solution, to the lipid matrix of SLN suspension before melting (222).

To assess internalization of SLN-1 and SLN-2, HaCaT cells and BJ cells, 300 µl of $1x10^5$ $cell \cdot ml^{-1}$ were grown in 8-well chamber slider (ibidi®) until approximately 80 % confluence and then incubated with 5 µl of SLN-1 or 1.2 µl SLN-2 (36 µg/µl) at 37 ºC for 1.5 h or 24 h. Non-internalized SLN were then removed by three PBS washes, then the plasmatic membranes of the cells were stained with wheat germ agglutinin (WGA) Alexa Fluor-488 (Molecular Probes) at 1 µg/ml for 25 minutes at 4 °C, cells were washed 3 times with PBS and were fixed with 3 % paraformaldehyde for 30 min at 25 °C. Subsequently, cells were washed 3 times with PBS and the nuclei were stained with 4',6-diamino-2-phenylindole dichlorate (DAPI) at 0.5 µg/ml for 15 minutes at 25 °C. Finally, cells were washed 3 times and mounting solution (PBS) was added for microscopic analysis. Images were acquired using a Leica TCS SP5 confocal laser scanning microscope (Leica Microsystems, Germany) with 63x oil immersion objective lens.

8.10.9.2 LIIPOPLEXES TRANSFECTION BY FLUORESCENCE MICROSCOPY

To confirm the ability of lipoplexes formed by SLN-4 or NLC-5 together with the plasmid EGFP (1:20 (w/w) of pDNA (1µg/µl):SLN-4 (36 µg/µl), to transfect murine immune cells in vitro, DC2.4 cells were transfected with lipoplexes for 72 h, and green fluorescent protein (EGFP) was visualized by fluorescence microscopy.

Briefly, DC2.4 cells were seeded onto 25 mm glass coverslips in a 6 well plate at a density of $3x10^5$ cells per well and incubated at 37 ºC in a 5% CO_2 humidified atmosphere for 24

h. Then, 20 ul of lipoplexe (1:20) was added to each well and incubated at 37 ºC for up to 72 h to allow cellular uptake of the lipoplexes and expression of green fluorescent protein (EGFP). Untreated cells and cells treated with plain SLN were used as a negative control and transfection with Lipofectamine® 2000 Transfection Reagent (1µg pDNA : 9µl lipofectamine) was used as positive control. Following incubation, the unbound SLN were removed by gentle washing with PBS three times. Cells were then fixed and permeabilized by adding 0.1% Triton X-100 with 4% PFA for 15 min. Subsequently, nuclear staining with DAPI was performed at room temperature for 15 min, followed by three washes with PBS. The coverslips were carefully mounted and sealed onto a glass slide using gold antifade reagent. Cellular imaging was performed using a Leica Epifluorescence microscope (Wetzlar, Hesse, Germany).

8.11 BIOPHARMACEUTICAL STUDIES

EX VIVO STUDY OF SKIN PERMEATION – DIFFUSION WITH FRANZ CELLS

The transdermal absorption of 1.0 ml of SLN of CHON, was estimated through an ex vivo permeation study, using porcine ear skin (n approx 5) with 0.6 mm thickness, with Franz-type diffusion Cells with a surface area of 0.64 cm^2 and receptor chamber capacity of 4.5 ml for all the mucous membranes, at 32 ºC.

Specimens Porcine ear skin were obtained ex vivo from female pigs (Landrace x Large White cross, 40–45 kg), resulting from surplus of surgical studies following the study protocol of the Animal Experimentation Ethics Committee of the University of Barcelona with ethics code 514/ 18. Animals were anesthetized with intramuscular (im) ketamine (3 mg/kg), xylazine (2.5 mg/kg), and midazolam (0.17 mg/kg) and, after the surgery practices, pigs received an intravenous (iv) overdose of sodium thiopental.

Immediately, porcine ear skin was excised, debrided in the laboratory to obtain the corresponding samples of tissues and frozen by placing them in containers with a phosphate buffered saline (PBS) mixture containing 4% albumin and 10% DMSO (as cryoprotective agents) and stored. at −80 °C in a mechanical freezer until their use. The day before their use, specimens were cut in 600 µm parallel slices with a mucotome GA 630 (Aesculap, Tuttlingen, Germany) (223–225)and mounted in vertical Franz-type cells of diffusion (Vidra Foc, Barcelona, Spain) to perform the ex vivo experiment (Figure 23).

8.11.1 PERMEATION TEST

In all, 1 ml of each sample was incubated in Franz cells and filled with MQH2O. In all experiments, a constant temperature, thermoregulated with a water jacket of 32° ± 0.5 °C was used, with agitation at 600 rpm. Samples were collected from the receiver compartment at 24 h. Sink conditions were maintained throughout the experiment.

To quantify the permeated amount of CHON in the tissues tested, drug concentration in receptor phase (water) was determined by a validated technique of UV-Vis detection (520 nm), using a Thermo Scientific Helyos B Uv-Vis Dual Beam Spectrophotometer. Transepidermal water loss values were used for skin integrity testing. The permeated amount of CHON at 24 h, expressed as percentage of CHON encapsulated, all the experiments were performed at least by quintuplicate, the results were also shown by median and range.

8.11.2 DRUG RETENTION INSIDE THE SKIN

At the end of the experiment, porcine ear skins were removed and cut according to the permeated area corresponding to 0.64 $cm^{2,}$ then carefully cleaned using a gauze soaked in a 0.05% solution of sodium lauryl sulphate, then washed with distilled water and blotted dry with filter paper. Then the skin was weighed and divided into smaller pieces, 1.2 ml of MQH2O water was added, it was sonicated for 20 minutes, it was centrifuged for 15 minutes at 12000 rpm and the supernatant was used for the analysis of the amount of CHON retained. on the skin. The amount of CP retained in each sample of skin (Qr, µg/cm^2/g) was estimated by a validated technique of UV-Vis detection (520 nm), using a Thermo Scientific Helyos B Uv-Vis Dual Beam Spectrophotometer. Transepidermal water loss values were used for skin integrity testing, and, all the experiments were performed by triplicate, the results were also shown by median and range.

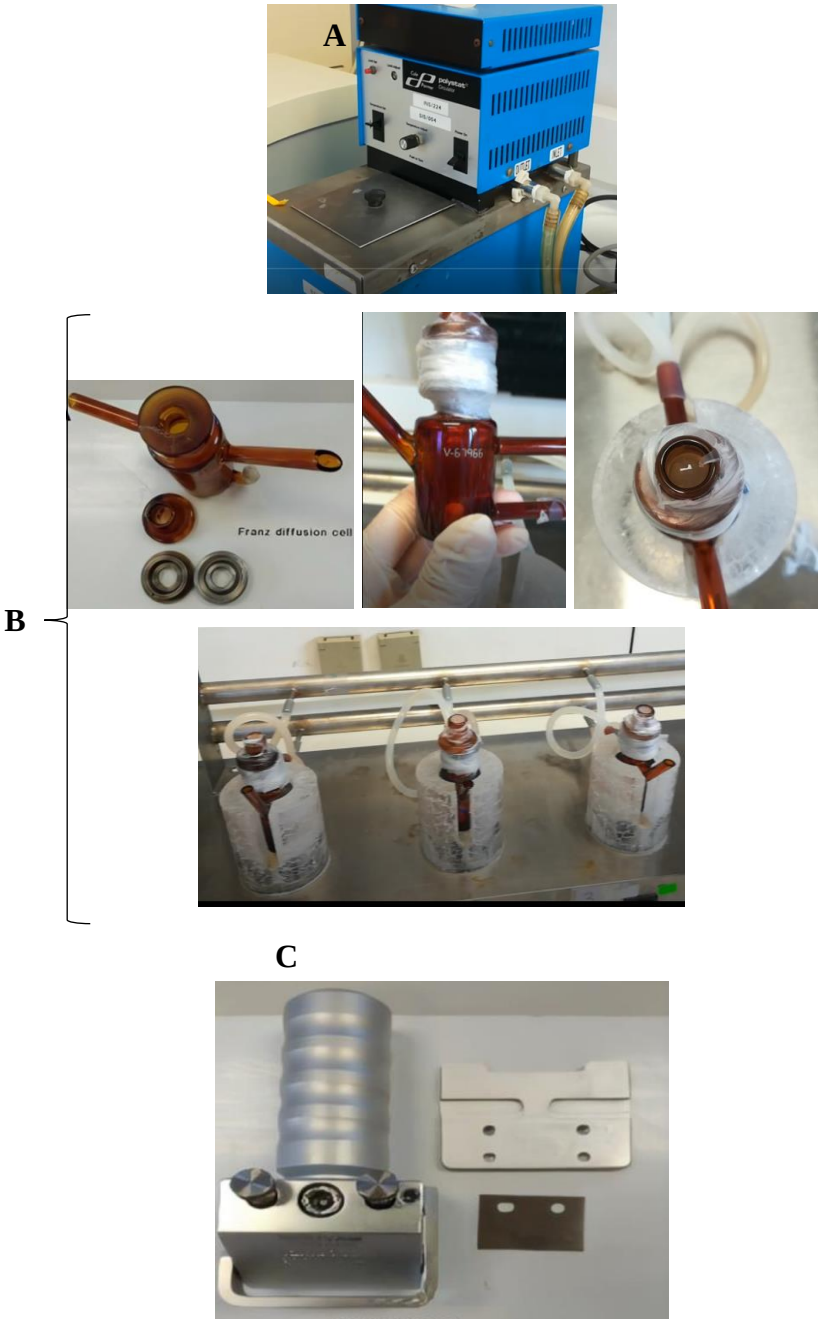

Figure 23. Tools used in permeation tests. Adapted from Gómez-Segura et al., 2020) (226). (A): Thermoregulator; (B): different parts that make up the instruments that house the Franz diffusion cell with its different components; and (C): Dermatome.

8.12 VALIDATION OF ANALYTICAL METHODS

A titration method and UV-Vis spectrophotometric method were validated to test entrapment efficiency of CHON. We evaluated the following parameters:

- Specificity
- Linearity
- Accuracy
- Precision
- Intermediate precision
- Robustness

8.12.1 SPECIFICITY – SELECTIVITY

An aliquot of the matrix, consisting of SLN prepared without CHON, was evaluated to determine if it consumed volume of the titrant or gave a spectrophotometric signal, depending on the method used.

For its part, for the spectrophotometric method, selectivity was determined in the presence or absence of possible interferences, evaluating samples containing CHON (0.4 mg/ml) in the presence of matrix (with interference) and samples of CHON (0.4 mg/ml) in aqueous medium. The discrepancy was calculated using the following formula (227):

$$\% \text{ discrepancy} = (Di - Ds)/ D_s * 100$$

Where:

D_i = mean response with interference

D_s = mean response without interference

The t test, for the significance of differences among experimental groups ($p< 0.05$) was obtained by Student'st test, and the percentage of discrepancy was established $\leq \pm 5\%$ as acceptable.

8.12.2 LINEARITY

Linearity of the CHON assay was calculated by analysis of three replicates of six matrix spiked with CHON at different concentrations (1.20, 1.00, 0.70, 0.40, 0.20, 0.10 mg/ml) by least square regression. The minimum acceptable Determination coefficient (R^2) to establish linearity was defined at 0.99 a priori.

8.12.3 ACCURACY

Accuracy was evaluated by performing the assay of samples and calculated the equivalence point of different samples by recovery method. Appropriate portions of CHON solution (1.0 mg/ml) were spiked into matrix to produce concentration of 80.0 to 120.0 % of target level (table 14). Accuracy was expressed as the percentage of CHON recovery and the acceptance criteria were defined as the relative standard deviation (RSD %) of the measurement, with a maximum limit of 5.3 according to OAAC (227) and an average recovery between 90.0 to 110.0 %.

Table 14. Composition of the samples spiked with matrix for the accuracy study.

Percentage (%)	**CHON concentration (mg/ml)**	**Matrix (ml)**	**CHON (1.0 mg/ml) (ml)**
120	0.48	10	10
100	0.40	8	12
80	0.32	6	14

8.12.4 PRECISION

Precision was calculated the EE% of 6 samples of CHON 1.0 mg/ml enriched with matrix and precision was defined as the relative standard deviation (RSD %) of the measurement, with a maximum limit of 5.3 according to OAAC (227).

8.12.5 INTERMEDIATE PRECISION

To determine the intermediate precision, 6 samples of CHON 1.0 mg /ml, enriched with matrix, on different days. The relative standard deviation (RSD %) was calculated and the maximum limit was 5.3 according to OAAC (227).

8.12.6 ROBUSTNESS.

Robustness of the proposed method was performed by keeping titration conditions constant with following deliberate variations. For the titration method, the following variations were evaluated: using two different titrant and changing in the titrant concentration from 1.0 mg/ml to 0.5 mg/ml.

In the case of robustness for the UV-Vis method, the response of samples from 80% to 100% of the 0.4 mg/ml concentration of CHON was evaluated at different wavelengths (517 nm - 520 nm - 523 nm). The response to varying the amount of sulfuric acid in the sample (4 ml - 5 ml - 6 ml) was also evaluated.

In summary, the table 15 shows the parameters and criteria established for the validation of the analytical methods used to determine the EE% of CHON in SLNs.

Table 15. Acceptance criteria for the validation of the analytical methods used for the determination of the % EE of CHON in SLN.

Parameters	**Acceptance requirements**
- Specificity	No interference with target / Discrepancy $\leq \pm 5\%$
- Linearity	R2 $\geq$ 0.99
- Accuracy	RSD < 5.3
	Average Recovery 90.0% to 110.0%
- Precision	RSD < 5.3
- Intermediate precision	RSD < 5.3
- Robustness.	Statistical test

RESULTS AND DISCUSSION

SLN PRODUCTION

1.Formulation of nanoparticles
2.Hot Microemulsion Method
3.Experimental Factorial Design
4.Stability Study - Lyophilization

SLN AS VEHICLE OF CHON - **PHYSICOCHEMICAL TECHNIQUES**

1. Morphological Analysis by Transmission Electron Microscopy (TEM)
2. Differential Scanning Calorimetry (DSC)
3. Determination Of Surface Charge (Zeta-Potential) And Particle Size
4. Viscosity Measurement
5. Scanning Electron Microscopy (SEM)
6. Atomic Force Microscopy (AFM)
7. X-Ray Diffraction (XRD)
8. High-Performance Liquid Chromatography (HPLC)
9. Titration Method
10. UV-Vis Spectroscopy Method

SLN AS VEHICLE OF CHON - **TECHNIQUES IN MOLECULAR AND CELLULAR BIOLOGY**

1. Cell Viability - Cytotoxicity (MTT)
2.Study of the anti-inflammatory activity
  1.RT-qPCR
  2.ELISA
3.Characterisation of SLN uptake by **Confocal Microscopy**

SLN AS VEHICLE OF CHON - **BIOPHARMACEUTICAL STUDIES**

1.Permeation test
2.Drug retention inside the skin

VALIDATION OF ANALYTICAL METHODS TO DETERMINE EE%

1. Specificity
2. Linearity
3. Accuracy
4. Precision
5. Intermediate precision
6. Robustness

SLN AS A VEHICLE OF pDNA

1.Morphological Analysis by Transmission Electron Microscopy (TEM)
2.Determination of Surface Charge (Zeta-Potential) And Particle Size
3.Plasmid preparation
4.Gel retardation assays
5.Cell viability - Cytotoxicity (MTT)
6. Confirmation of lipoplexes transfection by **Fluorescence Microscopy**

SLN PRODUCTION

In the characterization of solid lipid nanoparticles as a vehicle for biomolecules, the ability of SLN to encapsulate biomolecules was studied. On the one hand, we worked with chondroitin sulfate (CHON) (Figure 24) of bovine origin, supplied by the Bioiberica company, and we also evaluated the ability of SLN to transport pDNA, by forming lipoplexes that are capable of transfecting cells.

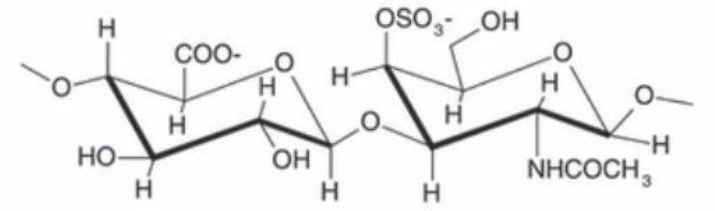

Figure 24. Molecular structure of the chondroitin sulfate biomolecule. Reproduced from Gandhi et al., 2008 (74).

The studies were carried out in different laboratories available at different stages of doctoral research. Most of the work was carried out in the research laboratories of the Faculty of Pharmacy and Food Sciences of the University of Barcelona, and in its final stage studies were carried out in the laboratory headed by Dr. Tang Bin, from the Department of Biomedical Engineering, Southern University of Science and Technology, Shenzhen, Guangdong, Republic of China, as well as in the Laboratory run by Dr. Peter Smooker of the School of Science, RMIT University, Bundoora, Australia.

9 SLN PRODUCTION

9.1 FORMULATION OF NANOPARTICLES

The formulation used for the manufacture of SLN as a CHON vehicle was the one proposed by Fábregas et al, 2017 (26). This formula results in solid cationic lipid nanoparticles, whose composition is based on neutral lipid component stearic acid, Poloxamer 188 as surfactant and octadecylamine as cationic lipid. Given the cationic characteristics of the formulation, it becomes a viable option to encapsulate CHON whose surface charge is negative, as well as a pDNA vehicle also with a negative charge, since in general the DNA molecule has a net negative charge (Figure 25), because the phosphates, which are part of the nucleotides that compose it, are arranged towards the outside of the double helix (228), therefore the union is facilitated by electrostatic interactions of cationic SLN with the nucleic acid and cell transfection can thus be achieved.

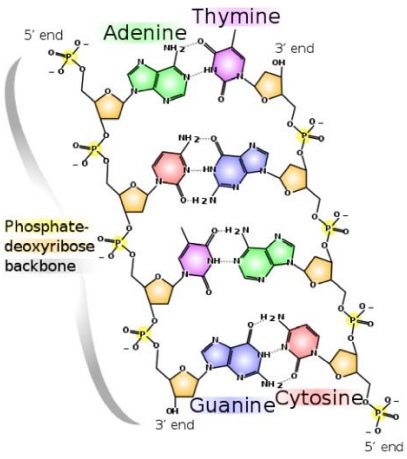

Figure 25. Structure of the DNA double helix. Reproduced from Gómez Ochoa, et al, 2019 (228). DNA presents a negative surface charge due to the phosphate anions that are arranged towards the outside of the molecule.

9.2 HOT MICROEMULSION METHOD

The hot microemulsion method (Figure 26) was used, both to manufacture the cationic SLN proposed by Fàbregas and other formulations containing changes in their composition, as shown in table 5 of the section *8.1.1 Hot Microemulsion Method of Methodology*. In total, 7 different formulations were manufactured, with the following acronyms or numbers to be recognized among them: SLN-1, SLN-2, NLC-3, SLN-4, NLC-5, 40/60, 70/30, and 95 /5.

The formulations SLN-1, SLN-2, NLC-3, 40/60, 70/30, and 95/5, were elaborated containing CHON, and were evaluated in different stages of the investigation to define the best combination of excipients in the formulation. SLN-4 and NLC-5 were used in the study of lipoplex formation and cell transfection.

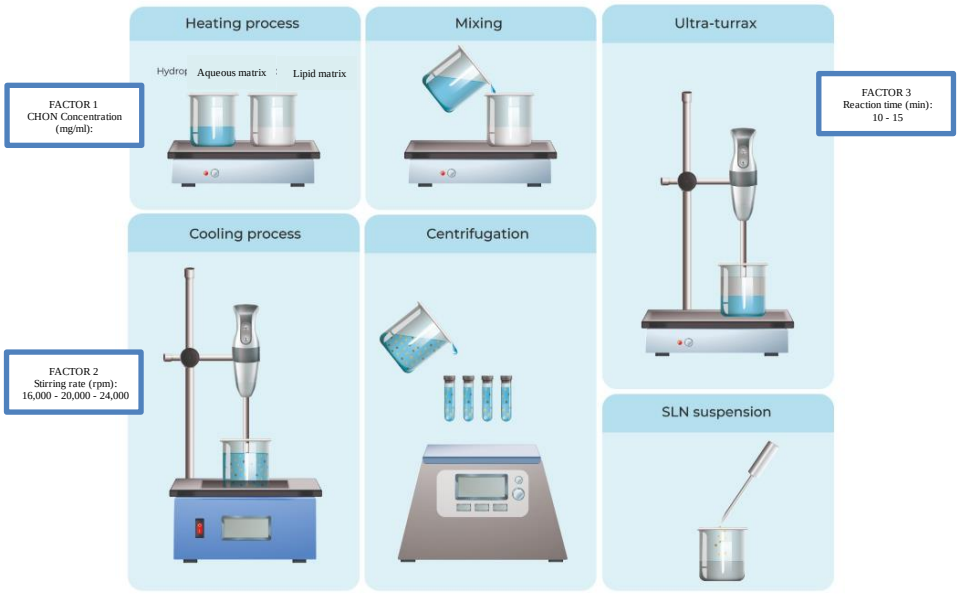

Figure 26. Schematic representation of Solid lipid nanoparticles with CHON, prepared by hot microemulsification process. Source: own elaboration. Production process of the SLN, a matrix lipid (stearic acid), a cationic lipid (octadecylamine), a surfactant (poloxamer 188) and the biomolecule under study (CHON), were used. In the process of optimizing the formulation, different parameters where evaluated.

For manufacturing, according to the method of Fábregas (26,29), a 43 to 48 µm filter was

used. The first thing that was optimized was the use of a double filter to improve the profile of nanoparticles in suspension. Therefore, from the preliminary study, the use of 2 filters was proposed, placing the 43 to 48 µm filter as the first filter in contact with the suspension, followed by a 7–9 µm filter. This change helped to reduce the presence of larger particles in the final formulation.

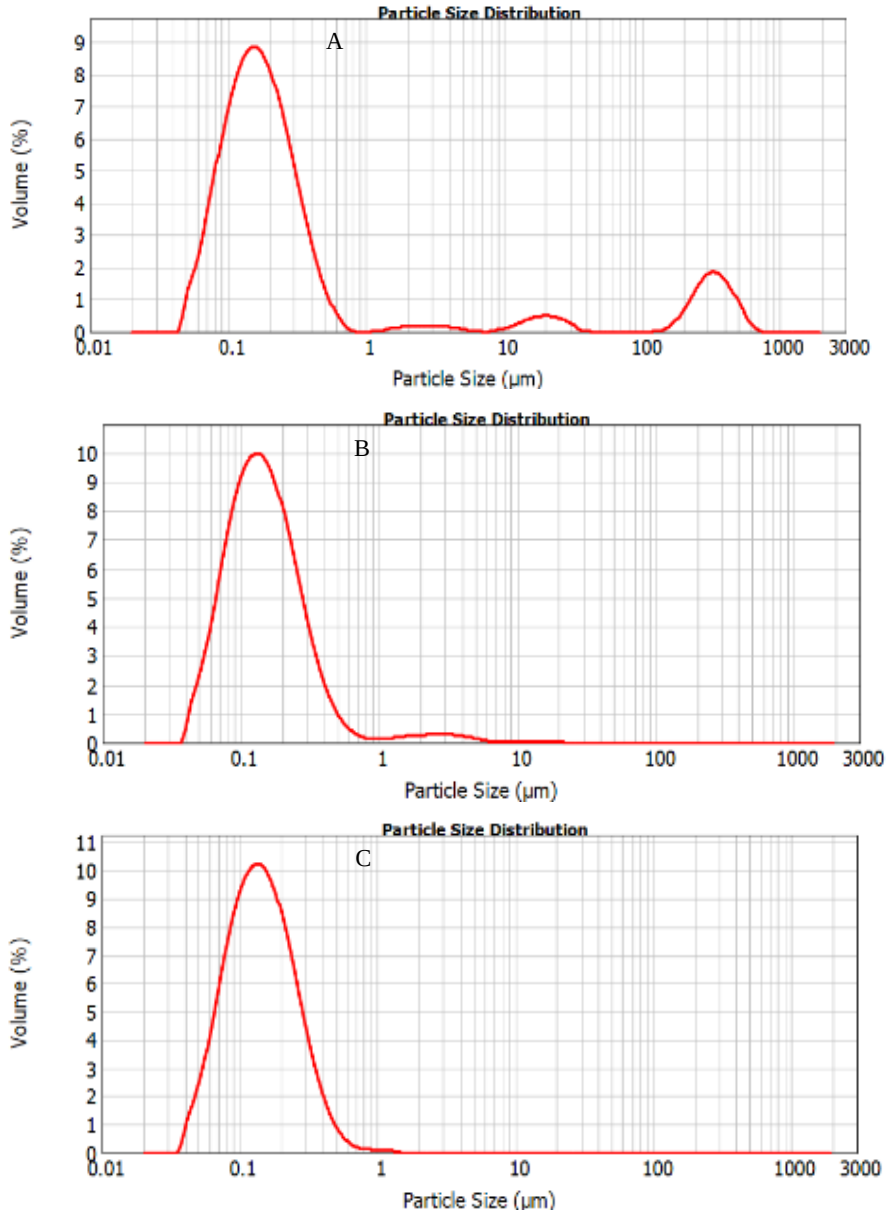

Figure 27. Optimization of the original SLN formulation by using an additional filter. Particle size distribution of (A) plain SLN filtered with a 43–48 µm filter, (B) plain

SLN filtered with a double filter, one 43–48 μm and one 7–9 μm, and (C) formulation of SLN-1 using a double filter, one from 43 to 48 μm and the other from 7–9 μm.

A decrease in the presence of aggregates is observed in figure 27, image A shows the size distribution of the nanoparticles filtered only with a 43 to 48 μm filter, with the presence of aggregates of more than 10 μm, while the images 2 and C have a more homogeneous size distribution, without the presence of aggregates with sizes greater than 10 μm, an improvement that was achieved by using 2 filters. In the subsequent formulations, two filters were used for the manufacture of nanoparticles.

9.3 EXPERIMENTAL FACTORIAL DESIGN (DOE)

To determine the best formulation to encapsulate CHON, a 3x3x2 full-factorial experimental design was proposed and different combinations of SLN were formulated in duplicate, each experiment evaluated in triplicate. The factors evaluated were Concentration (mg/ml), Stirring rate (rpm), and Reaction time (min) and the variables analyzed as results were defined as the percentage of CHON Encapsulation Efficiency, using a validated method of volumetric titration, as well as the Z Potential and the Size of the nanoparticles obtained. As shown in table 8 of the section *8.1.2 Experimental Factorial Designof the Methodology*, the criteria for choosing the best results include the highest Entrapment efficiency of CHON (EE%), a Zeta potential (mV) < -25 and Particle size (nm) the least size possible.

According to the DOE 3x3x2, with three factors at three and two levels, respectively (table 16), 18 combinations were established to study the proposed factors. The average of three measurements for each experiment, carried out in duplicate, is reported. The factors and levels are shown below, at the stage of the process involved.

Table 16. Experimental Factorial Design (3x3x2) for the optimization of the formulation of SLN-1 and the results obtained for each experiment analyzed.

Experiment	Concentration (mg/ml)	Stirring rate (rpm)	Reaction time (min)	EE %		Pot Z (mV)		Size (nm)		Size Johnson´s Transformation
				Mean	SD	Mean	SD	Mean	SD	
1	0,4	16000	10	48.24	1.21	-45.67	0.98	155.33	2.08	**1.62853**
2	0,4	16000	15	52.77	1.48	-41.67	0.72	136.67	0.58	**0.97257**
3	0,4	20000	10	59.57	1.27	-39.10	1.61	118.50	0.71	**-0.30277**
4	0,4	20000	15	55.16	0.55	-38.17	1.29	115.50	0.71	**-0.71042**
5	0,4	24000	10	56.80	0.00	-39.43	0.23	121.00	2.00	**-0.03776**
6	0,4	24000	15	53.37	0.02	-40.13	1.70	180.00	11.31	**1.69187**
7	0,7	16000	10	35.54	1.29	-47.53	1.10	147.50	0.71	**2.01961**
8	0,7	16000	15	44.27	0.00	-46.83	0.97	143.00	1.41	**1.23266**
9	0,7	20000	10	45.74	0.97	-41.90	0.44	123.00	0.00	**0.14203**
10	0,7	20000	15	33.15	0.05	-40.33	0.15	120.00	1.73	**-0.13758**
11	0,7	24000	10	30.34	0.06	-38.13	0.61	121.67	12.50	**0.02488**
12	0,7	24000	15	31.86	0.00	-44.83	0.40	121.50	2.52	**0.00949**
13	1,0	16000	10	22.67	0.62	-50.97	0.64	161.00	4.36	**1.77747**
14	1,0	16000	15	17.41	0.62	-48.03	1.40	127.00	8.66	**0.44232**
15	1,0	20000	10	25.44	0.00	-48.47	0.61	111.67	0.58	**-1.52134**
16	1,0	20000	15	22.23	0.00	-44.67	0.45	130.00	8.19	**0.63032**
17	1,0	24000	10	26.18	0.44	-49.73	0.90	129.67	7.51	**0.61069**
18	1,0	24000	15	41.17	0.03	-51.23	0.67	122.33	0.58	**0.08473**
19	0,4	16000	10	48.25	0.00	-36.63	0.31	139.00	2.83	**1.07435**
20	0,4	16000	15	59.85	1.49	-40.37	0.81	112.00	0.00	**-1.42783**
21	0,4	20000	10	63.01	0.00	-29.53	0.51	117.33	3.79	**-0.44696**
22	0,4	20000	15	51.38	0.60	-39.75	0.35	112.33	2.31	**-1.34042**
23	0,4	24000	10	52.77	1.05	-35.87	0.95	112.00	2.00	**-1.42783**
24	0,4	24000	15	55.91	0.00	-40.00	0.53	116.00	3.46	**-0.63329**
25	0,7	16000	10	30.80	0.00	-41.47	1.53	120.00	0.00	**-0.13758**
26	0,7	16000	15	39.99	0.44	-43.93	1.56	125.00	2.65	**0.30055**
27	0,7	20000	10	48.56	0.02	-46.03	0.86	130.00	1.41	**0.63032**
28	0,7	20000	15	33.85	0.36	-46.77	0.40	109.00	2.83	**-2.67674**
29	0,7	24000	10	29.48	0.72	-47.57	1.43	124.67	0.58	**0.27540**
30	0,7	24000	15	32.00	0.00	-44.37	0.15	117.67	3.21	**-0.40416**
31	1,0	16000	10	23.83	0.30	-51.70	0.50	143.67	0.58	**1.25732**
32	1,0	16000	15	18.73	0.00	-46.93	1.90	117.33	3.06	**-0.44696**
33	1,0	20000	10	25.27	0.29	-49.13	0.78	110.67	0.58	**-1.84872**
34	1,0	20000	15	19.83	0.85	-46.33	0.87	112.50	0.50	**-1.29876**
35	1,0	24000	10	25.31	0.00	-51.70	0.36	116.00	0.00	**-0.63329**
36	1,0	24000	15	39.77	0.88	-47.07	0.71	117.33	2.31	**-0.44696**

The table reports the mean and standard deviation for n=3 in each experiment.

Once the results of all the formulations proposed in the DOE were obtained, the statistical analysis of the data was carried out, to find the formulation with the best characteristics in terms of size, Z potential and efficiency in CHON encapsulation.

9.3.1 PREMISES EVALUATION - EXPERIMENTAL FACTORIAL DESIGN

To carry out the statistical analysis of the results, the statistical premises were first evaluated (Figure 28):

- Normality of residues
- Linearity
- Homoscedasticity
- Independence

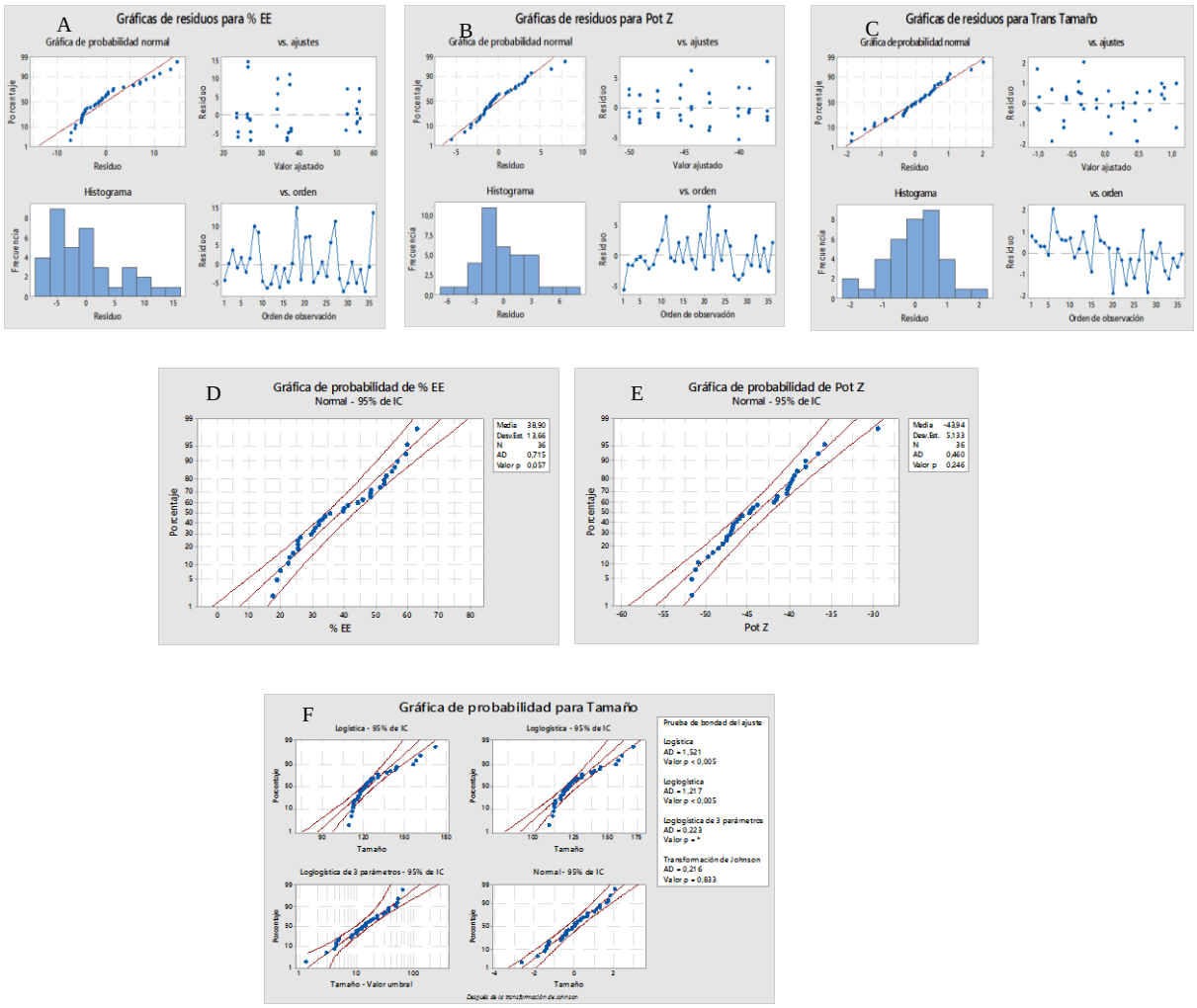

Figure 28. Plots of the DOE premises evaluation. Graphs A, B and C are used to evaluate the normality of the residuals, linearity, independence, and homoscedasticity. Graphs D, E and F help to assess the normality of the data, with a value of $p \geq 0.05$.

According to the previous figure, the statistical premises for the proposed model are met:

- **Normality of residuals and linearity:** it is shown when the residuals are aligned to the red line, in the upper left box of images A, B and C. images D, E and F show a p value greater than 0.05, indicating a normal distribution. In the case of the

evaluation of the size values, a Johnson transformation was required, image F, for which the transformed data, used in the statistical results, is reported in table 16.

- **Homoscedasticity:** The fitted value of the residuals shows values above and below zero, as shown in the second box at the top right of images A, B and C**.**

- **Independence:** when evaluating the residuals vs. order of observation, in the boxes at the bottom right of images A, B and C, there is no order that stands out, some pattern above or below, which indicates that there is independence.

The model met the statistical premises, so each factor proposed in the formulation was evaluated. The study of the impact of the factors on the results of the EE%, particle size and Zeta Potential, was evaluated using a Pareto Chart, Figure 29.

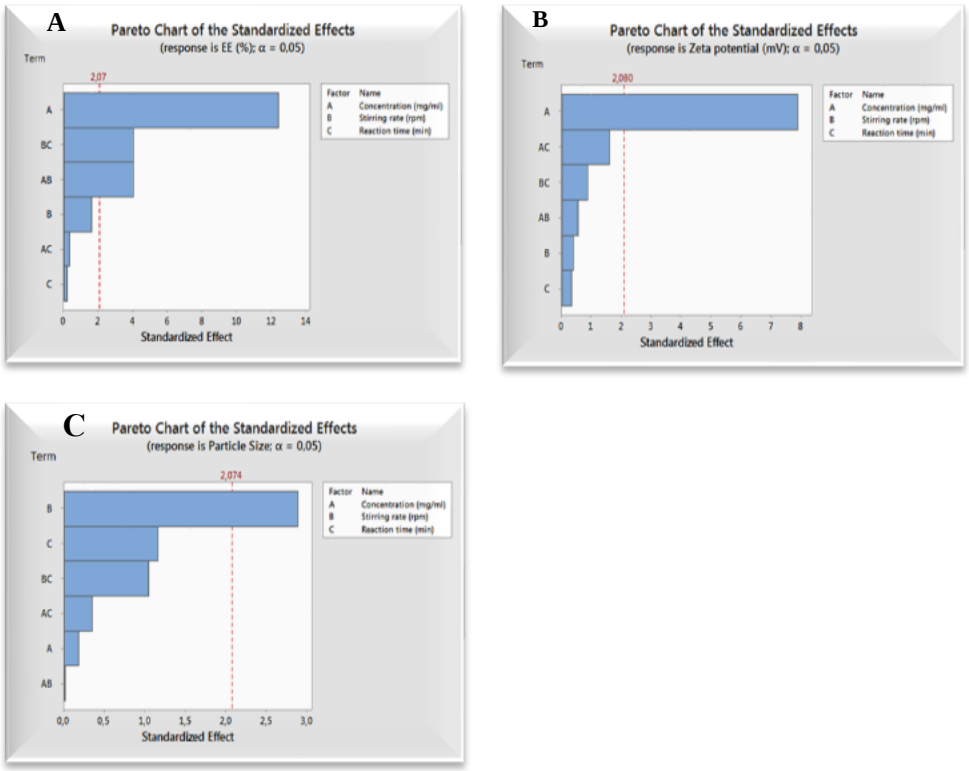

Figure 29. Pareto Chart of main effects in DOE. It is used to determine the magnitude and the importance of the effects in the responses. Bars that cross the reference line are statistically significant at the 0.05 level with the current model terms.

The main effects that are statistically significant ($\alpha = 0.05$) are those that exceed the intermittent vertical red line. The null hypothesis is that the coefficient of the term is equal to zero, which implies that there is no association between the term and the response.

Value $p \leq \alpha$: The association is statistically significant.

If the p-value is less than or equal to the significance level, there is a statistically significant association between the response variable and the term.

Value $p > \alpha$: The association is not statistically significant

If the p-value is greater than the significance level, it cannot be concluded that there is a statistically significant association between the response variable and the term.

The EE% is mainly influenced by the Concentration of CHON. However, the combination of factors such as: Stirring rate with the Concentration and Stirring rate with the Reaction time have an important effect, and they should be considered in the production of SLN (A). Only the factor Concentration is statistically significant for the zeta potential (B). Stirring rate is statistically significant for the Particle Size response (C).

To determine which level had a greater impact on the results, the main effects plot was used, as shown in Figure 30.

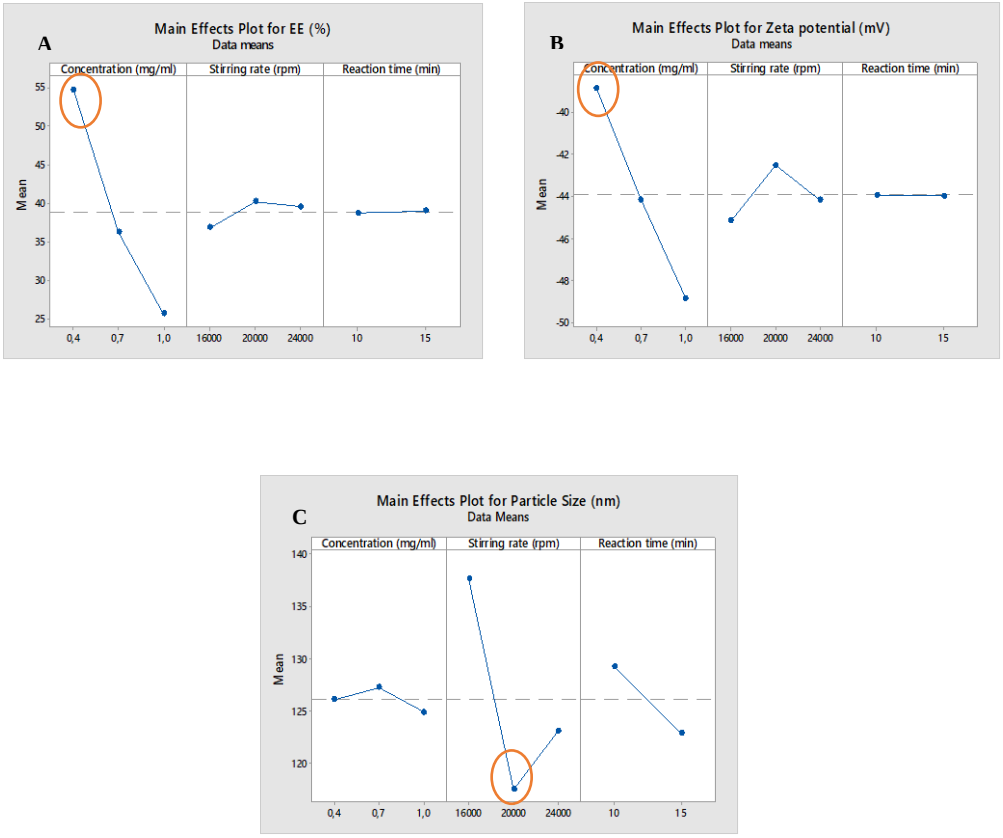

Figure 30. Graph of the main effects, according to the factors and levels defined in DOE.

The concentration level of 0.4 mg/ml is statistically significant to produce the highest EE% around 55 %. The level of Stirring rate of 20,000 rpm is the main effect for EE%. The reaction time is not statistically significant (A). Likewise, the 0.4 mg/ml level of concentration of CHON is a main effect for Zeta potential, with values around -40 mV.

The Stirring factors and the reaction time do not significantly influence the response (B). The particle size shows not statistically significant changes for the different levels of the factors: Concentration and Reaction time, however, the Stirring factor of 20,000 rpm, is

statistically significant to obtain particle size less than 120 nm (C). The two-way ANOVA results are statistically significant at the 0.05 level with the current model term.

Once the DOE is finished, the best conditions are established: use a CHON concentration of 0.4 mg/ml and use a speed of 20,000 rpm and a time of 10 minutes for the SLN manufacturing process. The summary of the optimal SLN that were obtained is shown in table 17.

Table 17. Factors and result of the best formulation obtained through the DOE.

CHON Concentration (mg/ml)	**Stirring rate (rpm)**	**Reaction time (min)**	**EE %**		**Pot Z (mV)**		**Size (nm)**	
			Mean	SD	Mean	SD	Mean	SD
0,4	20000	10	**61.29**	2.05	**-34.32**	5.35	**117.80**	2.77

The other DOE data can be seen in Annex 1, where the best fit equations and all the DOE details are included, together with the progressive exclusion of variables.

9.4 STABILITY STUDY - LYOPHILIZATION

To establish the stability of the nanoparticles, the determination of Surface Charge (Zeta-Potential) and Particle Size was performed. On the one hand, the stability of nanoparticles in aqueous medium and of the lyophilized nanoparticles was evaluated, as shown in Table 18. On the other hand, the stability of the lyophilized nanoparticles was monitored for up to 6 y 8 months.

Stability of fresh nanoparticles was evaluated at different temperatures: 4 °C, room temperature and 37 °C. The evaluated nanoparticles were SLN-1, SLN-2 and NLC-3, which were stored in hermetically sealed glass vials. This last formulation was also

manufactured by the sonication method, explained in the section *8.1.1 Hot Microemulsion Method of Methodology*. The sonication method was briefly evaluated as an alternative possibility to the method used in the other formulations.

As observed in the results of Table 18, for the initial formulation exposed by Fábregas, the formulation presents a progressive increase in the size of the nanoparticles but more stability at 37 °C, since at room temperature after 3 days it observed particle sizes around 663 nm, and for 4 °C, after 7 days. The Z Potential is maintained in the tens of -40 mV.

In the case of the SLN-2 formulations, the stability data show the presence of nanoparticles at the 3 temperatures evaluated, up to 28 days after their manufacture. Being that Cholesteryl oleate gives greater stability to the formulation over time. The surface charge ranges from -25.8 to -51.6 mV, apparently not affecting the presence of nanoparticles smaller than 200 nm.

NLC-3 show greater stability compared to SLN-1 and less stability compared to SLN-2. At 4°C, nanoparticles smaller than 150 nm are obtained up to 7 days after their manufacture, while at room temperature a progressive increase in size is observed, but even 63 days later, the nanoparticles have a size of less than 300 nm. The 37 °C temperature provided an adequate medium to maintain nanoparticles smaller than 200 nm up to 63 days after manufacturing. The Z potential ranges from -31.5 to -50.9 mV.

The NLC-3_Sonicated Formulation, maintain the same ingredients as the NLC-3, with certain variants in its manufacture, mainly the use of a sonicator instead of ultraturrax and the initial mixture of all the components in the same container. Its stability behavior is similar to that of NLC-3, with a stability of 14 days at 4 °C, presenting nanoparticles of 162 nm and with average sizes of 135 and 117 nm at room temperatures and 37 °C respectively. Up to 28 days into the study, nanoparticles smaller than 150 nm and Z potentials between -27.9 and -51.2 mV are obtained. The sonication technique allowed

obtaining stable nanoparticles like NLC-3 manufactured by the original method studied and with similar sizes.

The temperature of 4 °C is the least favorable for the stability of the nanoparticles in an aqueous medium, while, except for SLN-1 whose stability is limited to 2 days at room temperature, in general room temperature is favorable in intervals less than 28 days old and a temperature of 37 °C presents a more homogeneous size profile in the study of stability over time.

Table 18. Particle size (nm) and Z Potential (Mv) in the study of stability of nanoparticles in aqueous medium.

SLN-1												
	Temperature 4 °C				Room temperature (RT)				Temperature 37 °C			
	Size (nm)				Size (nm)				Size (nm)			
Day	D[3,2]	SD	Pot Z	SD	D[3,2]	SD	Pot Z	SD	D[3,2]	SD	Pot Z	SD
0	**114**	1.1	**-40,0**	0.5	**114**	1.1	**-40,0**	0.5	**114**	1.1	**-40,0**	0.5
1	**138**	2.3	**-45,0**	0.3	**271**	5.0	**-45,3**	0.7	**123**	2.0	**-40,1**	0.3
2	**126**	4.4	**-46,2**	0.6	**274**	22.3	**-46,3**	0.2	**149**	6.1	**-40.3**	0.5
3	**163**	2.4	**-46,2**	0.8	**663**	32.6	**-47,6**	0.9	**191**	63.5	**-41.2**	0.4
6	**209**	6.1	**-49,1**	0.9	**39000**	336.5	**-45,5**	0.2	**229**	58.7	**-42.8**	1.1
7	**616**	28.5	**-46,5**	0.5	**43000**	3265.4	**-44,4**	0.3	**278**	31.1	**-44.8**	0.9
9	**1335**	216.6	**-45,9**	1.0	**47000**	3413.8	**-45,6**	0.5	**336**	35.9	**-44.6**	0.6
SLN-2												
	Temperature 4 °C				Room temperature (RT)				Temperature 37 °C			
	Size (nm)				Size (nm)				Size (nm)			
Day	D[3,2]	SD	Pot Z	SD	D[3,2]	SD	Pot Z	SD	D[3,2]	SD	Pot Z	SD
0	**124**	1.5	**-46.9**	0.5	**124**	1.5	**-46.9**	0.5	**124**	1.5	**-46.9**	0.5
3	**129**	2.9	**-50.0**	0.2	**118**	0.6	**-49.8**	0.5	**128**	12.7	**-51.3**	0.3
7	**129**	2.8	**-48.1**	1.4	**125**	3.2	**-51.6**	1.0	**125**	3.2	**-48.4**	0.2
14	**124**	2.6	**-50.8**	0.2	**127**	2.3	**-47.6**	1.7	**131**	10.4	**-40.4**	1.0
21	**143**	1.7	**-26.9**	0.4	**130**	3.1	**-47.6**	0.7	**123**	2.9	**-45.4**	1.0
23	**128**	2.0	**-31.4**	0.7	**130**	3.5	**-25.8**	0.9	**162**	21.2	**-48.5**	1.2
28	**213**	4.5	**-48.1**	0.8	**128**	1.7	**-42.4**	0.7	**139**	1.0	**-47.1**	1.2
NLC-3												
	Temperature 4 °C				Room temperature (RT)				Temperature 37 °C			
Day	Size (nm)				Size (nm)				Size (nm)			
	D[3,2]	SD	Pot Z	SD	D[3,2]	SD	Pot Z	SD	D[3,2]	SD	Pot Z	SD
1	**117**	2.1	**-42.0**	1.0	**117**	2.1	**-42.0**	1.0	**117**	2.1	**-42.0**	1.0
7	**135**	8.7	**-45.8**	1.9	**139**	0.6	**-47.8**	0.8	**133**	32.1	**-47.5**	1.0
14	**665**	30.6	**-40.7**	0.3	**141**	7.2	**-50.9**	0.6	**210**	16.5	**-48.6**	1.0
21	**76967**	2388.0	**-31.5**	1.0	**155**	14.1	**-49.2**	0.5	**117**	7.5	**-46.9**	0.9
29	**41779**	11498.0	**-34.0**	2.0	**191**	23.1	**-45.4**	0.3	**116**	7.5	**-46.0**	0.4
35	-	-			**240**	12.3	**-43.3**	0.3	**118**	9.9	**-45.8**	1.0
63	-	-			**295**	10.5	**-41.0**	0.4	**176**	20.1	**-47.4**	0.4

Table continues in the following page.

NLC-3_SONICATED FORMULATION												
	Temperature 4 °C				Room temperature (RT)				Temperature 37 °C			
	Size (nm)				Size (nm)				Size (nm)			
Day	D[3,2]	SD	Pot Z	SD	D[3,2]	SD	Pot Z	SD	D[3,2]	SD	Pot Z	SD
0	**117**	2.5	**-44.1**	0.2	**117**	2.5	**-44.1**	0.2	**117**	2.5	**-44.1**	0.2
3	**163**	21.1	**-48.5**	0.8	**137**	15.5	**-47.7**	0.1	**143**	23.1	**-46.5**	0.4
7	**143**	17.0	**-47.5**	0.3	**138**	4.0	**-51.2**	1.1	**135**	8.1	**-47.1**	0.8
14	**162**	11.4	**-42.3**	0.2	**150**	29.2	**-46.0**	1.2	**133**	4.0	**-45.4**	0.2
21	**40424**	27805.0	**-33.9**	1.6	**145**	10.4	**-39.3**	0.6	**147**	26.6	**-32.6**	1.1
28	**89587**	5912.0	**-27.9**	0.3	**135**	3.6	**-39.3**	0.4	**117**	0.6	**-39.0**	0.6

Table 19. Measurement of the particle size and Z potential of lyophilized nanoparticles, after different storage times at room temperature.

SLN-1				
Date / Condition	**Size (nm)**	**SD**	**Pot Z**	**SD**
Day 1_aquous medium	114	1.1	-40	0.5
Day 1_Freeze-dried	183	43.3	-39.3	1.2
Month 6_Freeze-dried	164	24.7	-43.8	1.7
Month 8_Freeze-dried	391.2	4.9	-32.55	1.08
SLN-2				
Date / Condition	**Size (nm)**	**SD**	**Pot Z**	**SD**
Day 1_aquous medium	124	1.5	-46.9	0.5
Day 1_Freeze-dried	137	4.2	-33.2	0.6
Month 6_Freeze-dried	179	9.3	-25.8	0.7
Month 8_Freeze-dried	400.7	4.9	-22.76	1.29
NLC-3				
Date / Condition	**Size (nm)**	**SD**	**Pot Z**	**SD**
Day 1_aquous medium	117	2.1	-42	1
Day 1_Freeze-dried	116	2.8	-35.3	0.5
Month 4_Freeze-dried	134	45.1	-31.9	0.15
Month 6_Freeze-dried	199.2	0.5	-16.65	0.56
SLN-4				
Date / Condition	**Size (nm)**	**SD**	**Pot Z**	**SD**
Day 1_aquous medium	135	11.6	28.1	0.4
Day 1_Freeze-dried	210	1.7	27.3	0.6
Month 4_Freeze-dried	188	0.6	26.1	0.6
Month 6_Freeze-dried	140	1.1	39.8	0.6
NLC-5				
Date / Condition	**Size (nm)**	**SD**	**Pot Z**	**SD**
Day 1_aquous medium	126	17.1	31.4	1.2
Day 1_Freeze-dried	201	41.0	33.9	1
Month 4_Freeze-dried	159	18.3	36.3	0.6
Month 6_Freeze-dried	162	0.8	46	1.5

The lyophilized nanoparticles were kept in hermetically closed vials with an elastomeric stopper and an aluminum cap. Considering that lyophilization provides greater stability to the nanoparticle formulation over time, and that it was necessary to transport the samples for analysis in other laboratories, they were kept at room temperature and the size and Z potential over time and before their use were measured. Table 19 lists the values obtained at different time intervals, depending on the nanoparticle studied. Formulations SLN-1, SLN-2, NLC-3, SLN-4 and NLC-5 present average particle sizes between 114 and 400 nm, measuring their values up to 6 and 8 months after manufacturing.

SLN-1 and SLN-2 present particle sizes around 400 nm after 8 months of lyophilization; however, this variation with respect to the previous values found, may be due to the equipment used, or to the fact that they were not completely resuspended and not wait the necessary time for the separation of the nanoparticles in the aqueous suspension, since if we compare the values with those found 11 months later and measured with the Nanoparticle Tracking Analysis (NTA) technology, Table 20, the average size values are around 250 nm. Likewise, an increase in the mean values of size with storage time is observed.

Table 20. Measurement of the particle size of lyophilized nanoparticles, after several months of manufacture and using the Nanoparticle Tracking Analysis software.

Sample	**Place / Time in months**	**Mean (nm)**	**D90 (nm)**	**Concentration (particle/ml)**
SLN-1	Barcelona / 4	149.2 ± 4.5	215.3 ± 12.8	1.55x10^11 ± 1.40x10^10
	Melbourne / 11	152.7 ± 2.0	267.1 ± 9.0	8.87x10^9 ± 1.41x10^8
SLN-2	Barcelona / 4	235.0 ± 3.4	319.9 ± 12.1	4.30 x10^11 ± 1.06 x10^10
	Melbourne / 11	276.4 ± 5.9	377.6 ± 18.2	1.59x10^11 ± 7.18x10^9
NLC-3	Barcelona / 2	157.8 ± 5.3	229.5 ± 6.8	3.63x10^11 ± 2.00x10^10
	Melbourne / 9	219.3 ± 2.6	277.8 ± 5.8	9.94x10^10 ± 3.73x10^9
SLN-4	Barcelona / 2	231.9 ± 0	327.5 ± 0	4.52x10^11 ± 0
	Melbourne / 9	251.6 ± 3.0	314.9 ±4.8	2.58x10^11 ± 1.73x10^10
NLC-5	Barcelona / 2	179.3 ± 0	328.9 ±0	2.14x10^11 ± 0
	Melbourne / 9	183.3 ± 1.3	267.1 ± 6.0	1.11x10^11 ± 4.19x10^9

Nanoparticle follow-up analysis (NTA) was also performed for formulations SLN-1, SLN-2, NLC-3, SLN-4 and NLC-5, on 2 separate occasions since their manufacture, either at 2 or 4 months or, at 9 or 11 months. The mean sizes in all cases remain with very small variations from one measurement to another, showing nanoparticles of mean size, in the range of 149.2 to 276.4 nm.

This technique, in particular, measures the concentration of particles per milliliter of suspension and in all cases, both the first and the second measurement, the concentration of the nanoparticles is in the 10^11 power, except for the SLN-1 and NLC-3 formulations. that a slight decrease in the nanoparticle count was observed with time and an increase in their size.

SLN-1 **NLC-5**

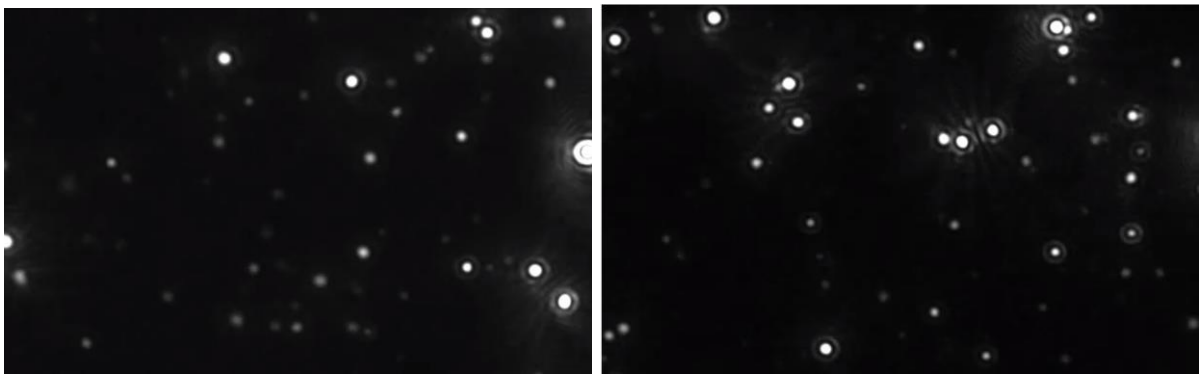

Figure 31. Image capture from a video of nanoparticles in Brownian motion by NTA. SLN-1 nanoparticle with carga superficial negative y NLC-5 con carga superficial positiva.

Figure 31 shows, in an illustrative way, a screenshot of a specific moment of the videos taken by NTA, in the analysis and counting of nanoparticles. The white circles correspond to the individual particles that are the nanoparticles, on the one hand SLN-1 with a negative surface charge and NLC-5 with a positive surface charge. The NTA allows observing the movement in each formulation, through a video of the analyzed sample. See Annex X.

From the stability study we have that lipid nanoparticles are highly diverse in size, due to their affinity for electrostatic interaction and aggregation. There are numerous variables that can cause high variability in SLN size, particularly the concentration of lipid species used, storage temperature, and method of synthesis (186,229).

SLN AS VEHICLE OF CHON-PHYSICOCHEMICAL TECHNIQUES

10 SLN AS VEHICLE OF CHON - PHYSICOCHEMICAL TECHNIQUES

VISUALITZACIÓN DE LAS NANOPARTÍCULAS

The nanoparticles obtained were observed by transmission electron microscopy (TEM) and scanning electron microscopy (SEM).

10.1 SCANNING ELECTRON MICROSCOPY (SEM)

Previous studies

To visualize the morphology and size of the SLN with CHON, the SEM technique was used at different concentrations of CHON in the nanoparticles. In the preliminary study, lyophilized samples with and without cryoprotectant (5% Trehalose) were used and finally the fresh sample was evaluated at the concentration defined as optimum in the manufacture of SLN.

A - Freeze-dried samples – without cryoprotectant

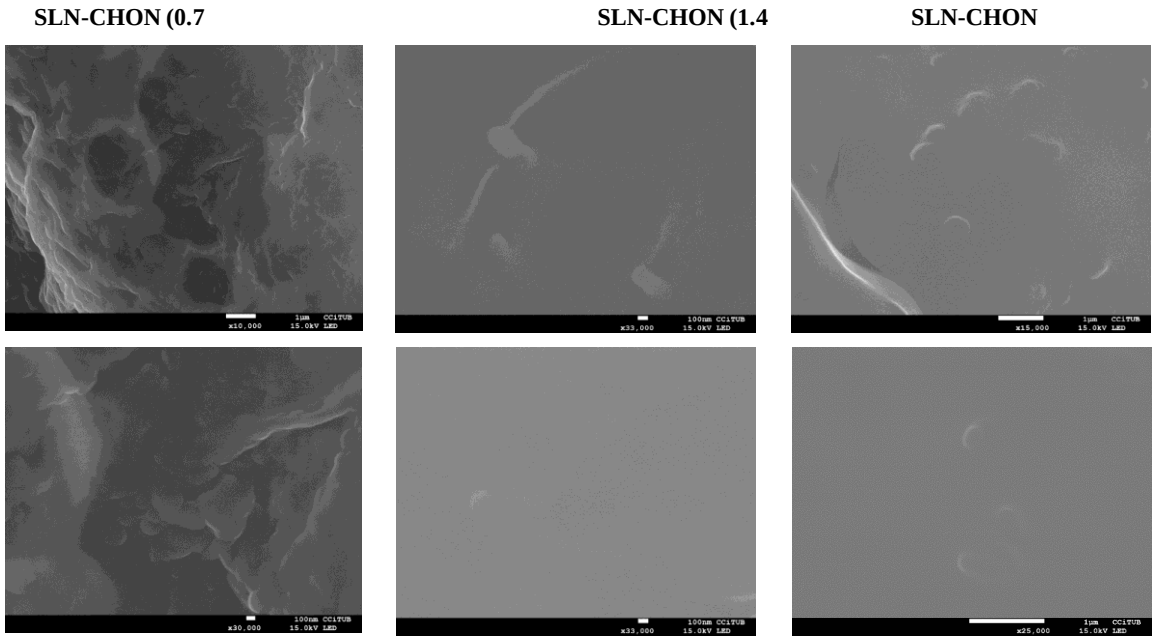

B - Freeze-dried samples – with cryoprotectant

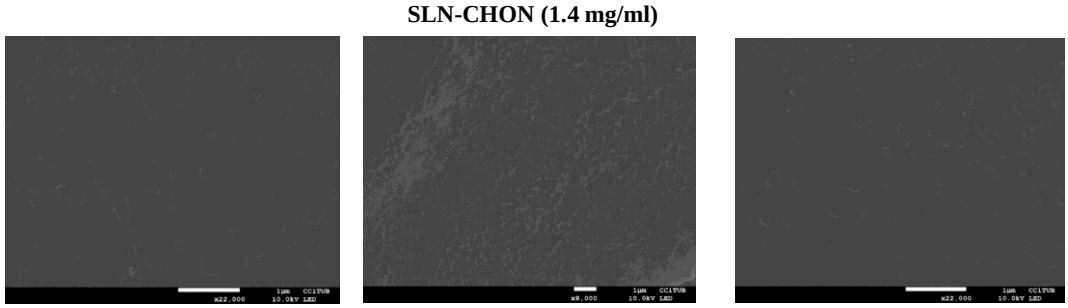

C - Fresh samples – without cryoprotectant

Figure 32. SEM images of SLN with CHON. A represents lyophilized samples without cryoprotectant, B lyophilized samples with cryoprotectant and C fresh samples without

cryoprotectant, nanoparticles with sizes of 127 nm and 92 nm are appreciated. Scale bar 1 μm and 100nm.

When carrying out the morphological study through SEM, difficulty was found in achieving an adequate visualization of the nanoparticles with lyophilized samples, both with or without cryoprotectant and using different concentrations of CHON in the nanoparticles, images A and B of figure 32. Therefore, fresh samples were used to analyze the final formulation of SLN with CHON (SLN-1), and as shown in figure 32, images C, nanoparticles of different sizes were found, including 127 nm and 92 nm.

In the case of the SLN encapsulating CHON, the characterization by SEM is preferable to carry out with fresh samples of the nanoparticles, without the presence of cryoprotectants.

10.2 MORPHOLOGICAL ANALYSIS BY TRANSMISSION ELECTRON MICROSCOPY (TEM)

Previous studies

To assess the morphology and size of the SLN with CHON, the TEM technique was also used. First, the quality of the images was evaluated using deposition or negative staining.

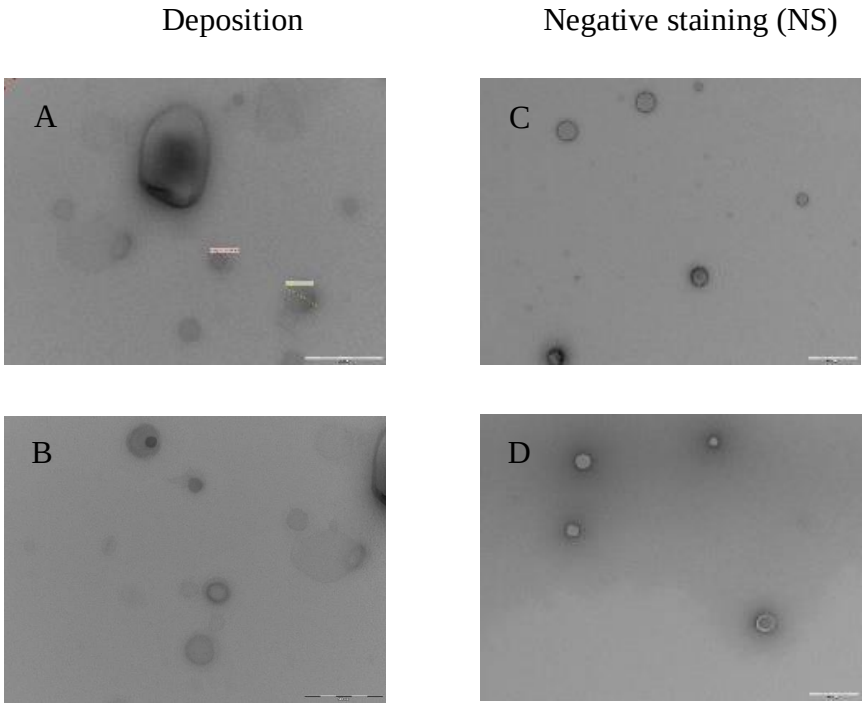

Figure 33. TEM images of SLN with CHON in aqueous medium. Images A and B on the left were obtained using the deposition technique, in image A, the measurement of 2 nanoparticles is shown, in red the diameter was 165.98 nm and in yellow 236.73 nm. For images C and D, the negative staining technique with 2% uranyl acetate was used. Scale bar 500nm.

When observing the images in figure 33, it is found that negative staining generates more defined and clear images than TEM images after deposition of SLN.

Evaluation of the formulations in the DOE

Considering that the concentration was a critical factor and once it was defined that the reaction time was not a critical factor and that the speed of 20,000 rpm was adequate, 3 formulations were manufactured using the CHON concentrations evaluated in the DOE, to optimize the process. used the shortest reaction time (10 min), to evaluate the morphology of the nanoparticles (figure 34).

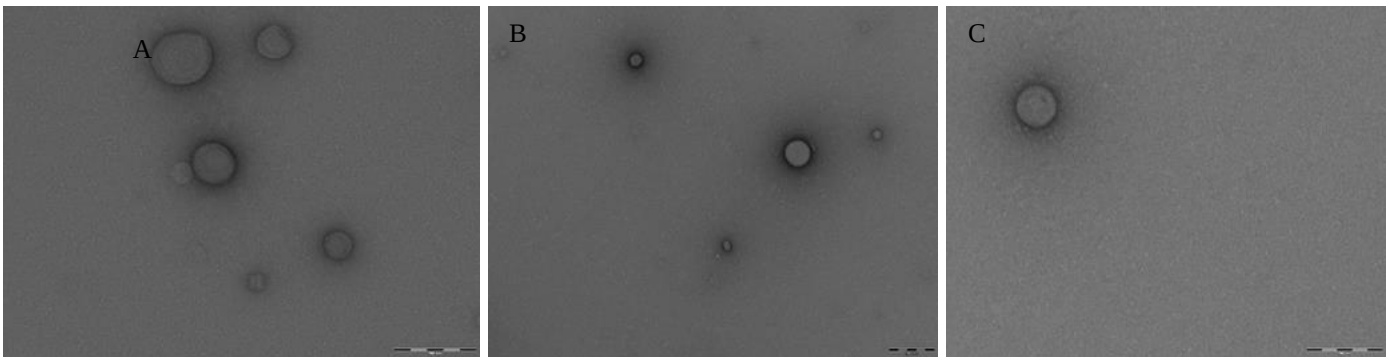

Figure 34. TEM images of SLN with CHON in aqueous medium as part of DOE study. Different concentrations were used of CHON. A) 0.4 mg/ml of CHON, B) 0.7 mg/ml of CHON and C) 1.0 mg/ml of CHON. Scale bar = 200 nm.

The morphology of the nanoparticles was analyzed through transmission electron microscopy (TEM). Images reveal that the nanoparticles showed spherical morphologies and the observed particle size remained around 150 nm in average diameter for the three concentrations studied. These findings confirm the average scores obtained for the formulations manufactured at the DOE.

The morphology of the different formulations was compared through the images obtained by TEM and the characterization of the size profile was performed by Atomic Force Microscopy.

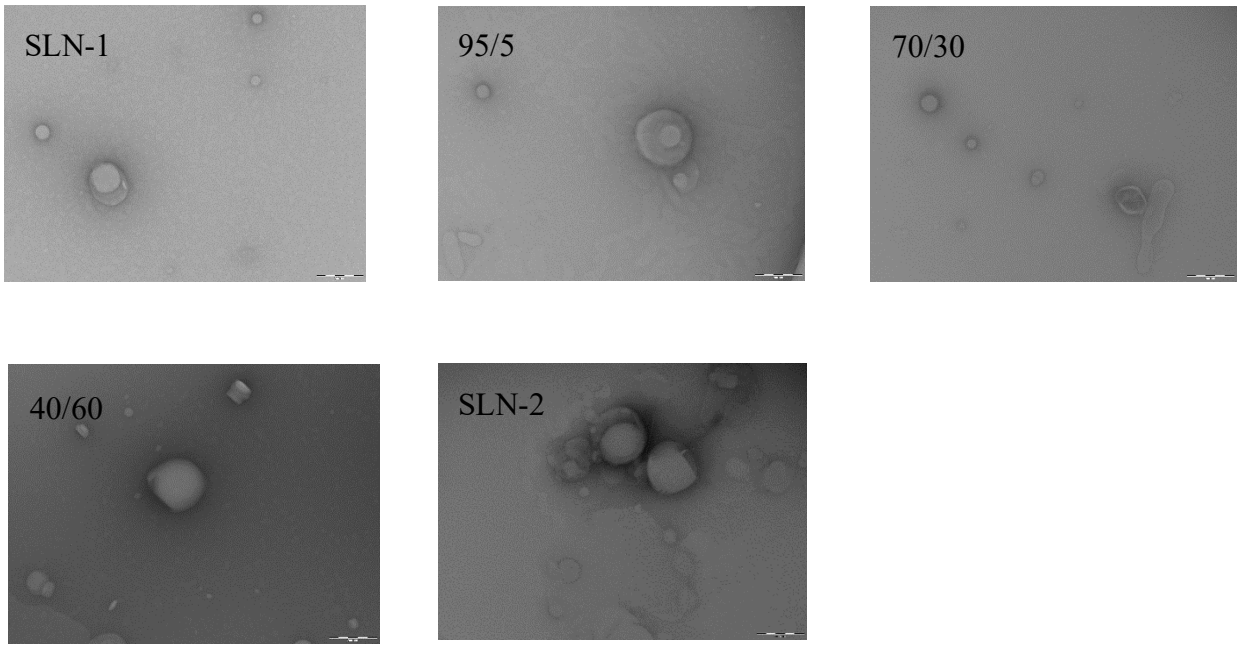

Figure 35. TEM images of different formulations of SLN containing CHON, in aqueous medium. Using the optimal conditions according to the DOE, several formulations were studied by TEM. Scale bar = 200 nm.

In all the formulations, circular nanoparticles with various sizes were observed, obtaining sizes smaller than 200 nm with a greater presence in the 70/30 formulation (Figure 35). SLN generally range in size from 10-1000 nm and are submicron colloidal carriers composed of physiological lipids, dispersed in an aqueous surfactant solution or in water (Mukherjee et al., 2009).

10.3 MORPHOLOGICAL ANALYSIS BY ATOMIC FORCE MICROSCOPY (AFM)

The AFM technique was used to characterize and confirm the morphology of the nanoparticles under study. This analysis allowed us to observe not only the image in two dimensions, but also to profile the height and diameter of the particles, as well as see the morphology in three dimensions.

As can be seen in Figure 36, the height profile and morphological visualization by AFM, were made to the formulations SLN-1, SLN-2, 40/60, 70/30, 95/5. The nanoparticles were evaluated freshly manufactured and in an aqueous medium. The first column corresponds to the two-dimensional images, and the particles in turquoise color correspond to the nanoparticles used to create a height and size profile per formulation.

The nanoparticles remain in the range of less than 200 nm in diameter, except for SLN-2 whose morphology showed a mean size of 285.3 nm. In all cases, nanoparticles with heterogeneous sizes and varied shapes are observed, with a predominance of circular shapes. The average heights found range from 11 nm for the 70/30 formulation, which in turn presents the smallest size of the nanoparticles, with an average of 81 nm, to the highest average height for the nanoparticles of the 40/60 formulation with 35 nm.

Formulation	2D Image	Height Profiles	3D Image

SLN-1

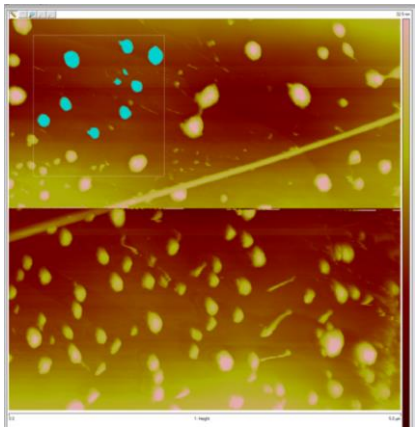

Parameter	Mean	Minimum	Maximum
Total Count:	10	10	10
Height (nm):	24.47	11.936	37.326
Diameter (nm):	143.134	58.309	204.081

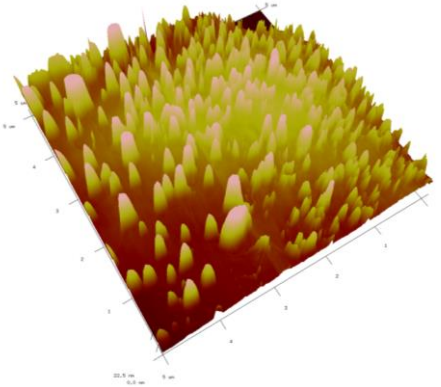

SLN-2

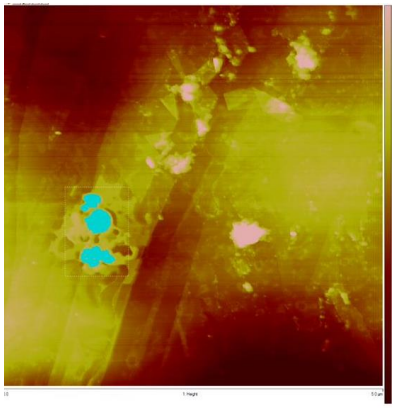

Parameter	Mean	Minimum	Maximum
Total Count:	3	3	3
Height (nm):	17.248	15.493	18.904
Diameter (nm):	285.294	222.307	318.800

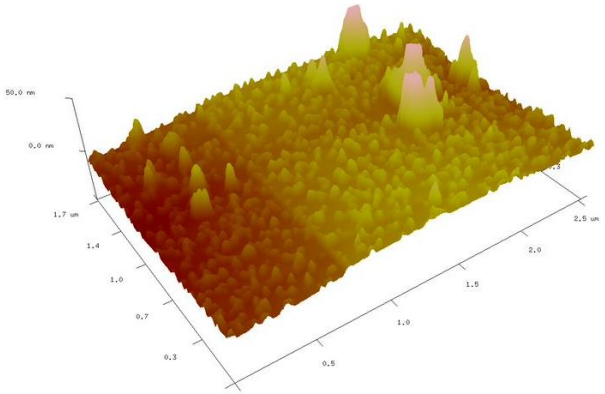

Figure continues in the following page.

Formulation	2D Image	Height Profiles	3D Image

40/60

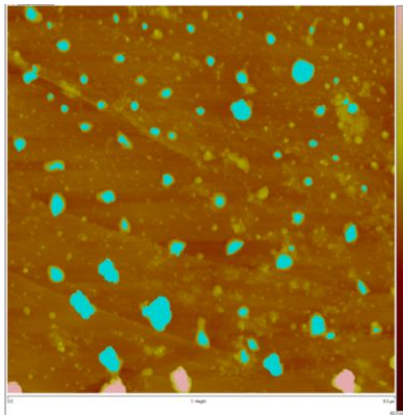

Parameter	Mean	Minimum	Maximum
Total Count:	63	63	63
Height (nm):	34.496	18.532	126.381
Diameter (nm):	124.255	55.097	365.636

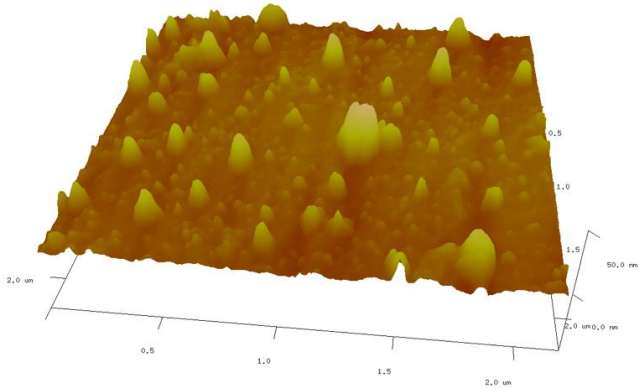

70/30

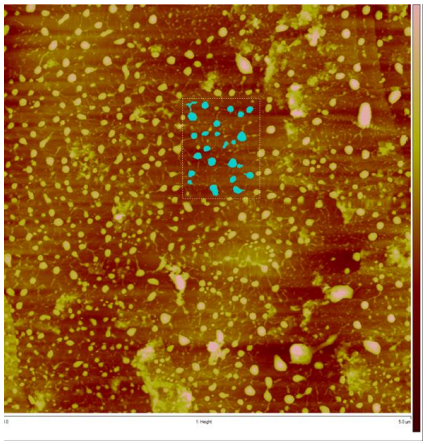

Parameter	Mean	Minimum	Maximum
Total Count:	24	24	24
Height (nm):	10.735	6.061	14.598
Diameter (nm):	81.299	55.097	112.376

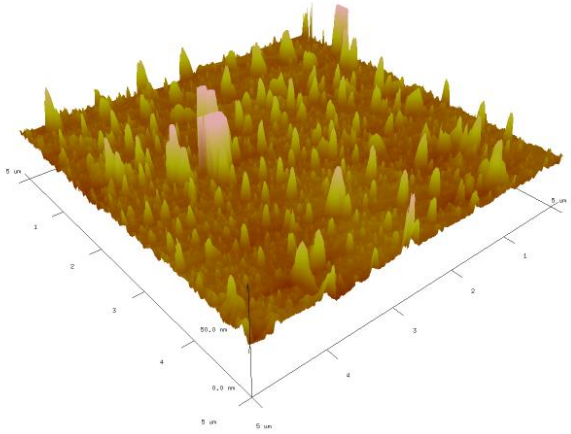

Figure continues in the following page.

Formulation	2D Image	Height Profiles	3D Image

95/5

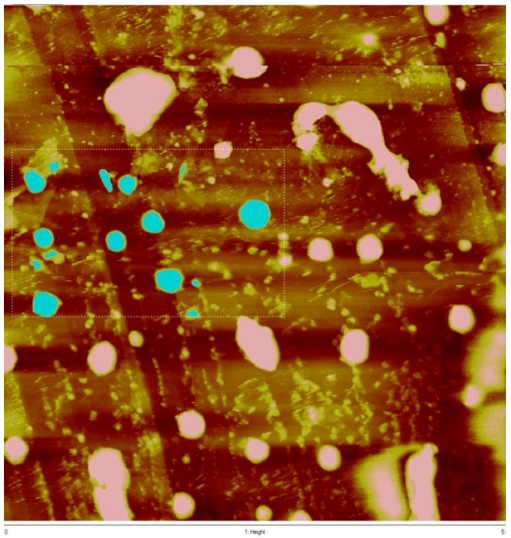

Parameter	Mean	Minimum	Maximum
Total Count:	15	15	15
Height (nm):	27.240	13.128	51.123
Diameter (nm):	147.078	59.341	277.460

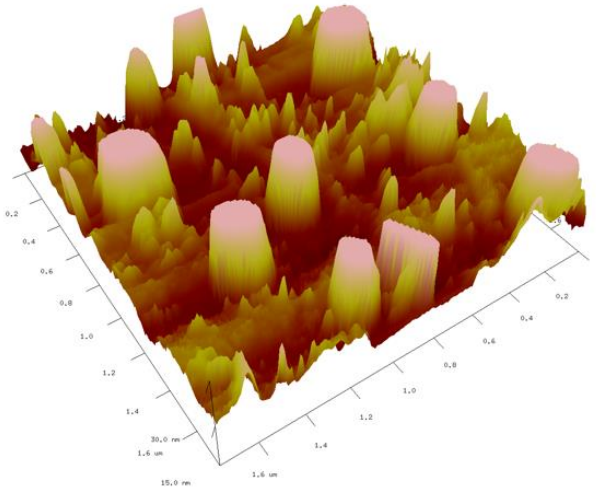

Figure 36. Typical AFM measurement of fresh nanoparticles. Study of different formulations of SLN containing CHON (SLN-1, SLN-2, 40/60, 70/30 and 95/5)) The nanoparticles marked in Turquoise Color are those used in the Height profile.

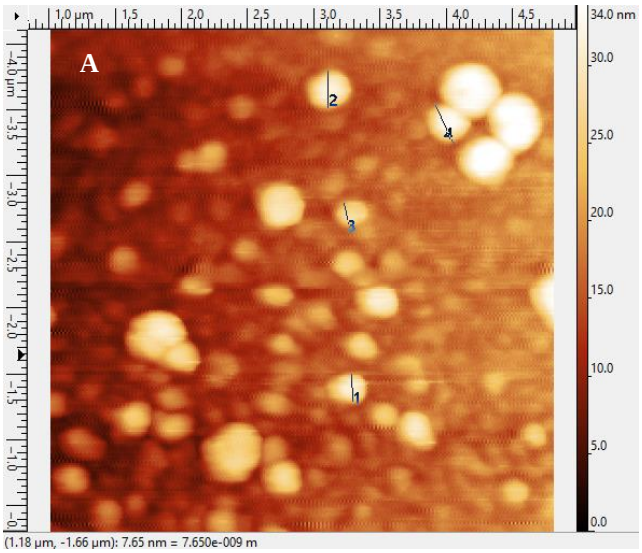

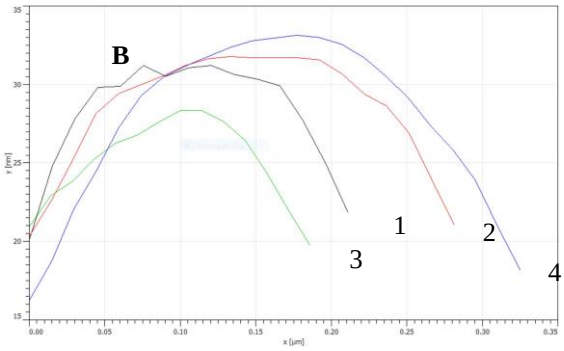

Nanoparticle	Height (nm)	Diameter (nm)
1	31.1	212.2
2	31.8	281.0
3	28.5	186.5
4	33.3	323.9
Mean	**31.2**	**250.9**
St. Dev.	**2.0**	**62.9**

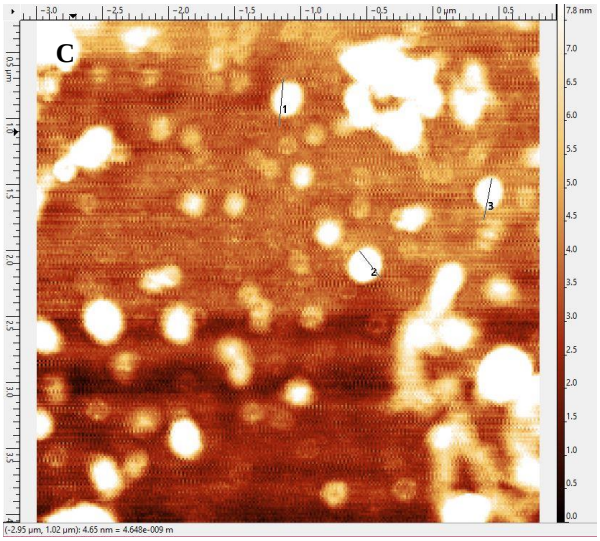

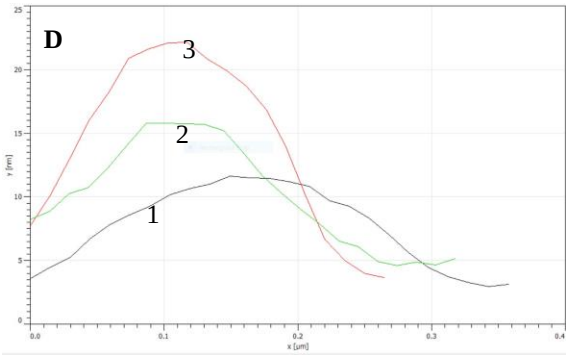

Nanoparticle	Height (nm)	Diameter (nm)
1	11.6	310.1
2	22.2	216.6
3	15.8	214.0
Mean	**19.0**	**246.9**
St. Dev.	**4.5**	**54.7**

Figure 37. Stability study of the SLN, after 6 months of lyophilization. The formulations were freeze-dried and storage at room temperature, visualization by typical AFM nanoparticle (SLN + CHON) measurement. (A) 2D image of SLN-1; (B) profile study of SLN-1; (C) 2D image of SLN-2; (D) profile study of SLN-2.

The Figure 37 corresponds to the morphological study by AFM after 6 months of storage at room temperature and in a lyophilized form of the SLN-1 and SLN-2 formulations, in all cases, the nanoparticles were found to be heterogeneous in size and circular in shape with an average diameter of around 200nm and 250nm. The heights remain similar to those found when manufacturing the nanoparticles and studying them in an aqueous medium (figure 36). The fresh SLN-1 presented a height in the range of 11.9 and 37.3 nm, while the lyophilized and studied 6 months later was 28.5 to 33.3 nm. In the case of SLN-2, the height range was from 15.4 to 18.9 nm, and 6 months later it was from 11.6 to 22.2 nm. It was therefore found that nanoparticles remain stable after 6 months of being manufactured and lyophilized.

10.4 DETERMINATION OF SURFACE CHARGE (ZETA-POTENTIAL) AND PARTICLE SIZE

The different formulations, recently formulated and in aqueous medium, were characterized by their size and surface charge. Table 21 shows the particle sizes reported as D50, and the Z potential, both characteristics measured in triplicate. The sizes generally stay in the range of 121 to 139 nm and the Z potential is around -40 mV.

Table 21. Average particle size (D50) and Z Potential of SLN with CHON, in different formulations.

Formulation	Particle size (nm)	Z Potential (mV)
SLN-1	121±8	-41.8±4.3
SLN-2	121±6	-41.9±2.5
NLC-3	139±27	-41.8±1.3
95/5	125±16	-40.7±2.3
70/30	116±7	-40.2±1.9
40/60	128±11	-42.8±1.8

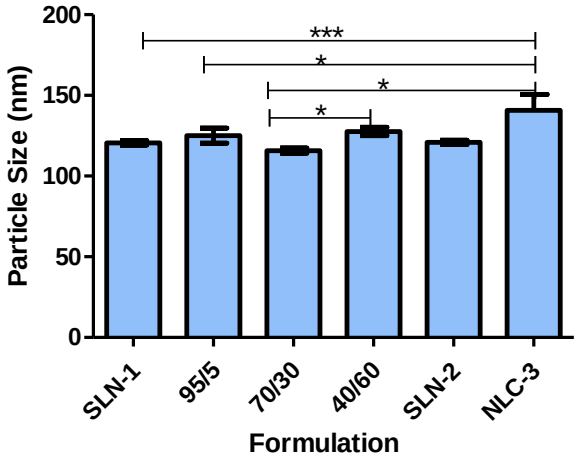

Figure 38.: Particle size of different formulations of SLN with CHON. One-way ANOVA test for the significance of differences among multiple experimental groups was performed, followed the Tukey's Multiple Comparison Test was performed for the significance of differences among each pair of experimental groups ($p< 0.05$). Data are expressed as mean ± SEM; *$p< 0.05$, **$p< 0.01$, ***$p< 0.001$ and ***$p< 0.0001$ significant difference between formulations.

The significant differences between the average sizes found are shown in figure 38. The largest size was found in the NLC-3 formulation and the smallest in the 70/30 formulation. Despite the differences, the sizes of the initial formulations are below 150 nm for all samples.

The zeta potential of the particles was studied, this parameter is directly related to the surface charge of the particles and therefore the electrostatic interaction (that is, attraction/repulsion) between the particles. It is defined as the electric potential at its shear or slip plane, which is a theoretical limit within the electric double layer separating the (bulk) liquid that shows the normal viscous behaviour of the Stern Layer, a layer that is predominantly composed of counter ions and considered to move with the particle (183,230).

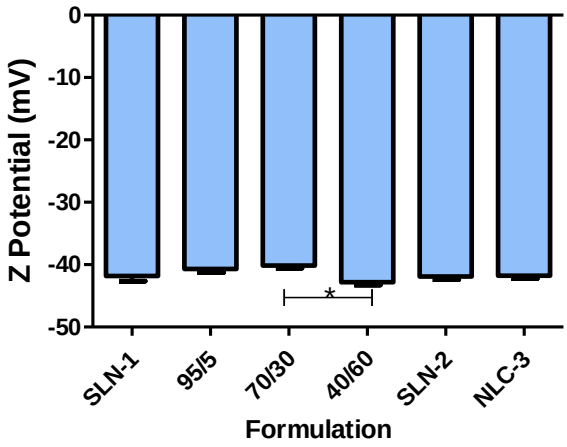

Figure 39. Z potential of different formulations of SLN with CHON. One-way ANOVA test for the significance of differences among multiple experimental groups was performed, followed the Tukey's Multiple Comparison Test was performed for the significance of differences among each pair of experimental groups ($p< 0.05$). Data are expressed as mean ± SEM; *$p< 0.05$, **$p< 0.01$, ***$p< 0.001$ and ***$p< 0.0001$ significant difference between formulations.

The Z potential is considered a primary indicator of the stability of the dispersion of nanomaterials and by convention a value below -25 mV and above 25 mV is considered stable. Among the factors that affect the obtained value of potential Z, the concentration and type of ions, as well as the pH of the solution, strongly affect the zeta potential (183).

According to figure 39, the Z potential does not present significant differences between the fresh samples of nanoparticles evaluated, except for the 70/30 and 60/40 formulations. However, the mean values are around -40 mV, which is considered stable and convenient for the nanoparticle preparations studied.

10.5 STUDY OF POSSIBLE CHON:EXCIPIENT INTERACTIONS BY DIFFERENTIAL SCANNING CALORIMETRY (DSC)

The thermograms were studied with the help of a Mettler Toledo Star System program, recording the position of the peaks, and quantifying the enthalpy values corresponding to each endotherm. The possible interactions were deduced from the modifications of these parameters in the thermograms of the mixtures with respect to those observed in the thermograms of the pure components (231).

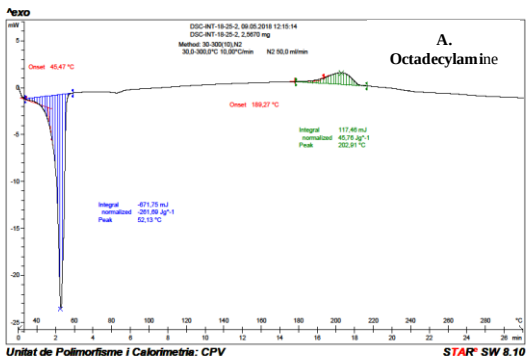

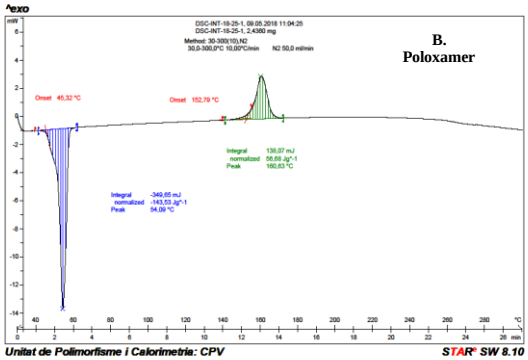

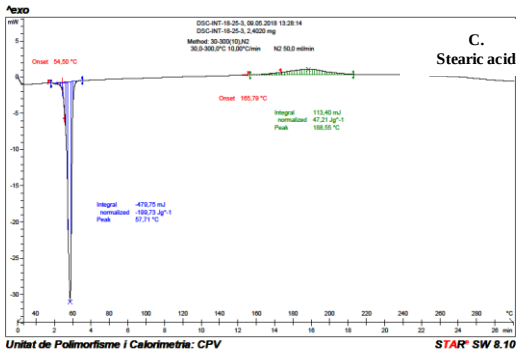

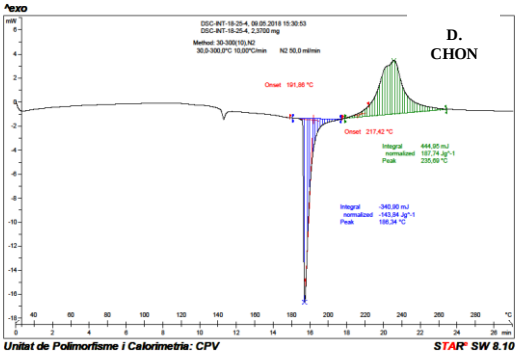

Figure continues in the following page.

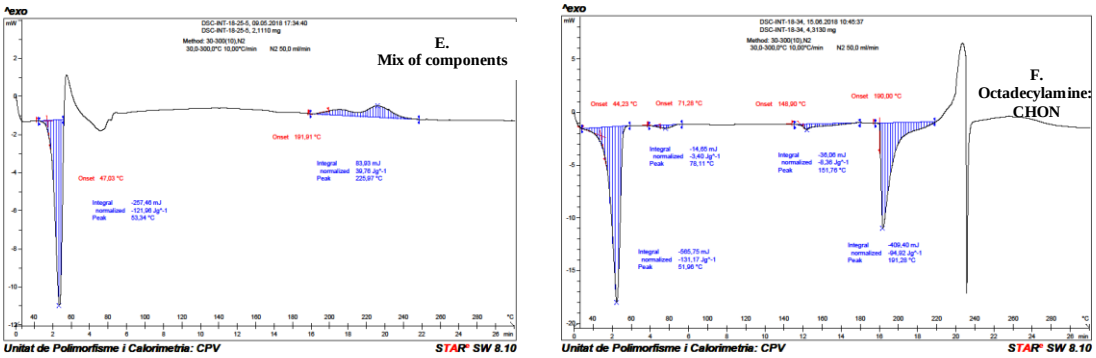

Figure 40. Thermograms obtained in the study of possible CHON:excipient interactions by Differential Scanning Calorimetry (DSC). Letters represent: A Octadecylamine thermogram; B poloxamer thermogram; C Stearic Acid thermogram; D CHON thermogram; E mix of the components of the SLN formulation in the original proportion; F mix of CHON and Octadecylamine in the original proportion of SLN formulation.

The corresponding figure 40 shows the DSC thermograms of CHON and of each of the excipients in isolation, all of them presenting defined endotherms that correspond to their fusion or fusion/decomposition processes.

Likewise, the DSC thermograms of the CHON mixture with the three excipients and with the octadecylamine excipient are shown. Although the figures E and F mixtures make it easier to observe the changes that occur in the characteristic peaks of each of the components due to mixing, the mixtures in the proportions in which they will form part of the formulation should more accurately reflect their actual behaviour (232).

The DSC record of octadecylamine, figure A, presents a first endothermic phenomenon starting at 45 ºC with an associated heat of 261.69 J/g and an exothermic phenomenon starting at 189 ºC with an associated heat of 45.76 J/g. The exothermic peak reflects the appearance of a new chemical species, product of the degradation of octadecylamine when subjected to a temperature higher than 189 ºC.

The DSC record of poloxamer, figure B, shows a first endothermic event starting at 45 ºC with an associated heat of 143.53 J/g and an exothermic event starting at 152 ºC with an associated heat of 56.68 J/g. The exothermic peak reflects the appearance of a new chemical species, product of the degradation of poloxamer when it is subjected to a temperature higher than 56 ºC, which must be considered in its experimental manipulation.

The DSC record of stearic acid, figure C, shows a first endothermic event starting at 54 ºC with an associated heat of 199.73 J/g and an exothermic event starting at 165 ºC with an associated heat of 47.21 J/g. The exothermic peak reflects the appearance of a new chemical species, product of the degradation of stearic acid when subjected to a temperature higher than 165 ºC.

The CHON DSC record, figure D, shows a first endothermic event starting at 191 ºC with an associated heat of 143.84 J/g and an exothermic event starting at 217 ºC with an associated heat of 187.74 J/g. The exothermic peak reflects the appearance of a new chemical species, product of CHON degradation when subjected to a temperature higher than 165 ºC.

The DSC record of the mixture of the four substances in the same proportions as required in the manufacture of SLN, figure E, shows a first endothermic phenomenon starting at 47 ºC with an associated heat of 121.46 J/g and an exothermic phenomenon starting at 191 ºC with an associated heat of 39.76 J. /g. There is a single exothermic peak, corresponding to the superposition of the three excipients used, the predominant one being the one found in the greatest amount; this overlap indicates that there is no interaction between the three substances, proving compatible with each other. As a new thermal phenomenon does not appear at a temperature lower than the first thermal phenomenon, the existence of a chemical interaction between the mixed substances can be ruled out and, therefore, the existence of possible chemical incompatibilities between them can be ruled out. The exothermic peak also corresponds to the superposition of those

presented by the substances individually, so it can be deduced that there is no interaction between them and, therefore, the chemical species are compatible with each other. All of this indicates that it is not foreseeable that relevant interactions of any kind will occur between the components (231,232), as long as they are used in the quantities in which they have been used in the mixture studied.

On the other hand, the record of the binary mixture CHON:octadecylamine, figure F, presents a first endothermic phenomenon from 44 ºC with an associated heat of 131.17 J/g, a second endothermic phenomenon from 71 ºC with an associated heat of 3 0.40 J/g, a third endothermic event starting at 148 ºC with an associated heat of 8.36 J/g and a fourth endothermic event starting at 190 ºC with an associated heat of 94.92 J/g. In this mixture, the characteristic endothermic peaks of the two substances can be observed when they are analysed separately, but two new endothermic peaks appear in the diffractogram, both with a temperature lower than that corresponding to the CHON endothermic peak, which clearly indicates that there is an interaction between both substances and that there is an incompatibility between them. However, this interaction, which is not seen in the mixture of the four substances together, can become apparent quickly when the mixture is subjected to a temperature above 70 ºC, being slow at normal storage temperatures.

10.6 STUDY OF POSSIBLE CHON:EXCIPIENT INTERACTIONS BY X-RAY DIFFRACTION (XRD)

The X-ray diffraction pattern was obtained to determine if the CHON and octadecylamine interactions, observed from the DSC experiments, imply the formation of new chemical entities, observable from the line intensities, which are characteristic for each component. depending on the atomic reflection centers. If there is no interaction, the XRD pattern results for CHON and octadecylamine should show an overlapping pattern when analyzing a molten mixture of both components.

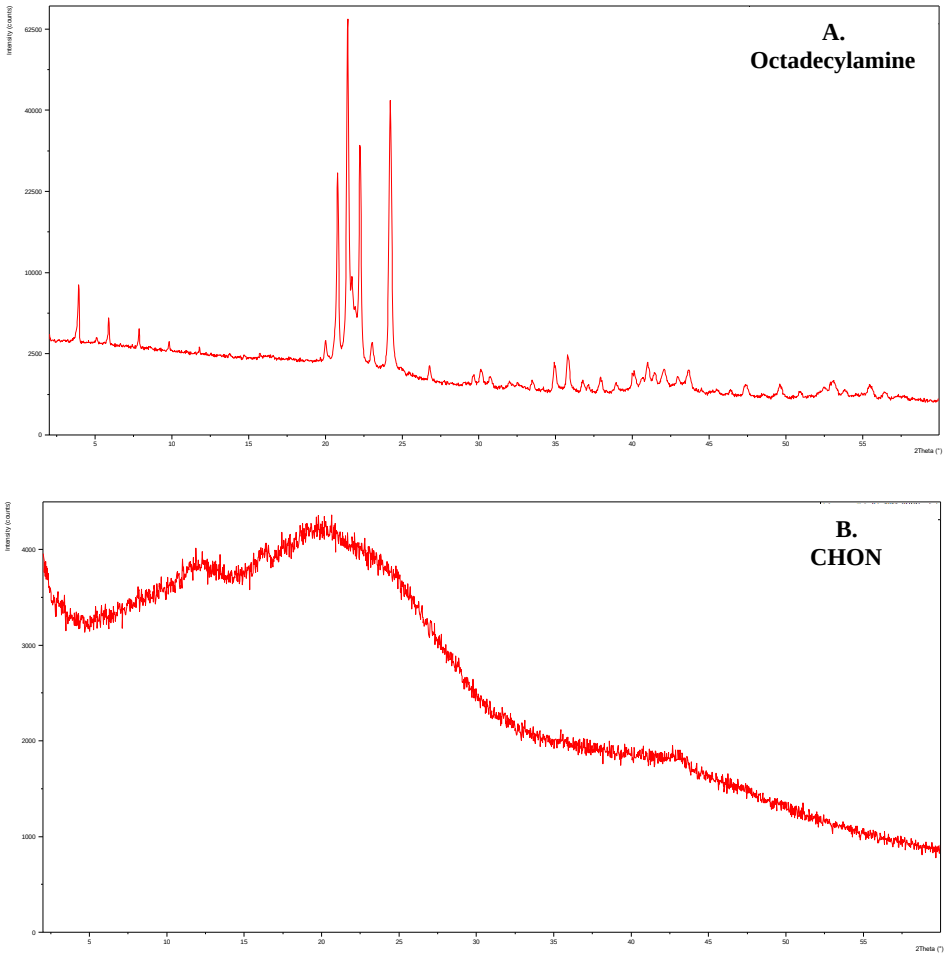

Figure continues in the following page.

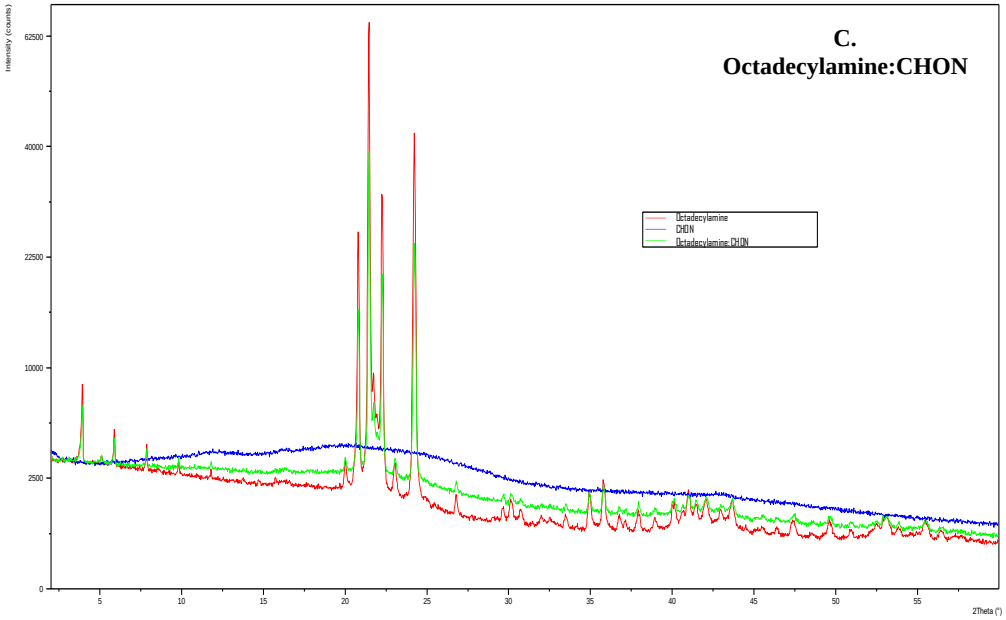

Figure 41. X-ray diffraction patterns obtained in the study of possible CHON:Octadecylamine interactions by X-Ray Diffraction (XRD). Figure A. Diffraction pattern obtained for Octadecylamine; Figure B. Diffraction pattern obtained for CHON; Figure C. Diffraction pattern obtained for a mixture (1:1) of CHON and Octadecylamine.

X-ray diffraction was performed by the powder method (figure 41), and the diagram obtained from the Octadecylamine sample indicates that the present phase is crystalline (Figure A). That of the CHON sample indicates that the phase present is fundamentally non-crystalline (amorphous) (Figure B). That of the CHON and octadecylamine mixture indicates that the sample is a physical mixture of the phases present in the Octadecylamine (crystalline) and CHON (amorphous) samples (Figure C). There are no appreciable or significant differences in the diffraction signal of the phases in the mixed sample compared to that observed in the individual samples.

10.7 STUDY OF THE VISCOSITY OF SLN FOR ITS APPLICATION ON SKIN

The flow properties in rotational rheological studies were determined, as well as the viscosity at 100 s^{-1} of the SLN formulation containing 0.7 mg/ml of CHON to characterize its rheological behavior and evaluate its possible topical application. In the same way, the rheological characteristics of the Milli Q grade water (without CHON), an aqueous solution with 0.7 mg/ml of CHON and of the plain SLN without CHON solution (matrix) were determined to assess the influence of the components on the rheological properties of the formulation. The graphs obtained are reproduced in **annex 2.**

The figure 42 shows examples of flow curves and viscosity curves obtained in the rheological characterization of the four formulations studied at t_0 and 25 ºC. **Table 22** shows the corresponding results after analysis of the data obtained.

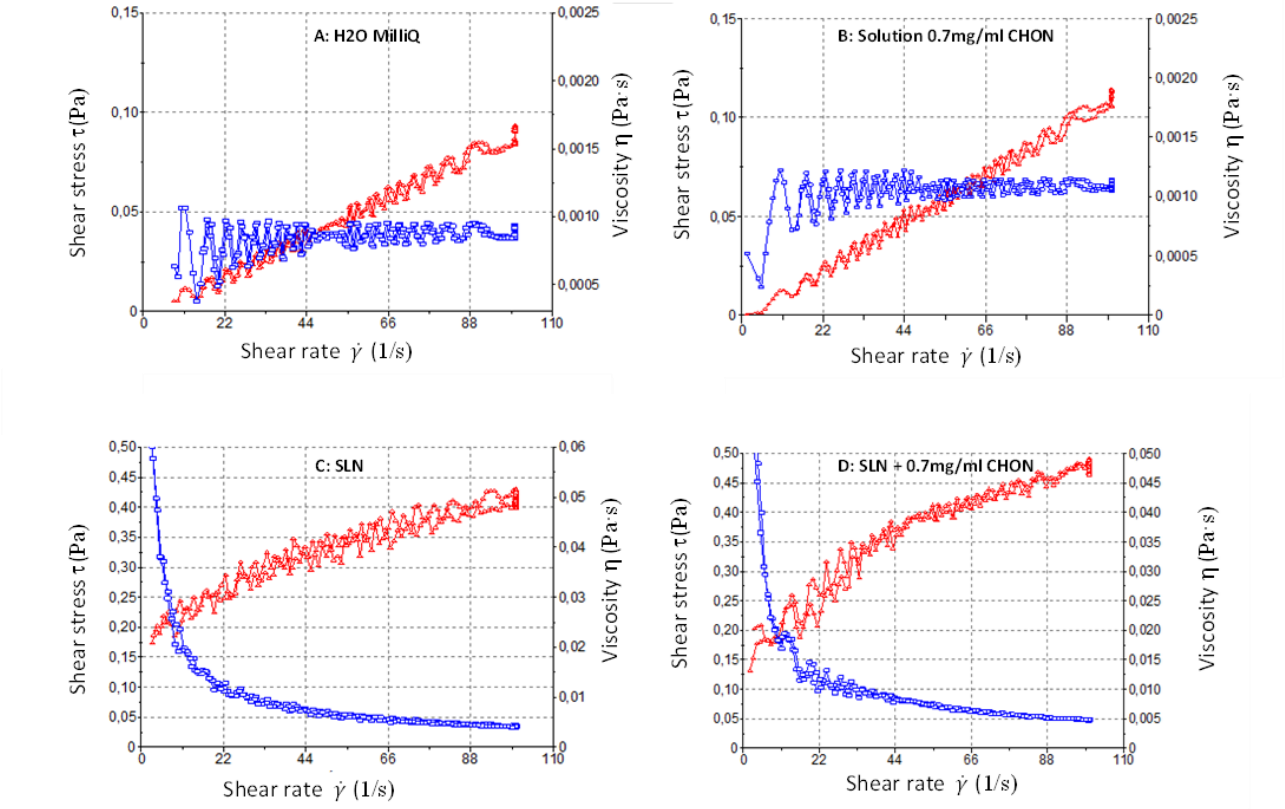

Figure 42. Study of the viscosity of the SLN containing CHON. Flow curves in red (Shear stress in Pa versus shear rate in s^{-1}), and viscosity curves in blue (Viscosity in Pa·s

versus shear rate in s-¹) of MilliQ Water (A), the 0.7 mg/ml solution of CHON (B), the plain SLN formulation without CHON (C) and with 0.7 mg/ml of CHON (D).

Table 22. Viscosity (Mean value ± *SD*), rheological behavior and mathematical fitting of MilliQ water, solution of CHON (0.7 mg/ml), SLN formulation and SLN + CHON (0.7 mg/ml) formulation, analyzed by duplicate o triplicate.

Formula/ Sample	Viscosity (mPa.s) at 100 s^{-1}	Viscosity mean value (mPa·s) at 100 s^{-1}	Rheological behavior	Mathematical model
H20 MilliQ/1	**0.895** ± *0.036*	**0.869 ± 0.038**	Newtonian	Ramp-up: Newton (r=0.9889); Ramp-down: Newton (r=0.9873)
H20 MilliQ/2	**0.882** ± *0.037*		Newtonian	Ramp-up: Newton (r=0.9872); Ramp-down: Newton (r=0.9830)
H20 MilliQ/3	**0.830** ± *0.039*		Newtonian	Ramp-up: Newton (r=0.9772); Ramp-down: Newton (r=0.9816)
Sol. CHON/1	**1.101** ± *0.034*	**1.097 ± 0.033**	Newtonian	Ramp-up: Newton (r=0.9943); Ramp-down: Newton (r=0.9926)
Sol. CHON/2	**1.092** ± *0.033*		Newtonian	Ramp-up: Newton (r=:0.9934); Ramp-down: Newton (r=0.9917)
Plain SLN/1	**4.449** ± *0.050*	**4.449 ± 0.059**	Shear thinning	Ramp-up: Cross (r=0.9943); Ramp-down Cross (r=0.969)
Plain SLN/2	**4.154** ± *0.069*		Shear thinning	Ramp-up: Cross (r=0.9799); Ramp-down Cross (r=0.9829)
SLN+CHON/1	**4.778** ± 0.063	**4.836 ± 0.060**	Shear thinning	Ramp-up: Cross (r=0.9738); Ramp-down Cross (r=0.9871)
SLN+CHON/2	**4.893** ± *0.057*		Shear thinning	Ramp-up: Cross (r=0.9928); Ramp-down Cross (r=0.9933)

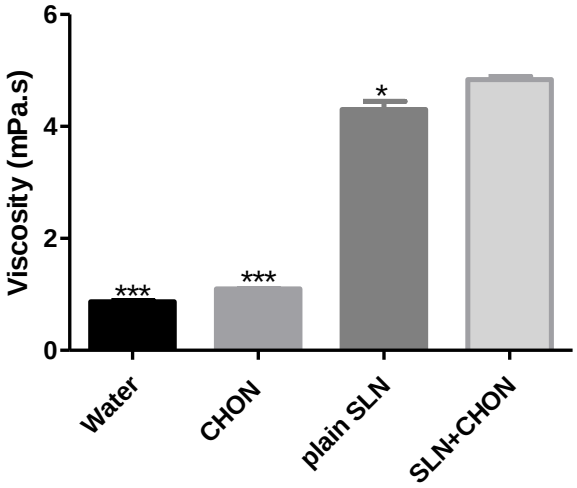

Figure 43. Comparison of the Viscosity of the SLN with respect to water. Viscosity (mPa.s) at 100 s^{-1}; Milli Q Water; 0.7 mg/ml CHON solution; SLN formulation without CHON and SLN with 0.7 mg/ml CHON. One-way ANOVA was performed to determine the significance of differences between groups, followed by Bonferroni test for the significance of differences among each experimental groups compared to SLN + CHON. Data are expressed as mean ± SD; *p< 0.05 and ***p< 0.001 significant difference compared to SLN + CHON.

As it is shown in figure 42, the flow curves of 0.7 mg/mL CHON solution (B) and MilliQ grade water without CHON (A) show a linear relationship between shear stress and shear rate, which is characteristic of Newtonian behavior, where the viscosity is independent of the intensity of the shear, therefore it remains constant (233).

Therefore, the addition of CHON to water continues to provide a fluid with Newtonian behavior. However, the solution is slightly more viscous, without the difference being significant ($p > 0.05$), with 0.869 ± 0.038 mPa·s being the viscosity of water alone and 1.097 ± 0.033 mPa·s that of the CHON solution, under the established experimental conditions.

The formulation of plain SLN without CHON (Figure 42-C) that contains mostly neutral and cationic lipids, together with a surfactant, as well as the formulation SLN with CHON

(Figure 42-D) present the characteristics of pseudoplastic fluids (*shear thinning behavior*), since the viscosity of both products decreases considerably with the increase in shear rate (234). In addition, the rheograms do not show signs of thixotropy since no well-defined hysteresis loop can be seen, as the ascending and descending sections of the curves practically coincide. This indicates that the perturbation of the microstructure of the system during the rheological test depends fundamentally on the intensity of the shearing. The model for the best fit of the experimental data was the Cross equation, which confirms the pseudoplastic character of these fluids (235).

Therefore, the incorporation of CHON to the SLN base does not affect the type of flow, remaining pseudoplastic. However, the viscosity of the mixture obtained is significantly more viscous ($p < 0.05$), being 4.449 ± 0.059 mPa·s the viscosity of the SLN vehicle without CHON and 4.836 ± 0.060 mPa·s than the same formula with 0.7 mg/ml CHON, under the experimental conditions. Then the addition of CHON to the plain SLN (matrix) adds texture to the system as in the case of the aqueous CHON formulation.

Comparing the results obtained from the two formulations with CHON, the type of vehicle used (Water or SLN) significantly affects the rheological characteristics of the preparation. A change in behavior from Newtonian to pseudoplastic is observed as well as a significant increase ($p < 0.05$) in viscosity (Figure 43) from 1.097 ± 0.033 to 4.836 ± 0.060 mPa·s to 100 s^{-1}, respectively for the aqueous solution of CHON and the formula SLN + CHON. In addition, the viscosity values of the formulations with CHON indicate that they are apt to be dispensed in the form of aerosols or fine jets from suitable containers. They could even be applied as a roll-on (233). For formulations for topical use such as SLN+CHON, the pseudoplastic behavior (more viscous system at rest and fluidizing when handled) is desirable, since it facilitates the processing and use of the product, particularly its spread on the skin when applying it (236,237).

10.8 DETERMINATION OF ENCAPSULATION EFFICIENCY (EE)

10.8.1 PRELIMINARY REVERSE-PHASE CHROMATOGRAPHY (RP-HPLC) STUDY

To determine the amount of CHON in a sample, other authors have used techniques such as Reverse-phase chromatography (RP-HPLC) (215), and the determination of viscosity (238). In the study of the EE% of CHON in the SLN, it was proposed to evaluate the amount of CHON encapsulated through RP-HPLC, however, due to limitations in its execution, it was subsequently decided to apply other methods.

In the case of the determination by RP-HPLC, when using the mobile phase with octane-sulfonic acid, the signal was not clear at 195nm with respect to the signal of the diluent used and the baseline fluctuated a lot (figure 44, B and C). At 240 nm, despite being able to see a characteristic CHON peak (figure 44, D and E), it was not very intense. Hence, other types of reagents were required, such as specific enzymes of high economic value, whose method is based on specific enzymatic hydrolysis of the Chondroitin Sulfate to produce disaccharides Di-4S, Di-6S and Di-0S (239,240)**,** or more specialized chromatographic columns and equipment, both to achieve greater resolution of the CHON peak with respect to the equipment's own noise, or to avoid damage to the columns and equipment, since the reagents used had strongly acid characteristics.

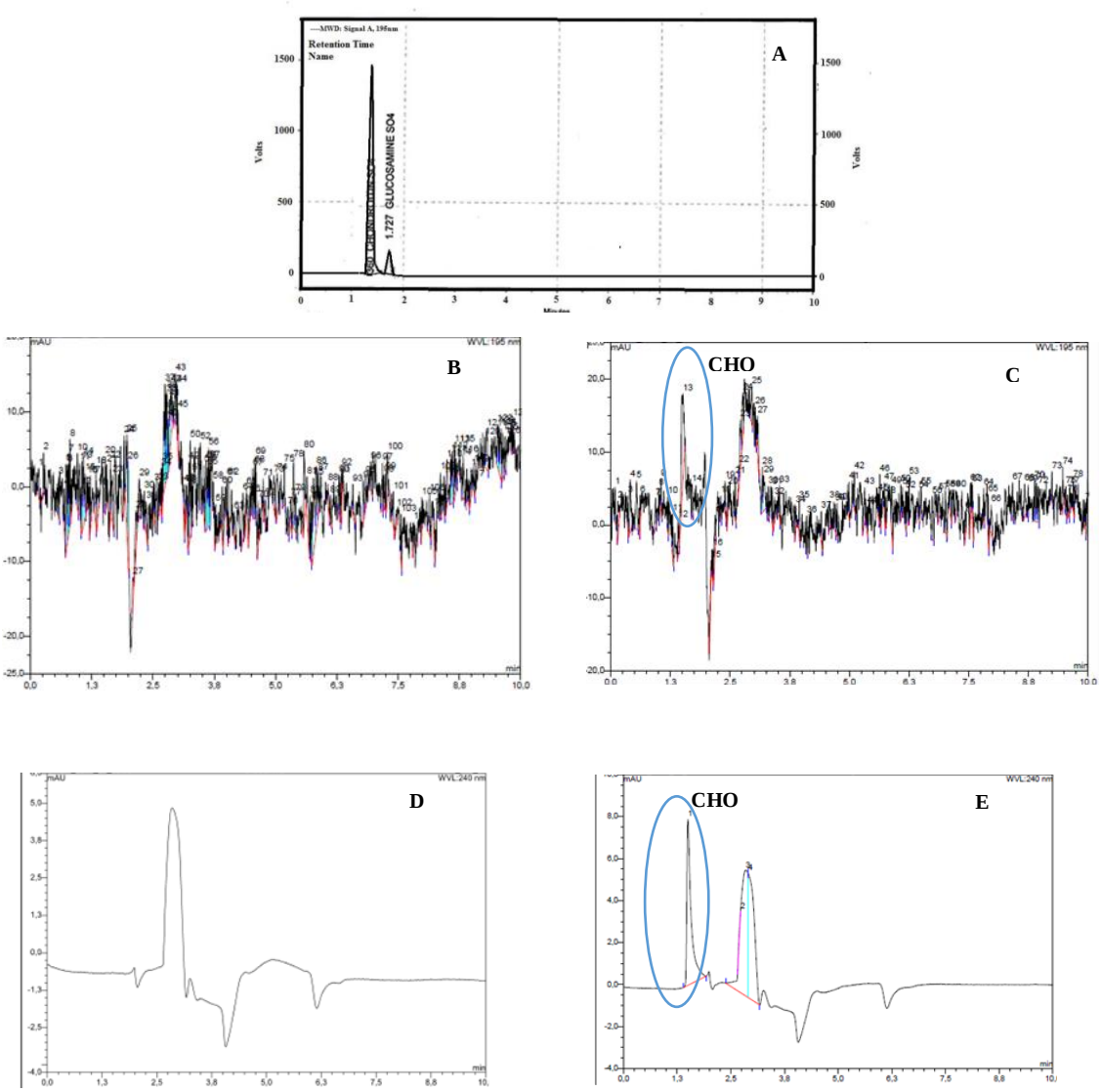

Figure 44. Chromatograms involve in the study of the determination of CHON by RC-HPLC. Image A: Typical chromatogram of Chondroitin sulphate (215); image B: diluent chromatogram at a wavelength of 195 nm; imagen C: CHON in aqueous medium at a wavelength of 195 nm; image D: diluent chromatogram at a wavelength of 240 nm; imagen C: CHON in aqueous medium at a wavelength of 240 nm.

10.8.2 DETERMINATION OF EE% BY THE TITRATION METHOD AND UV-Vis SPECTROSCOPY METHOD

The determination of the EE% was carried out by two different validated methods, titration method and UV-vis spectroscopy method.

The first method validated and used in the research was the volumetric titration method that involves a precipitation reaction between CHON and Cetylpyridinium chloride Monohydrate.

10.8.2.1 Confirmation of CHON encapsulation

Since the volumetric titration method was initially validated and used in the DOE study to determine the CHON encapsulation efficiency (EE%), preliminary studies confirmed that CHON remained bound to SLN during the titration and that only CHON not bound to the nanoparticles reacted.

Different options were evaluated:

1. Addition of concentrated Hydrochloric acid to break the SLN and release the CHON, however, when carrying out the titration, a reaction with the titrant was not achieved. After adding the 37% Hydrochloric acid and stirring, methylene blue (which lost color in contact with the acidic mixture) was subsequently added and no color change was noted when titrating.

2. Heating above the melting point higher than that of the components of the formulation, however, when titrating only a small higher percentage of CHON was found, around 4%. According to the statistical analysis (Table 23), the value of p (0.3725) is greater than 0.05, therefore no significant differences were found between the original nanoparticles and those after being heat treated, indicating that the increase in the temperature did not disrupt the nanoparticles or allow the release of the encapsulated CHON.

Table 23. Measurement of the percentage of Free CHON found in the samples analyzed by the titration method before and after being subjected to heating to break the nanoparticles.

Sample	EE% in SLN-1	EE% in SLN-1 after heating
1	78.92	81.59
2	82.13	80.52
3	73.15	81.00
4	73.15	-
Mean	**76.84**	**81.04**
STD	4.46	0.54
P value*	0.3725	

*The significance of differences among experimental groups was performed by *Student's t* test; *$p < 0.05$ significant difference between samples.

3. Addition of an excess of NaOH according to the stoichiometric ratio with the stearic acid present in the formulation, an irreversible saponification reaction was produced, which released the encapsulated CHON and at the same time the base used did not interfere in the reaction with the titrant.

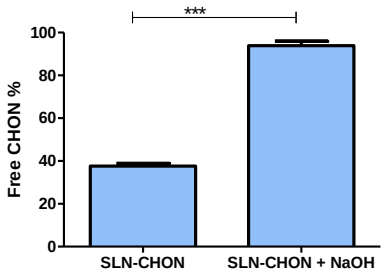

Figure 45. Study of CHON encapsulation confirmation. Free CHON percentage found in the reference samples (SLN containing CHON (0.4 mg/ml)) and in reference samples previously treated with NaOH (0.7 % w/v), by titration method. Data are expressed as

mean ± SEM; the significance of differences among experimental groups was performed by Student's t test; *p< 0.05, **p< 0.01 and ***p< 0.001 significant difference between samples.

Table 24. Measurement of the percentage of Free CHON found in the samples analyzed by the titration method.

Sample	SLN-CHON (%)	SLN-CHON + NaOH (%)
1	39.41	93.22
2	37.26	97.53
3	33.06	94.93
4	39.52	97.37
5	39.05	86.17
Mean ± SEM	37.66 ± 1.220 N=5	93.84 ± 2.079 N=5

SLN-CHON: were nanoparticles containing CHON (0.4 mg/ml) and SLN-CHON + NaOH: the same samples previously treated with NaOH (0.7% w/v).

As can be seen in Figure 45 and table 24, in the SLN samples containing CHON, when evaluated by volumetric titration, a significantly lower percentage of free CHON was found, around 40%, compared to the same samples previously treated with NaOH, where the amount of free CHON was about 93%. NaOH forms an irreversible saponification reaction with stearic acid, which breaks the nanoparticle and releases CHON. When sodium hydroxide and stearic acid react with each other results in the formation of sodium salt and water (Figure 46).

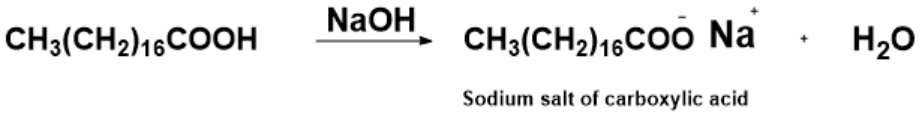

Figure 46. Chemical reaction between stearic acid and sodium hydroxide. Taken from Wolff, 2019 (241)**.** The final products are water and sodium salt of carboxylic acid.

10.8.3 COMPARISON OF METHODS TO DETERMINE EE%

We worked with 2 different methods, previously validated, to know the EE % of the CHON in the nanoparticles. One method used the volumetric titration technique and another by determination by UV-Vis spectrophotometry.

According to the optimal conditions established for the manufacture of nanoparticles bound to CHON, different formulations were made, with changes in the ingredients of the preparation and the encapsulation efficiency was evaluated, both by the volumetric titration method and by the previously spectrophotometric method.

Table 25. CHON encapsulation efficiency in different SLN formulations, by titration method.

Sample	**EE %**				
	SLN-1	**95/5**	**70/30**	**40/60**	**SLN-2**
1	60.6	52.0	49.8	48.4	84.5
2	62.7	49.8	56.3	48.4	88.1
3	66.9	52.4	62.8	43.8	78.3
4	66.9	50.2	61.8	43.8	80.3
5	60.5	49.4	61.8	47.4	84.8
6	68.4	50.5	76.0	45.3	72.4
7	61.0	49.3	49.4	43.0	70.3
8	63.1	49.3	49.4	45.1	78.2
9	-	-	47.2	-	-
Mean (%)	**63.8**	**50.4**	**57.2**	**45.7**	**79.6**
Standard deviation	3.2	1.2	9.4	2.1	6.2
Standard error of the mean	1.1	0.4	3.1	0.8	2.1

The table 25 shows the results of the EE% obtained by the volumetric titration method in the 5 formulations evaluated. The percentages range from a lower efficiency for the 40/60 formulation with 45.7 % encapsulation of CHON, up to 79.6 % as the highest encapsulation efficiency achieved with the SLN-2 formula.

Table 26. CHON encapsulation efficiency in different SLN formulations, by spectrophotometric method.

Sample	EE %				
	SLN-1	**95/5**	**70/30**	**40/60**	**SLN-2**
1	77.6	74.2	69.0	64.7	88.1
2	76.4	74.3	71.4	70.8	86.2
3	78.8	75.6	82.5	71.2	81.4
4	83.4	75.1	81.3	75.3	82.3
5	80.2	71.4	78.1	76.7	87.0
6	82.5	74.0	71.5	75.4	87.2
7	74.9	71.1	71.2	76.1	84.8
8	83.7	70.1	73.8	65.2	82.1
9	83.7	83.0	85.9	66.4	98.3
10	83.1	82.9	-	75.9	81.6
11	-	-	-	-	91.5
12	-	-	-	-	93.6
13	-	-	-	-	89.1
Mean (%)	**80.4**	**75.2**	**76.1**	**71.8**	**87.2**
Standard deviation	3.3	4.5	6.0	4.8	5.1
Standard error of the mean	1.1	1.4	2.0	1.5	1.4

It was also validated and worked with a UV-Vis spectrophotometry method, the results are shown in table 26, as this method is more sensitive than the volumetric titration method, higher encapsulation percentages were obtained, from 71.8% to 87.2%.

Graphically, the EE percentages of each formulation can be observed in figures 47 and 48. In both cases, the graph on the left shows the behavior of the percentages found, linked with a line. The same direction of decrease and increase of the EE% is observed according to each formula. The graph on the right shows the significant differences between the formulations, in both methods, the SLN-1 and SLN-2 formulations have the highest

percentages of encapsulation. Since the highest efficiency was obtained with the SLN-2 formulation, it presents significant differences with all the other formulas and by both methods studied.

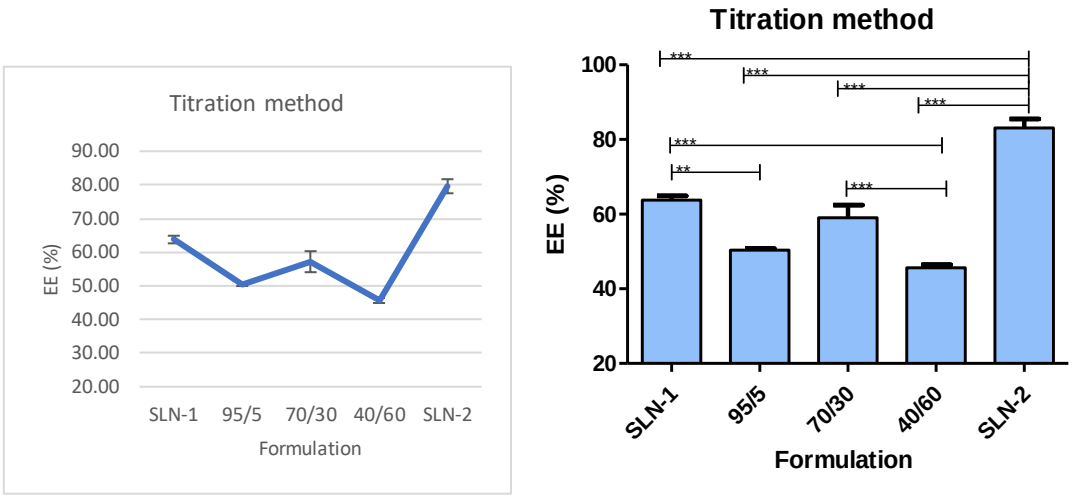

Figure 47. CHON encapsulation efficiency in different SLN formulations, by titration method. Data are expressed as mean ± SEM; *p< 0.05, **p< 0.01, ***p< 0.001 and ***p< 0.0001 significant difference between formulations.

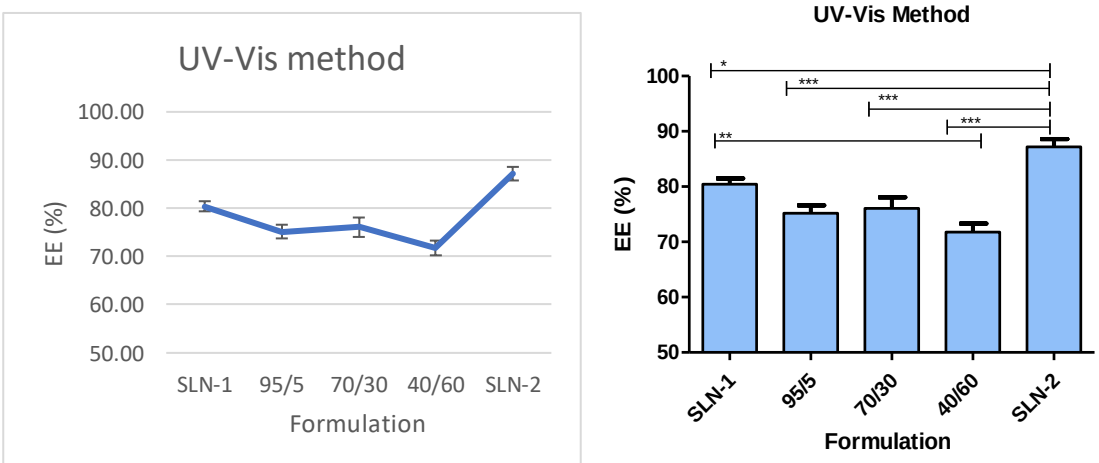

Figure 48. CHON encapsulation efficiency in different SLN formulations, by spectrophotometric method. Data are expressed as mean ± SEM; *p< 0.05, **p< 0.01, ***p< 0.001 and ***p< 0.0001 significant difference between formulations.

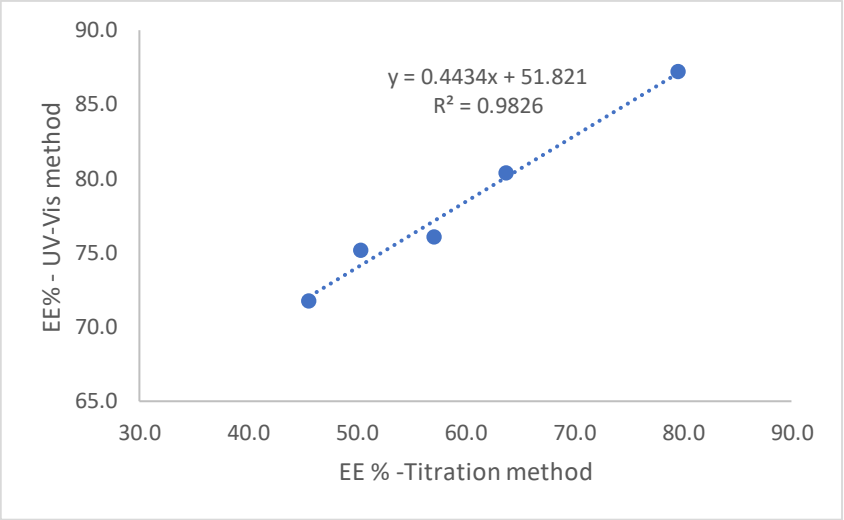

Figure 49. Linear correlation of the validated methods to determine the EE% of CHON. Comparison of CHON encapsulation efficiencies in different SLN formulations, using the spectrophotometric method and the titration method.

Since both methods were able to obtain the EE% and graphically have the same tendency of increase and decrease in the results, the correlation equation between both methods was sought (Figure 49), and the following equation was obtained with a 98.2% correlation:

EE % of UV_Vis method = (0.443 * EE % of titration method) + 51.821 $R^2 = 0.9826$

In this way, having the results with one method, it is possible to calculate the data that would be obtained with the other method.

The UV-Vis method allows to analyze smaller sample volumes and obtain higher results than the titration method, however it has limitations when the nanoparticle samples are lyophilized with trehalose, since the sugar reacts with the acid that the UV-Vis method requires. If concentrated sulfuric acid is added to the sugar, the complete dehydration of the carbohydrate occurs, which causes it to turn into carbon (242), and forms an intense black color that measurement of the absorbance of the sample.

SLN AS VEHICLE OF CHON-TECHNIQUES IN MOLECULAR AND CELLULAR BIOLOGY

11 LN AS VEHICLE OF CHON - TECHNIQUES IN MOLECULAR AND CELLULAR BIOLOGY

11.1 CELL VIABILITY

To assess the viability of the cells in the presence of the nanoparticles, the cell cytotoxicity assay with MTT was performed. The study was carried out in different cell lines. First, the concentration that did not generate cellular cytotoxicity was studied for use in the following cellular internalization assays and anti-inflammatory capacity studies.

This type of assay precedes others that are required such as cell internalization, cell transfection, among others. Since it is required to know the concentration or amount of nanoparticles that can be added to a specific amount of cells and achieve a studied effect, without causing cellular cytotoxicity.

First, the Cell viability was evaluated in the cell lines: BJ, HACAT and HT 29.

11.1.1 HT-29 cell line - studies

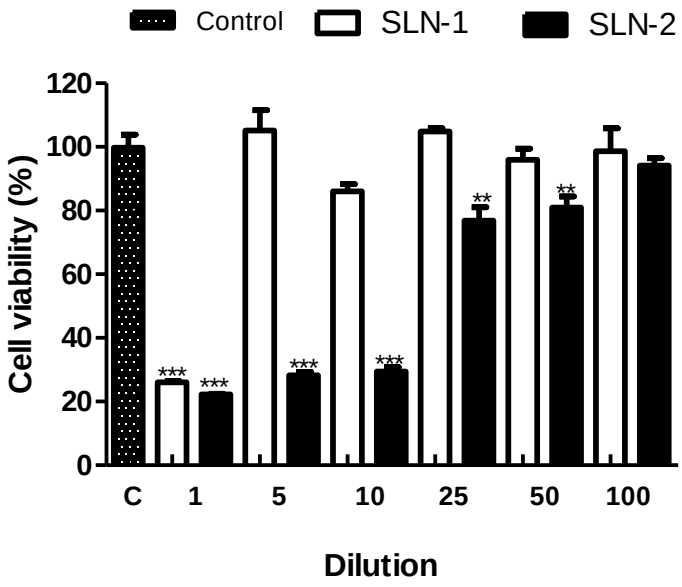

Figure 50. Effect of different formulations of SLN with CHON on viability of *HT-29* cells (intestinal epithelial) at 24 h. MTT reduction values of untreated control cells were set as 100% cell viability. One-way ANOVA was performed, followed by Bonferroni test for the significance of differences among multiple experimental groups. Data are expressed as mean ± SEM; *p< 0.05, **p< 0.01 and ***p< 0.001 significant difference compared to control cells. The numbers 1, 5, 10, 25, 50, 100 means the SLN dilution before adding to the cells plate.

Cellular cytotoxicity of SLN-1 and SLN-2 in the Human colon adenocarcinoma cell line (HT-29) was previously evaluated. As observed in figure 50, for SLN-1, from a dilution of 5, a high cell viability is observed, without significant differences with respect to the control. In the case of the SLN-2 formulation, there is greater cytotoxicity at low dilutions, being necessary to dilute up to 100 times to avoid having significant differences with respect to the control.

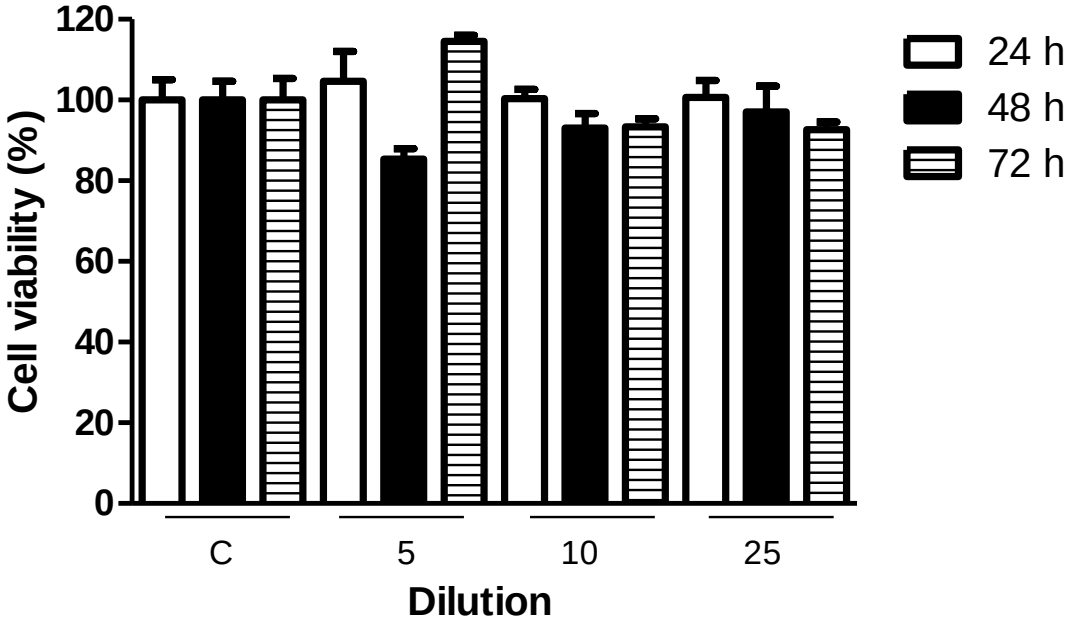

Figure 51. Effect of SLN-1 on viability of *HT-29* cells (intestinal epithelial) at 24 h, 48 h and 72 h. MTT reduction values of untreated control cells were set as 100% cell viability. One-way ANOVA was performed, followed by Bonferroni test for the significance of differences among multiple experimental groups. Data are expressed as mean ± SEM; *p< 0.05, **p< 0.01 and ***p< 0.001 significant difference compared to control cells. The numbers 5, 10 and 25 means the SLN dilution before adding to the cells plate.

Once the preliminary study was carried out in HT-29 cells, at 24 h and using SLN-1 and SLN-2, the most convenient dilutions were obtained to evaluate cell viability at times of 24, 48 and 72 h.

The study was extended with the same type of HT-29 cell line. For the previously defined conditions, it can be seen in figures 51 and 52 that for the working dilutions, both for the SLN-1 with dilutions of 5, 10 and 25, and for the SLN-2 with dilutions greater than 25, 50 and 100, there is no cellular cytotoxicity and there is a cellular viability without significant differences with respect to the 100% of the control that consisted of untreated cells.

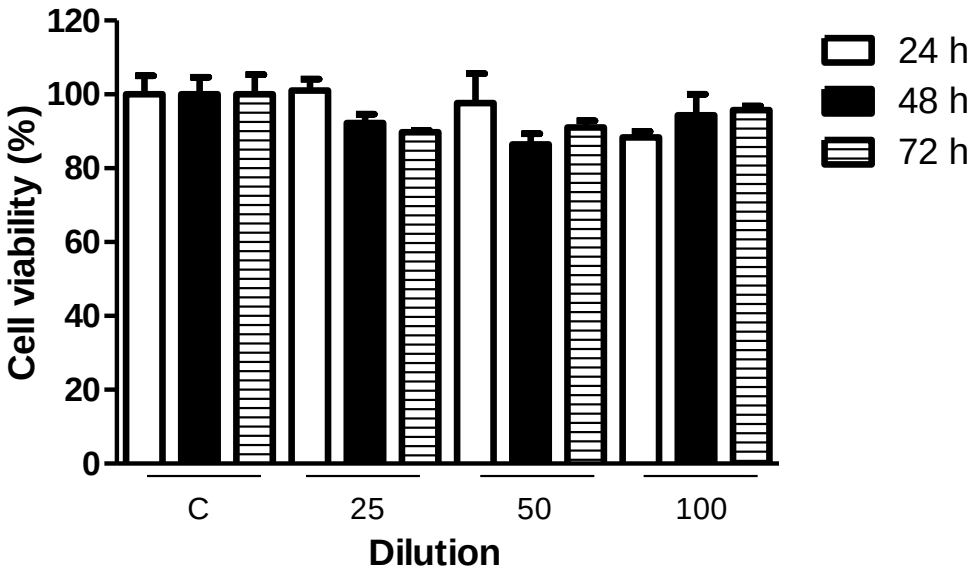

Figure 52. Effect of SLN-2 on viability of *HT-29* cells (intestinal epithelial) at 24 h, 48 h and 72 h. MTT reduction values of untreated control cells were set as 100% cell viability. One-way ANOVA was performed, followed by Bonferroni test for the significance of differences among multiple experimental groups. Data are expressed as mean ± SEM; *p< 0.05, **p< 0.01 and ***p< 0.001 significant difference compared to control cells. The numbers 25, 50 and 100 means the SLN dilution before adding to the cells plate.

Therefore, for the HT-29 cell line, a dilution of SLN-1 starting at 5 and for SLN-2 starting at 25, allows the cells to grow without cell death induced by the treatment with the nanoparticles.

11.1.2 HaCaT cell line- studies

Another cell line included in the study of the cell viability of SLN-1 and SLN-2 nanoparticles was Human keratinocyte cells (HaCaT).

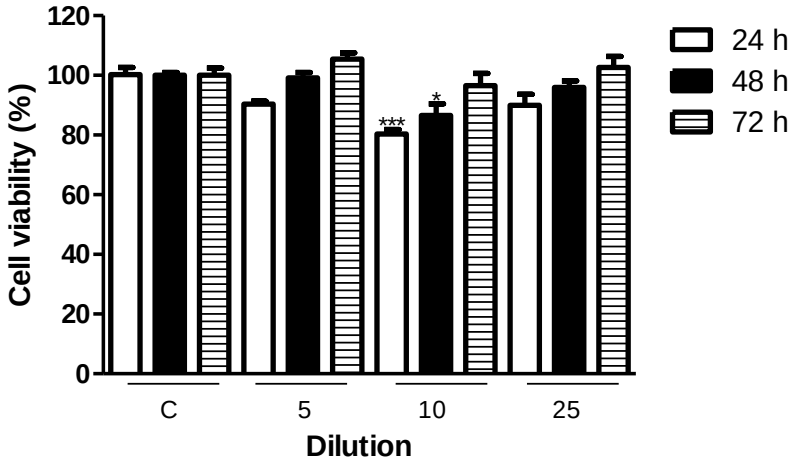

Figure 53. Effect of SLN-1 on viability of *HaCaT cells* (keratinocyte): at 24 h, 48 h and 72 h. MTT reduction values of untreated control cells were set as 100% cell viability. One-way ANOVA was performed, followed by Bonferroni test for the significance of differences among multiple experimental groups. Data are expressed as mean ± SEM; *p< 0.05, **p< 0.01 and ***p< 0.001 significant difference compared to C: control cells. The numbers 5, 10, 25 mean the SLN dilution before adding to the cells plate.

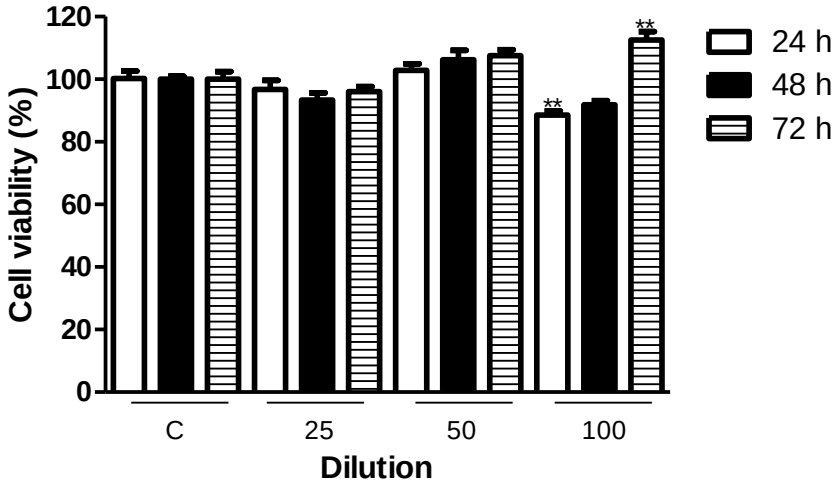

Figure 54. Effect of SLN-2 on viability of *HaCaT cells (*keratinocyte): at 24 h, 48 h and 72 h. MTT reduction values of untreated control cells were set as 100% cell viability. One-way ANOVA was performed, followed by Bonferroni test for the significance of differences among multiple experimental groups. Data are expressed as mean ± SEM;

*p< 0.05, **p< 0.01 and ***p< 0.001 significant difference compared to control cells. C: Control. The numbers 25, 50, 100 mean the SLN dilution before adding to the cells plate.

The conditions established in the cell viability study of HT-29 cells were used for both SLN-1 and SLN-2 formulations (Figures 53 and 54), no cell cytotoxicity was found at the established dilutions and times, except for the first 24 h and 48 h of treatment of the SLN-1 at a dilution of 10, where there were significant differences with respect to the control. In the case of the SLN-2, the significant difference with respect to the control was obtained in the dilution of 100 and in the first 24 hours of treatment; however, cell recovery occurred after 72 hours and even in the case of the SLN-2, cell growth was greater compared to the control.

11.1.3 BJ cell line - studies

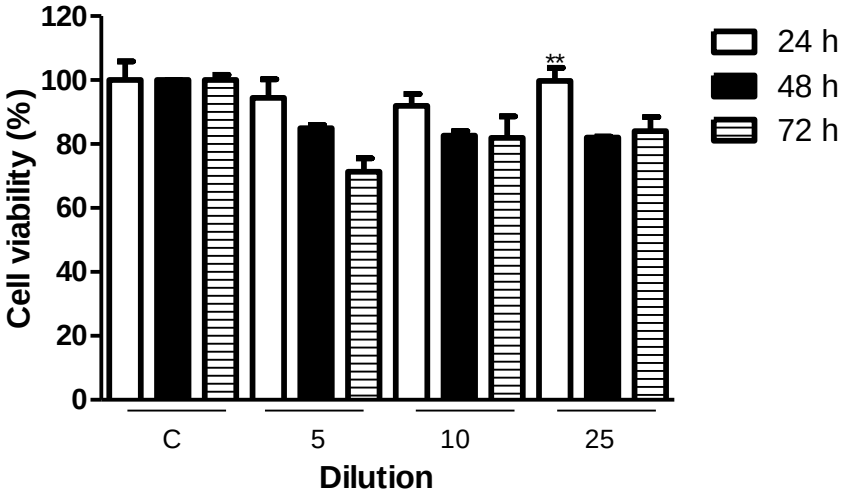

Figure 55. Cell viability assays in *BJ cells* (fibroblasts) with SLN-1 at 24, 48 h and 72 h. One-way ANOVA was performed, followed by Bonferroni test for the significance of differences among multiple experimental groups. Data are expressed as mean ± SEM. C: Control. The number 5, 10 and 25 mean the SLN dilution before adding to the cells plate.

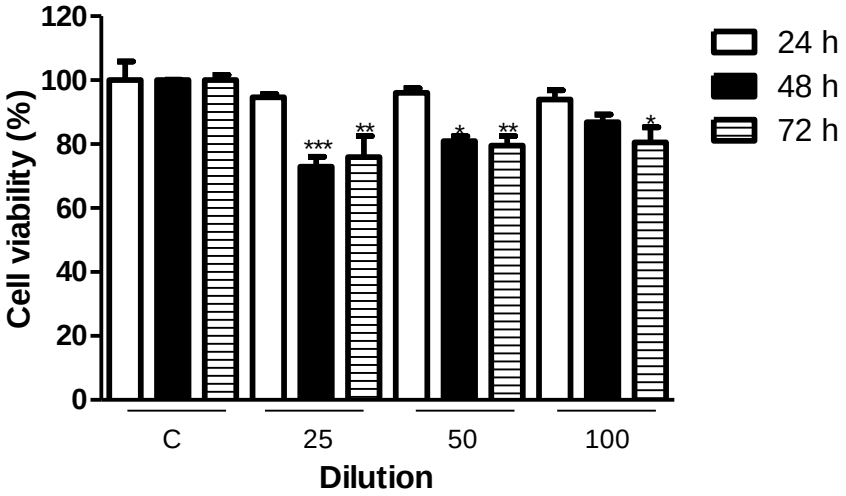

Figure 56. Cell viability assays in *BJ cells* (fibroblasts) with SLN-2 at 24, 48 h and 72 h. One-way ANOVA was performed, followed by Bonferroni test for the significance of differences among multiple experimental groups. Data are expressed as mean ± SEM. C: Control. The number 25, 50 and 100 mean the SLN dilution before adding to the cells plate.

The Human skin fibroblast cell line (BJ) were also evaluated regarding the viability of these cells in the presence of nanoparticles under the conditions already studied with the two previously mentioned cell lines.

In the case of the SLN-1 (figure 55), there were no significant differences in the cell viability of the treated cells compared to the control without treatment, in any of the incubation times worked.

The SLN-2 (figure 56) showed cellular cytotoxicity at dilutions 25 and 50 in the first 24 and 48 h treatment times; however, cellular cytotoxicity was not observed in these treatments at 72 h. While for the dilution of 100 there were significant differences at 72 h with respect to the control.

11.1.4 OA Chondrocyte cell line - studies

The study was conducted in cell models at the Research Scientist, Department of Biomedical Engineering of the Southern University of Science and Technology (SUSTech), Shenzhen, China. Cell viability in OA chondrocytes was evaluated to later study the anti-inflammatory capacity of CHON encapsulated in different nanoparticles.

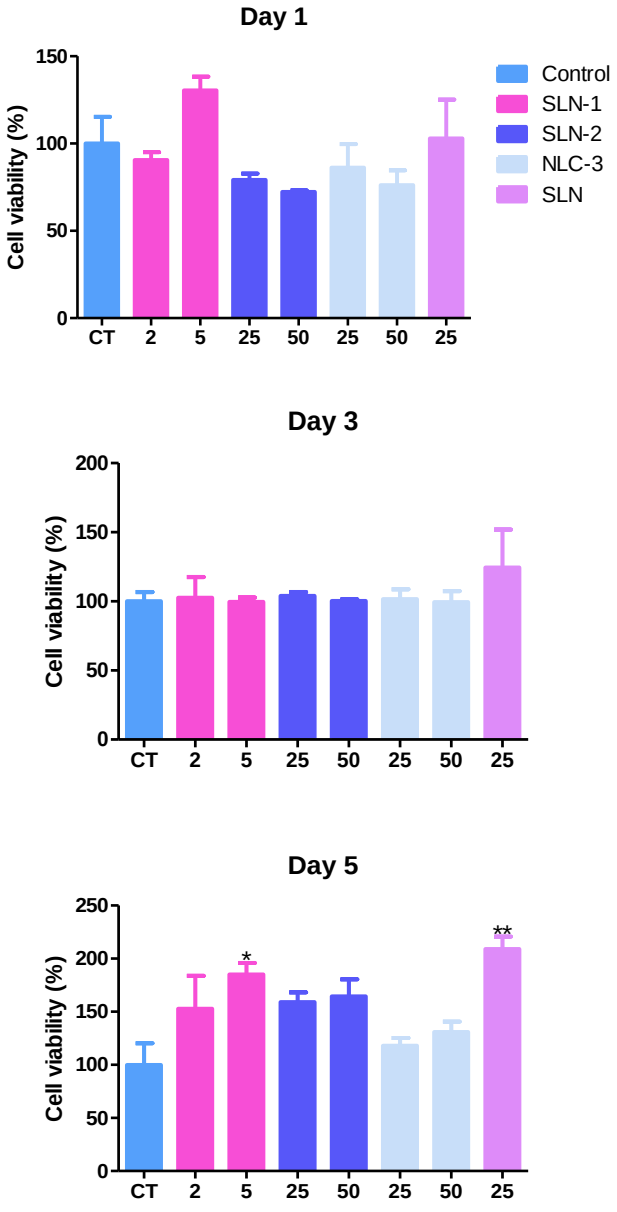

Figure 57. Effect of different formulations of SLN with CHON on viability of OA chondrocyte cells. MTT reduction values of untreated control cells were set as 100% cell viability. One-way ANOVA was performed, followed by Bonferroni test for the

significance of differences among multiple experimental groups. Data are expressed as mean ± SEM; *p< 0.05, **p< 0.01 and ***p< 0.001 significant difference compared to control cells. The numbers 2, 5, 25 and, 50 mean the SLN or NLC dilution before adding to the cells plate.

In the cell viability study carried out with OA chondrocytes, the cells were treated with different formulations SLN-1, SLN-2, NLC-3 as well as nanoparticles without CHON and the study was carried out at three different times: 1, 3 and 5 days. In no case was there cytotoxicity, both in the different treatments and in the dilutions studied. No significant differences were found in cell growth compared to control cells.

11.2 STUDY OF THE ANTI-INFLAMMATORY ACTIVITY OF CHON ENCAPSULATED IN SLN

The anti-inflammatory or regenerative activity of the CHON encapsulated in the nanoparticles was evaluated. Three formulations SLN-1, SLN-2 and NLC-3 were studied as carriers of the CHON biomolecule.

11.2.1 RT-qPCR

Using the RT-qPCR technique, the change in markers of inflammation in OA disease was measured. Table 27 shows the cytokines studied, their role or activity in OA and what is required after treatment of the disease.

Table 27. Cytokines evaluated in the study of CHON inflammatory activity carried by SLN.

Cytokine	Activity	Condition in OA
IL-1β / IL-8 / MMP13 / MMP9 / IL6 / iNOS / BMP2 / COL X or COL 10	Inflammatory	They are elevated, they must be decreased
ACAN /COLII	Regenerative	They are low, they must be increased

Taken from (97–99)

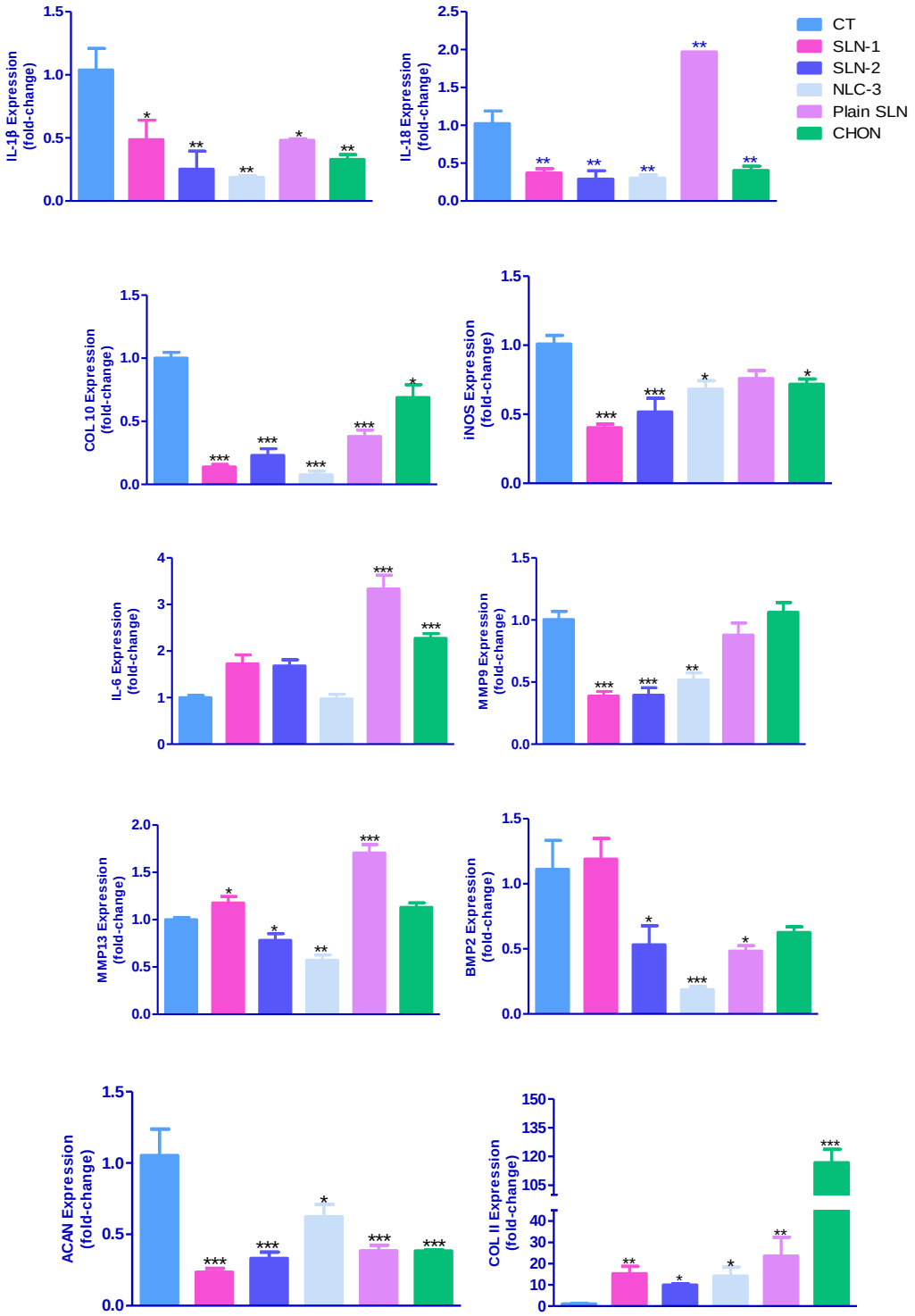

Figure 58. Gene expression analysis of OA chondrocytes after SLN + CHON treatment. CT: control was OA chondrocytes without treatment; SLN-1: cells treated with SLN-1 formulation, dilution 5; SLN-2: cells treated with SLN including cholesteryl oleate with CHON, dilution 25; NLC-3: cells treated with SLN using oleylamine with CHON, dilution 25: SLN: cells treated with plain SLN, dilution 25; and CHON: cells

treated with CHON 4.0 mg/ml in aqueous medium, dilution 25. Data are present as mean ± SEM for at least three biological replicates. One-way ANOVA test was conducted. In those cases, were p-values were < 0.05, a Bonferroni post-hoc test was conducted. Bonferroni corrected p-values are shown; *p< 0.05, **p< 0.01 and ***p< 0.001 significant difference compared to control cells. Dilutions used: SLN-1: 5; SLN-2: 25: NLC-3:25; plain SLN: 25; CHON (4.0 mg/ml): 25.

As it is indicated in the graphs of figure 58, the behavior in the decrease or increase of the cytokines studied was highly varied and dependent on the treatment used. In general, it is described for each cytokine:

- **IL-1β**: all the treatments used presented a significant decrease in IL-1β, favoring anti-inflammatory activity.

- **IL-18**: This cytokine was significantly decreased, except when treating chondrocytes only with nanoparticles without CHON, which favored the presence of IL-18.

- **COL10**: all the treatments used presented a significant decrease, generating an anti-inflammatory activity and improving the regenerative capacity of the chondrocyte.

- **iNOS**: all the treatments used presented a significant decrease, generating an anti-inflammatory activity, except for the treatment with plain SLN, which did not show significant changes.

- **IL-6**: For IL-6 a significant increase was observed with treatment with plain SLN and with CHON. Although with the SLN- and SLN-2 no significant differences were found, an increase was recorded. This behaviour may be due to the dual nature of IL-6, which on the one hand acts as an inflammatory agent but also has an anti-inflammatory capacity in another way (98).

- **MMP9**: The treatment of CHON delivered with SLN-1, SLN-2 and NLC-3 achieved a significant decrease in this cytokine, while the treatment with CHON in an aqueous medium or plain SLN did not generate significant differences.

- **MMP13**: Although the treatment with CHON in an aqueous medium, generated significant changes, the SLN-1 and plain SLN formulations presented a significant increase in this marker, while SLN-2 and NLC-3 achieved a significant decrease.

- **BMP2**: A significant decrease of this marker was obtained with the SLN-2 and NLC-3 formulations.

- **COLII and ACAN**: As previously described (Ma et al., 2017) regarding the effect of treating OA chondrocytes with CHON, in terms of markers of chondrocyte deterioration, it was found that all treatments significantly decreased the ACAN, while in the case of COLII a significant increase was achieved with all treatments.

11.2.2 ELISA

On the other hand, the anti-inflammatory capacity of CHON in SLN-2 nanoparticles was analyzed by Enzyme-Linked ImmunoSorbent Assay. The study was carried out in HaCat cells, which were induced to inflammation by adding TNF-µ.

A significant decrease in IL-8 was obtained with the SLN-2 treatment and a significant increase in IL-6, agreeing with the results obtained in the RT-qPCR study (figure 59).

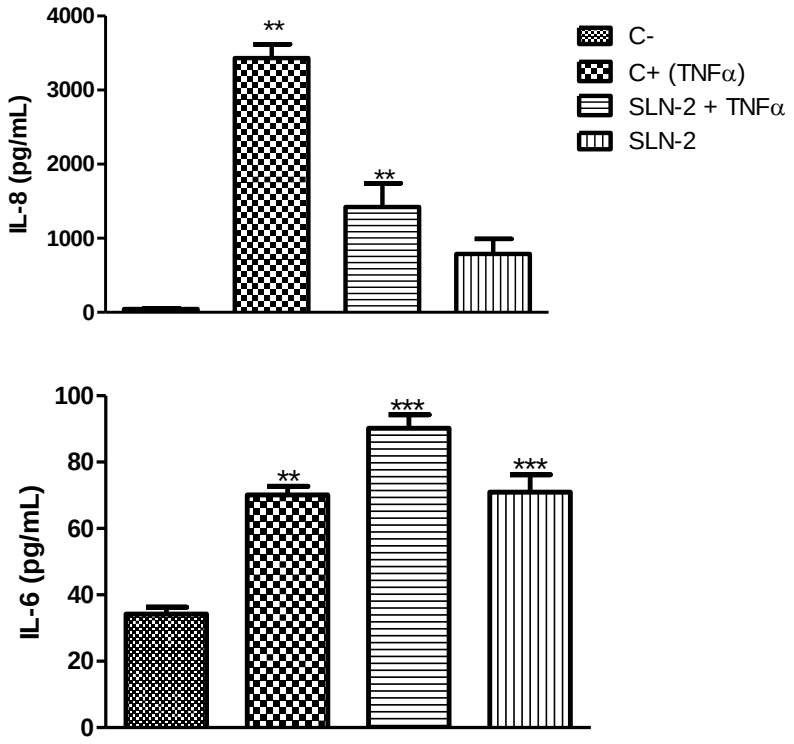

Figure 59. Quantification of secreted proinflammatory cytokines in *HaCaT cells* (keratinocyte) induced inflammation. Cells were incubated in the absence and presence of SLN-2 for 24 h. C-: Negative control, untreated control cells. C+ (TNF-α) cells previously induced to inflammation with TNF-α 20 ng/ml. Values are expressed as mean ± SD; One-way ANOVA test was conducted. In those cases, were p-values were < 0.05, a Bonferroni post-hoc test was conducted. Bonferroni corrected p-values are shown; *p< 0.05, **p< 0.01 and ***p< 0.001 significant difference compared to negative control cells.

The study of the anti-inflammatory capacity of CHON delivered with SLN shows that the biomolecule had the ability to enter the cell and generate a variation in the response of different cytokines. The nanoparticles studied have the ability to be a CHON vehicle and thus generate anti-inflammatory and cartilage regeneration activity in OA chondrocytes. Although there are differences between the formulations, the global effect of each one compensates for the unexpected effect of some responses, in general there is positive inflammatory activity.

Of the formulations studied, those with the presence of cholesteryl oleate in their composition, SLN-2 and NLC-3, present the best anti-inflammatory and regenerative profile of chondrocytes, regardless of the cationic lipid (solid or liquid) used.

11.3 CHARACTERISATION OF SLN UPTAKE BY CONFOCAL MICROSCOPY

A cellular uptake study was performed to evaluate the ability of nanoparticles to enter cells. To determine the ability of the nanoparticles to internalize cells, the SLN-1 and SLN-2 formulations were labeled with Nile red which is a fluorescent dye that interacts with lipids and allows them to be visualized without dissolving them (243).

In figure 60, the internalization of the SLN-1 nanoparticles in HaCat cells is observed, using a non-cytotoxic concentration, according to the data from the cell viability study, and at times of 1.5 h and 24 h. It is shown that in both cases there was internalization, with the presence of the labeled nanoparticles being more intense at 1.5 h than 24 h after, indicating endosomal processing and metabolism of particles after 1.5 h.

Subsequently, the internalization capacity of SLN-1 and SLN-2 in BJ cells was evaluated at a time of 1.5 h. The presence of particles marked in red inside the cells is evident in both cases (Figure 61).

CONTROL 1.5 h

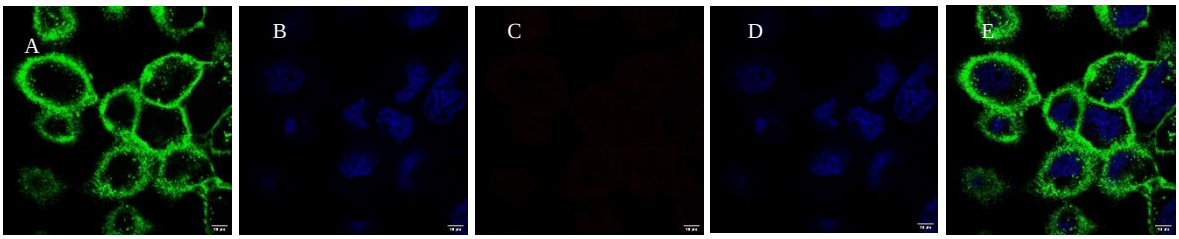

CONTROL 24 h

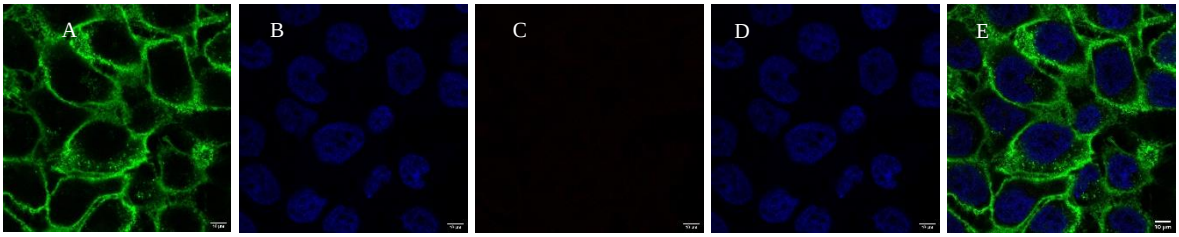

INTERNALIZATION 1.5 H – SLN-1

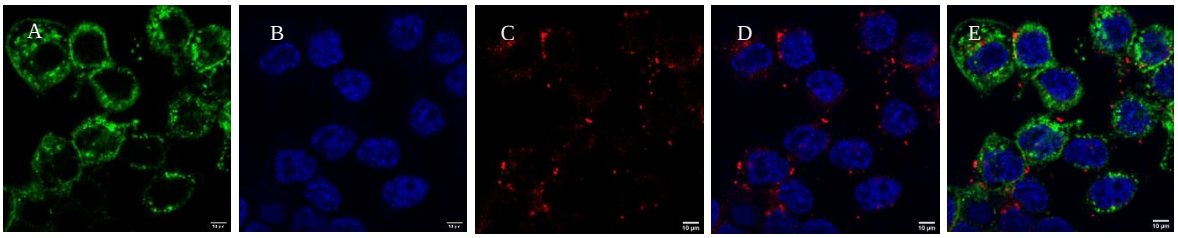

INTERNALIZATION 24 H – SLN-1

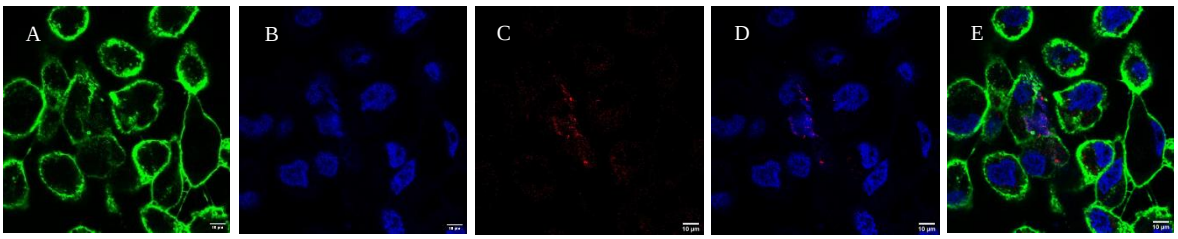

Figure 60. Cellular uptake by confocal microscopy analysis in *HaCaT cells*. Cells were incubated 1.5h and 24 h, with the indicated Nile red SLN-1 formulation. (A) membrane staining with WGA, (B) nuclei staining with DAPI; (C) fluorescence of internalized CHON-SLN, (D) merged B and C and (E) merged A, B and C. Figure scale bar corresponds to 10 μm.

CONTROL

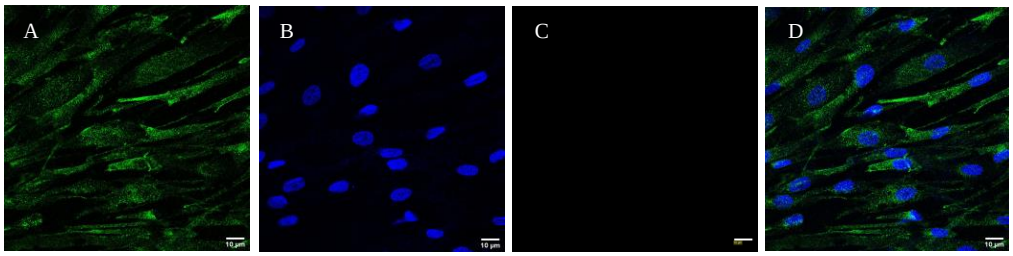

INTERNALIZATION – SLN-1

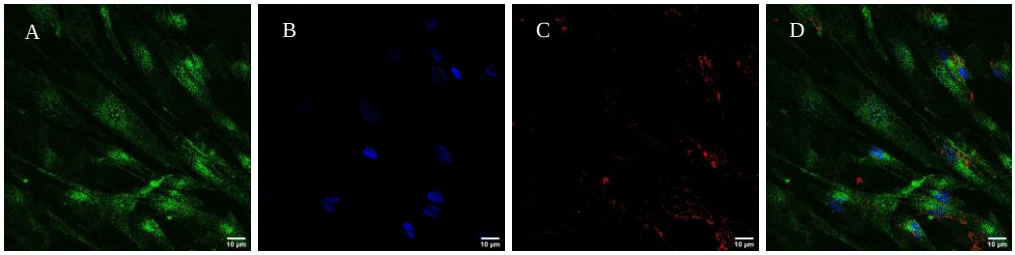

INTERNALIZATION – SLN-2

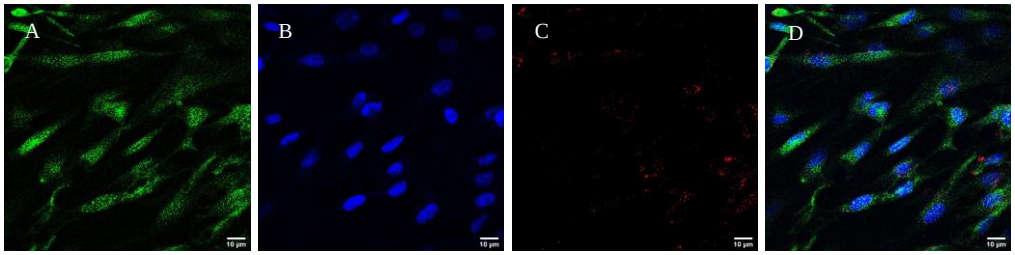

Figure 61. Cellular uptake by confocal microscopy analysis of *BJ cells*. Cells were incubated 1.5 h with the indicated Nile red SLN-1 formulation and Nile red SLN-2 formulation. (A) membrane staining with WGA, (B) nuclei staining with DAPI; (C) fluorescence of internalized SLN+CHON, (D) merged A, B and C. Figure scale bar corresponds to 10 μm.

12 EX VIVO STUDY OF SKIN PERMEATION OF CHON IN SLN

According to studies carried out, CHON has a very low permeability in the skin, due to its high molecular weight. (244,245), Therefore, new proposals are required to improve bioavailability through topical administration. (Figure 62).

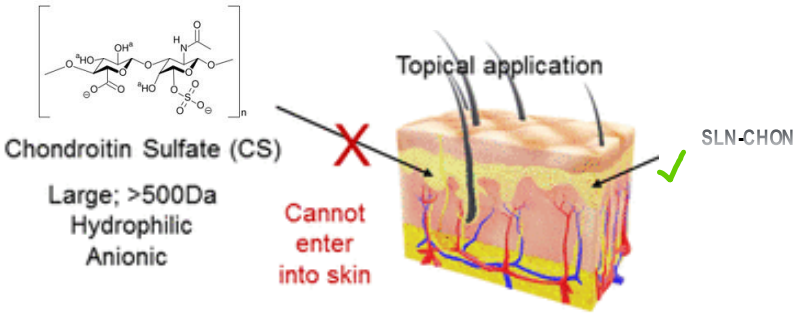

Figure 62. Use of SLN as a vehicle to internalize CHON through the skin. Modified from: (245)**.** Skin has natural barriers that do not allow certain substances with large sizes to enter, such as the case of CHON, which presents sizes up to more than 500 Da. SLNs are an alternative for the transport and entry of CHON through the skin

12.1 PERMEATION TEST

The transdermal absorption of SLN of CHON was studied, through an ex vivo permeation study, using porcine ear skin. The permeated amount of CHON at 24 h, expressed as percentage of CHON encapsulated, was also shown by median and range.

Table 28. CHON skin permeation results expressed in mg of CHON and percentage, through an ex vivo permeation study, using porcine ear skin

Sample	CHON cumulative permeate amount (mg)	Percentage permeate of CHON (%)	Median and range (%)
Control[b,c,d]	0.0060	1.47	2.44 (1.47 - 3.41)
	0.0140	3.41	
	0.0070	1.82	
	0.0120	3.06	
	0.0070	1.66	
	0.0130	3.22	
SLN-1[a,d]	0.2119	86.98	77.03 (58.4 - 86.98)
	0.1968	84.96	
	0.1784	77.03	
	0.1353	58.40	
	0.1661	71.70	
SLN-2[a]	0.3048	91.80	52.80 (27.48 - 94.6)
	0.3141	94.60	
	0.1753	52.80	
	0.0912	27.48	
	0.0980	29.51	
NLC-3[a,b]	0.1413	61.00	56.40 (44.64 - 65.26)
	0.1386	59.83	
	0.1034	44.64	
	0.1063	45.89	
	0.1512	65.26	
	0.1227	52.96	

Statistically significant differences between CHON Permeate Percentage (%) per group were evaluated. One-way ANOVA without parametric testing for the significance of differences between multiple experimental groups was performed. Followed by the t test (non-parametric test), the significance of the differences between each pair of experimental groups ($p< 0.05$) was obtained using the Mann Whitney test: **[a]**: statistically significant difference with the control (CHON 0.4 mg/ml in aqueous solution); **[b]**: statistically significant difference with the SLN-1; **[c]**: statistically significant difference with the SLN-2; **[d]**: statistically significant difference with the NLC-3. Data are expressed as median and range.

The CHON concentration in the SLN formulation was 0.4 mg/ml, achieving around 60 % encapsulation for the SLN-1 and NLC-3 formulation, while for the formulation it was 83 %. From that encapsulated percentage, the amount permeated through the pig ear skin was calculated. Permeation through the skin was achieved with the different formulations, compared to CHON 0.4 mg/ml in aqueous solution (Table 28). It gave the biological variability that occurs in this type of analysis, for example, in the thickness and in the section of biological tissue, as well as the differences in the skin of the different animals, in some formulations great variability is observed in the permeate percentage or accumulated.

SLN are a viable option for transporting CHON through the skin. CHON has low skin penetration given its high molecular size and nanoparticles have proven to be an effective transport for CHON, since they contain lipids that are also present in the human body, making it easier for them to cross the layers of the skin.

12.2 DRUG RETENTION INSIDE THE SKIN

Table 29. CHON acummulative retention amoung porcine ear skin, expressed by median and range, , through an ex vivo permeation study.

Sample	Amount retained in skin (Qr, µg/g/cm^2)	Median and range
Control[b,c,d]	4.51 8.83 4.49 8.82	6.67 (4.49 – 8.83)
SLN-1[a]	173.20 435.46 567.01 564.05	499.80 (173.20 – 567.01)
SLN-2[a]	1548.51 1084.10 281.46 295.83	690.00 (281.46 – 1548.51)
NLC-3[a]	556.60 865.51 38.98 30.98	297.80 (30.98 – 865.51)

Statistically significant differences between the accumulated amount of CHON in the skin (µg/g/cm^2) per group were evaluated. One-way ANOVA nonparametric test for the significance of differences among multiple experimental groups was performed. Following the t test (Nonparametric test), the significance of differences among each pair of experimental groups ($p < 0.05$) was obtained by Mann Whitney test: **[a]**: statistically significant difference with control (CHON 0.4 mg/ml in aqueous solution); **[b]**: statistically significant difference with the SLN-1; **[c]**: statistically significant difference with the SLN-

2; **[d]**: statistically significant difference with the NLC-3. Data are expressed as median and range.

On the other hand, as can be seen in Table 29, the CHON retained in the skin was significantly higher, when comparing the CHON in aqueous solution with respect to the formulations with SLN. This indicates a capacity of the nanoparticles to form CHON depots in the skin, which will become available over time.

Thus, a completely non-invasive method was used to deliver a bio-macromolecule into the skin without using injections or abrasive procedures.

VALIDATION OF ANALYTICAL METHODS

13 VALIDATION OF ANALYTICAL METHODS TO DETERMINE EE%

A titration method was validated to test entrapment efficiency of CHON. Cetylpyridinium chloride monohydrate was used as titrant. We evaluated the following parameters:

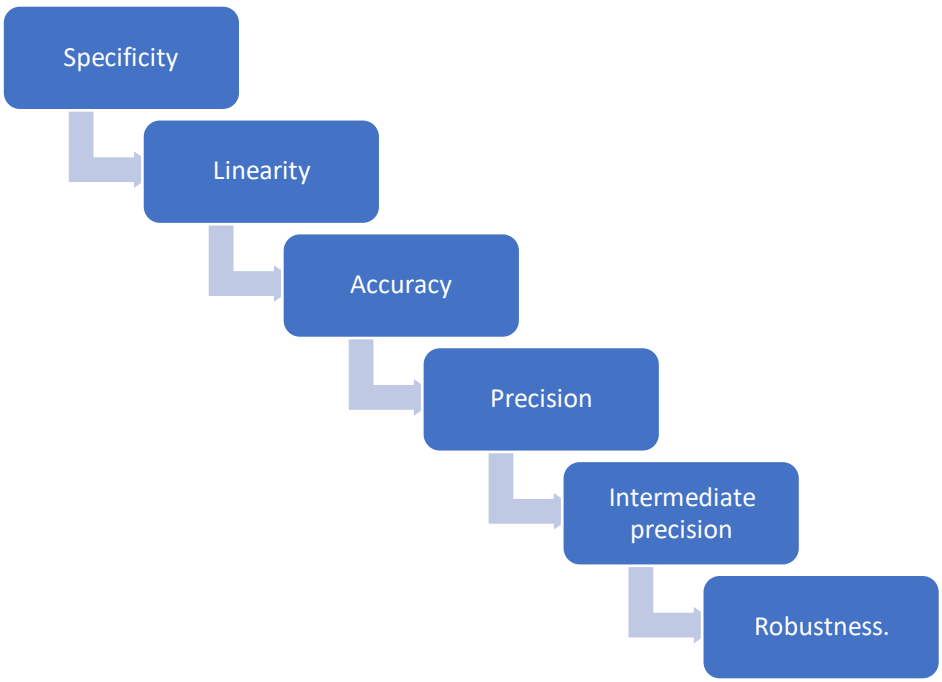

Figure 63. Analytical validation parameters. List of parameters evaluated in the validation of the analytical methods for the determination of the EE% of the CHON in the nanoparticles.

13.1 Specificity

Specificity is a parameter to determine the ability of the method to distinguish between the analyte and the other substances or excipients present (158,246).

13.1.1 TITRATION METHOD

Volumetric titration was performed in triplicate, of the matrix that consisted of a formulation of nanoparticles without the presence of CHON and not showed a consumption of titrating solution by the matrix, therefore no precipitate was formed, indicating that the method is specific to determine the presence of CHON and that the excipients of the formulation do not interfere in the analysis.

13.1.2 UV-Vis SPECTROPHOTOMETRIC METHOD

In the case of the spectrophotometric method, the determinations made on the matrix of excipients show a signal from the matrix. For this reason, the effect of matrix interference on the determination of the active ingredient in the formulation was quantified.

For the selectivity of the spectrophotometric method, the percentage of discrepancy between the signal obtained by the CHON 0.4 mg/ml sample in aqueous solution was calculated with respect to a matrix sample enriched with CHON 0.4 mg/ml.

Table 30. Study of the selectivity of the Spectrophotometric Method, by determining the percentage of discrepancy in the signal obtained.

Determination	Matriz + CHON (Abs)	CHON in aqueous medium (Abs)
1	1.010	0.820
2	1.022	0.832
3	1.115	0.925
4	1.182	0.998
Mean	**1.082**	**0.894**
SD	0.081	0.084
Discrepancy (%)	**21.09**	
Student´s t test	**p < 0.0001**	

The t test, for the significance of differences among experimental groups ($p< 0.05$) was obtained by Student's t test, and it was found that there are significant differences, with a p value less than 0.0001.

In addition, as observed in table 30 Study of the selectivity of the Spectrophotometric Method, a positive bias of 21.09 % is observed, so it does not meet the selectivity criterion, since the value of the percentage of discrepancy is greater than 5. %.

This high discrepancy value is partly due to the varied and lipid nature of the matrix, so the value obtained from the matrix alone must always be subtracted from each sample of nanoparticles analysed. Thus, it is necessary to evaluate the matrix signal in each experiment and subtract it from the value obtained with the nanoparticles loaded with CHON.

13.2 Linearity

The proportionality of the amount of analyte present in the sample was evaluated, with respect to the signal obtained or the amount of titrant consumed. (158,246). Responses from samples containing different amounts of analyte are obtained from the test method. Linearity of the CHON assay was determined by analysis of three replicates of six concentrations of CHON. The acceptance criterion to determine linearity was the coefficient of determination (R^2) > 0.99.

13.2.1 TITRATION METHOD

To titration method, the coefficient of determination (R^2) obtained was 0.9994, showing an excellent linear relation between the consumed volume of titrant and the amount of CHON present in the sample (figure 64).

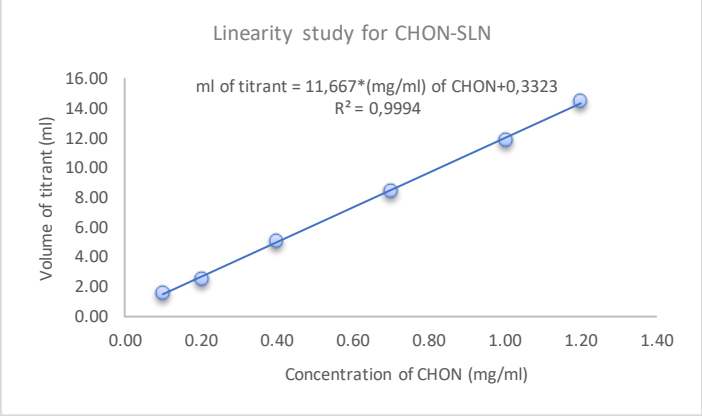

Figure 64. Linear regression curve for the assay of CHON in SLN.

Table 31. Linear regression results for the assay of linearity of CHON in SLN by titration method.

CHON concentration (mg/ml)	Average volume of titrant (ml)			
	Sample 1	Sample 2	Sample 3	Average
1.20	14.50	14.55	14.50	14.52
1.00	11.90	11.90	11.90	11.90
0.70	8.45	8.45	8.45	8.45
0.40	5.05	5.00	5.05	5.03
0.20	2.60	2.60	2.60	2.60
0.10	1.65	1.60	1.60	1.62

The values of the volume of titrant consumed increase linearly as the concentration of CHON increases (Table 31).

13.2.2 UV-Vis SPECTROPHOTOMETRIC METHOD

For the spectrophotometric method, a high determination coefficient of 0.995 was obtained (Figure 65), fulfilling the linearity criterion of the method.

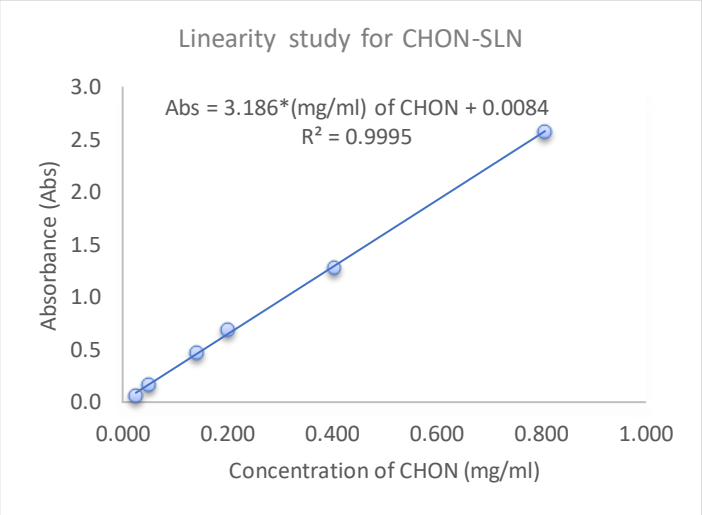

Figure 65. Linear regression curve for the assay of CHON in SLN.

Table 32. Linear regression results for the assay of linearity of CHON in SLN by UV-Vis spectrophotometric method.

CHON concentration	**Absorbance (Abs)**			
(mg/ml)	**Sample 1**	**Sample 2**	**Sample 3**	**Average**
0.808	2.541	2.620	2.582	2.581
0.404	1.284	1.281	1.279	1.281
0.202	0.700	0.667	0.685	0.684
0.141	0.477	0.471	0.474	0.474
0.051	0.163	0.163	0.163	0.163
0.025	0.064	0.067	0.064	0.065

The tables 31 and 32 show the individual values in the determination of the linear regression line of the studied methods. As the concentration of CHON in the enriched

matrix increases (1.20, 1.00, 0.70, 0.40, 0.20, 0.10 mg/ml) both the amount consumed by the titrant in the volumetric titration or the spectrophotometric signal obtained increases.

13.3 Accuracy

"The accuracy of an analytical procedure expresses the closeness of agreement between the value which is accepted either as a conventional true value or an accepted reference value and the value found" (158,247).

The accuracy of a matrix enriched to (80 – 100 – 120) % of the final concentration of CHON (0.4 mg/ml) used in the nanoparticles was evaluated. The acceptance criteria were defined as the relative standard deviation (RSD %) of the measurement, with a maximum limit of 5.3 according to OAAC (227) and an average recovery between 90.0 to 110.0 %.

13.3.1 TITRATION METHOD

The volumetric titration method meets the established accuracy criteria (table 33), since the RSD value was 1.4 less than 5.3 previously established and a recovery percentage of 93.3%, it is within the range 90.0% to 110.0%.

Table 33. Results of the accuracy determination for the study of CHON in SLN by titration method.

Determination	Sample concentration (%)	Volume of titrant (ml)	CHON recovery (%)
1	80	3.80	93.8
2	80	3.80	93.8
3	80	3.90	93.8
4	100	4.80	91.7
5	100	4.80	91.7
6	100	4.80	91.7
7	120	6.00	93.9
8	120	6.00	93.9
9	120	6.00	95.3
Mean			**93.3**
SD			**1.3**
RSD			**1.4**

13.3.2 UV-Vis SPECTROPHOTOMETRIC METHOD

Table 34. Results of the accuracy determination for the study of CHON in SLN by spectrophotometric method

Determination	Sample concentration (%)	Absorbance (Abs)	CHON recovery (%)
1	80	0.754	91.3
2	80	0.766	93.2
3	80	0.766	93.2
4	100	0.961	99.5
5	100	0.965	100.0
6	100	0.950	98.1
7	120	1.010	88.1

8	120	1.022	89.4
9	120	1.115	99.3
Mean			**94.7**
SD			**4.6**
RSD			**4.9**

The CHON recovery percentage in the matrix, with the spectrophotometric method, was higher than that obtained by the volumetric titration method, 94.7%, being also within the established range of 90.0% to 110.0% recovery (Table 34).

The variability found was higher with respect to the volumetric method, with an RSD of 4.9, even so it is less than 5.3. The variability in this method can be influenced, among other factors, by the volume of sulfuric acid required, since being a dense substance, the volume added can fluctuate and affect the final percentage recovered.

For both methods, it was fulfilled that the RSD value is below the proposed limit of 5.3, according to the AOAC regulations and within the set CHON recovery percentage (227).

13.4 Precision and intermediate precision

The consistency of the results obtained was evaluated, evaluating six samples at each level of analyte analyzed, as recommended in the ICH Q2 standards (158,247)**.**

13.4.1 TITRATION METHOD

To determine the precision of the method, two different titrants were analyzed on the same day, and intermediate precision was determined on different days with the same titrant.

Table 35. Results of intermediate precision determination for the study of CHON in SLN by titration method.

Determination	Sample concentration (%)	CHON recovery (%)	Mean	SD	RSD
T1-1	80	94.7	94.1	1.1	**1.1**
T1-2	80	92.7			
T1-3	80	94.7			
T1-4	80	94.7			
T1-5	80	92.7			
T1-6	80	94.7			
T2-1	80	96.1	94.2	0.9	**1.0**
T2-2	80	94.0			
T2-3	80	94.0			
T2-4	80	94.0			
T2-5	80	94.0			
T2-6	80	94.0			
D1-1	100	95.0	94.7	1.2	**1.3**
D1-2	100	95.0			
D1-3	100	96.6			
D1-4	100	95.0			
D1-5	100	93.4			
D1-6	100	93.4			
D2-1	100	93.5	93.9	0.7	**0.7**
D2-2	100	93.5			
D2-3	100	93.5			
D2-4	100	94.3			
D2-5	100	93.5			
D2-6	100	95.1			
Mean		**94.2**			
SD		**1.0**			
RSD		**1.0**			

* D: day: T: Titrant

When determining the CHON recovery percentage in the Matrix (Table 35), it is found that when determining the presence in 6 repeated measurements, for the 2 titrants used, the RSD value was 1.1 and 1.0 respectively and when doing the analysis with the same titrant on different days the RSD is 1.3 on day 1 and 0.7 on day 2. In general, the method is accurate, the RSD values per titrant group or per day were less than 5.3.

When evaluating the total data, taking the values obtained when using different titrants and on different days, the RSD is 1.0, which shows that it meets the intermediate precision of the method, since the global RSD value is less than 5, 3.

13.4.2 UV-Vis SPECTROPHOTOMETRIC METHOD

The precision of the spectrophotometric method was evaluated with 6 measurements of a sample and the intermediate precision, when analyzing the samples on different days.

Table 36. Results of intermediate precision determination for the study of CHON in SLN by spectrophotometric method

Determination	**Absorbance (Abs)**	**CHON recovery (%)**	**Mean**	**SD**	**RSD**
D1-1	0.496	92.0	95.1	3.5	3.7
D1-2	0.503	93.2			
D1-3	0.550	101.9			
D1-4	0.515	95.5			
D1-5	0.508	94.1			
D1-6	0.508	94.1			
D2-1	0.495	89.8	89.3	2.0	2.3
D2-2	0.494	89.6			
D2-3	0.499	90.5			
D2-4	0.488	88.6			
D2-5	0.500	90.7			
D2-6	0.467	85.0			
D2-7	0.508	90.9			
Mean		92.0			
SD		4.0			
RSD		4.4			

Given the greater variability of the spectrophotometric method found in the determination of accuracy, there is also a higher RSD than that of the volumetric method. As is shown in the table 36, for day 1 the RSD was 3.7 and for day 2 it was 2.3 and for the intermediate precision, that involves the joint values found in the 2 days, it was 4.4. Even so, the UV-Vis method is accurate with RSD values less than 5.3.

13.5 Robustness

When evaluating the robustness of the method, small changes in its conditions were introduced to assess whether they are critical factors when applying the method (158).

13.5.1 TITRATION METHOD

For the volumetric titration method, the effect of changing the titrant was evaluated, using another commercial brand (Table 37).

Table 37. Results of variation of the amount of volume of titrant in the determination of robustness for the study of CHON in SLN by titration method.

Determination	**Titrant**	**Volume of titrant (ml)**	**CHON recovery (%)**	**Mean**	**SD**	**RSD**
1	1	1.20	89.5	92.3	2.4	2.6
2		1.25	93.7			
3		1.25	93.7			
4	2	1.25	92.1	92.1	0.0	0.0
5		1.25	92.1			
6		1.25	92.1			
Valor p	0.6579					

The t test (Nonparametric test), for the significance of differences among experimental groups ($p< 0.05$) was obtained by Mann Whitney test, and no significant differences were found, with a p value of 0.6579.

Therefore, the change proposed for the study of robustness in the volumetric method does not affect the analytical test for the determination of CHON in SLN.

13.5.2 UV-Vis SPECTROPHOTOMETRIC METHOD

In the robustness study of the spectrophotometric method, specific changes were introduced, on the one hand, the variation of the wavelength, ±3 nm of the fixed working wavelength 520 nm, and on the other hand, changes in the volume (± 1 ml) of sulfuric acid added for the acid hydrolysis of glycosaminoglycans.

Table 38. Results of Wavelength (nm) variation in the robustness determination for the study of CHON in SLN by spectrophotometric method.

Determination	Sample concentration (%)	Wavelength (nm)	Absorbance (Abs)	CHON recovery (%)
1	120	520	1.726	96.0
2			1.725	96.0
3			1.714	95.3
4		517	1.724	96.3
5			1.722	96.2
6			1.713	95.7
7		523	1.719	95.8
8			1.717	95.6
9			1.706	95.0
10	100	520	1.322	87.6
11			1.435	95.3
12			1.417	94.1
13		517	1.411	94.0
14			1.323	87.9
15			1.440	96.0
16		523	1.315	87.3
17			1.425	94.8
18			1.408	93.7
19	80	520	1.136	93.6
20			1.108	91.2
21			1.136	93.6
22		517	1.142	94.3
23			1.112	91.7
24			1.141	94.2
25		523	1.125	92.9
26			1.099	90.7
27			1.124	92.9
Mean				93.6
SD				2.6
RSD				2.8

The data in Table 38 show the results of the analysis of matrix samples spiked with different concentrations of CHON and evaluated at the different wavelengths. On average, a recovery of 93.6% and an RSD DE 2.8 was obtained.

A One-way ANOVA test was performed for the significance of differences among multiple experimental groups was performed, not finding differences between groups, with an overall p value of 0.8078. Followed the Tukey's Multiple Comparison Test was performed for the significance of differences among each pair of experimental groups ($p< 0.05$), and the results are presented below.

Table 39. Tukey's Multiple Comparison Test for changes in wavelength in the robustness study.

Groups evaluated	Significant? P < 0.05?	Summary
520 nm vs 517 nm	No	ns
520 nm vs 523 nm	No	ns
517 nm vs 523 nm	No	ns

ns: no significant differences

No significant differences were found in the different groups, analyzed by wavelength analyzed (Table 39). Therefore, a variation of ±3 nm in the wavelength does not affect the spectrophotometric analytical method.

In the study of the influence of the volume of sulfuric acid in the determination of the EE% of CHON in the nanoparticles, Table 40 shows the results when varying the volumes of sulfuric acid.

Table 40. Results of absorbance variation in the robustness determination for the study of CHON in SLN by spectrophotometric method.

Determination	Volume of sulfuric acid (ml)	Absorbance (Abs)	CHON recovery (%)	Mean	SD	RSD
1	5	0.652	93.7	93.6	2.2	2.3
2		0.666	95.8			
3		0.637	91.4			
4	4	0.537	76.4	76.5	3.3	4.3
5		0.560	79.8			
6		0.516	73.2			
7	6	0.453	63.7	63.6	2.0	3.2
8		0.465	65.5			
9		0.438	61.5			

The One-way ANOVA test was performed for the significance of differences among multiple experimental groups was performed, finding significant differences in the global analysis between groups, with a value of $p < 0.0001$. Followed by the Bonferroni's Multiple Comparison Test for the significance of differences among each pair of experimental groups ($p< 0.05$), and the results are presented below.

Table 41. Bonferroni's Multiple Comparison Test for changes in the volume of sulfuric acid used in the robustness study.

Groups evaluated	Significant? P < 0.05?	Summary
H_2SO_4 (5.0 mL) vs H_2SO_4 (4.0 mL)	Yes	***
H_2SO_4 (5.0 mL) vs H_2SO_4 (6.0 mL)	Yes	***
H_2SO_4 (4.0 mL) vs H_2SO_4 (6.0 mL)	Yes	**

*p< 0.05, **p< 0.01 and ***p< 0.001

Since there are statistically significant differences between the recovery percentages according to the volume of acid added (Table 41), and very low results (76.5 % and 63.6 %) are obtained using 4.0 or 6.0 ml respectively, it is necessary to be sure to add the 5.0 ml volume.

Table 42. Summary of the results obtained in the validation of the analytical methods for the determination of the EE% of CHON in the SLN.

Parameter	**Method Title**	**UV-Vis method**
Specificity / Selectivity No reaction with the matrix / % discrepancy ≤ ± 5%	White does not react with titrant	Discrepancy (%) 21.09 Student'st test $p < 0.0001$
Linearity ($r^2 > 0.99$)	0.9994	0.9995
Precision (%CV ≤ 5.3)	1,3	3.7
Precision intermediate (%CV ≤ 5.3)	1.1	3.0
Accuracy–SLN(%) RSD < 5.3 Recovery between 90.0 and 110.0%	 1.4 93.3	 4.9 94.7
Robustness Statistical test	Changes do not affect the results	Different volumes of sulfuric acid produce significant changes in the result.

In general, according with table 42, both methods met the established validation criteria. The volumetric method presents less variation in the means compared to the spectrophotometric method; the latter being influenced by the precision in the addition of sulfuric acid. The spectrophotometric method achieved a higher CHON recovery percentage and always requires the measurement and correction of the matrix signal.

SLN AS VEHICLE OF pDNA

14 SLN AS VEHICLE OF DNA

14.1 MORPHOLOGICAL ANALYSIS BY TRANSMISSION ELECTRON MICROSCOPY (TEM) DE LAS SLN AND LIPOPLEXES

The morphological analysis with the characteristic TEM technique also to characterize the recently lyophilized SLN-4 and NLC-5 nanoparticles and after 12 months of storage at room temperature, which were used in the study of pDNA transfection through the formation of lipoplexes.

In figure 66, in all cases, the nanoparticles were found to be heterogeneous in size and circular in shape with an average diameter of around 200 nm. SLN-4 contain octadecylamine, a cationic lipid that is solid at room temperature, and NLC-5, a cationic lipid that is liquid at room temperature. Figures A and B represent the lyophilized cationic nanoparticles at time zero and C and D represent the lyophilized cationic nanoparticles at time zero and after 12 months, all cases show nanoparticles with a size of around 200 nm, confirming the size data in the stability study, being possible the use of the formulations after this storage time.

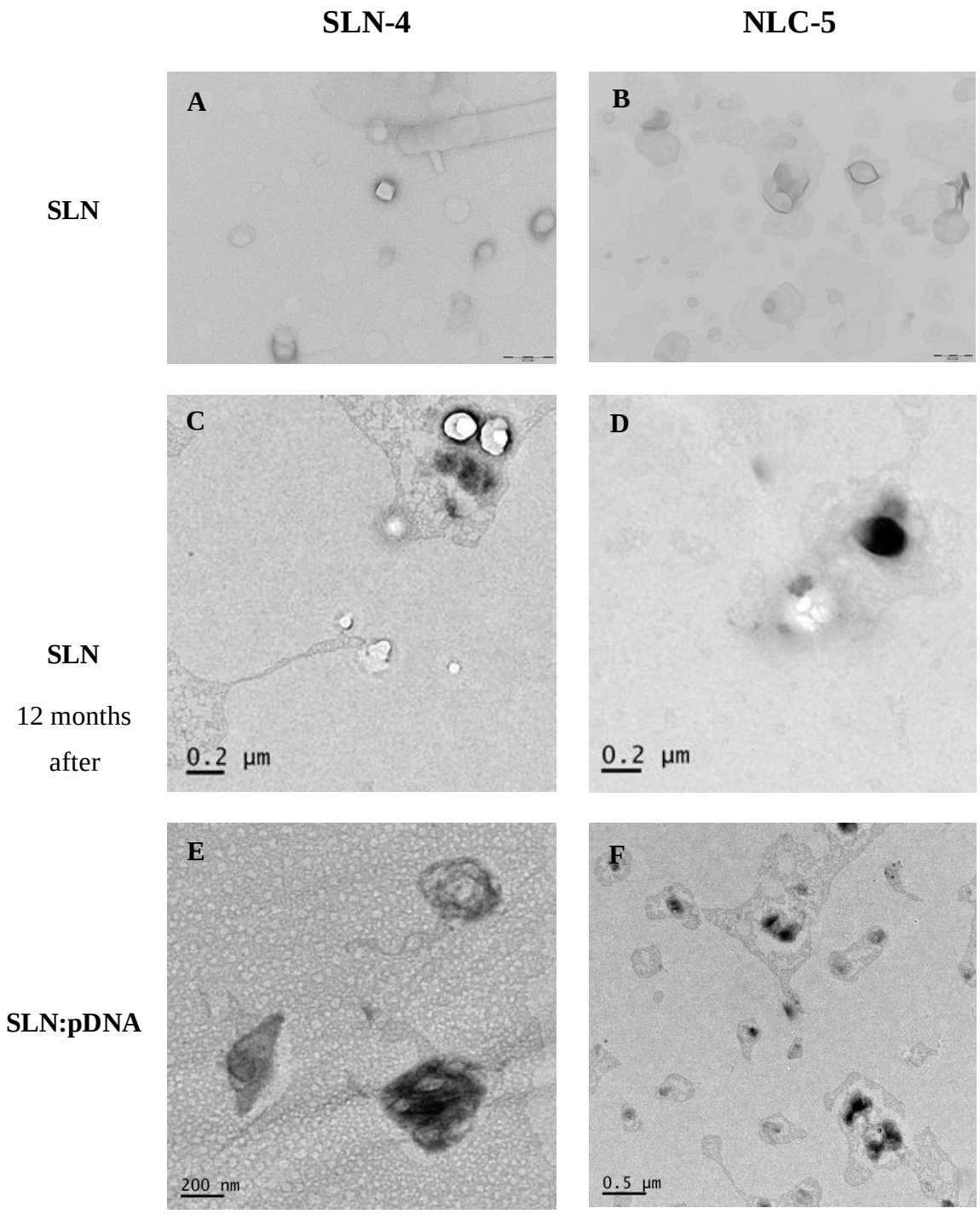

Figure 66. Morphological study of lipoplexes by TEM. TEM micrographs of deposited (A and B) freshly freeze-dried solid lipid nanoparticle (SLN), (C and D) solid lipid nanoparticle (SLN) freeze-dried and stored at room temperature for 12 months and

lipoplexes using SLN freeze-dried and stored at room temperature for 12 months (1:20) pDNA:SLN. Scale bar 0.2 µm (200 nm), except figure F, 0.5 µm (500 nm).

The figure 66, micrographs E and F show the formation of lipoplexes with both formulations, pDNA:SLN complexes were found to be larger in size compared to nanoparticles alone, with more heterogeneous shapes and undefined edges. Previous research has shown that the size and shape of the nanoparticles change with DNA loading, which may be due to the complete coating of the nanoparticles, darkening the edges and giving the lipoplexes a different shape (248,249).

14.2 DETERMINATION OF SURFACE CHARGE (ZETA-POTENTIAL) AND PARTICLE SIZE

The size and Z potential of the different lipoplex ratios studied (1:2, 1:5, 1:10 and 1:20) were measured.

Table 43. Sizes, PDIs and superficial charges (Z Potential) of lipoplexes (SLN binding pDNA), formed in different ratios (w/w), by mixing an aqueous solution of 1µl of the EGFP plasmid (1 mg/ml) together with different amount of SLN suspension (36 µg/µl).

Formulation	SLN-4			NLC-5		
	Size (nm)	PDI	Z Potential (mV)	Size (nm)	PDI	Z Potential (mV)
Plain SLN	140.7 ± 1.1	0.174 ±0.023	45.2 ± 0.8	162.0 ± 0.8	0.225 ± 0.014	46.0 ± 1.5
1:1	161.4 ± 12.0	0.409 ± 0.064	39.8 ± 0.7	161.8 ± 2.1	0.228 ± 0.009	44.7 ± 0.4
1:2	309.6 ± 17.0	0.639 ± 0.106	-13.8 ± 1.3	113.5 ± 3.1	0.279 ± 0.026	-45.8 ± 1.8
1:5	2849.5 ± 1061.9	0.158 ± 0.018	24.4 ± 0.7	108.9 ± 1.4	0.293 ± 0.040	-43.7 ± 0.2
1:10	1784.3 ± 390.9	0.527 ± 0.131	34.3 ± 0.5	132.9 ± 7.2	0.303 ± 0.011	-47.9 ± 0.2
1:20	302.1 ± 23.5	0.417 ± 0.055	38.2 ± 1.3	275.0 ± 3.5	0.271 ± 0.038	± 1.0

The table 43 shows the values obtained in the measurement of the size and Z potential of the lipoplexes, with their respective standard deviations. Graphically, the distribution of sizes and charges can be seen in Figure 67.

For the SLN-4 formulation, with all the lipid components in solid form, the size is maintained between 140.7 nm and 309.6 nm, except for the 1:5 and 1:10 ratios that present a size greater than 1700 nm due to agglomeration accommodation. specificity of the cationic nanoparticles with the pDNA. The Z potential remains positive except for the 1:2 ratio, where the negative surface charge of the pDNA predominated. Since the 1:20 lipoplex remains smaller than the 1:5 and 1:10 lipoplexes and has a positive surface charge, it is considered a suitable choice for other cell transfection studies.

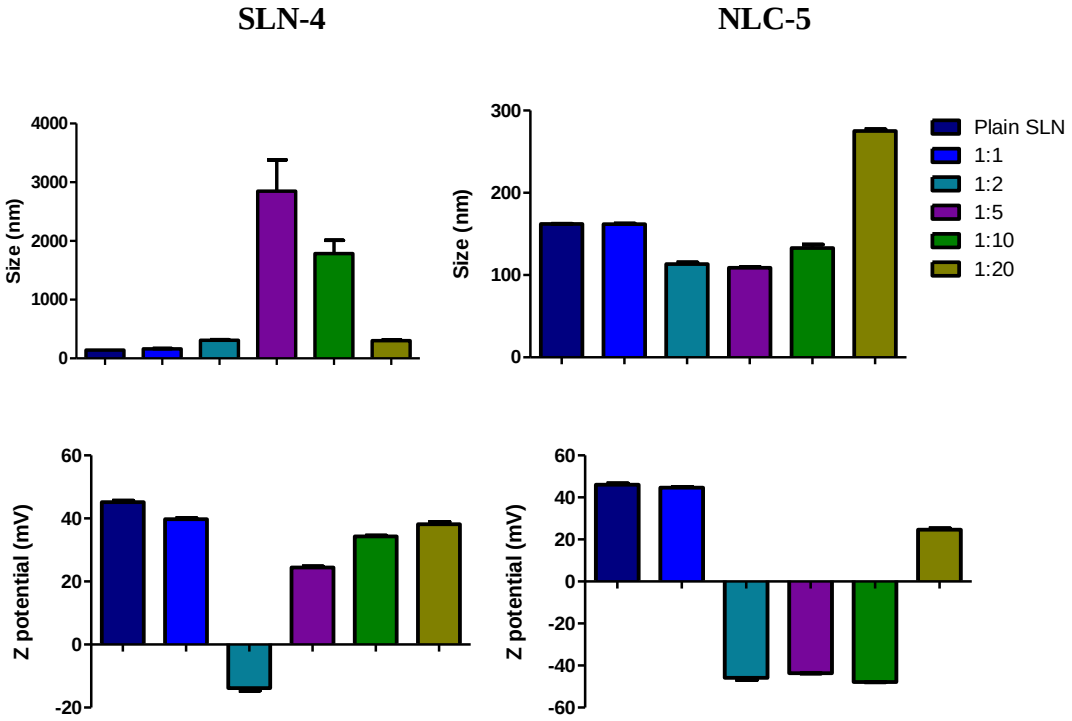

Figure 67. Sizes and superficial charges of lipoplexes. Study of size and Z Potential of lipoplexes (SLN binding pDNA), formed in different ratios (w/w), by mixing an aqueous solution of 1µl of the EGFP plasmid (1 mg/ml) together with different amount of SLN suspension (36 µg/µl).

A different behavior was obtained from the formation of lipoplexes with the NLC-5 formulation (Figure 67), which contained a liquid cationic lipid at room temperature. All the sizes of the lipoplexes remained smaller than 275 nm and the Z potential was positive

for the 1:1 and 1:20 ratios. Similarly, the 1:20 lipoplex is considered the most appropriate option for the study of cell transfection due to the greater number of positive charges, the increased zeta-potential resulting in increased transfection.

14.3 PLASMID PREPARATION

For the study of cell transfection, the pEGFP plasmid was used, which contains an ampicillin-resistant gel, as observed in the circular map of the plasmid (Figure 68). The plasmid sequence was confirmed by restriction digest and agarose gel electrophoresis. HindIII and EcoRI were used as restriction enzymes to excise the encoded EGFP gene from the plasmid backbone. Undigested and digested vector samples were visualized by agarose gel electrophoresis by visualizing the samples on a 1.0% agarose gel. Agarose gels were imaged using the Bio-Rad Chemidoc system (Bio-Rad, USA).

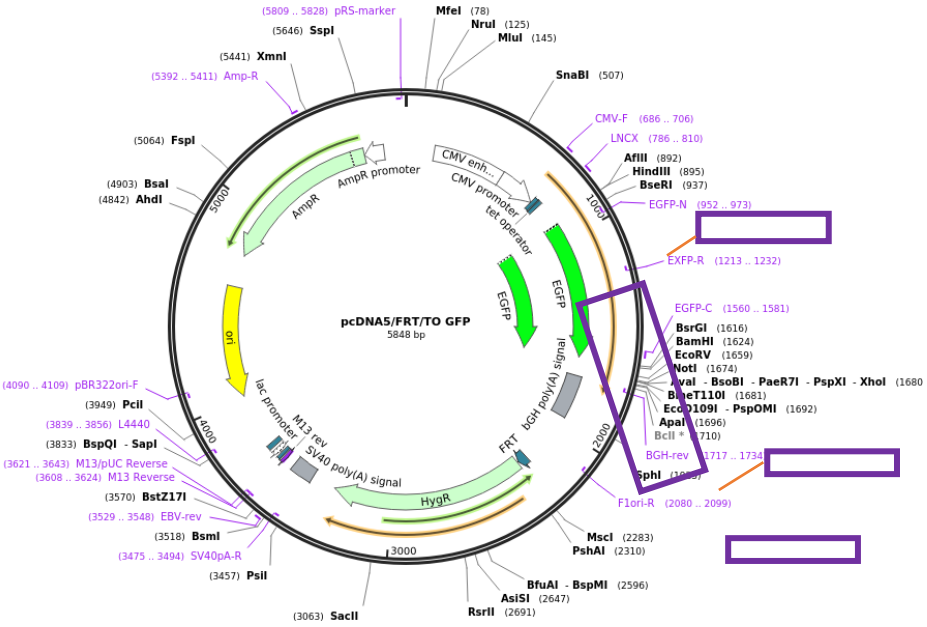

Figure 68. pEGFP Plasmid circular map. The sites where the restriction enzymes HindIII and EcoRI would act are indicated with orange lines. Adapted from (221).

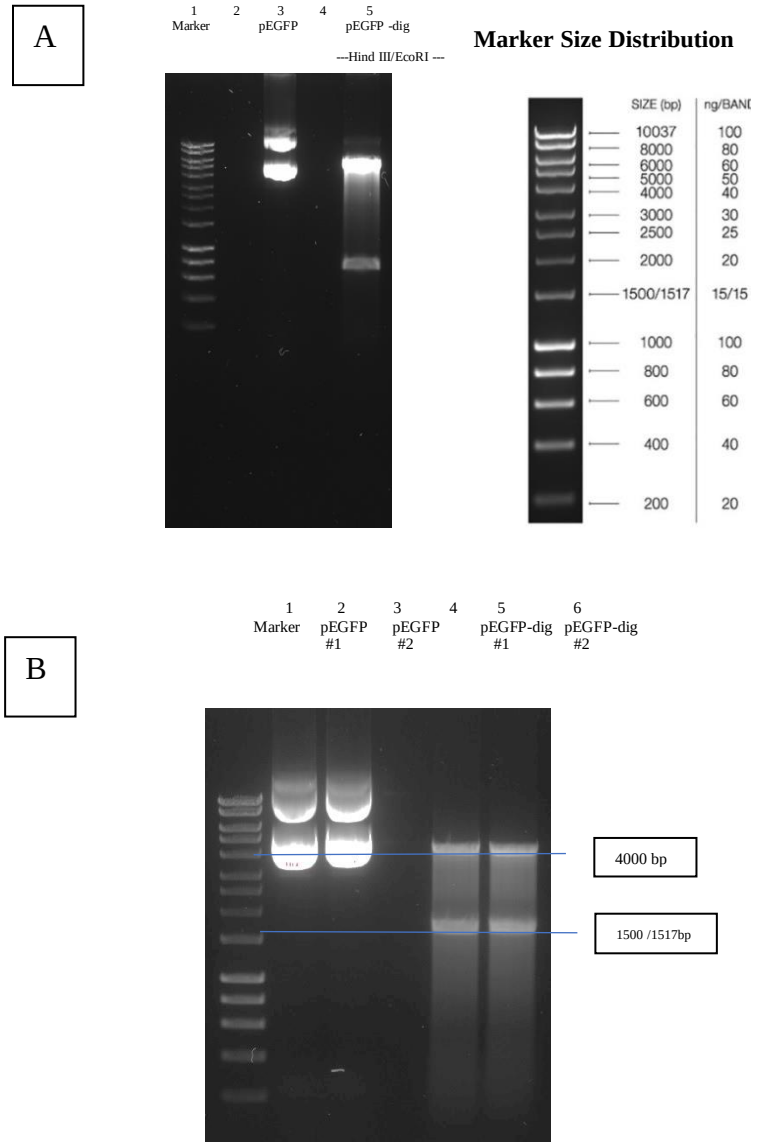

Figure 69. Plasmid digestion with Hind III and EcoRI. Confirmation of pEGFP vector functionality through doble enzymatic digestion by agarose gel electrophoresis. Image A presents in lane 1: the size marker, lane 2 and 4: empty, lane 3: the EGFP plasmid, lane 5: the EGFP plasmid digested with restriction enzymes. Image B presents lane 1: the size marker, lane 4: empty, lane 2 and 3: the EGFP plasmid, lane 5 and 6: the EGFP plasmid digested with restriction enzymes (HidIII and EcoRI). HyperLadder™ 1kb was used as a marker. The experiment was performed in triplicate (A and B).

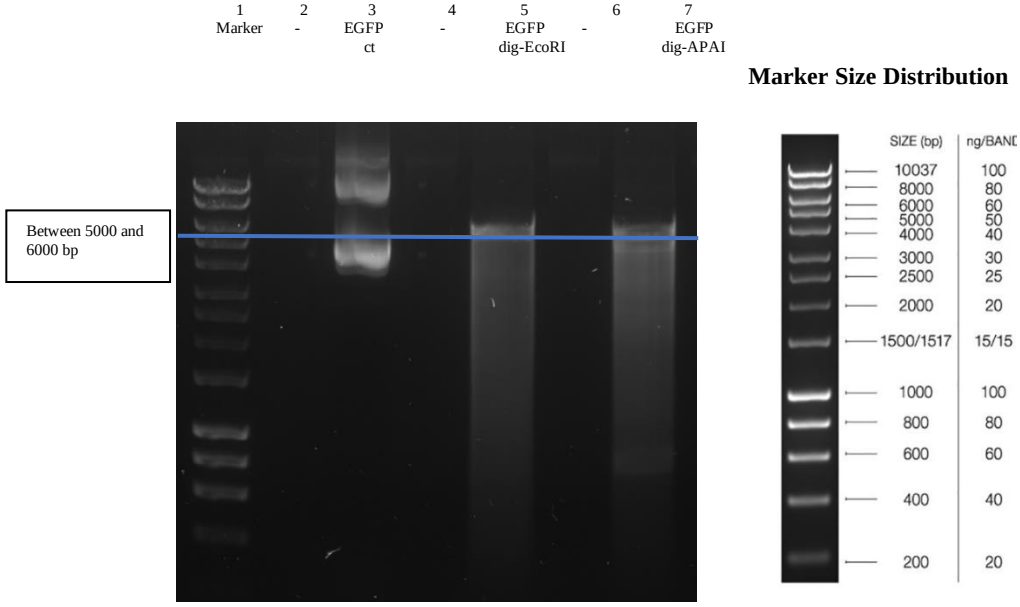

Figure 70. Plasmid digestion with ApaI and EcoRI. Confirmation of pEGFP vector functionality through single enzymatic digestion (ApaI or EcoRI) by agarose gel electrophoresis. Lane 1: the size marker, lanes 2, 4 and 6: empty, lane 3: the EGFP plasmid, lane 5 the EGFP plasmid digested with EcoRI restriction enzyme and lane 7 the EGFP plasmid digested with ApaI restriction enzyme. HyperLadder™ 1kb was used as a marker.

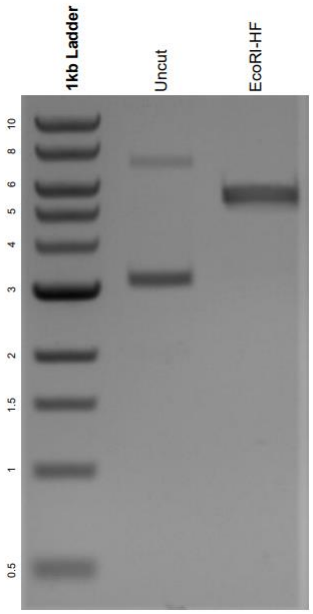

Figure 71. pEGFP digested with EcoRI-HF single digest for 2 hours. Taken from Addegene, n.d. (250)

Enzymatic digestion tests of the plasmid served to confirm the identity and purity of the EGFP plasmid used. The figures 69 and 70 confirm the size of the plasmid around 1500 bp. The uncut plasmid showed the profile reported on the Addgene supplier webpage, with two characteristic bands and the single digestion showed the total size of the plasmid between band 3 and 4 of the size marker, also reported by the manufacturer (Figure 71).

14.4 GEL RETARDATION ASSAYS

14.4.1 Agarose gel based assays

Gel retardation assays were performed to assess the binding ability of SLN to pDNA and to protect it in the presence of DNase enzymes. The composition of DNA:SLN weight ratios (v/v) was characterized by agarose gel electrophoresis (Figure 72). The principle

of this assay is that the free DNA migrates forward within the electric field, whereas the DNA interacting with any substance remains in the well (251).

First, band 2 of the free plasmid EGFP is observed, which showed complete DNA migration, and then from band 3 to lane 14, the bands obtained from the lipoplexes are seen, where all the ratios of DNA-SLN complexes, except 1:1 ratio whose signal is similar to that of the free plasmid, displayed complete retardation of DNA movement. This indicates the integrity of DNA-SLN complexes. Lanes 3 and 9 show no bands, as expected for the signal from the SLN-4 and NLC-5 formulations without DNA. Lanes 4-8 and 10-14 present the DNA signal but its intensity decreases as the amount of nanoparticles present per 1 ug of DNA increases, and for lipoplexes 1:10 and 1:20 the bands are less intense than all other combinations showing strong binding of SLN to DNA. The two evaluated formulations SLN-1 and SLN-2 show greater binding to plasma DNA as the amount of nanoparticles increases.

14.4.2 DNase protection assay

The DNase protection assay was carried out to analyze the level of protection of SLN bound DNA from DNases. The results are shown in Figure 72, images A, lane 15 onwards, and image B, from lanes 2 to 7. The lane 15 of the image A, showed a naked plasmid DNA which was completely digested by DNase in the same time. As shown in this test, the DNA was affected by DNase digestion in all ratios of DNA-SLN-4 complexes; the DNA:NLC-5 lipoplex samples, ratio 1:5, 1:10 and 1:20, a minor amount of DNA appearing to escape, which implies the protection of DNA against DNases.

14.4.3 SDS induced release assay

To determine the ability of SLN-4 and NLC-5 nanoparticles to protect plasmid DNA from degradation by the DNase enzyme, all samples were treated with DNase I and subsequently DNA release from the SLN was provided for its visualization, using SDS.

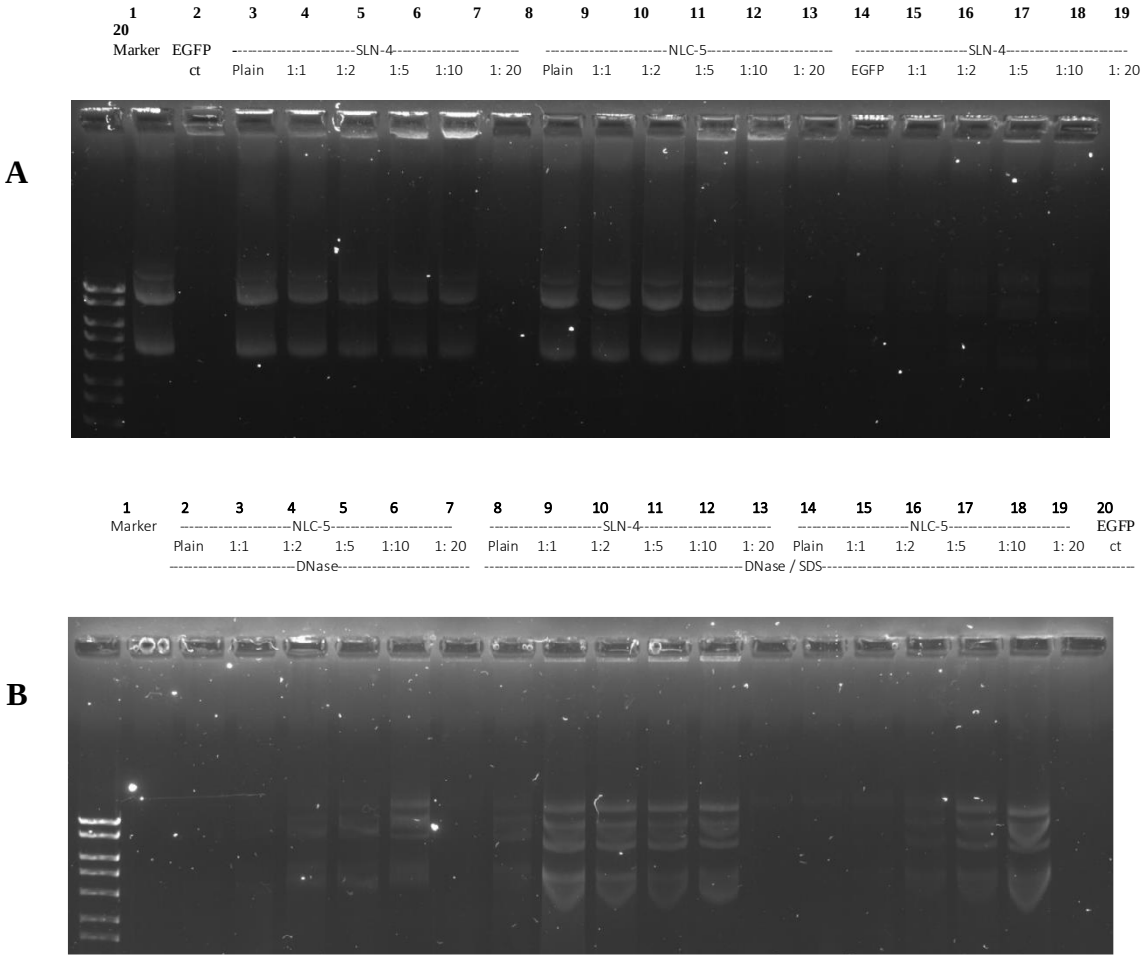

Figure 72. Agarose gel electrophoresis of a range of lipoplexes pDNA:SLN-4 and pDNA:NLC-5 w/w ratios. A: pDNA binding Assay and DNase I protection assay. B: continues DNase I protection assay and DNase I and subsequently released from particles by SDS treatment. Marker: Hyperladder I; EGFP ct: 1 µg of plasmid DNA only; Plain: SLN only; 1:1, 1:2, 1:5, 1:10, 1:20 (w/w) of pDNA (1µg/µl):SLN (36 µg/µl) ratio lipoplexes. DNase: DNase I protection assay: DNase/SDS: sample treated with DNase I and subsequently released from particles by SDS treatment.

To release the pDNA protected by the nanoparticles, SDS, an anionic detergent, was used to disrupt the interaction of the lipid nanoparticle with the pDNA, both to the pDNA-SLN-4 complexes and to the pDNA:NLC-5 complexes. This assists the evaluation of conformational integrity of the released plasmid. In figure 72, image B, from lane 8 to 20, the SDS induced release assay was performed, also showing a characteristic SDS band that did not appear in the previous tests on the agarose gel. Lane 20 shows the naked plasmid treated with the DNase enzyme and subsequently with SDS, there is no signal on the gel. In the case of the SLN-4 formulation, observe for all the lipoplex ratios, from lane 9 to 13, the signal of the plasmid released from the nanoparticles and appears in its native conformation. In the case of the lipoplexes with the NLC-5 formulation, lanes 15 to 19, the release from lipoplexes 1:5 to 1:20 is observed, showing the characteristic signal of the intact plasmid, indicating effective protection against DNases by nanoparticles.

This assay confirms the ability of the two formulations studied to protect pDNA from attack and digestion by the DNase I enzyme, the SLN-4 formulation being more effective than NLC-5, since all pDNA-SLN-4 were able to protect the plasmid when treated with DNase I, while free pDNA was totally degraded. After the treatment with SDS, pDNA was able to migrate from the loading wells, which demonstrates its ability to be released from SLN-4 and NLC-5 vectors.

14.5 CELL VIABILITY - CYTOTOXICITY (MTT)

The cellular viability studies of cells treated with SLN and lipoplexes was performed using Dendritic cells treated with different ratios of lipoplexes.

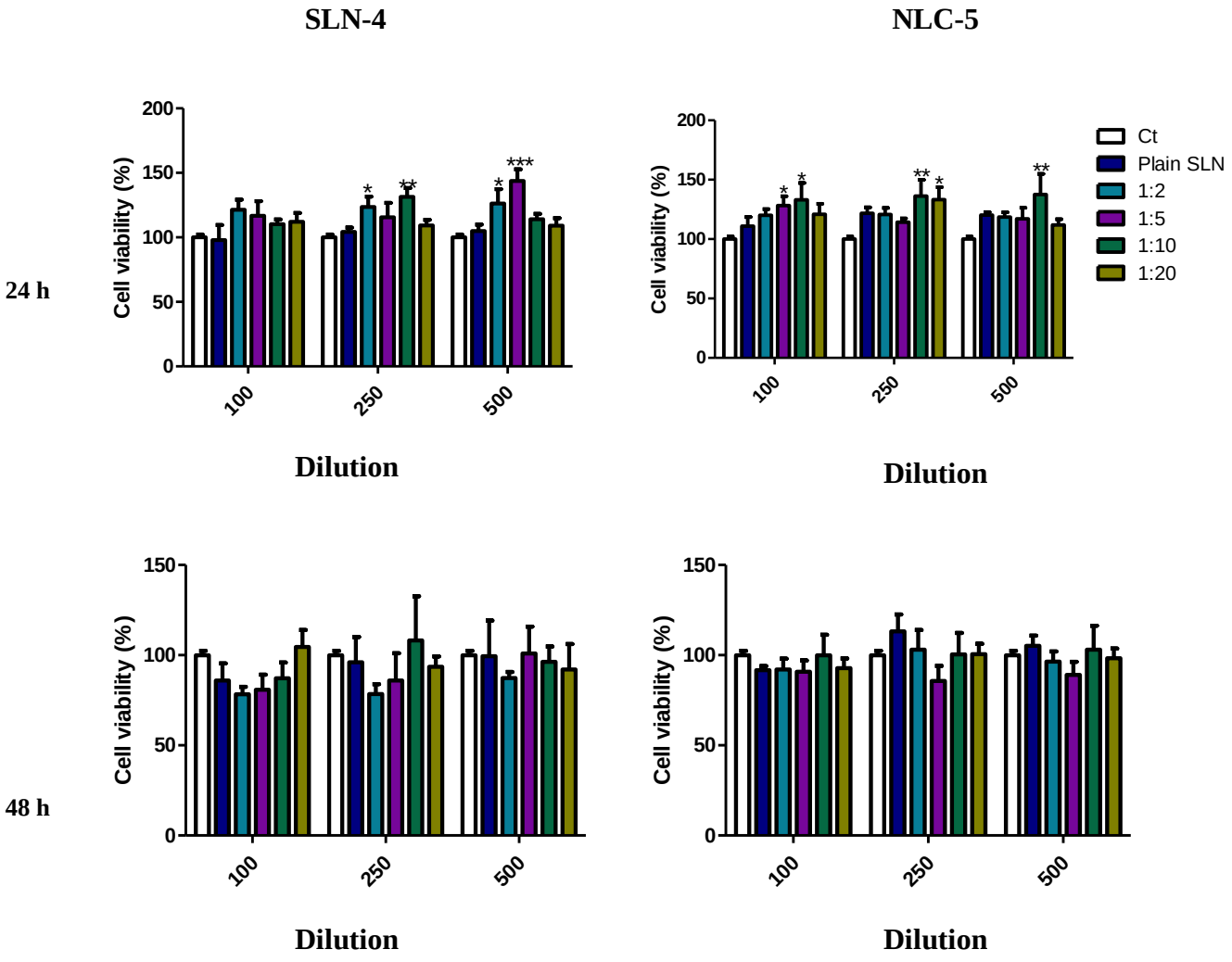

Figure continues in the following page.

72 h

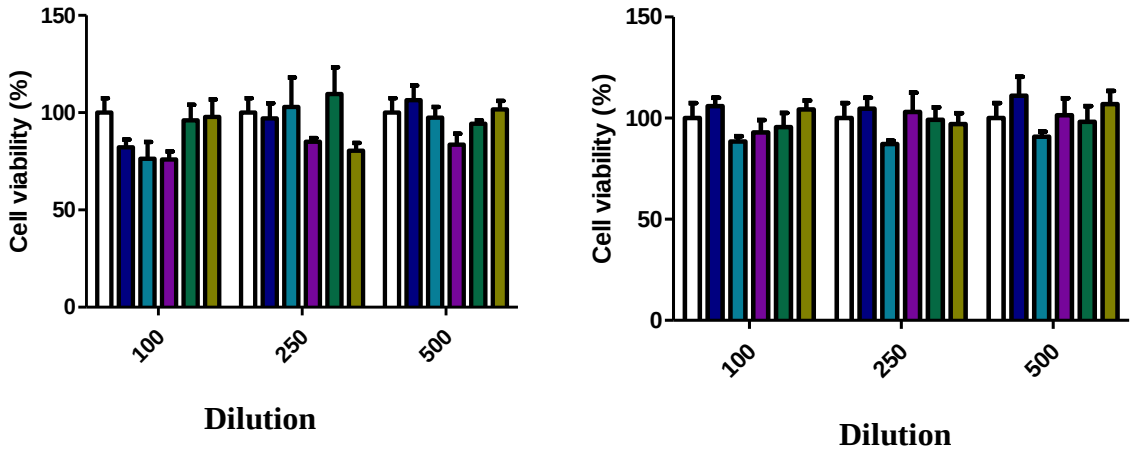

Figure 73. Cell viability assays in DC2.4 cells with lipoplexes at 24, 48 h and 72 h. Different ratios of Lipoplexes were studied (1:2; 1:5; 1:10; 1:20 (w/w) of pDNA (1µg/µl):SLN-4 (36 µg/µl)) on viability of DC2.4 cells at 24 h, 48 h and 72 h. Different dilution of the lipoplexes where evaluated. MTT reduction values of untreated control cells were set as 100% cell viability. Two-way ANOVA was performed, followed by Bonferroni test for the significance of differences among multiple experimental groups. Data are expressed as mean ± SEM; *p< 0.05, **p< 0.01 and ***p< 0.001 significant difference compared to control cells.

The study of the cell viability of the cells in contact with different concentrations of pEGFP:SLN-4 and pEGFP:NLC-5 lipoplexes, was evaluated in DC2.4 cells at 24 h, 48 h and 72 h. Different ratios of lipoplexes were used, 1:2, 1:5, 1:10 and 1:20, in three different dilutions in contact with the cells.

In general, both SLN-4 and NLC-5 formulations in the form of lipoplexes did not present cellular cytotoxicity at any of the times or concentrations studied (Figure 73). Within 24 h, significant differences were observed in favor of cell growth for some combinations of lipoplexes. In the study at 48 h and 72 h, there were no significant differences, showing normal cell growth, compared to the control cells without treatment.

14.6 CONFIRMATION OF LIPOPLEXES TRANSFECTION BY FLUORESCENCE MICROSCOPY

The study of transfection capacity of nanoparticles as a vehicle of pDNA was performed. The cell transfection capacity of SLN-4 and NLC-5 was evaluated in DC2.4 cells exposed to lipoplexes formed by pEGFP:SLN-4 and pEGFP:NLC-5, for 72 h by fluorescence microscopy. DAPI-stained cell nuclei are shown in blue and the expression of the GFP protein is shown in green.

The figure 74 shows the ability of the nanoparticles to internalize the cell nucleus and achieve the expression of the GFP protein, in comparison with control cells, not treated with any treatment, and cells treated with SLN without the DNA plasmid, which they did not show the presence of a signal of the protein in green color.

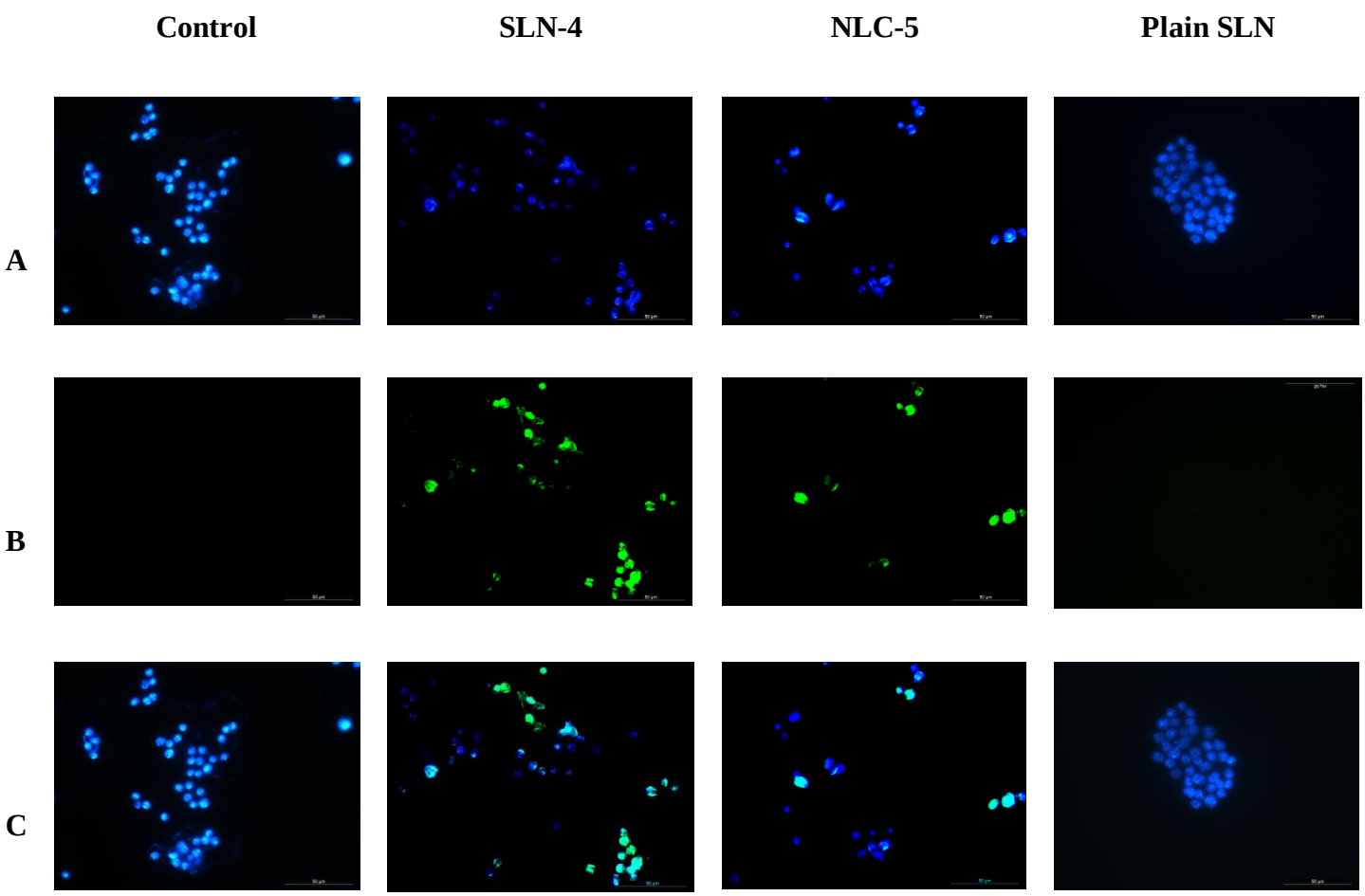

Figure 74. Fluorescence micrograph of DAPI-stained DC2.4 cells (blue; nuclei) expressing green fluorescent protein (EGFP). Cells were transfected with lipoplex (pEGFP SLN loaded with nanoparticles, 1:20, dilution 100) for 72 h. Negative control correspond DC2.4 cells without transfection. A) DAPI-stained (blue; nuclei), B) EGFP expression and, C) Merge of images A and B. Scale bar 50 µm.

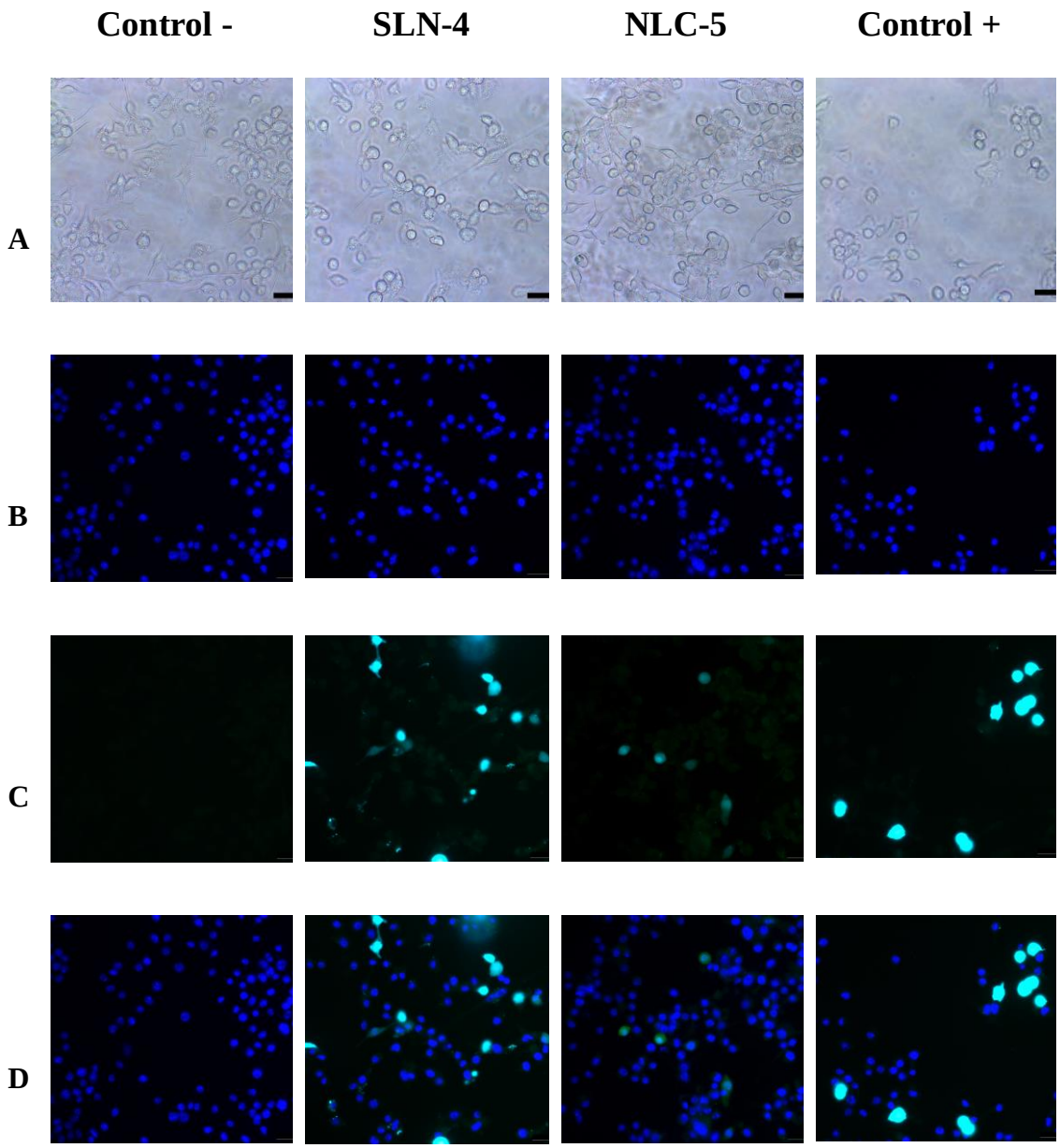

Figure 75. Fluorescence micrograph of DAPI-stained DC2.4 cells expressing green fluorescent protein (EGFP). Cells were transfected with lipoplex (pEGFP SLN loaded with nanoparticles, 1:20, dilution 100) for 72 h. Negative control correspond DC2.4 cells without transfection and positive control correspond to cells treated with Lipofectamine as a vector of pEGFP. A) Gray images correspond to the respective transmitted light to each condition to visualize the extension of the cytoplasm, B) DAPI-stained (blue; nuclei), C) EGFP expression and, D) Merge of images B and C. Scale bar 50 µm.

The transfection capacity of the pEGFP:SLN-4 and pEGFP:NLC-5 lipoplexes was also qualitatively compared to the positive control cells, which contained lipofectamine as vector of DNA. DAPI-stained cell nuclei are shown in blue and GFP protein expression is shown in green.

The figure 75 shows that although the green signal corresponding to the expression of the GFP protein is less intense than that achieved with lipofectamine as a vector, there is the ability of the nanoparticles to internalize the cell nucleus and achieve the expression of the GFP protein. These results allow us to observe that cationic solid lipid nanoparticles enhance the ability of nucleic acids to complete endosomal escape by neutralizing the differential charge between the endosomal membrane and DNA (186,252).

This makes nanoparticles an alternative for cell transfection, compared to liposomal transfection reagents such as lipofectamine, which is a substance that, although commercially available for liposomal transfection, has reduced stability and low encapsulation efficiency in alive compared to other solid lipids. nanoparticle formulations (186).

CONCLUSIONS

1. The production of Solid lipid nanoparticles (SLN) of CHON has been optimized according to a DOE and the factors CHON concentration of 0.4 mg/ml, Stirring rate of 20,000 rpm and a Reaction time of 10 minutes were found to be optimal. Different formulations of nanoparticles with average sizes smaller than 150 nm were fabricated; and zeta potential values around -40 mV were obtained for the formulations SLN-1, SLN-2, NLC-3, 40/60, 70 /30 and 95/5, while the SLN-4 and NLC-5 formulations had a cationic surface charge between 28 and 31 mV.

2. The stability was mainly evaluated by measuring the size (nm) and Z potential (mV). It was possible to manufacture nanoparticles with the capacity to maintain stability in an aqueous medium from 9 days at 37 °C for SLN-1 and up to 60 days at 37 °C for NLC-3. Once lyophilized, the stability of the nanoparticles was evaluated for up to 11 months, being stable during this time.

3. The morphological characterization of the nanoparticles was carried out by different methods, allowing the TEM and AFM techniques to observe mainly spherical shapes. It has been verified by techniques of DSC and XRD that there are no significant interactions between the components of the nanoparticles, therefore the composition or final functionality of the SLN are not altered.

4. The nanoparticles containing CHON presented a characteristic viscosity of pseudoplastic fluids, which is desired for formulations with topical application, which shows the potential of SLN to be applied to human skin in different presentations such as roll-on.

5. Two analysis methods for the determination of CHON encapsulation efficiency (EE%) in nanoparticles were proposed and validated. Both methods: volumetric

titration and UV-Vis Spectrophotometry, en el rango del 80 % al 120 % de la concentración 0.4 mg/ml de CHON se encontró que cumplen the validation criteria, de acuerdo a los siguientes parámetros Specificity, Selectivity Linearity, Accuracy, Precision, Intermediate precision and Robustness. The methods presented a correlation between the measurement results greater than 98%, and with the correlation equation EE% of UV-Vis method = (0.443 * EE% of titration method) + 51.821.

6. It was demonstrated that the SLN-1 formulation has the ability to internalize in HaCaT and BJ cells, and the SLN-2 to internalize in BJ cells, since the presence of nanoparticles marked in red with the confocal microscopy, was observed. The optimal dilution for the cell viability study was determined, where each formulation containing CHON did not cause cell toxicity, according to the cell line evaluated (BJ, HACAT, HT 29 and Chondrocyte OA). For SLN-1, dilutions 5, 10 and 25 did not cause cytotoxicity, for SLN-2 the dilutions were higher 25, 50 and 100 and for NLC-3 25 and 50 worked in OA chondrocytes.

7. SLN-1, SLN-2 and NLC-3 have shown the ability to transport CHON into the cell, by modifying the inflammatory response of OA chondrocytes. SLN-2 being the formulation with the greatest effectiveness in modifying the response in inflammation markers.

8. It was verified that the nanoparticles of the SLN-1, SLN-2 and NLC-3 formulations are an effective vehicle for the transport of CHON through the skin of pig ears, showing a greater permeation of CHON in the nanoparticle, compared to CHON in an aqueous medium.

9. Formulations SLN-4 and NLC-5 showed the ability to form lipoplexes and protect pEGFP from degradation by DNase I enzymes. The binding ratio (v/v) of pDNA:SLN of 1:20 presents the best profile. protection in the 1% agarose gel assay.

10. The different ratios of lipoplexes studied for the SLN-4 and NLC-5 formulations did not present cytotoxicity to dendritic cells, in the dilutions and times studied. Serving these data to establish the concentration to be used in the other cell transfection studies.

11. The 1:20 lipoplexes for both the SLN-4 and NLC-5 formulations presented sizes around 300 nm and a positive Z potential, which gave them the appropriate characteristics to be studied in cell transfection. The SLN-4 and NLC-5 formulations were capable of achieving cell transfection of pEGFP, at a ratio of 1:20 in dendritic cell lines.

12. The SLN formulations, developed and studied in this research, showed the capacity of carrying biomolecules such as CHON and pDNA, becoming a promising alternative in the field of non-viral delivery of biomolecules.

BIBLIOGRAPHY

1. Geszke-Moritz M, Moritz M. Solid lipid nanoparticles as attractive drug vehicles: Composition, properties and therapeutic strategies. Materials Science and Engineering C. 2016;68:982–94.
2. Soler Illia G. Nanotecnología: el desafío del siglo XXI. Buenos Aires, Argentina: Ed. Eudeba; 2010.
3. Pinto Reis C, Neufeld RJ, Ribeiro AJ, Veiga F. Nanoencapsulation I. Methods for preparation of drug-loaded polymeric nanoparticles. Nanomedicine. 2006;2(1):8–21.
4. Rajagopal K, Schneider JP. Self-assembling peptides and proteins for nanotechnological applications. Curr Opin Struct Biol. 2004;14(4):480–6.
5. Küchler S, Herrmann W, Panek-Minkin G, Blaschke T, Zoschke C, Kramer KD, et al. SLN for topical application in skin diseases-Characterization of drug-carrier and carrier-target interactions. Int J Pharm. 2010;390(2):225–33.
6. Dwivedi P, Nayak V, Kowshik M. Role of gold nanoparticles as drug delivery vehicles for chondroitin sulfate in the treatment of osteoarthritis. Biotechnol Prog. 31(5):1416–22.
7. Umerska A, Matougui N, Groo AC, Saulnier P. Understanding the adsorption of salmon calcitonin, antimicrobial peptide AP114 and polymyxin B onto lipid nanocapsules. Int J Pharm. 2016;506(1–2):191–200.
8. Carrillo C, Sánchez-Hernández N, García-Montoya E, Pérez-Lozano P, Suñé-Negre JM, Ticó JR, et al. DNA delivery via cationic solid lipid nanoparticles (SLNs). European Journal of Pharmaceutical Sciences [Internet]. 2013;49(2):157–65. Available from: http://dx.doi.org/10.1016/j.ejps.2013.02.011
9. Zoubari G, Staufenbiel S, Volz P, Alexiev U, Bodmeier R. Effect of drug solubility and lipid carrier on drug release from lipid nanoparticles for dermal delivery. European Journal of Pharmaceutics and Biopharmaceutics. 2017;110:39–46.
10. del Pozo-Rodríguez A, Solinís MÁ, Rodríguez-Gascón A. Applications of lipid nanoparticles in gene therapy. European Journal of Pharmaceutics and Biopharmaceutics. 2016;109:184–93.
11. Kundu AK, Chandra PK, Hazari S, Pramar Y V., Dash S, Mandal TK.

Development and optimization of nanosomal formulations for siRNA delivery to the liver. European Journal of Pharmaceutics and Biopharmaceutics. 2012;80(2):257–67.

12. Rodríguez Bonilla DM del P. Biochemical, Molecular Nanoencapsulation of Stilbenes by Cyclodextrins. Study of Applications, Chromatographic and Antioxidant. UNIVERSIDAD DE MURCIA; 2015.
13. Kumari A, Yadav SK, Yadav SC. Biodegradable polymeric nanoparticles based drug delivery systems. Colloids Surf B Biointerfaces. 2010;75(1):1–18.
14. Rostami E, Kashanian S, Azandaryani AH, Faramarzi H, Dolatabadi JEN, Omidfar K. Drug targeting using solid lipid nanoparticles. Chem Phys Lipids. 2014;181:56–61.
15. Weber S, Zimmer A, Pardeike J. Solid Lipid Nanoparticles (SLN) and Nanostructured Lipid Carriers (NLC) for pulmonary application: A review of the state of the art. European Journal of Pharmaceutics and Biopharmaceutics. 2014;86(1):7–22.
16. Severino P, Szymanski M, Favaro M, Azzoni AR, Chaud M V., Santana MHA, et al. Development and characterization of a cationic lipid nanocarrier as non-viral vector for gene therapy. European Journal of Pharmaceutical Sciences. 2015;66:78–82.
17. Yu YH, Kim E, Park DE, Shim G, Lee S, Kim YB, et al. Cationic solid lipid nanoparticles for co-delivery of paclitaxel and siRNA. European Journal of Pharmaceutics and Biopharmaceutics. 2012;80(2):268–73.
18. Ding Y, Jiang Z, Saha K, Kim CS, Kim ST, Landis RF, et al. Gold Nanoparticles for Nucleic Acid Delivery. Molecular Therapy. 2014;22(6):1075–83.
19. De Jesus MB, Zuhorn IS. Solid lipid nanoparticles as nucleic acid delivery system: Properties and molecular mechanisms. Journal of Controlled Release. 2015;201:1–13.
20. Vaghasiya H, Kumar A, Sawant K. Development of solid lipid nanoparticles based controlled release system for topical delivery of terbinafine hydrochloride. European Journal of Pharmaceutical Sciences. 2013;49(2):311–22.
21. Doktorovova S, Souto EB, Silva AM. Nanotoxicology applied to solid lipid

nanoparticles and nanostructured lipid carriers - A systematic review of in vitro data. European Journal of Pharmaceutics and Biopharmaceutics. 2014;87(1):1–18.

22. Kovacevic A, Savic S, Vuleta G, Muller RH, Keck CM. Polyhydroxy surfactants for the formulation of lipid nanoparticles (SLN and NLC): Effects on size, physical stability and particle matrix structure. Int J Pharm. 2011;406(1–2):163–72.
23. Kalaycioglu GD, Aydogan N. Preparation and investigation of solid lipid nanoparticles for drug delivery. Colloids Surf A Physicochem Eng Asp. 2016;510:77–86.
24. Islan GA, Tornello PC, Abraham GA, Duran N, Castro GR. Smart lipid nanoparticles containing levofloxacin and DNase for lung delivery. Design and characterization. Colloids Surf B Biointerfaces. 2016;143:168–76.
25. Müller, R. H., Mäder, K., Gohla S. Solid lipid nanoparticles (SLN) for controlled drug delivery ± a review of the state of the art. 2000;50.
26. Fàbregas A, Prieto S, Suñé-Pou M, Boyero-Corral S, Ticó JR, García-Montoya E, et al. Improved formulation of cationic solid lipid nanoparticles displays cellular uptake and biological activity of nucleic acids. Int J Pharm [Internet]. 2017;516(1–2):39–44. Available from: http://dx.doi.org/10.1016/j.ijpharm.2016.11.026
27. Vasile C, Nistor MT, Cojocariu A maria. Nano-Sized Polymeric Drug. In: Nanotechnology and Drug Delivery. CRC Press; 2014. p. 81–141.
28. Lakkireddy HR, Urmann M, Besenius M, Werner U, Haack T, Brun P, et al. Oral delivery of diabetes peptides ? Comparing standard formulations incorporating functional excipients and nanotechnologies in the translational context. Adv Drug Deliv Rev. 2016;106:196–222.
29. Fàbregas A. Nanopartícules lipídiques sòlides catiòniques (cSLN) com a sistema d'elecció per a transfecció cel·lular de DNA/RNA. Universitat de Barcelona; 2015.
30. Pájaro Castro N, Olivero Verbel J, Redondo Padilla J. Nanotecnología aplicada a la medicina. Revista Guillermo de Ockham. 2013 Jun 1;11(1):125.
31. Patra JK, Das G, Fraceto LF, Campos EVR, Rodriguez-Torres M del P, Acosta-Torres LS, et al. Nano based drug delivery systems: recent developments and future prospects. J Nanobiotechnology. 2018 Dec 19;16(1):71.
32. Thieman WJ, Palladino MA, Muñoz Céspedes A. Introducción a la biotecnología.

Thieman W PMMCA, editor. Pearson Educación; 2010.

33. Western Governors University. Medical Biotechnology: Advancement and Ethics [Internet]. Nursing & Healthcare. 2021 [cited 2022 Sep 23]. Available from: https://www.wgu.edu/blog/medical-biotechnology-advancements-ethics1811.html#close
34. Jain KK. The role of nanobiotechnology in drug discovery. Drug Discov Today. 2005 Nov;10(21):1435–42.
35. Kumar Dash D, Kant Panik R, Kumar Sahu A, Tripathi V. Role of Nanobiotechnology in Drug Discovery, Development and Molecular Diagnostic. Applications of Nanobiotechnology. IntechOpen; 2020.
36. Olvera Carranza C. La importancia de lo diminuto: aplicaciones de la nanobiotecnología. Quiurevista. 2017.
37. Nair SB, Dileep A, Rajanikant GK. Nanotechnology Based Diagnostic and Therapeutic Strategies for Neuroscience with Special Emphasis on Ischemic Stroke. Curr Med Chem. 2012 Feb 1;19(5):744–56.
38. Vasir JK, Labhasetwar V. Targeted Drug Delivery in Cancer Therapy. Technol Cancer Res Treat. 2005 Aug 24;4(4):363–74.
39. Jain K. Nanodiagnostics: application of nanotechnology in molecular diagnostics. Expert Rev Mol Diagn. 2003 Mar 9;3(2):153–61.
40. Qi B, Wang C, Ding J, Tao W. Editorial: Applications of Nanobiotechnology in Pharmacology. Front Pharmacol. 2019;10.
41. Villafuerte Leopoldo R. Nanotecnología Farmacéutica. 2009;1(68):1–20.
42. Ulbrich W, Lamprecht A. Targeted drug-delivery approaches by nanoparticulate carriers in the therapy of inflammatory diseases. J R Soc Interface [Internet]. 2010 Feb 6;7(suppl_1). Available from: https://royalsocietypublishing.org/doi/10.1098/rsif.2009.0285.focus
43. Jain KK. The Role of Nanobiotechnology in Drug Discovery. In 2009. p. 37–43.
44. Zazo H, Colino CI, Lanao JM. Current applications of nanoparticles in infectious diseases. Journal of Controlled Release. 2016 Feb;224:86–102.
45. Pund S, Joshi A. Nanoarchitectures for Neglected Tropical Protozoal Diseases: Challenges and State of the Art. Nano- and Microscale Drug Delivery Systems:

Design and Fabrication. 2017 Jan 1;439–80.

46. Mishra B, Patel BB, Tiwari S. Colloidal nanocarriers: a review on formulation technology, types and applications toward targeted drug delivery. Nanomedicine. 2010 Feb;6(1):9–24.
47. Faraji AH, Wipf P. Nanoparticles in cellular drug delivery. Bioorg Med Chem. 2009 Apr;17(8):2950–62.
48. Gasco MR. Method for producing solid lipid microspheres having a narrow size distribution. U.S. Patent No. 5,250,236; 1993.
49. Cervantes Covarrubias P. Preparación y caracterización de nanopartículas lipídicas sólidas (SLN) que contienen capsaicina por el método emulsificación-difusión. [Mexico]: Autonomous University of Baja California; 2016.
50. Hajipour H, Hamishehkar H, Nazari Soltan Ahmad S, Barghi S, Maroufi NF, Taheri RA. Improved anticancer effects of epigallocatechin gallate using RGD-containing nanostructured lipid carriers. Artif Cells Nanomed Biotechnol. 2018 Oct 31;46(sup1):283–92.
51. Tamjidi F, Shahedi M, Varshosaz J, Nasirpour A. Nanostructured lipid carriers (NLC): A potential delivery system for bioactive food molecules. Innovative Food Science & Emerging Technologies. 2013 Jul;19:29–43.
52. Doktorovova S, Souto EB. Nanostructured lipid carrier-based hydrogel formulations for drug delivery: A comprehensive review. Expert Opin Drug Deliv. 2009 Feb 24;6(2):165–76.
53. Villafuerte R. L, García F. B, Garzón S. M de L, Hernández L. A, Vázquez R. ML. Nanopartículas lipídicas sólidas. Revista Mexicana de Ciencias Farmacéuticas [en linea] [Internet]. 2008 [cited 2022 Nov 23];39(1):38–52. Available from: https://www.redalyc.org/articulo.oa?id=57939107
54. Lingayat VJ, Zarekar NS, Shendge RS. Solid Lipid Nanoparticles: A Review. Nanoscience and Nanotechnology Research [Internet]. 2017;4(2):67–72. Available from: http://pubs.sciepub.com
55. Müller RH, Shegokar R, Keck CM. 20 Years of Lipid Nanoparticles (SLN & NLC): Present State of Development & Industrial Applications. Curr Drug Discov Technol. 2011;8:207.

56. Garcês A, Amaral MH, Sousa Lobo JM, Silva AC. Formulations based on solid lipid nanoparticles (SLN) and nanostructured lipid carriers (NLC) for cutaneous use: A review. European Journal of Pharmaceutical Sciences. 2018 Jan 15;112:159–67.
57. Shah R, Eldridge D, Palombo E, Harding I. Lipid Nanoparticles: Production, Characterization and Stability. ASTM Manual on Zirconium and Hafnium. Springer; 2015.
58. Voet D, Voet J, Pratt C. Fundamentos de Bioquímica. La vida molecular. 4th ed. Editorial Médica Panamericana; 2016.
59. Voet D, Voet J. Bioquímica. 3rd ed. Buenos Aires: Editorial Médica Panamericana; 2006.
60. Russell PJ. Genetics [Internet]. 3rd ed. Lincoln, United Kingdom: Harper Collins; 1992 [cited 2022 Nov 24]. Available from: https://www.creative-proteomics.com/pronalyse/main-hplc-components.html
61. National Human Genome Research Institute. Deoxyribonucleic Acid (DNA) [Internet]. National Institutes of Health (NIH). 2020 [cited 2022 Jan 2]. Available from: https://www.genome.gov/about-genomics/fact-sheets/Deoxyribonucleic-Acid-Fact-Sheet
62. National Human Genome Research Institute. Ribonucliec Acid (RNA) [Internet]. National Institutes of Health (NIH). 2022 [cited 2022 Dec 28]. Available from: https://www.genome.gov/genetics-glossary/RNA-Ribonucleic-Acid
63. Rodríguez Gascón A, Solinís Aspiazu M, Pozo Rodríguez A. Nanopartículas sólidas lipídicas para terapia génica. An R Acad Farm. 2016;408–23.
64. Gallegos PSA. Design and evaluation of non-viral vectors based on solid lipid nanoparticles for the treatment of x-linked juvenile retinoschisis by gene therapy . 2015.
65. Torrecilla Alzola J. Diseño de un vector no viral basado en nanopartículas lipídicas para el tratamiento de la hepatitis C mediante ARN de interferencia. 2016 May 5 [cited 2022 Nov 11]; Available from: http://addi.ehu.es/handle/10810/19030
66. Suñé-Pou M, Limeres MJ, Nofrerias I, Nardi-Ricart A, Prieto-Sánchez S, El-Yousfi Y, et al. Improved synthesis and characterization of cholesteryl oleate-

loaded cationic solid lipid nanoparticles with high transfection efficiency for gene therapy applications. Colloids Surf B Biointerfaces. 2019 Aug 1;180:159–67.

67. Parashar D, Rajendran V, Shukla R, Sistla R. Lipid-based nanocarriers for delivery of small interfering RNA for therapeutic use. European Journal of Pharmaceutical Sciences [Internet]. 2020 Jan;142:105159. Available from: https://linkinghub.elsevier.com/retrieve/pii/S0928098719304324
68. Limeres MJ, Suñé-Pou M, Prieto-Sánchez S, Moreno-Castro C, Nusblat AD, Hernández-Munain C, et al. Development and characterization of an improved formulation of cholesteryl oleate-loaded cationic solid-lipid nanoparticles as an efficient non-viral gene delivery system. Colloids Surf B Biointerfaces. 2019;184:110533.
69. Sandoval Rodríguez A, Armendáriz-Borunda J, Salazar Montes A. Vectores virales en terapia génica. Ventajas de los vectores adenoasociados. Rev Gastroenterol Mex [Internet]. 2005 Feb 22 [cited 2023 Jan 2];70(2). Available from: https://studylib.es/doc/7060543/vectores-virales-en-terapia-g%C3%A9nica.-ventajas-de-los
70. Romero E, Morilla M, Bakas L. Vectores lipídicos, nuevas estrategias aplicadas a la terapia génica. Medicina (B Aires). 2001;61(1):205–14.
71. Macarulla J, Goñi F. Biomoléculas: Lecciones de Bioquímica Estructural [Internet]. 3rd ed. Barcelona: Reverté; 2002. Available from: https://books.google.es/books?hl=es&lr=&id=WUzrV3z3NogC&oi=fnd&pg=PA1&dq=biomol%C3%A9cula&ots=tJvpSMDYzx&sig=lyZtZ6QPgz2AniiT_v3TyFMyijk#v=onepage&q=biomol%C3%A9cula&f=false
72. Sánchez Amador S. Biomoléculas: qué son, tipos, funciones y características [Internet]. Psicología y mente. 2021. Available from: https://psicologiaymente.com/salud/biomoleculas
73. MedlinePlus. Chondroitin Sulfate [Internet]. National Library of Medicine (NLM). 2022 [cited 2022 Sep 29]. Available from: https://medlineplus.gov/druginfo/natural/744.html
74. Gandhi NS, Mancera RL. The Structure of Glycosaminoglycans and their Interactions with Proteins. Chem Biol Drug Des. 2008 Dec;72(6):455–82.

75. Möller I, Vergés J, Martínez G. Revisión farmacoclínica del condroitín sulfato. Seminarios de la Fundación Española de Reumatología. 2005 Dec 1;6(4):162–75.
76. Cañas Fernández N. Efecto neuroprotector del condroitin sulfato en modelos de isquemia y neuroinflamación. 2008 [cited 2022 Nov 11]; Available from: https://dialnet.unirioja.es/servlet/tesis?codigo=31168&info=resumen&idioma=SPA
77. Tornero JI, Olarte H, Escudero F, Gómez G. Experiencia a largo plazo con condroitín sulfato sódico en pacientes con síndrome de vejiga dolorosa. Actas Urol Esp. 2013 Sep 1;37(8):523–6.
78. Giménez S. El paciente con artritis. Farmacia Profesional [Internet]. 2006;20(9):52–7. Available from: https://www.elsevier.es/es-revista-farmacia-profesional-3-articulo-el-paciente-con-artritis-13094208
79. Buys LM, Wiedenfeld SA. Osteoarthritis. In: DiPiro JT, Yee GC, Michael Posey L, Haines ST, Nolin TD, Ellingrod VL, editors. DiPiro: Pharmacotherapy A Pathophysiologic Approach, 12e [Internet]. New York, NY: McGraw Hill; 2021. Available from: accesspharmacy.mhmedical.com/content.aspx?aid=1196908668
80. Gruber S, Lezcano B, Hylland S. Rheumatoid Arthritis. In: DiPiro JT, Yee GC, Posey LM, Haines ST, Nolin TD, Ellingrod V, editors. Pharmacotherapy: A Pathophysiologic Approach, 11e [Internet]. New York, NY: McGraw-Hill Education; 2020. Available from: accesspharmacy.mhmedical.com/content.aspx?aid=1182451431
81. Langford CA, Mandell BF. Arthritis Associated with Systemic Disease, and Other Arthritides. In: Loscalzo J, Fauci A, Kasper D, Hauser S, Longo D, Jameson JL, editors. Harrison's Principles of Internal Medicine, 21e [Internet]. New York, NY: McGraw-Hill Education; 2022. Available from: accessmedicine.mhmedical.com/content.aspx?aid=1190523624
82. Ayala Vizcaíno JR, Mejía Mendoza DA, Rosero Caiza JA, Rosero Caiza GE. Medicamentos biológicos en el tratamiento de la Artritis Reumatoide (AR). RECIMUNDO. 2021;5(3):197–204.
83. Massardo L. Artritis reumatoide temprana. Rev Med Chil. 2008;136(11).
84. Guo Q, Wang Y, Xu D, Nossent J, Pavlos NJ, Xu J. Rheumatoid arthritis:

pathological mechanisms and modern pharmacologic therapies. Bone Res. 2018;6(1):15.

85. Radu AF, Bungau SG. Management of Rheumatoid Arthritis: An Overview. Cells [Internet]. 2021 Nov 1 [cited 2022 Nov 11];10(11). Available from: https://pubmed.ncbi.nlm.nih.gov/34831081/
86. Jagampalli A. Insights of rheumatoid arthritis risk factors and associations. 2019;1–5.
87. Ngian G. Rheumatoid arthritis. Aust Fam Physician. 2010 Sep 1;39(9):626–8.
88. Borenstein D. Glucosamine and Chondroitin Sulfate Use in Arthritis -What You Need to Know [Internet]. The Arthritis Connection. 2021 [cited 2022 Aug 30]. Available from: thearthritisconnection
89. Liu K, Zhang D, Wang W. Nanoparticle-Based Drug Delivery System—A Target Strategy for Osteoarthritis Treatment. J Nanomater. 2021 Oct 20;2021:1–15.
90. Li Z, Huang Z, Bai L. Cell Interplay in Osteoarthritis. Front Cell Dev Biol. 2021 Aug 3;9.
91. Johnson BE. Arthritis: Osteoarthritis, Gout, & Rheumatoid Arthritis. In: South-Paul JE, Matheny SC, Lewis EL, editors. CURRENT Diagnosis & Treatment: Family Medicine, 4e [Internet]. New York, NY: McGraw-Hill Education; 2015. Available from: accessmedicine.mhmedical.com/content.aspx?aid=1106848754
92. Barbour KE, Helmick CG, Boring M, Brady TJ. Vital Signs: Prevalence of Doctor-Diagnosed Arthritis and Arthritis-Attributable Activity Limitation — United States, 2013–2015. MMWR Morb Mortal Wkly Rep. 2017 Mar 10;66(9):246–53.
93. McQueen CE. Herbal and Nonherbal Dietary Supplements. In: Sutton SS, editor. McGraw Hill's NAPLEX® Review Guide, 4e [Internet]. New York, NY: McGraw-Hill Education; 2020. Available from: accesspharmacy.mhmedical.com/content.aspx?aid=1179737069
94. Giménez Basallote S. Tratamiento de la artrosis en Atención Primaria: revisión de los fármacos de acción sintomática lenta (SYSADOA). SEMERGEN - Medicina de Familia. 2008 Oct;34(8):400–6.
95. Goldring SR, Goldring MB. The Role of Cytokines in Cartilage Matrix

Degeneration in Osteoarthritis. Clin Orthop Relat Res. 2004 Oct;427:S27–36.

96. Gato L. Estandarización del plasma rico en plaquetas como medicamento para la artrosis. [Coruña]: University of A Coruña; 2019.

97. López-Armada MJ, Vaamonde-García C, Caramés B, Lires-Deán M, Cillero-Pastor B, Blanco García FJ. Evidencia de mecanismos inflamatorios en la osteoartritis. Reumatol Clin. 2007 Oct;3:S23–7.

98. Gary S F, Ralph C B, Sherine E G, Iain B M, James R O. Firestein's Textbook of Rheumatology. 10th ed. Elsevier, editor. Vol. 2. 2017. 34–57 p.

99. Bosch I, Xhaja K, Estevez L, Raines G, Melichar H, Warke R v., et al. Increased Production of Interleukin-8 in Primary Human Monocytes and in Human Epithelial and Endothelial Cell Lines after Dengue Virus Challenge. J Virol. 2002 Jun;76(11):5588–97.

100. Xing Z, Gauldie J, Cox G, Baumann H, Jordana M, Lei XF, et al. IL-6 is an antiinflammatory cytokine required for controlling local or systemic acute inflammatory responses. J Clin Invest [Internet]. 1998 Jan 15 [cited 2022 Nov 11];101(2):311–20. Available from: http://www.jci.org

101. Park E, Lee CG, Han SJ, Yun SH, Hwang S, Jeon H, et al. Antiosteoarthritic Effect of Morroniside in Chondrocyte Inflammation and Destabilization of Medial Meniscus-Induced Mouse Model. International Journal of Molecular Sciences 2021, Vol 22, Page 2987 [Internet]. 2021 Mar 15 [cited 2022 Nov 11];22(6):2987. Available from: https://www.mdpi.com/1422-0067/22/6/2987/htm

102. Zhong L, Huang X, Karperien M, Post JN. Correlation between Gene Expression and Osteoarthritis Progression in Human. International Journal of Molecular Sciences 2016, Vol 17, Page 1126 [Internet]. 2016 Jul 14 [cited 2022 Nov 11];17(7):1126. Available from: https://www.mdpi.com/1422-0067/17/7/1126/htm

103. Ma FB, Liu N, Hu N, Wen CY, Tang B. Synthesis of strontium chondroitin sulfate and the evaluation of its capability to attenuate osteoarthritis. Carbohydr Polym. 2017;170:217–25.

104. Simmons DL, Botting RM, Robertson PM, Madsen ML, Vane JR. Induction of an acetaminophen-sensitive cyclooxygenase with reduced sensitivity to nonsteroid

antiinflammatory drugs. Proceedings of the National Academy of Sciences [Internet]. 1999;96(6):3275–80. Available from: https://www.pnas.org/doi/abs/10.1073/pnas.96.6.3275

105. Fermor B, Brice Weinberg J, Pisetsky DS, Misukonis MA, Banes AJ, Guilak F. The effects of static and intermittent compression on nitric oxide production in articular cartilage explants. Journal of Orthopaedic Research [Internet]. 2001 Jul 1 [cited 2022 Nov 11];19(4):729–37. Available from: https://onlinelibrary.wiley.com/doi/full/10.1016/S0736-0266%2800%2900049-8
106. Lee KB, Taghavi CE, Song KJ, Sintuu C, Yoo JH, Keorochana G, et al. Inflammatory Characteristics of rhBMP-2 In Vitro and in an In Vivo Rodent Model. Spine (Phila Pa 1976). 2011 Feb;36(3):E149–54.
107. Hori M, Sawai H, Tsuji Y, Okamura H, Koyama K. Bone Morphogenetic Protein-2 Counterregulates Interleukin-18 mRNA and Protein in MC3T3-E1 Mouse Osteoblastic Cells. Connect Tissue Res. 2006 Jan 6;47(3):124–32.
108. Zara JN, Siu RK, Zhang X, Shen J, Ngo R, Lee M, et al. High Doses of Bone Morphogenetic Protein 2 Induce Structurally Abnormal Bone and Inflammation *In Vivo*. Tissue Eng Part A. 2011 May;17(9–10):1389–99.
109. Nguyen V, Meyers CA, Yan N, Agarwal S, Levi B, James AW. BMP-2-induced bone formation and neural inflammation. J Orthop. 2017 Jun;14(2):252–6.
110. Alonso Bernardo E. Absorción oral de glucosamina y condroitín sulfato. Universidad Complutense. Madrid; 2018.
111. Fernández Dorta L. Glucosamina y sulfato de condroitina en el tratamiento de la osteoartritis. Revista CENIC Ciencias Biológicas. 2016 Aug;47(2):93–9.
112. Leite CBS, Coelho JM, Muehlmann LA, de Azevedo RB, Sousa MH. Skin Delivery of Glucosamine and Chondroitin Sulphates—A Perspective on the Conservative Treatment for Osteoarthritis of the Knee. J Biosci Med (Irvine). 2017;05(04):11–20.
113. Fernández-Martín S, González-Cantalapiedra A, Muñoz F, García-González M, Permuy M, López-Peña M. Glucosamine and Chondroitin Sulfate: Is There Any Scientific Evidence for Their Effectiveness as Disease-Modifying Drugs in Knee Osteoarthritis Preclinical Studies?-A Systematic Review from 2000 to 2021.

Animals (Basel) [Internet]. 2021 Jun 1 [cited 2022 Nov 11];11(6). Available from: https://pubmed.ncbi.nlm.nih.gov/34072407/

114. Calvo R. Sulfato de glucosamina y condroitín sulfato, fármacos para el tratamiento de la artrosis, acusados de no presentar eficacia clínica. ¿Culpables? Gaceta Médica de Bilbao. 2012 Oct 1;109(4):158–64.
115. Desai PP, Date AA, Patravale VB. Overcoming poor oral bioavailability using nanoparticle formulations – opportunities and limitations. Drug Discov Today Technol. 2012 Jun;9(2):e87–95.
116. Öztürk AA, Aygül A, Şenel B. Influence of glyceryl behenate, tripalmitin and stearic acid on the properties of clarithromycin incorporated solid lipid nanoparticles (SLNs): Formulation, characterization, antibacterial activity and cytotoxicity. J Drug Deliv Sci Technol. 2019 Dec 1;54.
117. Suñé-Pou M, Prieto-Sánchez S, el Yousfi Y, Boyero-Corral S, Nardi-Ricart A, Nofrerias-Roig I, et al. Cholesteryl oleate-loaded cationic solid lipid nanoparticles as carriers for efficient gene-silencing therapy. Int J Nanomedicine. 2018 May 30;13:3223–33.
118. Szliszka E, Czuba ZP, Domino M, Mazur B, Zydowicz G, Krol W. Ethanolic Extract of Propolis (EEP) Enhances the Apoptosis- Inducing Potential of TRAIL in Cancer Cells. Molecules. 2009 Feb 13;14(2):738–54.
119. Huang Y, Yang M, Wang N, Li S, Liu Z, Li Z, et al. Intracellular delivery of messenger RNA to macrophages with surfactant-derived lipid nanoparticles. Mater Today Adv. 2022 Dec 1;16.
120. Khalil RM, Abd-Elbary A, Kassem MA, Ghorab MM, Basha M. Nanostructured lipid carriers (NLCs) versus solid lipid nanoparticles (SLNs) for topical delivery of meloxicam. Pharm Dev Technol. 2014;19(3):304–14.
121. Chen CC, Tsai TH, Huang ZR, Fang JY. Effects of lipophilic emulsifiers on the oral administration of lovastatin from nanostructured lipid carriers: Physicochemical characterization and pharmacokinetics. European Journal of Pharmaceutics and Biopharmaceutics. 2010 Mar;74(3):474–82.
122. Salih M, Omolo CA, Agrawal N, Walvekar P, Waddad AY, Mocktar C, et al. Supramolecular amphiphiles of Beta-cyclodextrin and Oleylamine for

enhancement of vancomycin delivery. Int J Pharm. 2020 Jan 25;574.

123. de Jesus MB, Zuhorn IS. Solid lipid nanoparticles as nucleic acid delivery system: Properties and molecular mechanisms. Vol. 201, Journal of Controlled Release. Elsevier; 2015. p. 1–13.

124. Tian JL, Zhao YZ, Jin Z, Lu CT, Tang QQ, Xiang Q, et al. Synthesis and characterization of Poloxamer 188-grafted heparin copolymer. Drug Dev Ind Pharm. 2010 Jul;36(7):832–8.

125. Mukherjee S, Ray S, Thakur R. Solid lipid nanoparticles: A modern formulation approach in drug delivery system. Indian J Pharm Sci. 2009;71(4):349.

126. Garzón M de L, Hernández A, Vázquez ML, Villafuerte L, García B. Preparación de nanopartículas sólidas lipídicas (SLN) y de Acarreadores lipídicos nanoestructurados (NLC). Revista Mexicana de Ciencias Farmacéuticas [Internet]. 2008;39(4):50–66. Available from: http://www.redalyc.org/articulo.oa?id=57911113008

127. Müller R, Stefan Lucks S. Arzneistofftra¨ger aus festen lipidteilchen — feste lipid nanospha¨ren (SLN). 1996.

128. Jenning V, Thü Nemann B AF, Gohla SH. Characterisation of a novel solid lipid nanoparticle carrier system based on binary mixtures of liquid and solid lipids [Internet]. Vol. 199, International Journal of Pharmaceutics. 2000. Available from: www.elsevier.com/locate/ijpharm

129. Yang SC, Zhu JB. Preparation and Characterization of Camptothecin Solid Lipid Nanoparticles. Drug Dev Ind Pharm [Internet]. 2002;28(3):265. Available from: www.dekker.com

130. Hu FQ, Jiang SP, Du YZ, Yuan H, Ye YQ, Zeng S. Preparation and characteristics of monostearin nanostructured lipid carriers. Int J Pharm. 2006 May 11;314(1):83–9.

131. Trotta M, Debernardi F, Caputo O. Preparation of solid lipid nanoparticles by a solvent emulsification-diffusion technique. Int J Pharm. 2003 May 12;257(1–2):153–60.

132. Shah R. Microwave-assisted Production of Solid Lipid Nanoparticles. Swinburne University of Technology; 2016.

133. Ghasemiyeh P, Mohammadi-Samani S. Solid lipid nanoparticles and nanostructured lipid carriers as novel drug delivery systems: Applications, advantages and disadvantages. Res Pharm Sci. 2018;13(4):288–303.
134. Draelos ZK. Cosmetic dermatology: products and procedures. Second edition. Draelos ZK, editor. Chichester, West Sussex ; Wiley Blackwell; 2016.
135. Schäfer-Korting M, Mehnert W, Korting HC. Lipid nanoparticles for improved topical application of drugs for skin diseases. Vol. 59, Advanced Drug Delivery Reviews. 2007. p. 427–43.
136. Bouwstra JA, Loan Honeywell-Nguyen P, Gooris GS, Ponec M. Structure of the skin barrier and its modulation by vesicular formulations [Internet]. Vol. 42, Progress in Lipid Research. 2003. Available from: www.elsevier.com/locate/plipres
137. Cevc G. Lipid vesicles and other colloids as drug carriers on the skin. Adv Drug Deliv Rev. 2004 Mar 27;56(5):675–711.
138. Barry BW. Drug delivery routes in skin: a novel approach. Adv Drug Deliv Rev [Internet]. 2002;54:31–40. Available from: www.elsevier.com/locate/drugdeliv
139. Barry BW. Breaching the skin's barrier to drugs. Nat Biotechnol [Internet]. 2004;22:165–7. Available from: http://www.nature.com/naturebiotechnology
140. Moser K, Kriwet K, Kalia YN, Guy RH. Enhanced skin permeation of a lipophilic drug using supersaturated formulations. Journal of Controlled Release [Internet]. 2001;73:245–53. Available from: www.elsevier.com/locate/jconrel
141. Teichmann A, Heuschkel S, Jacobi U, Presse G, Neubert RHH, Sterry W, et al. Comparison of stratum corneum penetration and localization of a lipophilic model drug applied in an o/w microemulsion and an amphiphilic cream. European Journal of Pharmaceutics and Biopharmaceutics. 2007 Nov;67(3):699–706.
142. Montenegro L, Lai F, Offerta A, Sarpietro MG, Micicchè L, Maccioni AM, et al. From nanoemulsions to nanostructured lipid carriers: A relevant development in dermal delivery of drugs and cosmetics. J Drug Deliv Sci Technol. 2016 Apr 1;32:100–12.
143. Gunst RF, Mason RL. Fractional factorial design. Wiley Interdiscip Rev Comput Stat. 2009;1(2):234–44.

144. Spall JC. Factorial Design for Efficient Experimentation. IEEE Control Syst. 2010;30(5):38–53.
145. Fangueiro JF, Andreani T, Egea MA, Garcia ML, Souto SB, Souto EB. Experimental factorial design applied to mucoadhesive lipid nanoparticles via multiple emulsion process. Colloids Surf B Biointerfaces [Internet]. 2012;100:84–9. Available from: http://dx.doi.org/10.1016/j.colsurfb.2012.04.014
146. Sankar PR, Snehalatha KS, Firdose ST, Babu PS. Applications of HPLC in Pharmaceutical Analysis. Int J Pharm Sci Rev Res. 2019;59:117–24.
147. Zotou A. An overview of recent advances in HPLC instrumentation. Vol. 10, Central European Journal of Chemistry. 2012. p. 554–69.
148. Creative Proteomics. Main High-Performance Liquid Chromatography (HPLC) Components [Internet]. 2022 [cited 2022 Jan 3]. Available from: https://www.creative-proteomics.com/pronalyse/main-hplc-components.html
149. Townshend A. TITRIMETRY | Overview. Encyclopedia of Analytical Science: Second Edition. 2005;105–13.
150. Zumbado Fernández H. Análisis químico de los alimentos métodos clásicos. Ciudad de La Habana: Editorial Universitaria; 2002.
151. Nagwa. Lesson Explainer: Volumetric Analysis, Chemistry [Internet]. 2022 [cited 2022 Oct 26]. Available from: https://www.nagwa.com/en/explainers/809181620245/
152. Kumar H. Advanced Techniques of Analytical Chemistry. Kumar H, Goyal A, editors. Vol. 1. Bentham Books; 2022. 1–15 p.
153. Hardesty JH, Attili B, College C. Spectrophotometry and the Beer-Lambert Law: An Important Analytical Technique in Chemistry. 2010.
154. Mettler Toledo. Espectroscopia ultravioleta-visible: conceptos básicos [Internet]. [cited 2022 Oct 27]. Available from: https://www.mt.com/es/es/home/applications/Application_Browse_Laboratory_Analytics/uv-vis-spectroscopy/uvvis-spectroscopy-explained.html#spectroscopy
155. Ruiz Blandón YR, Paizano Hernández MD. Validación del método espectrofotométrico UV-Visible para la cuantificación y disolución de Tinidazol Table de 500 mg. 2015.

156. Verma G, Mishra M. Development and Optimization of UV-VIS Spectroscopy - A Review. Govinda et al World Journal of Pharmaceutical Research [Internet]. 2018;7(11):1170–80. Available from: www.wjpr.net
157. Rockville M. <1225> Validation of Compendial Procedures. In: USP 40/NF 35, United States Pharmacopeia. 40th ed., National Formulary. 35th ed. 35th ed. The United States Pharmacopeia Convention; United Book Press, Inc; 2017.
158. ICH Harmonised Tripartite Guideline. Validation of Analytical Procedures: Text And Methodology Q2(R1) [Internet]. 2005 [cited 2022 Sep 16]. Available from: https://somatek.com/wp-content/uploads/2014/06/sk140605h.pdf
159. Agency EM. Validation of Analytical Procedures: Text and Methodology [Internet]. 1995. Available from: http://www.emea.eu.int
160. European Medicines Agency. ICH Topic Q 2 (R1) Validation of Analytical Procedures: Text and Methodology [Internet]. London; 1995 [cited 2022 Sep 16]. Available from: https://www.ema.europa.eu/en/documents/scientific-guideline/ich-q-2-r1-validation-analytical-procedures-text-methodology-step-5_en.pdf
161. Carter CB, Williams D. Transmission Electron Microscopy: Diffraction, Imaging, and Spectrometry. Carter CB, Williams D, editors. 2016.
162. Zinin P. Transmission Electron Microscope [Internet]. Advanced Techniques in Geophysics and Materials Science; 2011 [cited 2022 Oct 23]. Available from: http://www.soest.hawaii.edu/HIGP/Faculty/sksharma/GG711/GG711Lec15TEM.pdf
163. Tang CY, Yang Z. Transmission Electron Microscopy (TEM). In: Membrane Characterization. Elsevier; 2017. p. 145–59.
164. Cortés Cortés M, Vigil Portales P. Aportes a la biomedicina y la enseñanza a noventa años del desarrollo de la microscopía electrónica. Educación Médica Superior. 2022;36(2).
165. Azad M, Avin A. Scanning Electron Microscopy (SEM): A REVIEW. In: International Conference on Hydraulics and Pneumatics - HERVEX. Băile Govora, Romania; 2018. p. 77–85.
166. Osorio Valencia S. Nanopartículas sólidas lipídicas para la encapsulación de

moléculas lipofílicas [Internet]. Universidad EIA; 2017. Available from: https://repository.eia.edu.co/handle/11190/1977

167. Castroviejo MP. Microscopía de Fuerza Atómica (AFM) [Internet]. Universidad de Burgos; 2022. Available from: https://www.ubu.es/parque-cientifico-tecnologico/servicios-cientifico-tecnicos/microscopia/microscopia-de-fuerza-atomica-afm
168. Gustafsson MGL, Clarke J. Scanning force microscope springs optimized for optical-beam deflection and with tips made by controlled fracture. J Appl Phys. 1994 Jul;76(1):172–81.
169. Raposo M, Ferreira Q, Ribeiro P. A Guide for Atomic Force Microscopy Analysis of Soft Condensed Matter. Modern Research and Educational Topics in Microscopy. 2007 Dec;1.
170. University of Greifswald. AFM (Atomic Force Microscope) [Internet]. 2022 [cited 2022 Dec 28]. Available from: https://physik.uni-greifswald.de/en/research-groups/soft-matter-and-biophysics-prof-christiane-helm/methods/afm-atomic-force-microscope/
171. AzoNano. Atomic Force Microscopes (AFM) What They Are, How They Work and What They Are Used For [Internet]. 2006 [cited 2022 Oct 28]. Available from: https://www.azonano.com/article.aspx?ArticleID=1688
172. Bunjes H, Unruh T. Characterization of lipid nanoparticles by differential scanning calorimetry, X-ray and neutron scattering. Adv Drug Deliv Rev. 2007 Jul 10;59(6):379–402.
173. Mehnert W, Mäder K. Solid lipid nanoparticles: Production, characterization and applications. Adv Drug Deliv Rev. 2012 Dec 1;64(SUPPL.):83–101.
174. Dong Y da, Boyd BJ. Applications of X-ray scattering in pharmaceutical science. Int J Pharm. 2011 Sep 30;417(1–2):101–11.
175. Malvern Panalytical. Differential Scanning Calorimetry (DSC) [Internet]. 2022 [cited 2022 Oct 28]. Available from: https://www.malvernpanalytical.com/en/products/technology/microcalorimetry/differential-scanning-calorimetry
176. Skoog DA. Principios de análisis instrumental. 6a ed. Holler FJames, Crouch SR,

editors. México: Cengage Learning; 2008.

177. Batalla Mayoral J, Cuadros Moreno A, San Martín Martínez E. Potencial zeta en la determinación de carga superficial de liposomas. Latin-American journal of physics education. 2014;8(4).

178. Gumustas M, Sengel-Turk CT, Gumustas A, Ozkan SA, Uslu B. Effect of Polymer-Based Nanoparticles on the Assay of Antimicrobial Drug Delivery Systems. Multifunctional Systems for Combined Delivery, Biosensing and Diagnostics. 2017 Jan 1;67–108.

179. Bard AJ. Electrochemical methods: fundamentals and applications. 2nd ed. Faulkner LR, editor. New York [etc: Wiley; 2001.

180. Holmberg K, Shah DO, Schwuger MJ. Handbook of applied surface and colloid chemistry. Holmberg K, Shah DO, Schwuger MJ (Milan J), editors. Chichester [etc: Wiley; 2002.

181. Kirby BJ, Hasselbrink Jr EF. Zeta potential of microfluidic substrates: 1. Theory, experimental techniques, and effects on separations. Electrophoresis. 2004;25(2):187–202.

182. Lopes MA, Monteiro FJ, Santos JD, Serro AP, Saramago B. Hydrophobicity, surface tension, and zeta potential measurements of glass-reinforced hydroxyapatite composites. J Biomed Mater Res. 1999;45(4):370–5.

183. Sikora A, Bartczak D, Geißler D, Kestens V, Roebben G, Ramaye Y, et al. A systematic comparison of different techniques to determine the zeta potential of silica nanoparticles in biological medium. Analytical Methods. 2015;7(23):9835–43.

184. Hilger I, Frühauf S, Linß W, Hiergeist R, Andrä W, Hergt R, et al. Cytotoxicity of selected magnetic fluids on human adenocarcinoma cells. J Magn Magn Mater. 2003 Apr;261(1–2):7–12.

185. Fröhlich E, Meindl C, Roblegg E, Griesbacher A, Pieber TR. Cytotoxity of nanoparticles is influenced by size, proliferation and embryonic origin of the cells used for testing. Nanotoxicology. 2012 Jun 31;6(4):424–39.

186. Francis JE, Skakic I, Dekiwadia C, Shukla R, Taki AC, Walduck A, et al. Solid Lipid Nanoparticle Carrier Platform Containing Synthetic TLR4 Agonist Mediates

Non-Viral DNA Vaccine Delivery. Vaccines (Basel). 2020 Sep 21;8(3):551.

187. Jin SE, Kim CK. Charge-mediated topical delivery of plasmid DNA with cationic lipid nanoparticles to the skin. Colloids Surf B Biointerfaces. 2014 Apr;116:582–90.

188. Ruenraroengsak P, Tetley TD. Differential bioreactivity of neutral, cationic and anionic polystyrene nanoparticles with cells from the human alveolar compartment: robust response of alveolar type 1 epithelial cells. Part Fibre Toxicol. 2015 Dec 2;12(1):19.

189. Shah RM, Malherbe F, Eldridge D, Palombo EA, Harding IH. Physicochemical characterization of solid lipid nanoparticles (SLNs) prepared by a novel microemulsion technique. J Colloid Interface Sci. 2014;428(428):286–94.

190. Vivek K, Reddy H, Murthy RSR. Investigations of the effect of the lipid matrix on drug entrapment, in vitro release, and physical stability of olanzapine-loaded solid lipid nanoparticles. AAPS PharmSciTech. 2007;8(4):E83.

191. Lambros MP. Rheology. In: Amiji MM, Cook TJ, Mobley WC, editors. Applied Physical Pharmacy, 2e [Internet]. New York, NY: McGraw-Hill Education; 2013. Available from: accesspharmacy.mhmedical.com/content.aspx?aid=1102749208

192. Malvern Instruments. A Basic Introduction to Rheology [Internet]. 2016 [cited 2022 Oct 29]. Available from: https://cdn.technologynetworks.com/TN/Resources/PDF/WP160620BasicIntroRheology.pdf

193. Molecular Devices. Desarrollo de líneas celulares [Internet]. 2022 [cited 2022 Oct 30]. Available from: https://es.moleculardevices.com/applications/cell-line-development#gref

194. National Human Genome RI. Plasmid [Internet]. 2022 [cited 2022 Dec 30]. Available from: https://www.genome.gov/genetics-glossary/Plasmid

195. Merck. Plasmid DNA Purification [Internet]. 2022 [cited 2022 Jan 2]. Available from: https://www.sigmaaldrich.com/ES/en/products/molecular-biology-and-functional-genomics/nucleic-acid-purification/plasmid-dna-purification

196. Rao X, Huang X, Zhou Z, Lin X. An improvement of the 2ˆ(–delta delta CT) method for quantitative real-time polymerase chain reaction data analysis. Biostat

Bioinforma Biomath [Internet]. 2013 Aug [cited 2022 Nov 12];3(3):71. Available from: /pmc/articles/PMC4280562/

197. Livak KJ, Schmittgen TD. Analysis of Relative Gene Expression Data Using Real-Time Quantitative PCR and the 2−ΔΔCT Method. Methods. 2001 Dec 1;25(4):402–8.
198. Wilson CR, Butz JK, Mengel MC. Methods for Analysis of Gastrointestinal Toxicants☆. In: Reference Module in Biomedical Sciences. Elsevier; 2014.
199. Abcam. ELISA principles and types [Internet]. [cited 2022 Nov 10]. Available from: https://www.abcam.com/kits/elisa-principle
200. Alhajj M, Farhana A. Enzyme Linked Immunosorbent Assay [Internet]. Treasure Island (FL): StatPearls . 2022 [cited 2022 Dec 20]. Available from: https://www.ncbi.nlm.nih.gov/books/NBK555922/
201. Scott V, Clark AR, Docherty K. The Gel Retardation Assay. In: Protocols for Gene Analysis. New Jersey: Humana Press; p. 339–48.
202. Thermo Fisher Scientific Inc. Gel Shift Assays–EMSA [Internet]. Protein Biology Resource Library. 2022 [cited 2022 Dec 30]. Available from: https://www.thermofisher.com/es/es/home/life-science/protein-biology/protein-biology-learning-center/protein-biology-resource-library/pierce-protein-methods/gel-shift-assays-emsa.html
203. Doroud D, Vatanara A, Zahedifard F, Gholami E, Vahabpour R, Rouholamini Najafabadi A, et al. Cationic Solid Lipid Nanoparticles Loaded by Cystein Proteinase Genes as a Novel anti-Leishmaniasis DNA Vaccine Delivery System: Characterization and in vitro Evaluations. Journal of Pharmacy & Pharmaceutical Sciences. 2010 Sep 6;13(3):320.
204. Karas VO, Westerlaken I, Meyer AS. Application of an In vitro DNA Protection Assay to Visualize Stress Mediation Properties of the Dps Protein. Journal of Visualized Experiments. 2013 May 31;(75).
205. Kim TK, Eberwine JH. Mammalian cell transfection: the present and the future. Anal Bioanal Chem. 2010 Aug 13;397(8):3173–8.
206. del Pozo-Rodríguez A, Delgado D, Solinís MA, Gascón AR, Pedraz JL. Solid lipid nanoparticles: Formulation factors affecting cell transfection capacity. Int J Pharm.

2007 Jul;339(1–2):261–8.

207. Villarino N, Landoni M. Administración transdérmica de fármacos: Una alternativa terapéutica. Analecta Vet. 2006;26(1):28–37.

208. Baena Aristizábal Y, Dallos J, Manso R, D'León L. Estandarización de celdas de Franz para la realización de ensayos de liberación de fármacos a partir de complejos con polielectrolitos. Revista Colombiana de Ciencias Qu'imicas y Farmacéuticas. 2011 Jan 1;40:174–88.

209. Aulton M. Pharmaceutics: the science of dosage form design. 2nd ed. London: Churchill Livingstone Eds; 2002. 294–506 p.

210. Vats S, Saxena C, Easwari TS, Shukla VK. Emulsion Based Gel Technique: Novel Approach for Enhancing Topical Drug Delivery of Hydrophobic Drugs. International Journal for Pharmaceutical Research Scholars. 2014 Feb 1;3:649–60.

211. Fàbregas A, Sánchez-Hernández N, Ticó JR, García-Montoya E, Pérez-Lozano P, Suñé-Negre JM, et al. A new optimized formulation of cationic solid lipid nanoparticles intended for gene delivery: Development, characterization and DNA binding efficiency of TCERG1 expression plasmid. Int J Pharm. 2014 Oct;473(1–2).

212. Malvern Panalytical. Nanoparticle Tracking Analysis (NTA) [Internet]. [cited 2022 Dec 13]. Available from: https://www.malvernpanalytical.com/en/products/technology/light-scattering/nanoparticle-tracking-analysis

213. el Moussaoui S, Fernández-Campos F, Alonso C, Limón D, Halbaut L, Garduño-Ramirez ML, et al. Topical Mucoadhesive Alginate-Based Hydrogel Loading Ketorolac for Pain Management after Pharmacotherapy, Ablation, or Surgical Removal in Condyloma Acuminata. Gels. 2021 Jan 23;7(1):8.

214. Binnig G, Quate CF, Gerber Ch. Atomic Force Microscope. Phys Rev Lett. 1986 Mar 3;56(9):930–3.

215. Nagarajan P, Dinakaran SK, Ghosh S, Avasarala H, Nallayya M, Banji D. Method Development and Validation for Glucosamine and Chondroitin Sulphate in Soflet Form by RP-HPLC. Research and Reviews Journal of Pharmaceutical Analysis. 2013;2(3):6–10.

216. Rockville M. Chondroitin Sulfato de Sodio. USP 38. Farmacopea de los Estados Unidos de América. NF 33. Formulario nacional., editor. 2015. 6411–6414 p.

217. European Pharmacopoeia 9.0. European Directorate for the Quality of Medicines. Vol. 01/2017. Strasbourg, France; 2017. 2064 p.

218. Bitter T, Muir HM. A modified uronic acid carbazole reaction. Anal Biochem. 1962 Oct;4(4):330–4.

219. Kosakai M, Yosizawa Z. Study on the factors yielding high color in the carbazole reaction with hexuronic acid-containinig substances. [Internet]. Vol. v. 84, Journal of Biochemistry. 1978 [cited 2022 Nov 7]. Available from: https://www.jstage.jst.go.jp/article/biochemistry1922/84/4/84_4_779/_pdf

220. Somashekar P, Sathish K, Javali C, Tripathy A, Kotanal R. Development and Validation of Spectrophotometric Method for the Estimation of Chondroitin Sulfate in Bulk Drug and Pharmaceutical Formulations. Chem Sci Trans. 2013 Oct 4;2(4):1427–33.

221. Addgene. Vector Database. Plasmid: pEGFP [Internet]. [cited 2022 Nov 4]. Available from: https://www.addgene.org/19444/

222. Vighi E, Montanari M, Ruozi B, Tosi G, Magli A, Leo E. Nuclear localization of cationic solid lipid nanoparticles containing Protamine as transfection promoter. European Journal of Pharmaceutics and Biopharmaceutics. 2010 Nov;76(3):384–93.

223. Brugués AP, Naveros BC, Calpena Campmany AC, Pastor PH, Saladrigas RF, Lizandra CR. Developing cutaneous applications of paromomycin entrapped in stimuli-sensitive block copolymer nanogel dispersions. Nanomedicine (Lond). 2015;10(2):227–40.

224. Netzlaff F, Schaefer UF, Lehr CM, Meiers P, Stahl J, Kietzmann M, et al. Comparison of bovine udder skin with human and porcine skin in percutaneous permeation experiments. Altern Lab Anim. 2006 Oct;34(5):499–513.

225. Seto JE, Polat BE, Lopez RFV, Blankschtein D, Langer R. Effects of ultrasound and sodium lauryl sulfate on the transdermal delivery of hydrophilic permeants: Comparative in vitro studies with full-thickness and split-thickness pig and human skin. Journal of controlled release. 2010;145(1):26–32.

226. Gómez-Segura L, Parra A, Calpena AC, Gimeno Á, Boix-Montañes A. Carprofen Permeation Test through Porcine Ex Vivo Mucous Membranes and Ophthalmic Tissues for Tolerability Assessments: Validation and Histological Study. Vet Sci. 2020 Oct 10;7(4):152.

227. AOAC International Officers and Committees. J AOAC Int. 1993 Jan 1;76(1):223–50.

228. Gómez Ochoa de Alda J, Marcos-Merino JM, Esteban Gallego R. Extracción de ADN con material cotidiano: desarrollo de una estrategia interdisciplinar a partir de sus fundamentos científicos. Educación Química. 2019 Feb 7;30(1):58.

229. Azhar Shekoufeh Bahari L, Hamishehkar H. The Impact of Variables on Particle Size of Solid Lipid Nanoparticles and Nanostructured Lipid Carriers; A Comparative Literature Review. Adv Pharm Bull. 2016 Jun 29;6(2):143–51.

230. Kaur I, Ellis LJ, Romer I, Tantra R, Carriere M, Allard S, et al. Dispersion of Nanomaterials in Aqueous Media: Towards Protocol Optimization. Journal of Visualized Experiments. 2017 Dec 25;(130).

231. Ford JL, Timmins P. Application of thermal analysis to compatibility studies for solid dosage forms. In: Rubinstein MH, editor. Pharmaceutical thermal analysis. Ellis Horwood. Chichester; 1989. p. 238–47.

232. Kerč J, Srčič S, Urleb U, Kanalec A, Kofler B, šMid-Korbar J. Compatibility study between acetylcysteine and some commonly used tablet excipients. Journal of Pharmacy and Pharmacology. 2011 Apr 12;44(6):515–8.

233. Schramm G. A Practical Approach to Rheology and Rheometry. 2nd ed. Karlsruhe, Germany: Gebrueder HAAKE GmbH; 2004.

234. Morés MP, Silva Treviño J. Implementación de una metodología para la determinación de propiedades reológicas. Proyecto fin de carrera. [Internet]. [España]: Escuela Universitaria Ingeniería Industrial de Zaragoza; 2010 [cited 2022 Sep 10]. Available from: https://zaguan.unizar.es/record/5221/files/TAZ-PFC-2010-251.pdf

235. Møller PCF, Fall A, Bonn D. Origin of apparent viscosity in yield stress fluids below yielding. Europhys Lett. 2009;87(3):38004-38004p6.

236. Provenza Bernal N. Caracterización y estudio de estabilidad de fórmulas

magistrales líquidas de administración oral. Calpena Campmany AC, Clares Naveros B, editors. [Barcelona]; 2014.

237. Pader M. Dentifrice rheology. In: Laba D, editor. The rheological properties of cosmetic and toiletries. New York: Marcel Dekker; 1993. p. 247–73.

238. Umerska A, Paluch KJ, Santos-Martinez MJ, Medina C, Corrigan OI, Tajber L. Chondroitin-based nanoplexes as peptide delivery systems – Investigations into the self-assembly process, solid-state and extended release characteristics. European Journal of Pharmaceutics and Biopharmaceutics. 2015;93:242–53.

239. Brunelle SL. Determination of Chondroitin Sulfate Content in Raw Materials and Dietary Supplements by High-Performance Liquid Chromatography with UV Detection After Enzymatic Hydrolysis: Single-Laboratory Validation First Action 2015.11. J AOAC Int [Internet]. 2016;99(1):53–4. Available from: https://academic.oup.com/jaoac/article/99/1/53-54/5657981

240. Ji D, Roman M, Zhou J, Hildreth J. Determination of chondroitin sulfate content in raw materials and dietary supplements by high-performance liquid chromatography with ultraviolet detection after enzymatic hydrolysis: single-laboratory validation. J AOAC Int. 2007;90(3):659–69.

241. Wolff R. Chemical reaction between stearic acid and Sodium Hydroxide [Internet]. OneClass. 2019 [cited 2022 Nov 23]. Available from: https://oneclass.com/homework-help/chemistry/3680105-write-a-chemical-reaction-betwe.en.html

242. Sánchez Soberón A, Bárcena Martín AI. El azúcar en la enseñanza secundaria [Internet]. 1st ed. Vol. 103. Real Sociedad Española de Química; 2007 [cited 2022 Dec 15]. 46–49 p. Available from: https://analesdequimica.es/index.php/AnalesQuimica/article/view/1521

243. Greenspan P, Mayer EP, Fowler SD. Nile red: a selective fluorescent stain for intracellular lipid droplets. J Cell Biol. 1985 Mar 1;100(3):965–73.

244. Kim Tae-gwon, Hyuk-cheol, Lee Kang, Tae-yi Chun, Mong Ji-young, Choi Jeong-eun, et al. Method for improving stickiness of cosmetic form using chondroitin sulfate [Internet]. South Korea; KR101609121B1, 2014 [cited 2022 Sep 1]. Available from: https://patents.google.com/patent/KR101609121B1/en

245. Mishra S, Reshma G B, Pal S, Bano S, Gupta A, Kumari A, et al. Topical Application of Peptide–Chondroitin Sulfate Nanoparticles Allows Efficient Photoprotection in Skin. ACS Appl Mater Interfaces. 2021;13(2):2382–98.
246. USP. <1225> Validation of Compendial Procedures. In: USP 40/NF 35, United States Pharmacopeia. 40th ed., National Formulary. 35th ed. 35th ed. Rockville, MD: The United States Pharmacopeia Convention; United Book Press, Inc; 2017.
247. Jenkins D, Diallo C, Bethea E, Kaale E, Layloff T. Method Validation Approaches for Pharmaceutical Assessments – Highlights with High Performance Thin Layer Chromatographic (HPTLC) Techniques. Calibration and Validation of Analytical Methods - A Sampling of Current Approaches. InTech; 2018.
248. Yuan H, Zhang W, Du YZ, Hu FQ. Ternary nanoparticles of anionic lipid nanoparticles/protamine/DNA for gene delivery. Int J Pharm. 2010 Jun 15;392(1–2):224–31.
249. Karagöz U, Kotmakçı M, Akbaba H, Çetintaş VB, Kantarcı G. Preparation and characterization of non-viral gene delivery systems with pEGFP-C1 Plasmid DNA. Brazilian Journal of Pharmaceutical Sciences. 2018 Jun 7;54(1).
250. Addgene. pEGFP-RNASEH1 Notes [Internet]. [cited 2019 Dec 19]. Available from: https://media.addgene.org/data/plasmids/108/108699/108699-notes_w6fDhcKvfHnDncK6MEY.pdf
251. Penumarthi A. Utilising Nanoparticles for DNA Vaccine Delivery. [Melbourne]: RMIT University; 2017.
252. Maugeri M, Nawaz M, Papadimitriou A, Angerfors A, Camponeschi A, Na M, et al. Linkage between endosomal escape of LNP-mRNA and loading into EVs for transport to other cells. Nat Commun. 2019 Sep 24;10(1):4333.

ANNEXES

15 ANNEX 1

15.1 Analysis of data- Experimental factorial design

Evaluation of statistical premises

NORMALITY

%EE Probability Plot

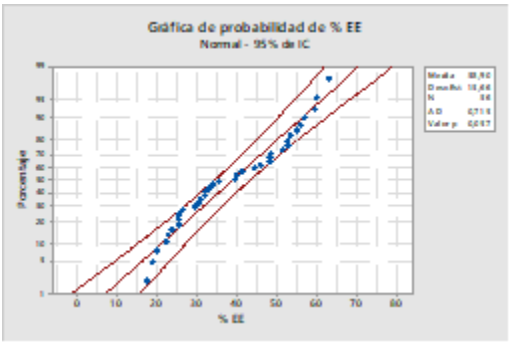

p value is greater than 0.05: follows normal distribution.

Pot Z probability plot

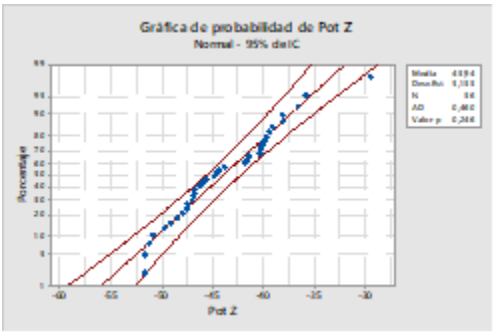

p value greater than 0.05: follows normal distribution.

Probability Plot of Size

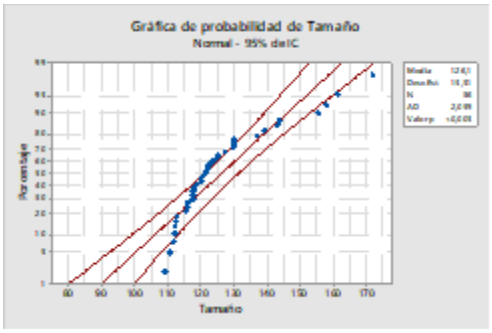

P value less than 0.05: Does not follow normal distribution.

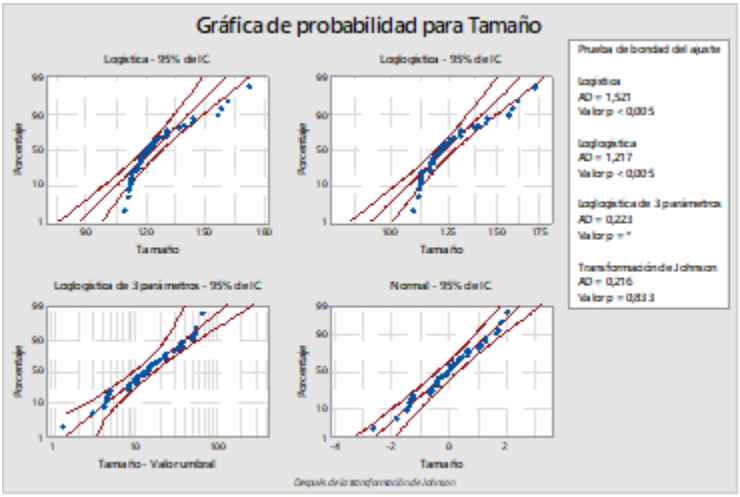

SIZE: p value greater than 0.05 for the Johnson distribution. The data is transformed.

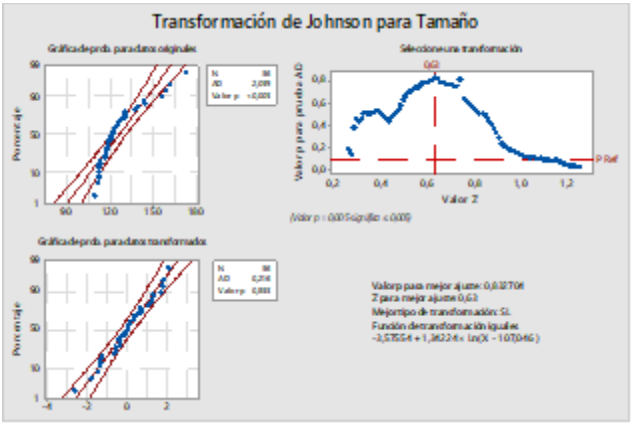

Transformed data follows a normal distribution.

ANOVA: % EE; Pot Z; Trans Size vs. Conc; Time; Speed

Factor information

Factor	Type	levels	Values
Conc	Permanent	3	0.4; 0.7; 1.0
Time	Permanent	2	10;15
Speed	Permanent	3	16000; 20000; 24000

Analysis of variance of % EE

Fountain	GL	SC	MC	F	P
Conc	2	5203.61	2601.81	62.52	0,000
Time	1	0.66	0.66	0.02	0.900
speed	2	77.84	38.92	0.94	0.404
Mistake	30	1248.52	41.62		
Total	35	6530.64			

Model Summary

S	R-sq	R-sq (tight)
6.45116	80.88%	77.70%

Pot Z Analysis of Variance

Fountain	GL	SC	MC	F	P
Conc	2	597,209	298,604	31.70	0,000
Time	1	0.020	0.020	0.00	0.963
Speed	2	42,413	21,206	2.25	0.123
Mistake	30	282,598	9,420		
Total	35	922,240			

Model Summary

S	R-sq	R-sq (tight)
3.06919	69.36%	64.25%

Analysis of Variance of Trans Size

Fountain	GL	SC	MC	F	P
Conc	2	0.3428	0.1714	0.19	0.830
Time	1	1.4572	1.4572	1.59	0.217
Speed	2	12.9035	6.4517	7.06	0.003

Mistake	30	27.4336	0.9145
Total	35	42.1371	

Model Summary

S	R-sq	R-sq (tight)
0.956270	34.89%	24.04%

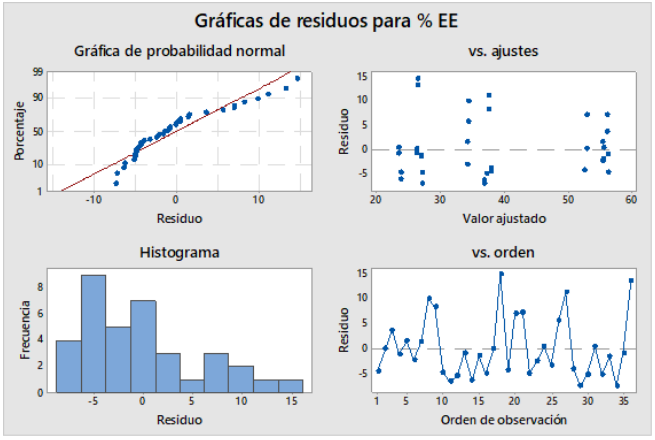

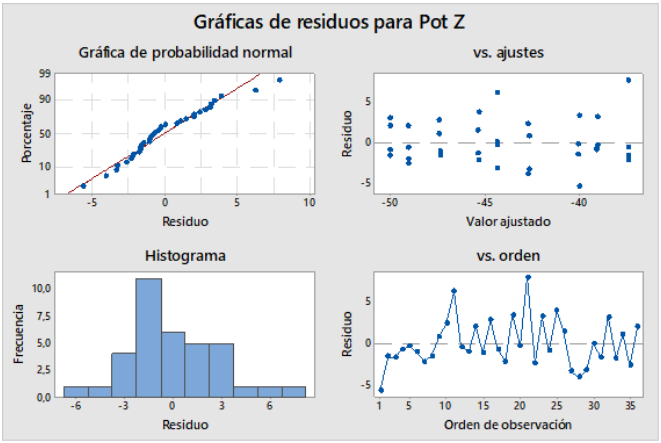

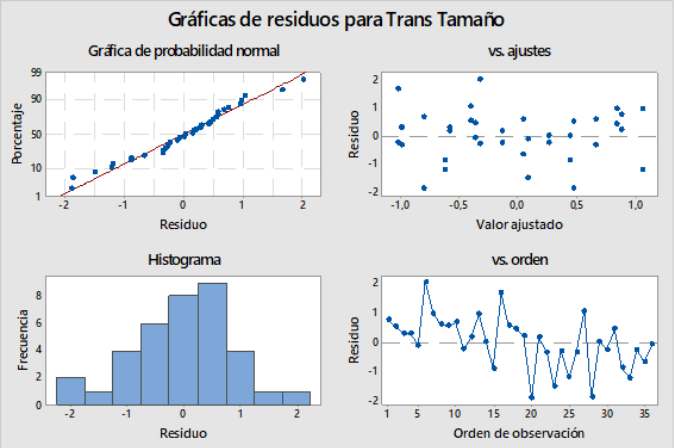

SUMMARY OF RESULTS FOR THE STATISTICAL ASSUMPTIONS

1. **Residual normality** : aligned to the red line.
2. **Independence:** residuals vs. order of observation : there is no attention - grabbing order : some pattern above or below . There is independence.
3. **Homoscedasticity** : second graph on the upper right. The residues are painted. The fitted value of the residuals shows values above and below zero.

General factorial regression: Trans Size vs. Conc; speed; Time

Factor information

Factor	levels	Values
Conc	3	0.4; 0.7; 1.0
Speed	3	16000; 20000; 24000
Time	2	10; fifteen

Variance analysis

Fountain	GL	SC Sec.	Contribution	SC Adj.	MC Adj.	F-value
Model	13	18.4378	43.76%	18.4378	1.41829	1.32
Linear	5	14.7035	34.89%	14.7035	2.94070	2.73
Conc	2	0.3428	0.81%	0.3428	0.17139	0.16
Speed	2	12.9035	30.62%	12.9035	6.45175	5.99
Time	1	1.4572	3.46%	1.4572	1.45723	1.35
2-term interactions	8	3.7343	8.86%	3.7343	0.46679	0.43
conc*speed	4	0.3573	0.85%	0.3573	0.08932	0.08
Conc*Time	2	0.6798	1.61%	0.6798	0.33990	0.32
speed*time	2	2.6972	6.40%	2.6972	1.34861	1.25
Mistake	22	23.6993	56.24%	23.6993	1.07724	
lack of fit	4	7.2056	17.10%	7.2056	1.80139	1.97
pure mistake	18	16.4937	39.14%	16.4937	0.91632	

Total	35	42.1371	100.00%

Fountain	p-value
Model	0.275
Linear	0.046
Conc	0.854
speed	0.008
Time	0.257
2-term interactions	0.888
conc*speed	0.987
Conc*Time	0.733
speed*time	0.306
Mistake	
lack of fit	0.143
pure mistake	
Total	

Model Summary

S	R-sq	R-sq (tight)	PRESS	R-sq (pred)
1.03790	43.76%	10.52%	63.4592	0.00%

coefficients

Finished	Coeff	ee of coef.	95% CI	T-value	p-value	IVF
Constant	-0.030	0.173	(-0.389, 0.329)	-0.17	0.865	
Conc						
0.4	-0.050	0.245	(-0.558, 0.457)	-0.21	0.839	1.33
0.7	0.136	0.245	(-0.371, 0.644)	0.56	0.583	1.33
speed						
16000	0.754	0.245	(0.247; 1.262)	3.08	0.005	1.33
20000	-0.710	0.245	(-1.218, -0.203)	-2.90	0.008	1.33
Time						
10	0.201	0.173	(-0.158, 0.560)	1.16	0.257	1.00
conc*speed						
0.4 16000	-0.112	0.346	(-0.830, 0.605)	-0.32	0.748	1.78
0.4 20000	0.090	0.346	(-0.627; 0.808)	0.26	0.797	1.78

0.7 16000	-0.007	0.346 (-0.725, 0.710)	-0.02	0.984	1.78
0.7 20000	0.093	0.346 (-0.624; 0.811)	0.27	0.790	1.78
Conc*Time					
0.4 10	-0.040	0.245 (-0.547, 0.467)	-0.16	0.872	1.33
0.7 10	0.185	0.245 (-0.323; 0.692)	0.75	0.458	1.33
speed*time					
16000 10	0.344	0.245 (-0.163; 0.852)	1.41	0.173	1.33
20000 10	-0.019	0.245 (-0.526, 0.488)	-0.08	0.939	1.33

regression equation

Trans Size = -0.030 - 0.050 Conc_0.4 + 0.136 Conc_0.7 - 0.086 Conc_1.0 + 0.754 Vel_16000
- 0.710 Vel_20000 - 0.044 Vel_24000 + 0.201 Time_10 - 0.201 Time_15
- 0.112 Conc*Vel_0.4 16000 + 0.090 Conc*Vel_0.4 20000 + 0.022 Conc*Vel_0.4
24000 - 0.007 Conc*Vel_0.7 16000 + 0.093 Conc*Vel_0.7 20000
- 0.086 Conc*Vel_0.7 24000 + 0.119 Conc*Vel_1.0 16000 - 0.183 Conc*Vel_1.0
20000 + 0.064 Conc*Vel_1.0 24000 - 0.040 Conc*Time_0.4 10
+ 0.040 Conc*Time_0.4 15 + 0.185 Conc*Time_0.7 10 - 0.185 Conc*Time_0.7
15 - 0.145 Conc*Time_1.0 10 + 0.145 Conc*Time_1.0 15
+ 0.344 Vel*Time_16000 10 - 0.344 Vel*Time_16000 15
- 0.019 Vel*Time_20000 10 + 0.019 Vel*Time_20000 15
- 0.325 Vel*Time_24000 10 + 0.325 Vel*Time_24000 15

Adjustments and diagnostics for unusual observations

Obs	Trans Size	ee of Adjustment	adjustment	95% CI	resided	resided its T.	resided delete	D of AA	cooking	DFITS
6	1,692	0.062	0.647	(-1,280; 1,405)	1,630	2.01	2.17	0.388889	0.18	1.73215
16	0.630	-1,047	0.647	(-2.389, 0.295)	1,677	2.07	2.25	0.388889	0.19	1.79504
25	-0.138	1,584	0.647	(0.242;	-1,722	-2.12	-2.32	0.388889	0.20	-

				2.926)					1.85433
28	-2,677	-0.877	0.647	(-2.220, 0.465)	-1,799	-2.22	-2.46	0.388889	0.22	- 1.96158

Obs
6 R.
16 R.
25 R.
28 R.

large residual R

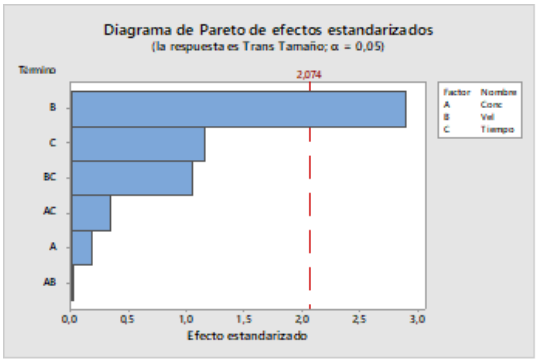

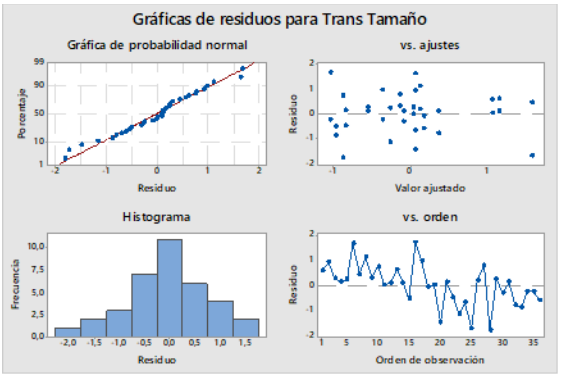

General factorial regression: Pot Z vs. Conc; speed; Time

factor information

Factor	levels	Values
Conc	3	0.4; 0.7; 1.0
speed	3	16000; 20000; 24000
Time	2	10; fifteen

Variance analysis

Fountain	GL	SC Sec.	Contribution	SC Adj.	MC Adj.	F-value
Model	13	706,750	76.63%	706,750	54,365	5.55
Linear	5	639,641	69.36%	639,641	127,928	13.06
Conc	2	597,209	64.76%	597,209	298,604	30.49
speed	2	42,413	4.60%	42,413	21,206	2.17
Time	1	0.020	0.00%	0.020	0.020	0.00
2-term interactions	8	67,109	7.28%	67,109	8,389	0.86

conc*speed	4	18,457	2.00%	18,457	4,614	0.47
Conc*Time	2	42,930	4.65%	42,930	21,465	2.19
speed*time	2	5,722	0.62%	5,722	2,861	0.29
Mistake	22	215,489	23.37%	215,489	9,795	
lack of fit	4	10,915	1.18%	10,915	2,729	0.24
pure mistake	18	204,575	22.18%	204,575	11,365	
Total	35	922,240	100.00%			

Fountain	p-value
Model	0,000
Linear	0,000
Conc	0,000
speed	0.139
Time	0.964
2-term interactions	0.566
conc*speed	0.756
Conc*Time	0.136
speed*time	0.750
Mistake	
lack of fit	0.912
pure mistake	
Total	

Model Summary

S	R-sq	R-sq (tight)	PRESS	R-sq (pred)
3.12969	76.63%	62.83%	577,013	37.43%

coefficients

Finished	Coeff	ee of coef.	95% CI	T-value	p-value	IVF
Constant	-43,944	0.522	(-45,026; -42,862)	-84.25	0,000	
Conc						

0.4	5,084	0.738	(3,554; 6,614)	6.89	0,000	1.33
0.7	-0.198	0.738	(-1,728; 1,332)	-0.27	0.791	1.33
speed						
16000	-1,200	0.738	(-2.730, 0.329)	-1.63	0.118	1.33
20000	1,429	0.738	(-0.101; 2.959)	1.94	0.066	1.33
Time						
10	0.024	0.522	(-1,058; 1,105)	0.05	0.964	1.00
conc*speed						
0.4 16000	-1.02	1.04	(-3.19, 1.14)	-0.98	0.337	1.78
0.4 20000	0.79	1.04	(-1.37, 2.96)	0.76	0.455	1.78
0.7 16000	0.40	1.04	(-1.76, 2.56)	0.38	0.705	1.78
0.7 20000	-1.05	1.04	(-3.21, 1.12)	-1.00	0.327	1.78
Conc*Time						
0.4 10	1,131	0.738	(-0.399, 2.660)	1.53	0.140	1.33
0.7 10	0.346	0.738	(-1,184; 1,876)	0.47	0.644	1.33
speed*time						
16000 10	-0.540	0.738	(-2.070; 0.990)	-0.73	0.472	1.33
20000 10	0.131	0.738	(-1,399; 1,660)	0.18	0.861	1.33

regression equation

Pot Z = -43.944 + 5.084 Conc_0.4 - 0.198 Conc_0.7 - 4.887 Conc_1.0 - 1.200 Vel_16000
+ 1.429 Spd_20000 - 0.228 Spd_24000 + 0.024 Time_10 - 0.024 Time_15
- 1.02 Conc*Vel_0.4 16000 + 0.79 Conc*Vel_0.4 20000 + 0.23 Conc*Vel_0.4 24000
+ 0.40 Conc*Vel_0.7 16000 - 1.05 Conc*Vel_0.7 20000 + 0.64 Conc*Vel_0.7 24000
+ 0.62 Conc*Vel_1.0 16000 + 0.25 Conc*Vel_1.0 20000 - 0.87 Conc*Vel_1.0 24000
+ 1.131 Conc*Time_0.4 10 - 1.131 Conc*Time_0.4 15 + 0.346 Conc*Time_0.7 10
- 0.346 Conc*Time_0.7 15 - 1.476 Conc*Time_1.0 10 + 1.476 Conc*Time_1.0 15
- 0.540 Vel*Time_16000 10 + 0.540 Vel*Time_16000 15 + 0.131 Vel*Time_20000 10
- 0.131 Vel*Time_20000 15 + 0.410 Vel*Time_24000 10 - 0.410 Vel*Time_24000 15

Adjustments and diagnostics for unusual observations

Obs	Pot Z	Adjustment	ee of adjustment	95% CI	resided	resided its T.	resided delete	AA	D of cooking	DFITS
1	-45.67	-40.47	1.95	(-44.52; -36.42)	-5.20	-2.12	-2.33	0.388889	0.21	-1.85698
twenty-one	-29.53	-35.35	1.95	(-39.40; -31.31)	5.82	2.38	2.70	0.388889	0.26	2.15093

Obs
1 R.
21 R.

large residual R

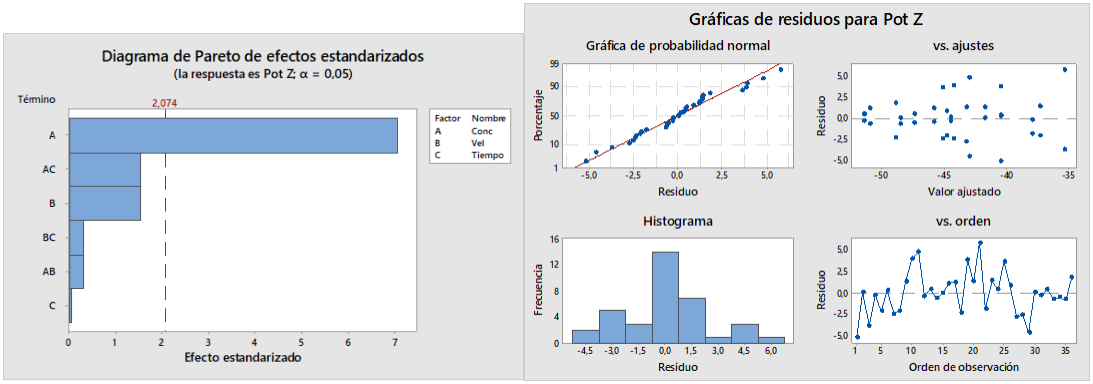

General factorial regression: % EE vs. Conc; speed; Time

factor information

Factor	levels	Values
Conc	3	0.4; 0.7; 1.0
speed	3	16000; 20000; 24000
Time	2	10; fifteen

Variance analysis

Fountain	GL	SC Sec.	Contribution	SC Adj.	MC Adj.	F-value
Model	13	6162.53	94.36%	6162.53	474.04	28.33
Linear	5	5282.12	80.88%	5282.12	1056.42	63.14
Conc	2	5203.61	79.68%	5203.61	2601.81	155.50
speed	2	77.84	1.19%	77.84	38.92	2.33
Time	1	0.66	0.01%	0.66	0.66	0.04
2-term interactions	8	880.41	13.48%	880.41	110.05	6.58

conc*speed	4	506.35	7.75%	506.35	126.59	7.57
Conc*Time	2	10.80	0.17%	10.80	5.40	0.32
speed*time	2	363.27	5.56%	363.27	181.63	10.86
Mistake	22	368.11	5.64%	368.11	16.73	
lack of fit	4	287.84	4.41%	287.84	71.96	16.14
pure mistake	18	80.27	1.23%	80.27	4.46	
Total	35	6530.64	100.00%			

Fountain	p-value
Model	0,000
Linear	0,000
Conc	0,000
speed	0.121
Time	0.844
2-term interactions	0,000
conc*speed	0.001
Conc*Time	0.728
speed*time	0.001
Mistake	
lack of fit	0,000
pure mistake	
Total	

Model Summary

S	R-sq	R-sq (tight)	PRESS	R-sq (pred)
4.09052	94.36%	91.03%	985,686	84.91%

coefficients

Finished	Coeff	ee of coef.	95% CI	T-value	p-value	IVF
Constant	38,903	0.682	(37,489; 40,317)	57.06	0,000	
Conc						
0.4	15,853	0.964	(13,853; 17,852)	16.44	0,000	1.33

0.7	-2,604	0.964	(-4.603, -0.604)	-2.70	0.013	1.33
speed						
16000	-2,042	0.964	(-4.041, -0.042)	-2.12	0.046	1.33
20000	1,364	0.964	(-0.636; 3.363)	1.41	0.171	1.33
Time						
10	-0.136	0.682	(-1,550; 1,278)	-0.20	0.844	1.00
conc*speed						
0.4 16000	-0.44	1.36	(-3.27, 2.39)	-0.32	0.750	1.78
0.4 20000	1.16	1.36	(-1.67, 3.99)	0.85	0.404	1.78
0.7 16000	3.39	1.36	(0.56; 6.22)	2.49	0.021	1.78
0.7 20000	2.66	1.36	(-0.16, 5.49)	1.95	0.064	1.78
Conc*Time						
0.4 10	0.153	0.964	(-1,847; 2,152)	0.16	0.876	1.33
0.7 10	0.581	0.964	(-1,418; 2,581)	0.60	0.553	1.33
speed*time						
16000 10	-1,838	0.964	(-3.837; 0.162)	-1.91	0.070	1.33
20000 10	4,469	0.964	(2,469; 6,468)	4.64	0,000	1.33

regression equation

%EE = 38.903 + 15.853 Conc_0.4 - 2.604 Conc_0.7 - 13.249 Conc_1.0 - 2.042 Vel_16000
+ 1.364 Spd_20000 + 0.678 Spd_24000 - 0.136 Time_10 + 0.136 Time_15
- 0.44 Conc*Vel_0.4 16000 + 1.16 Conc*Vel_0.4 20000 - 0.72 Conc*Vel_0.4 24000
+ 3.39 Conc*Vel_0.7 16000 + 2.66 Conc*Vel_0.7 20000 - 6.05 Conc*Vel_0.7 24000
- 2.95 Conc*Vel_1.0 16000 - 3.82 Conc*Vel_1.0 20000 + 6.78 Conc*Vel_1.0 24000

+ 0.153 Conc*Time_0.4 10 - 0.153 Conc*Time_0.4 15 + 0.581 Conc*Time_0.7 10
- 0.581 Conc*Time_0.7 15 - 0.734 Conc*Time_1.0 10 + 0.734 Conc*Time_1.0 15
- 1,838 Spd*Time_16000 10 + 1,838 Spd*Time_16000 15 + 4,469 Spd*Time_20000 10
- 4,469 Spd*Time_20000 15 - 2,631 Spd*Time_24000 10 + 2,631 Spd*Time_24000 15

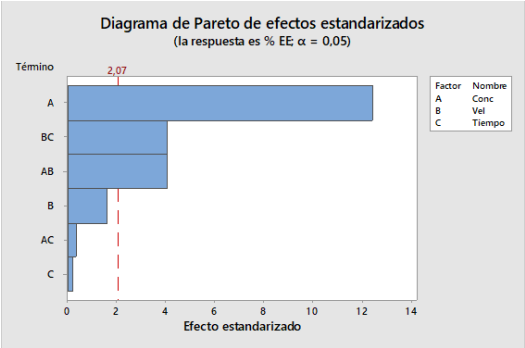

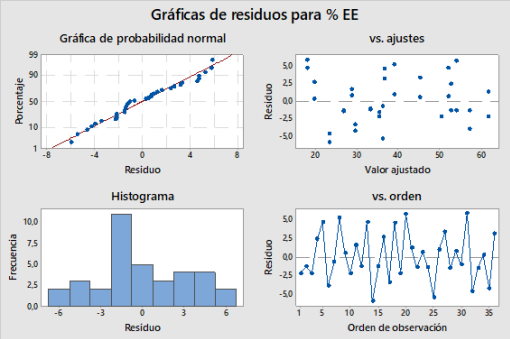

EE% ADJUSTMENT WITH LESS VARIABLES

General factorial regression: % EE vs. Conc; speed; Time

factor information

Factor	levels	Values
Conc	3	0.4; 0.7; 1.0
speed	3	16000; 20000; 24000
Time	2	10; fifteen

Variance analysis

Fountain	GL	SC Sec.	Contribution	SC Adj.	MC Adj.	F-value
Model	6	5577.68	85.41%	5577.68	929.61	28.29
Linear	2	5203.61	79.68%	5203.61	2601.81	79.18
Conc	2	5203.61	79.68%	5203.61	2601.81	79.18
2-term interactions	4	374.07	5.73%	374.07	93.52	2.85
Conc*Time	2	10.80	0.17%	10.80	5.40	0.16
speed*time	2	363.27	5.56%	363.27	181.63	5.53
Mistake	29	952.97	14.59%	952.97	32.86	
lack of fit	11	872.70	13.36%	872.70	79.34	17.79

pure mistake	18	80.27	1.23%	80.27	4.46
Total	35	6530.64	100.00%		

Fountain	p-value
Model	0,000
Linear	0,000
Conc	0,000
2-term interactions	0.042
Conc*Time	0.849
speed*time	0.009
Mistake	
lack of fit	0,000
pure mistake	
Total	

Model Summary

S	R-sq	R-sq (tight)	PRESS	R-sq (pred)
5.73244	85.41%	82.39%	1468.54	77.51%

coefficients

Finished	Coeff	ee of coef.	95% CI	T-value	p-value	IVF
Constant	38,903	0.955	(36,949; 40,857)	40.72	0,000	
Conc						
0.4	15.85	1.35	(13.09; 18.62)	11.73	0,000	1.33
0.7	-2.60	1.35	(-5.37, 0.16)	-1.93	0.064	1.33
Conc*Time						
0.4 10	0.15	1.35	(-2.61, 2.92)	0.11	0.911	1.33
0.7 10	0.58	1.35	(-2.18, 3.34)	0.43	0.670	1.33
speed*time						
16000 10	-1.84	1.35	(-4.60, 0.93)	-1.36	0.184	1.33
20000 10	4.47	1.35	(1.71; 7.23)	3.31		1.33

regression equation

%EE = 38.903 + 15.85 Conc_0.4 - 2.60 Conc_0.7 - 13.25 Conc_1.0 + 0.15 Conc*Time_0.4 10 - 0.15 Conc*Time_0.4 15 + 0.58 Conc*Time_0.7 10 - 0.58

Conc*Time_0.7 15
- 0.73 Conc*Time_1.0 10 + 0.73 Conc*Time_1.0 15 - 1.84
Vel*Time_16000 10
+ 1.84 Spd*Time_16000 15 + 4.47 Spd*Time_20000 10 - 4.47
Spd*Time_20000 15
- 2.63 Spd*Time_24000 10 + 2.63 Spd*Time_24000 15

Adjustments and diagnostics for unusual observations

Obs	%EE	Adjustment	ee of adjustment	95% CI	resided	resided its T.	resided delete	AA	D of cooking	DFITS	
14	17.41	28.23	2.53	(23.06; 33.40)	-10.82	-2.10	-2.24	0.194444	0.15	1.10228	-R.
18	41.17	29.02	2.53	(23.85; 34.19)	12.16	2.36	2.58	0.194444	0.19	1.26926	R.
36	39.77	29.02	2.53	(23.85; 34.19)	10.75	2.09	2.23	0.194444	0.15	1.09451	R.

large residual R

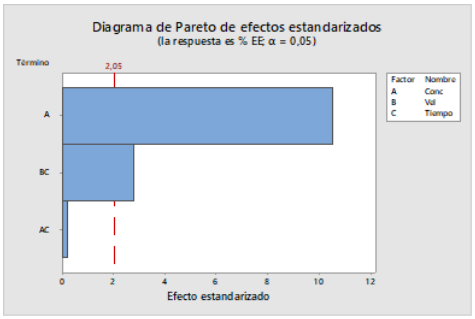

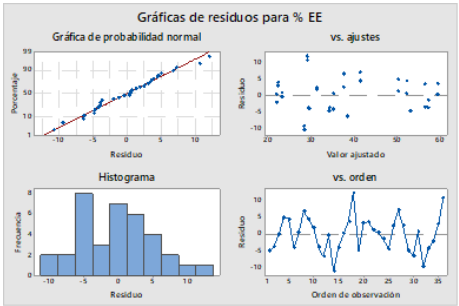

EE% ADJUSTMENT WITH LESS VARIABLES

General factorial regression: % EE vs. Conc; speed; Time

factor information

Factor	levels	Values
Conc	3	0.4; 0.7; 1.0
speed	3	16000; 20000; 24000
Time	2	10; 15

Variance analysis

Fountain	GL	SC Sec.	Contribution	SC Adj.	MC Adj.	F-

						value
Model	4	5566.88	85.24%	5566.88	1391.72	44.77
Linear	2	5203.61	79.68%	5203.61	2601.81	83.69
Conc	2	5203.61	79.68%	5203.61	2601.81	83.69
2-term interactions	2	363.27	5.56%	363.27	181.63	5.84
speed*time	2	363.27	5.56%	363.27	181.63	5.84
Mistake	31	963.77	14.76%	963.77	31.09	
lack of fit	13	883.50	13.53%	883.50	67.96	15.24
pure mistake	18	80.27	1.23%	80.27	4.46	
Total	35	6530.64	100.00%			

Fountain	p-value
Model	0,000
Linear	0,000
Conc	0,000
2-term interactions	0.007
speed*time	0.007
Mistake	
lack of fit	0,000
pure mistake	
Total	

Model Summary

S	R-sq	R-sq (tight)	PRESS	R-sq (pred)
5.57577	85.24%	83.34%	1299.73	80.10%

coefficients

Finished	Coeff	ee of coef.	95% CI	T-value	p-value	IVF
Constant	38,903	0.929	(37,008; 40,798)	41.86	0,000	
Conc						
0.4	15.85	1.31	(13.17; 18.53)	12.06	0,000	1.33

0.7	-2.60	1.31	(-5.28, 0.08)	-1.98	0.057	1.33
speed*time						
16000 10	-1.84	1.31	(-4.52, 0.84)	-1.40	0.172	1.33
20000 10	4.47	1.31	(1.79; 7.15)	3.40	0.002	1.33

regression equation

%EE = 38.903 + 15.85 Conc_0.4 - 2.60 Conc_0.7 - 13.25 Conc_1.0 - 1.84 Vel*Time_16000 10 + 1.84 Spd*Time_16000 15 + 4.47 Spd*Time_20000 10 - 4.47 Spd*Time_20000 15 - 2.63 Spd*Time_24000 10 + 2.63 Spd*Time_24000 15

Adjustments and diagnostics for unusual observations

Obs	%EE	Adjustment	ee of adjustment	95% CI	resided	its T.	resided delete	AA	D of cooking	DFITS	
18	41.17	28.29	2.08	(24.05; 32.52)	12.89	2.49	2.74	0.138889	0.20	1.10054	R.
36	39.77	28.29	2.08	(24.05; 32.52)	11.48	2.22	2.38	0.138889	0.16	0.95622	R.

large residual R

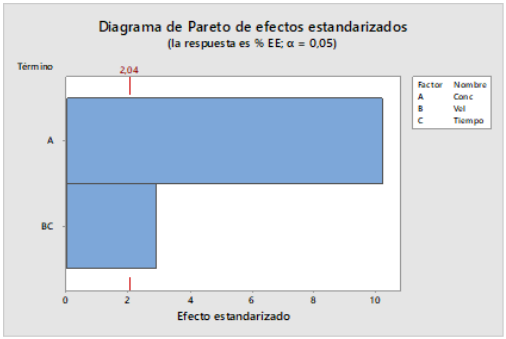

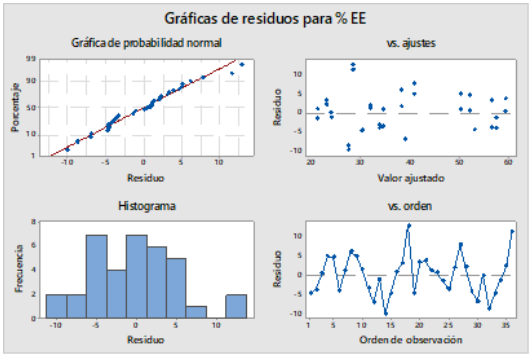

POT Z ADJUSTMENT WITH LESS VARIABLES

General factorial regression: Pot Z vs. Conc

factor information

Factor	levels	Values
Conc	3	0.4; 0.7; 1.0

Variance analysis

Fountain	GL	SCContribution	SC Adj.	MC Adj.	F-	p-

		Sec.				value	value
Model	2	597.2	64.76%	597.2	298,604	30.32	0,000
Linear	2	597.2	64.76%	597.2	298,604	30.32	0,000
Conc	2	597.2	64.76%	597.2	298,604	30.32	0,000
Mistake	33	325.0	35.24%	325.0	9,849		
lack of fit	15	120.5	13.06%	120.5	8,030	0.71	0.749
pure mistake	18	204.6	22.18%	204.6	11,365		
Total	35	922.2	100.00%				

Model Summary

S	R-sq	R-sq (tight)	PRESS	R-sq (pred)
3.13838	64.76%	62.62%	386,814	58.06%

coefficients

Finished	Coeff	ee of coef.	95% CI	T-value	p-value	IVF
Constant	-43,944	0.523	(-45,008; -42,880)	-84.01	0,000	
Conc						
0.4	5,084	0.740	(3,579; 6,589)	6.87	0,000	1.33
0.7	-0.198	0.740	(-1,703; 1,307)	-0.27	0.791	1.33

regression equation

Pot Z = -43.944 + 5.084 Conc_0.4 - 0.198 Conc_0.7 - 4.887 Conc_1.0

Adjustments and diagnostics for unusual observations

Obs	Pot Z	Adjustment	ee of adjustment	95% CI	resided	resided its T.	resided delete	AA	D of cooking
1	-45,667	-38,860	0.906	(-40,703; -37,017)	-6,807	-2.27	-2.43	0.0833333	0.16
21	-29,533	-38,860	0.906	(-40,703; -37,017)	9,326	3.10	3.63	0.0833333	0.29

Obs	DFITS	
1	-0.73192	R.
21	1.09519	R.

large residual R

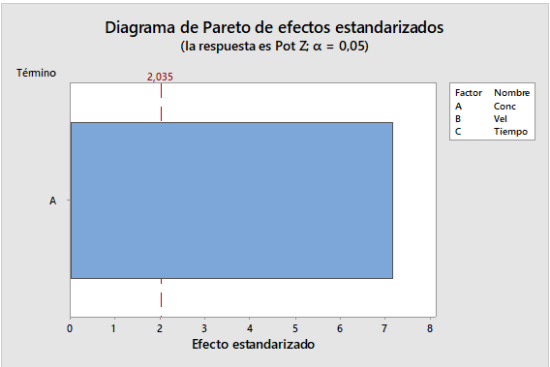

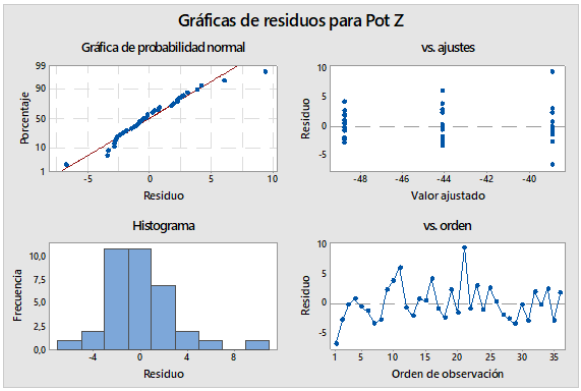

SIZE ADJUSTMENT WITH LESS VARIABLES

General factorial regression: Trans Size vs. speed

factor information

Factor	levels	Values
speed	3	16000; 20000; 24000

Variance analysis

Fountain	GL	SC Sec.	Contribution	SC Adj.	MC Adj.	F-value	p-value
Model	2	12.90	30.62%	12.90	6.4517	7.28	0.002
Linear	2	12.90	30.62%	12.90	6.4517	7.28	0.002
speed	2	12.90	30.62%	12.90	6.4517	7.28	0.002
Mistake	33	29.23	69.38%	29.23	0.8859		
lack of fit	fifteen	12.74	30.23%	12.74	0.8493	0.93	0.554
pure mistake	18	16.49	39.14%	16.49	0.9163		
Total	35	42.14	100.00%				

Model Summary

S	R-sq	R-sq (tight)	PRESS	R-sq (pred)
0.941205	30.62%	26.42%	34.7904	17.44%

coefficients

Finished	Coeff	ee of coef.	95% CI	T-value	p-value	IVF

Constant	-0.157	(-0.349, 0.030	-0.19	0.850		
		0.289)				
speed						
16000	0.754	0.222	(0.303; 1.206)	3.40	0.002	1.33
20000	-0.222	(-1.162, 0.710	-0.259)	-3.20	0.003	1.33

regression equation

Trans Size = -0.030 + 0.754 Spd_16000 - 0.710 Spd_20000 - 0.044 Spd_24000

Adjustments and diagnostics for unusual observations

Obs	Trans Size	Adjustment	ee of adjustment	95% CI	resided	resided its T.	resided delete	AA	D of cooking
20	-1,428	0.724	0.272	(0.172; 1.277)	-2,152	-2.39	-2.59	0.0833333	0.17
28	-2,677	-0.740	0.272	(-1.293, -0.187)	-1,937	-2.15	-2.28	0.0833333	0.14

Obs	DFITS
20	-0.779712 R.
28	-0.688059 R.

large residual R

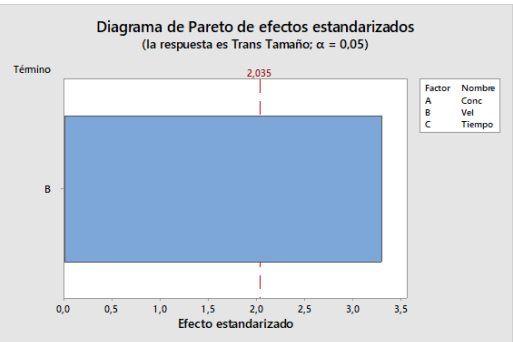

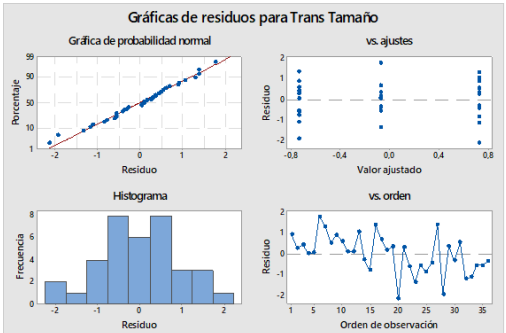

Factorial plots for %EE

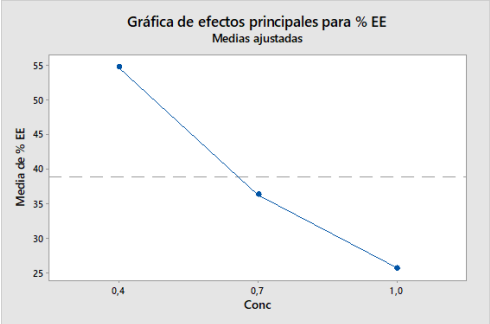

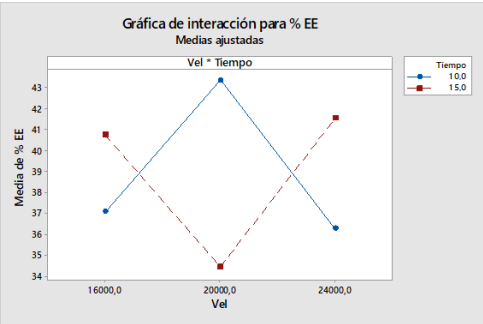

Factorial plots for Pot Z

***NOTE* There are no valid interactions to graph.**

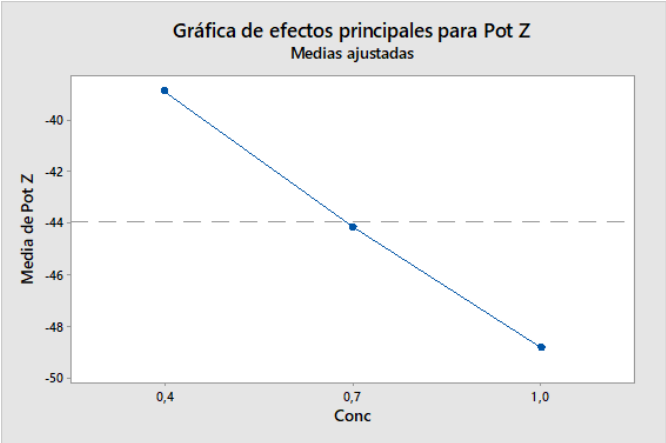

Factorial Plots for Trans Size

***NOTE* There are no valid interactions to graph.**

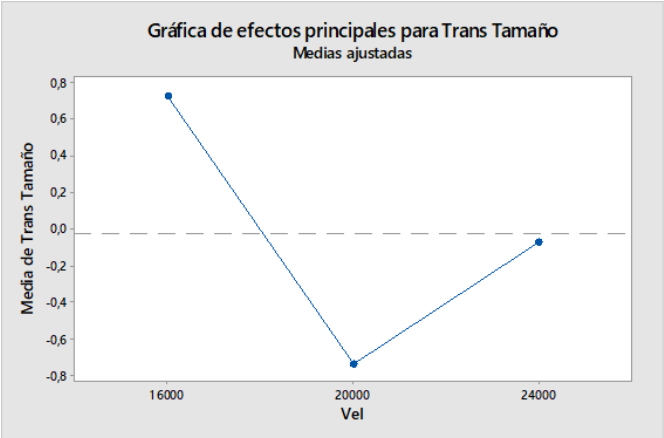

16 ANNEX 2

16.1 Viscosity study

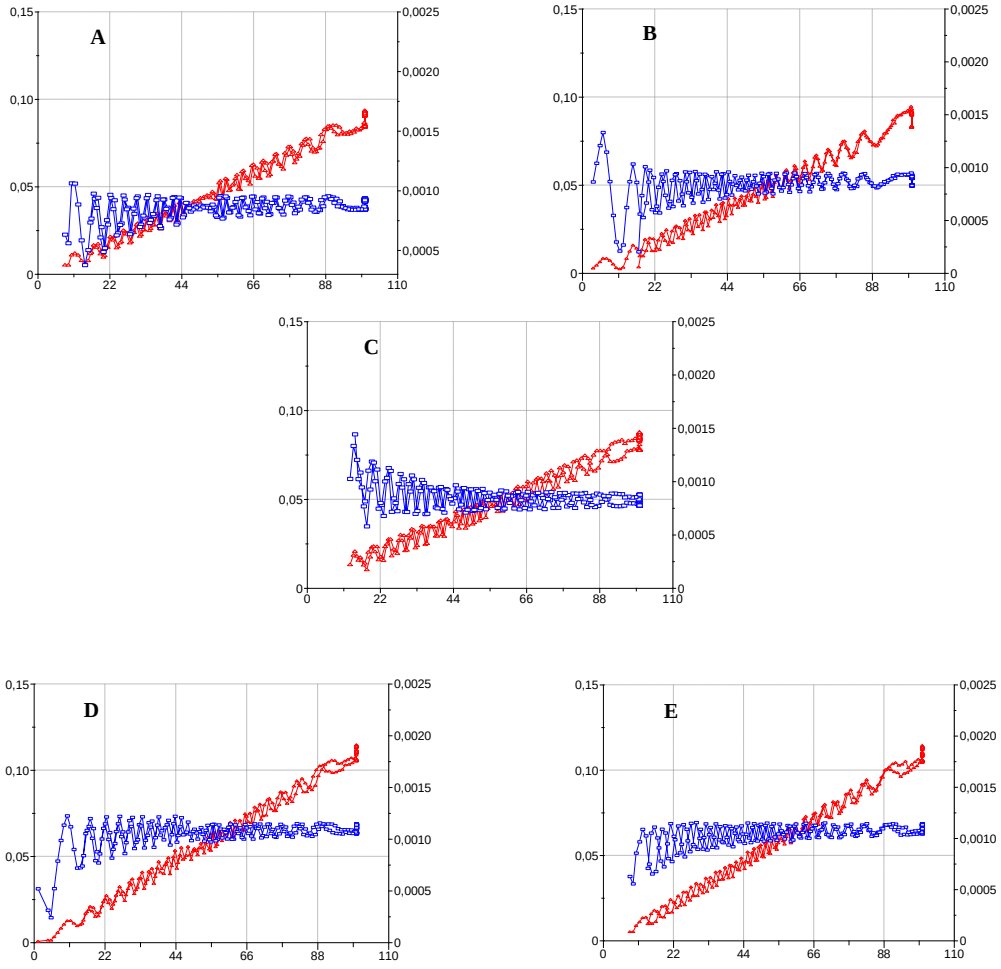

Figure 1-a. Flow curves in red (Shear *stress* in Pa versus *shear rate* in s^{-1}), and viscosity curves in blue (Viscosity *in* Pa s versus shear rate in s^{-1}) Milli Q Water (A, B and C), and CHON 0.7 mg/ml solution (D and E).

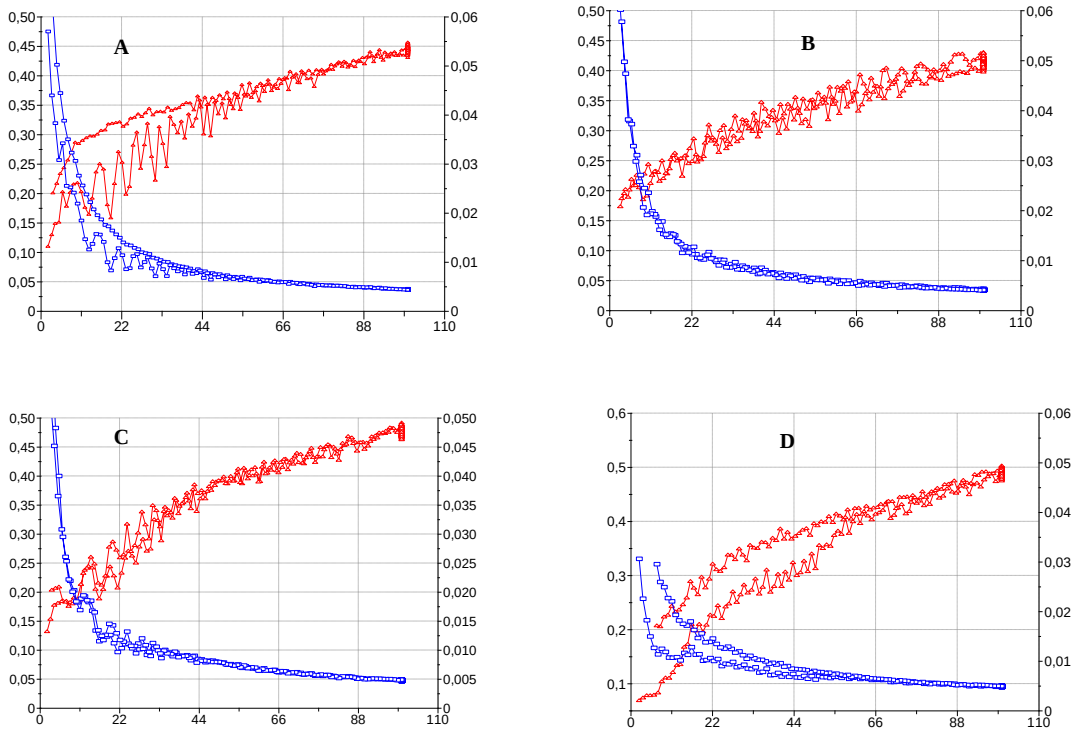

Figure 2-a. Flow curves in red (Shear *stress* in Pa versus *shear rate* in s^{-1}), and viscosity curves in blue (Viscosity *in* Pa s versus shear rate in s^{-1}) of an SLN formulation without CHON (A and B) and with 0.7 mg/ml of CHON (C and D).

17 ANNEX 3

17.1 COMMUNICATIONS IN CONGRESSES

The work presented in this dissertation has been developed with the financial support givenby the following grants:

- The Innovation and Human Capital Program for Competitiveness (PINN), Ministerio de Ciencia, Innovación, Tecnología y Telecomunicaciones (MICIT), Costa Rica.
- Office of International Affairs and External Cooperation (OAICE), University of Costa Rica.

Posters

1. Marta Eduviges Bustos Araya, JR Ticó, Ana C. Calpena, Anna Nardi-Ricart, Pilar Pérez-Lozano, Encarna García-Montoya, JM Suñe-Negre, Montserrat Miñarro-Carmona "**Study of Ex-vivo permeation of Chondroitin sulfate loaded to Solid Lipid Nanoparticles**". APGI (Association de Pharmacie Galénique Industrielle) and Skin Forum. Reims-France on the 23&24th September 2019.
2. Eduviges Bustos Araya, Anna Nardi-Ricart, Pilar Pérez-Lozano, Encarna García-Montoya, JM Suñé-Negre, JR Ticó, Montserrat Miñarro-Carmona. "**Validation of a titration method to determine chondroitin sulfate loaded to solid lipid nanoparticles in an experimental factorial design**". NanoBio&Med2018 International Conference. Barcelona-Spain, November 2018.
3. Eduviges Bustos Araya, Marc Suñé-Pou, Débora Mercadé Frutos, Isaac Nofrerias-Roig, Anna Nardi-Ricart, PilarPérez-Lozano, Encarna García-Montoya, JM Suñé-Negre, J R Ticó and Montserrat Miñarro-Carmona. **Experimental factorial design to optimize the formulation of solid lipid nanoparticles of chondroitin sulfate.** 23rd International Conference on Nanomaterials science & Nanoengineering & Technology and International Conference and Exhibition on Pharmaceutical Nanotechnology and Nanomedicine. April 18-19, 2018, Las Vegas, USA.